SHAPE STABILISATION OF CELLULOSE-POLY(ETHYLENE GLYCOL) PHASE CHANGE COMPOSITES FOR BUILDING CONSTRUCTION

A thesis submitted for the degree of Doctor of Philosophy (PhD)

By

Amende Sivanathan

Department of Civil and Environmental Engineering (CEE)

College of Engineering, Design and Physical Sciences (CEDPS)

Brunel University London

October 2023

Abstract

In this thesis a series of unique formulations were developed and investigated for the stabilisation of PEG using cellulose fibre (CF) as the supporting material by implementing the highly feasible tricarboxylic acid (TCA) crosslinking reaction using deionised water as solvent. This resulted in producing a series of shape stabilised TCA crosslinked composite PCMs of different chemical compositions. The TCA crosslinked composite PCMs were characterised by FTIR, XRD, SEM, DSC, TGA and POM analysis.

FTIR results confirmed the formation of a crosslinked structure, and the presence of weak intermolecular forces of attraction between the unreacted PEG particles and CF. Hence, leakage problem of solid-liquid PEG PCM was successfully overcome in the current study; and therefore, PEG was able to retain its original solid state during the phase transition process. Microwave (MW) irradiation had no major effects on the final structure of TCA composite PCM, but it appeared to have reduced the moisture content significantly since the intensity of peak appearing at 3450 cm-1 corresponding to the presence of OH groups had reduced significantly which may indicate moisture loss or changes in the polarity strength of the O-H group.

XRD results indicated that the crystallinity of pristine PEG had changed drastically after TCA crosslinking reaction. The major two crystalline peaks appearing at $2\theta =$ 19.10 and 23.23° disappeared after chemical crosslinking reaction; thus, broad humps existed in the composite PCMs indicating the presence of amorphous structures which was attributed to the incorporation of amorphous polymer (e.g., CF). The crystallinity index (CI) value of PEG8000 was 52.94% while TCA composite PCMs had CI value in the range 8.92 to 45.3%. The crystallinity of the resulting composite PCMs were dictated by the PEG content, PEG/CF ratio and PEG/CA ratio. Ten minutes MW radiation exposure was observed to enhance the crystallinity of TCA composite PCM with blend ratio of 4.0:1:7.5 from 35.65 to 47.96% (e.g., 34.53% increase) but twenty minutes MW radiation exposure reduced it from 35.65 to 32.32% (e.g., 9.34% decrease) which was attributed to destruction of PEG crystal lattice structure by the thermal effect of MW radiation.

DSC results showed that pristine PEG8000 had a very high latent heat capacity of 181.5 J/g which was attributed to the fact that PEG was comprised of simple linear polymer chains. This indicated that pristine PEG8000 are susceptible to crystallisation;

I

thus, could easily form crystals. After TCA crosslinking reaction the latent heat capacity of PEG had reduced significantly. Thus, TCA crosslinked composite PCMs had latent heat capacity in the range 18.19 to 58.08 J/g which was attributed to the reduced flexibility of the PEG chain during the crystallisation process. The phase transition temperature of PEG changed after TCA crosslinking reaction which was due to the changes in the thickness of the crystal lamellae. TGA results showed that the thermal stability of PEG had increased after TCA crosslinking reaction attributed to the formation of the crosslinked structure.

POM images indicated major changes in the spherulitic crystal structure of PEG after chemical crosslinking reaction due to the formation of the TCA crosslinked structure. Hence, the crystal structure became less prominent, and its size was observed to have reduced significantly attributed to the formation of crystal defects during chemical crosslinking reaction.

SEM images indicated the possibility of enhancing the structural integrity; thus, the homogeneity of the resulting composite PCMs using MW radiation exposure for ten minutes MW radiation exposure was observed to produce composite PCMs with compact structure and even topography; however, results suggested that twenty minutes MW radiation exposure was undesirable since cracks were observed to have formed due to severe moisture loss by the thermal effect of MW radiation.

Acknowledgements

I take this opportunity to appreciate my principal supervisor Professor Mizi Fan for his invaluable guidance, support, and encouragement. I am thankful to him for providing me with this opportunity to work with him in this project. I also wish to express my sincere thanks to Professor Xiangming Zhou, Head of Department of Civil and Environmental Engineering for proving me with the all the facilities required for this research.

Secondly, I am thankful to the senior technician of the Civil and environmental engineering (CEE) department Mr. Neil Macfadyen for the guidance, encouragement and help in the laboratory. I would like to thank the Experimental Technique Centre (ETC) for allowing me to use their facilities throughout this project.

Finally, I would like to wish to express my special gratitude to my beloved mother Christine; and my siblings Joash, Melessa and Jennifer for their moral support, continuous encouragement, and unconditional love through the difficult times they have provided me with which allowed me to complete my PhD project successfully. I dedicate this thesis to them.

Declaration

The work included within this thesis are based on research carried out, in accordance with the requirements of the University's Regulations and Code of Practice for Research Programs, at Brunel University London, United Kingdom (UK). I hereby declare that the research presented in the current thesis is my own work except where otherwise stated, and I confirm that this work has not been submitted for the completion of any other degree.

Table of Contents

VIII

List of Figures

XX

List of Tables

List of Equations

List of Abbreviations

MDI	4,4'-diphenylmethane diisocyanate
MW	Microwave
ATR-FTIR	Attenuated Total Reflectance Fourier Transform Infrared
XRD	X-ray diffraction
DSC	Differential scanning calorimetry
TGA	Thermogravimetric analysis
POM	Polarised Optical microscopy
SEM	Scanning electron microscopy
Mw	Molecular weight
SHS	Sensible heat storage
LHS	Latent heat storage
MF	melamine-formaldehyde
UF	urea-formaldehyde
LDPE-EVA	low-density polyethylene ethylvinylacetate
CNF	carbon nanofibers
SG	sterilised gelatine
AG	arabic gum
AA	Agar-agar
GO	graphene oxide
PLLA	poly(L-lactic acid)
CDA	cellulose diacetate
EP	expanded perlite
EG	expanded graphite
TiO2	titanium dioxide
RD	Raw diatomite
CNT	carbon nanotubes
PVA	poly(vinyl alcohol)

mPEGI	poly(ethylene glycol) monomethyl ether iodide
PGMA	poly(glycidyl methacrylate)
CNC	cellulose nanocrystal
GA	Glutaraldehyde
PGI	Poly(glycerol-itaconic acid)
CMC	carboxymethyl cellulose
EXO	exothermic
CI	crystallinity index
min	minutes
T_m	Melting temperature
T_c	Crystallisation temperature
H_m	Latent heat of melting
H_c	Latent heat of crystallisation
ST	supercooling temperature
T_{onset}	Onset temperature
T_{max}	Maximum temperature
DMF	N,N-Dimethylformamide
DI	deionised
TES	thermal energy storage
SHS	Sensible heat storage
LHS	Latent heat storage
LHTES	Latent heat thermal energy storage
CHS	Chemical heat storage
OH	hydroxyl
COOH	carboxyl
NCO	isocyanate
PCM	Phase Change Material
PEG	Poly(ethylene glycol)
PU	Polyurethane
TCA	Tricarboxylic acid

MCC	microcrystalline cellulose
CF	Cellulose fibre
TDI	Toluene diisocyanate
CA	Citric acid
MDI	4,4'-diphenylmethane diisocyanate

Chapter 1: Introduction

Abstract

This chapter introduces the research background, aims and objectives of current research, and gives an outline of the thesis structure. The gaps in knowledge and motivation are also discussed.

1.1 Research background

The building sector is reported as the highest energy consumers in the world. The international energy agency (IEA) reports that buildings contribute to one-third of the world total energy consumption; therefore, is responsible for more than 38% greenhouse emissions. Energy demand of buildings has grown considerably over the years, and studies predict that it will continue to increase by 50% in 2050 attributed to the rapidly growing and developing society (Nazir et al., 2019; Subin et al., 2021). Therefore, researchers have endeavoured the advancement of building energy performance by implementing Phase Change Material (PCM) technology to make significant energy-saving and decarbonisation in the built environment (Al-Yasiri and Szabó, 2023; Cao et al., 2016). The baseline concept of PCM technology is storing energy in form of latent heat and extracting the stored energy when required. PCMs is widely found in other fields such as thermal energy storage (TES), battery thermal management, electric and power peak regulation, and textiles for the fabrication of smart thermal fibres/ clothing (Hua et al., 2021; Shin et al., 2005).

The building envelope is mainly comprised of building materials including bricks, cement, and concrete, which are all sensible heat storage (SHS) materials of relatively low specific heat capacity (e.g., between 0.75 to 1 kJ/kgK) while paraffin PCMs has a latent heat storage capacity in the range 180 to 230 J/g which means less volume of material will be required to store the same amount of energy (Pomianowski et al., 2013; Trigui et al., 2013). Therefore, integration of PCMs in building energy systems or building envelopes can overcome the existing seasonal mismatch issues, and reduce the total premium fuel consumed by decreasing the heating and cooling loads (Jouhara et al., 2020).

PCMs are usually incorporated directly or in form of encapsulated particles in bricks, wallboards, gypsum boards and concrete slabs, to enhance the thermal mass of the

building materials or components (e.g., ability to accumulate energy) which consequently enhances its energy efficiency (Mousavi et al., 2021; Singh Rathore et al., 2020). The thermal performance of the PCM integrated building material/ component is reported to decrease over time due to the poor shape stability of solid-liquid paraffin PCMs. To overcome this problem PCMs are encapsulated within the chosen polymeric film via physical and chemical encapsulation approaches. However, the encapsulation technology has major drawbacks including requirement of very expensive equipment, and the encapsulation processes are highly complex.

Majority of previous studies has mainly performed investigation on paraffin based PCMs for building applications which are fossil derivatives; and therefore, it is important to reduce its usage by replacing it with alternative PCMs of similar characteristics such as poly(ethylene glycol) (PEG). PEG is an environmentally friendly polymer commonly used other fields such as biomedical, textile and pharmaceutical because it is susceptible to chemical modifications. The major drawback of PEG that limits its potential usage as PCMs is its poor shape stability which cannot be overcome via the encapsulation technology due to its hydrophilic nature. However, previous literature has resolved this problem by employing physical and chemical shape stabilisation approaches like vacuum impregnation and chemical crosslinking reactions.

Vacuum impregnation involves filling the pores of the chosen supporting material with liquid PEG; and therefore, resulting composite PCMs suffer from phase segregation as result of being subjected to repeated heating and cooling cycles which impacts its thermal performance undesirably. Also, majority of the previous studies have showed great interest in using synthetic polymers like PMMA, poly(urea-urethane) and polyamide as supporting material but widening the use of biopolymers like cellulose which is abundantly available at relatively low costs would be beneficial. Moreover, preparing PEG-cellulose composite PCMs for building applications would be ideal since raw materials are environmentally friendly.

1.2 Gap in knowledge

PEG based composite PCMs have been prepared via physical and chemical approaches in the past for thermal energy storage (TES) applications and is yet to be prepared for building applications. The factors impacting the intrinsic phase change properties of PCMs during the shape stabilisation approach is unclear; however, this should be understood very well to produce shape stabilised composite PCMs for building and TES applications.

Crosslinking reaction between PEG and cellulose has been demonstrated in the past via the polyurethane (PU) chemical reaction which relies on the utilisation of toxic crosslinking agents (e.g., crosslinker) including toluene-2,4-diisocyanate (TDI) or methylene diphenyl diisocyanate (MDI) which are both isocyanates based crosslinking agents; and therefore, contains the cyanide functional group. However, it is highly desirable to prepare composite PCMs using non-toxic crosslinking agents like citric acid (CA) (e.g., tricarboxylic acid (TCA) crosslinker) which has widely been used in previous literature to prepare environmentally friendly hydrogels for biomedical applications successfully but is yet to be used for the preparation of PEG-cellulose composite PCMs for TES related applications. Also, the influence of crystallinity which determines the rigidity of the composite PCM on thermal properties must be understood thoroughly to widen the potential use of PEG and to widen their potential use in the building sector. The changes caused to the undesirable 'supercooling behaviour' of PEG after chemical crosslinking reaction needs to be evaluated.

1.3 Project aims and objectives

This project aims at stabilising PEG, a solid-liquid organic PCM using cellulose fibre (CF) and citric acid (CA) through the employment of highly feasible green approaches; thereby, encourage the sustainability of the shape stabilisation technology. Also, to address and solve the major problems of PEG which is its poor shape stability, extremely high operating temperature and supercooling behaviours which must be overcome when considering its use in building construction applications as PCMs.

1.4 Specific objectives

1. Conduct a comprehensive review on phase change materials and approaches employed to overcome the leakage problem for the identification of the most

3

suitable and feasible approach for the synthesis of PEG-cellulose composite PCMs.

2. To investigate and identify the most suitable crosslinking agent and content of crosslinker in wt.% for the stabilisation of PEG with cellulose fibre.

3. Compose and investigate unique formulations for the stabilisation of PEG through chemical crosslinking reactions to determine the influence of chemical composition on the thermal performance of the shape stabilised composite PCMs.

4. Evaluate the influence of TCA crosslinking reaction on the crystalline properties, thermal properties, thermal stability, and crystal morphology of PEG in the TCA crosslinked composite PCMs.

5. Evaluate the impacts of MW irradiation on the thermal and crystalline properties of PEG in the TCA crosslinked composite PCMs.

6. Study the surface morphology to understand the interfacial compatibility between PEG and cellulose which is necessary for the development of composite PCMs of enhanced structural integrity.

1.5 Thesis Outline

This thesis is comprised of 8 Chapters and an outline of each chapter is presented below:

Chapter 1: Introduction

This Chapter gives an overview of PCM technology and attempts made to overcome the major leakage problems of solid-liquid PCMs is discussed. The aims and objects of research are also stated.

Chapter 2: Literature review

This Chapter extensively overviews the state-of-art of PCM technology and the shape stabilisation technology. Mainly to create a database for the preparation of environmentally friendly PEG based composite PCMs via chemical crosslinking.

Chapter 3: Raw materials and methodology

This Chapter explains thoroughly the procedures followed for the preparation of composite PCMs via chemical crosslinking reactions, and the analytical techniques used for the characterisation of raw materials and the corresponding PCMs.

Chapter 4: Characterisation of raw materials

In this Chapter the research materials used for the preparation of the composite PCMs are characterised fully using FTIR, XRD, DSC, TGA, POM and SEM analysis. The information compiled in this Chapter will later be used to study the changes in the intrinsic thermal and crystalline properties of PEG after the chemical crosslinking reactions. The effects of MW radiation exposure on the thermal and crystalline properties of PEG were investigated and evaluated.

Chapter 5: Influence of chemical composition on the thermal properties of PEG in the PU crosslinked composite PCMs

Composite PCMs prepared via the PU crosslinking reaction were characterised using FTIR, XRD and DSC analysis to study the influence of chemical composition on the thermal and crystalline properties of PEG. The PU crosslinked composite PCMs were successfully stabilised; however, they were observed to suffer from serious degradation/ phase segregation problems.

Chapter 6: Development and characterisation of TCA crosslinked composite PCMs

The stabilisation of PEG8000 via TCA crosslinking reaction using CA crosslinker was investigated and PEG-CF-CA crosslinked composite PCMs were developed successfully. The influence of chemical composition on thermal properties and crystalline properties of PEG was investigated and evaluated.

Chapter 7: Synthesis of composite PCMs via the innovative MW radiation assisted TCA crosslinking reaction

MW radiation assisted TCA crosslinking reaction was employed for the synthesis of TCA crosslinked composite PCMs and the influence of MW irradiation on thermal properties and crystalline properties of PEG8000 was studied and evaluated.

Chapter 8: Conclusion and recommended future work

This chapter summarises the findings of the current research, and concludes the established statements made within the current thesis. Recommended work that can be carried out in the future are also outlined.

Chapter 2: Literature review

Abstract

This Chapter comprehensively summarises the different categories of PCMs available in market. The final properties of encapsulated PCMs and composite PCMs resulting from different microencapsulation and shape stabilisation approaches are compared and discussed. A concise review of PEG based composite PCMs resulting from the shape stabilisation technology is included to reveal the benefits of PEG, and its processing techniques. Moreover, the information provided in this Chapter will serve as a useful database for the development of PEG based composite PCMs for building and TES applications. This Chapter aims at meeting specific objective 1 listed in section 1.4.

2.1 Thermal energy storage (TES) technology

The intended purpose of a thermal energy storage (TES) system is to store thermal energy for the utilisation later when required, and it is known to play an important role in meeting the constantly increasing energy demand of the world in a sustainable manner. TES systems usually function by undergoing three fundamental activities: thermal charging (e.g., process by which energy gets absorbed from the surrounding); thermal storing (e.g., storing the absorbed energy); and thermal discharging (e.g., process of extracting the stored energy) (Wei et al., 2013). There are in total three different TES techniques namely thermochemical, sensible heat and latent heat.

2.2 TES through physical processes

Sensible heat storage (SHS) and latent heat storage (LHS) technologies store energy via physical methods; and the heat transfer mechanism results in storing energy either in form of sensible heat or latent heat. The capability of the material to retain the stored energy is dictated by its thermophysical properties (e.g., thermal conductivity).

2.2.1 Sensible Heat Storage (SHS)

Sensible heat storage (SHS) materials absorb, store and release energy by conduction, convection, or radiation (e.g., without undergoing a phase change) when subjected to a temperature change. The change in temperature is directly proportional to the thermal energy stored by the material. Major advantages of SHS technology includes it is simple, easy, and inexpensive; thus, a mature technology with high

reliability ideal for long-term storage, seasonal storage and to conserve primary energy consumption (Li, 2016); however, their undesirable characteristics such as relatively low energy storage density, and loss of stored energy at any temperature prevents their potential application greatly.

There are two types of sensible heat storage materials: (1) solid storage materials; and (2) liquid storage materials. Examples of solid sensible heat storage materials includes metals and non-metals (e.g., concrete, rock, gravel, brick, marble, granite and sandstone rocks, stones, dry and wet earth/soil, iron, wood plasterboard, corkboard etc.); and liquid sensible heat storage materials includes water, oil, molten salt oils, pure and derivatives of alcohols (Ayyappan et al., 2016).

Solid media are commonly used for both low and high temperature storage purposes since their operating temperatures cover a wide range, usually from range 40 to -70 °C for concrete while its over 160 °C for metals. For operations that requires elevated temperatures above 100 °C, molten salts, oils, and liquid metals are commonly used, whereas for other purposes like heating the air, rock-bed type materials are preferable (Lafri et al., 2019). Solid metals are highly suitable for high temperature storage applications, especially when good thermal conductivity is required; however, high cost limits their usage (Tatsidjodoung et al., 2013).

Liquid storage media are preferred for low temperature applications (e.g., temperatures below 100 °C) due to their inherently low energy storage capacity and thermal conductivity. Water is the commonly used liquid media due to its relatively high specific heat capacity, and abundant availability at a relatively low cost (Nazir et al., 2019). Molten salts have desirable thermophysical properties, and therefore can be adopted in various elevated temperature TES applications, provided special measures are taken to prevent corrosion because this will rapidly increase the overall cost of the storage system.

The effectiveness of both solid and liquid SHS materials are dictated by their intrinsic characteristics. Partial factors that determine the quantity of energy stored by the SHS systems includes the quantity of material used, temperature variation and specific heat capacity of material; and may be represented by equation (1) (Cárdenas and León, 2013; Sharma et al., 2009).

$$Q = \int_{T_i}^{T_f} mC_p dT = mC_p(T_f - T_i) \tag{1}$$

Where Q= quantity of energy stored (J); m= mass of storage material (g); C_p = specific heat capacity of storage material at constant pressure (Jg^{-1}K^{-1}); T_f = final temperature (K); T_i = initial temperature (K).

2.2.2 Latent Heat Storage (LHS)

Latent heat storage (LHS) systems utilise 'Phase Change Materials' (PCMs), which can be defined as a class of materials capable of absorbing, storing, and releasing thermal energy by undergoing a phase change as its operating temperature under isothermal conditions. In PCMs, the thermal energy is accumulated at the molecular level which consequently results in phase transformations taking place attributed to its molecules gaining internal energy. Major advantages of PCMs are that they consist of a singular storage capacity with small temperature intervals, and they experience small volume changes (e.g., less than 10%) during the phase transition process (Elias and Stathopoulos, 2019), with negligible pressure change; therefore, can implemented in buildings for thermal management purposes.

PCMs are classified based on the physical transformation they experience during the phase transition process. The following forms of phase change are possible:

(1) from solid to solid (solid-solid); (2) from solid to liquid (solid-liquid); (3) from solid to gas (solid-gas); and (4) from liquid to gas (liquid-gas)

In solid-solid PCMs thermal energy is stored by the material when it experiences a phase change from crystalline phase to amorphous phase vice versa (Salunkhe and Shembekar, 2012). Compared to solid-liquid PCMs, they have lower latent heat capacities which is attributed to the insignificant volume changes they experience during phase change. Therefore, solid-liquid PCMs are the conventionally investigated PCM because it can store and release a significant amount of thermal energy over a narrow temperature range. Solid-gas and liquid-gas PCMs both present higher latent heat capacities attributed to the significant volume changes they experience during the phase transition process (e.g., a gaseous phase is involved). This makes them

impractical for any application due the requirement of more stringent containers attributed to the generation of high vapor pressure.

The storage capacity of a LHS system may be represented by equations (2) and (3) (Cárdenas and León, 2013). The main intrinsic characteristics of materials making them attractive in TES applications is their ability to provide high energy storage density and capability of storing thermal energy under isothermal conditions (e.g., constant temperature) (Sharma et al., 2009).

$$Q = \int_{T_i}^{T_m} mC_p dT + ma_m \Delta h_m + \int_{T_m}^{T_f} mC_p dT \qquad (2)$$

$$Q = m\left[C_{sp}(T_m - T_i) + a_m \Delta h_m + C_{lp}(T_f - T_m)\right] \qquad (3)$$

Where Q= quantity of energy stored (J); m= mass of storage material (kg); C_p= specific heat (J/kgK); C_{sp}= average specific heat between T_i and T_m (J/kgK); C_{lp}= average specific heat between T_m and T_f (J/kgK); a_m= fraction melted; Δh_m= heat of fusion per unit mass (J/kg).

2.3 TES through chemical processes

2.3.1 Chemical Heat Storage (CHS)
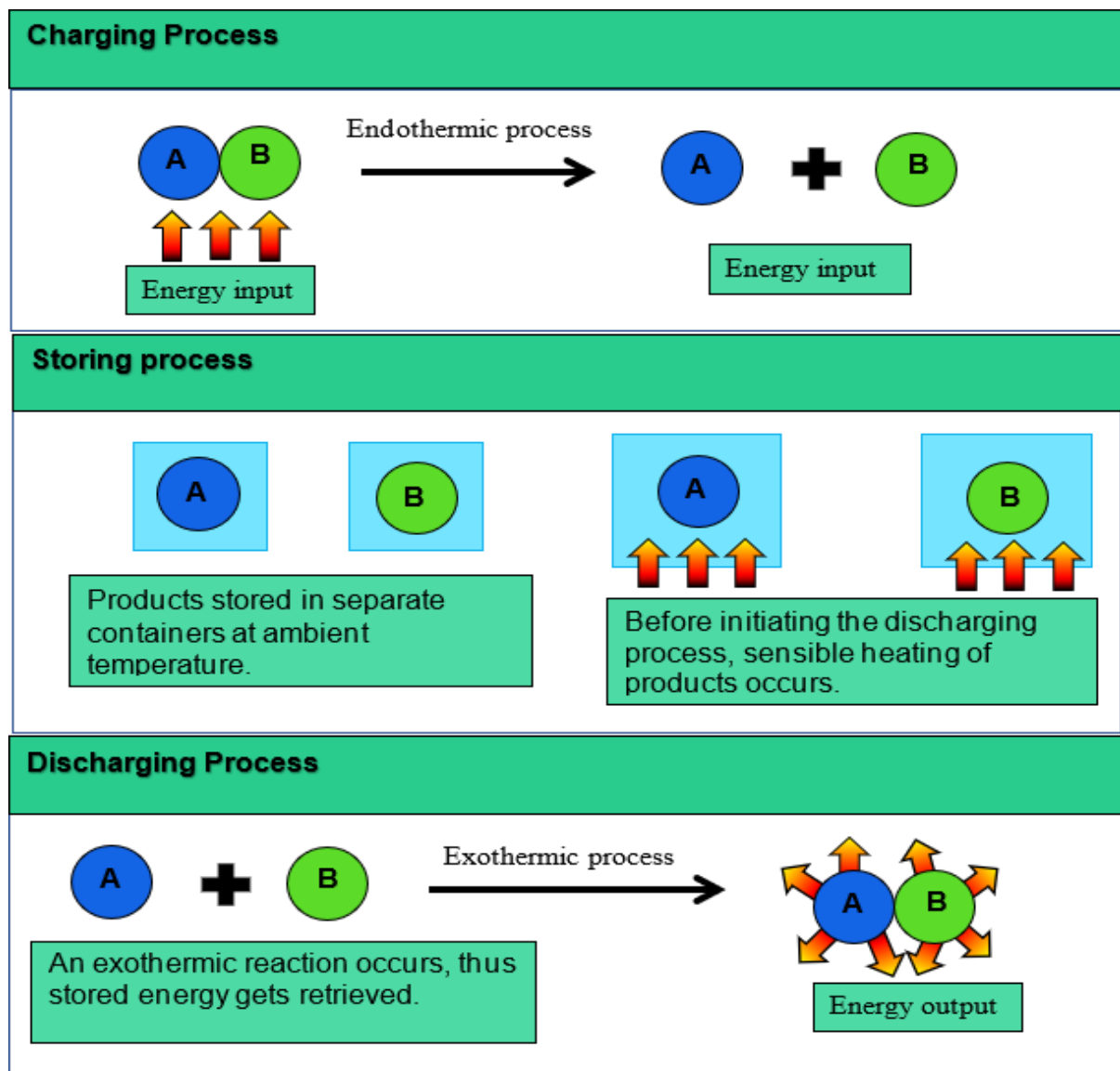
Figure 2. 1 Schematic representation of charging, storing, and discharging process of the thermochemical storage system.

The principle of chemical energy storage (e.g., thermochemical energy storage) is based on initiating a reversible chemical reaction (e.g., forward, and backward reactions occur simultaneously) using an energy source; and depending upon the reaction mechanism involved they can be classified as chemical energy storage with or without sorption (Fang et al., 2009). Sorption storage process comprises of absorption and adsorption. In the adsorption process, gas molecules combine with the surface of a solid material via forming bonds, so no new material gets formed, while in the absorption process a new compound gets produced. The heat stored by the system depends mainly upon the amount of storage material used, the endothermic

heat of reaction and the extent of conversion. The major operation of the thermochemical energy storage system is charging, storing, and discharging as shown in Figure 2.1.

The charging process involves extracting energy from the surrounding; therefore, it is an endothermic reaction (Sunku Prasad et al., 2019). The energy absorbed by the compound will be used to decompose the chemical reactants into products (e.g., exothermic process). The sensible heat contained in the products will be recovered in a heat exchanger. The products formed will be separated and stored in individual containers by sealing the connection during the storing period at ambient temperature until the requirement of energy extraction from the system (e.g., discharging). The stored heat can only be kept for a long time if the products of reaction are stored separately. Provided the sensible heat effect is negligible compared to the heat of reaction, no heat loss is likely to occur. Before initiating the discharging process, the products are preheated to reach the reaction temperature. Afterwards the products are combined via an exothermic reaction to retrieve the reactants. Energy will be released during the discharging process.

Desirable characteristics of thermochemical energy storage materials includes high reaction enthalpy, rapid reaction kinetics, high thermal conductivity, good cyclic stability, abundant availability and non-toxic with no side reactions (Li et al., 2022). Thermochemical energy storage is considered as the most viable and effective technology, especially for long-duration thermal energy storage and transport. However, its potential application is limited attributed to the fact that this technology is still in an infant stage; and therefore, several questions in terms of its cyclic stability and ease of its integration with concentration solar power remains unanswered (Mehrpooya and Pakzad, 2020; Prieto et al., 2016).

2.4 Characteristics of the TES techniques

Physical heat transfer approaches like SHS and LHS can store energy; and the capability of both systems to store the absorbed energy depends mainly upon its thermophysical properties (Yu et al., 2021). LHS systems are more advantageous than SHS systems since the latter has lower storage capacity; and therefore, requires more space (Oliver, 2012). Characteristics of different storage mechanisms are summarised in Table 2.1.

12

Table 2. 1 Summary of the properties of the different storage techniques.

Technique name	Sensible heat storage	Latent heat storage	Chemical heat storage	References
Storage media	Solid: gravel, metal, soil, ceramic materials Liquid: water, alcohol and their derivatives, oil	Solid-liquid PCMs Solid-solid PCMs	Metal chlorides, Metal hydrides, Metal Oxides	(Elias and Stathopoulos, 2019; Jouhara et al., 2020)
Type	Water-based system e.g., water tank and aquifer	Active storage	Thermal sorption	(Xu et al., 2014)
	Rock or ground-based system	Passive storage	Reversible reaction	
Advantages	Environmentally friendly and cheap materials are used.	High energy storage density	High energy storage density	(Jouhara et al., 2020; Xu et al., 2014)
	Simplest technology	PCMs have high latent heat storage capacity	Negligible heat loss	
	Reliable			
Disadvantages	Low energy density	Poor thermal stability	Poor heat transfer	(Elias and Stathopoulos, 2019; Jouhara et al., 2020)
	Experiences self-discharge at any temperature		Poor mass transfer	
	High site construction cost	Low thermal conductivity	Unsure cyclability	
			High material cost	

2.5 Phase Change Materials (PCMs)

Phase change materials (PCMs) are a group of functional materials that supports the same purpose as the function of temperature with intrinsic capability of absorbing, storing, and releasing thermal energy in form of latent heat (Mondal, 2008; Souayfane et al., 2016), at their operating temperatures under isothermal conditions. In general, PCMs are distinguished according to the phase change they experience during the phase transition process; and thus, are classified based on their physical transformation of absorbing/storing or releasing thermal energy capabilities, as result of undergoing designated phase transformations from one state to another (e.g., solid to liquid or liquid to gas vice versa) at their operating temperatures (Kee et al., 2018).

PCMs have played a vital role over the last few decades in efficient latent heat storage applications, as advanced latent heat thermal energy storage (LHTES) materials (Milián et al., 2017). Hence, they are incorporated in TES systems to store energy efficiently (Eanest Jebasingh and Valan Arasu, 2020). Technically, they can store 5-14 times more thermal energy per unit volume than conventional SHS materials like rock, masonry, or water (Yang and Cai, 2019). Thus, PCMs have high storage densities; and therefore, more compact energy storage systems can be designed and constructed (Pomianowski et al., 2013).

Moreover, the availability of PCMs in a wide range of phase transition temperatures makes them suitable for an unlimited number of real-world applications including (1) developing smart thermal microgrids; (2) portable thermal batteries; (3) indoor thermal management systems; (4) thermoregulating textiles, (5) warm supplies thermal protection; (6) in solar-driven cookers, (7) in solar heating systems; (8) water heaters; (9) refrigerators; (10) air-conditioning; (11) for cooling; (12) for the enhancement of thermal comfort in buildings; (13) thermal performance of building materials; (14) for the fabrication of energy-saving equipment, (15) in healthcare; and (16) food preservation (Ng et al., 2017; Umair et al., 2019).

Recently, the principle of PCM is being exploited and developed in building energy conservation systems and in solar heating, mainly to enhance their energy efficiency (Fabiani et al., 2020; Saafi and Daouas, 2019). The suitable working temperature ranges of PCMs for building applications is 19-26°C (Kahraman et al., 2018). Employing PCM technology in buildings will lower the heating and cooling loads by

reducing the heat transferred through the building envelope; thereby, the indoor temperature will be maintained within the thermal comfort range of occupants by reducing temperature swings and consequently, energy consumption of buildings will be reduced drastically (Souayfane et al., 2016). However, the thermal performance of PCMs integrated in the building envelope is dictated by its intrinsic characteristics including its phase transition temperature, thermal conductivity, and thermal energy storage density (Kasaeian et al., 2017). When designing heat storage systems, other factors including the cost, safety, material availability and processes involved should also be considered (Deng and Yang, 2017).

PCM integration methods reported in previous literature includes direct incorporation, immersion, shape-stabilisation, and encapsulation (e.g., nano-, micro- and macro-encapsulation) (Berardi and Gallardo, 2019); however, the macro-encapsulation approach has not proven to be practical in the past (L. Liu et al., 2019). Direct incorporation of PCM is the most practical approach available which involves impregnation of liquid PCM into the pores of the chosen construction material like gypsum boards (Park et al., 2019), concrete blocks or bricks (L. Liu et al., 2017). This leads to the production of PCM integrated building materials susceptible to phase segregation (Pasupathy et al., 2008). Overall, PCMs have two major drawbacks including their inherently low thermal conductivity and leakage problem which tends to limit their potential application. The leakage problem is the most serious one because it undesirably suppresses the potential practical application of solid-liquid PCMs in building applications. Fortunately, it can be overcome by employing either the encapsulation or shape stabilisation technology.

2.5.1 PCM working mechanism

Figure 2.2 illustrates the working mechanism of solid-liquid PCMs under isothermal conditions. Heating the solid PCM, results in its internal molecules gaining energy (e.g., temperature increases) until the phase transition temperature (e.g., melting point) of the PCM is reached. Eventually, the T_m of PCM is reached, and at this instant the temperature of the PCM stops increasing. The supplied energy will now be used by the PCM to undergo a phase change from solid to liquid (e.g., melting process) under isothermal conditions (e.g., constant temperature). As result, the PCM will start to absorb and store energy from the surrounding in form of latent heat. This will subsequently induce a 'cooling effect' which can be used to prevent overheating during summer. The melting process is complete once the solid phase has been converted into a liquid phase.

Continuous supply of energy results in increasing the temperature further; and thus, vaporisation point will be reached, and similar processes that occurred in first phase change is repeated. The cooling (e.g., crystallisation) process is very similar to the melting process, making it possible for the extraction of latent heat at a constant temperature. In the crystallisation process (e.g., solidification) the thermal energy stored within the PCM will be released to the surrounding which consequently induces a warming effect, and thereby can prevent cooling during winter. Overall, the indoor
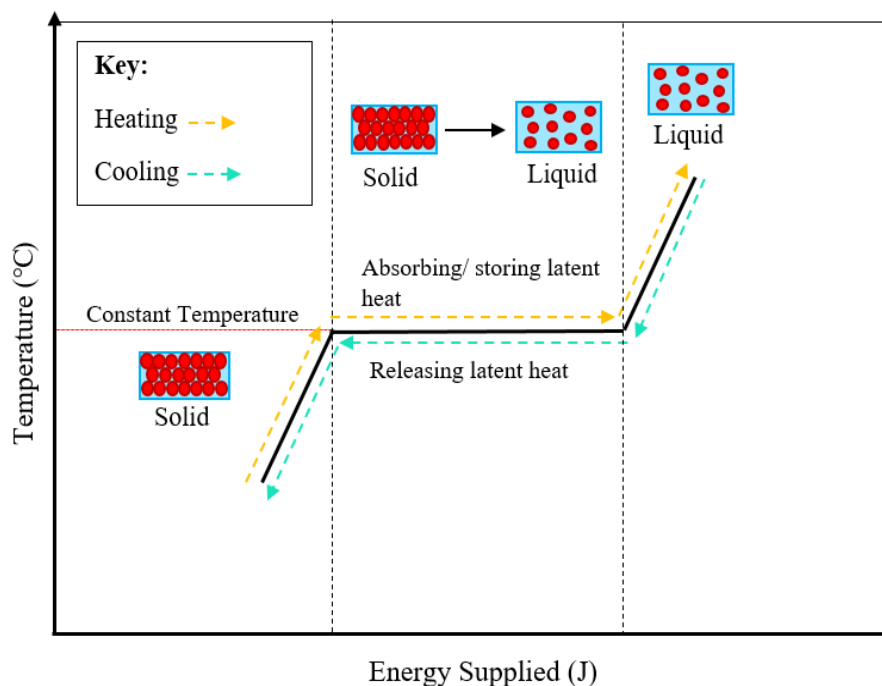
Figure 2. 2 The phase change mechanism of solid-liquid PCMs.

conditions of buildings integrated with PCM will be enhanced greatly which results in reducing the heating and cooling loads.

2.5.2 Classification of PCMs

PCMs used for latent heat thermal energy storage (LHTES) can be classified into four states according to the phase change mechanism they are subjected to and the phase transition temperature: (1) solid-solid (S-S) (e.g. metal based PCMs); (2) solid-liquid (S-L) (e.g., paraffin and PEG); (3) solid-gas (S-G) (e.g., non-existent); and (4) liquid-gas (L-G) (e.g., non-existent).

For practical purposes, solid-liquid PCMs are commonly used because other varieties such solid-solid PCMs have very low latent heat capacities. Solid-solid PCMs have the advantage of experiencing no liquid leakage during phase change which will subsequently reduce its overall cost; however, its major drawback (e.g., low latent heat capacity) suppresses its potential use (Fallahi et al., 2017). Technically, solid-gas and liquid-gas has the highest latent heat capacity of all attributed to the large volume changes that occur during phase change. However, they are impractical due to major technical limitations such as experiences large volume changes during the phase transition process which generates significant vapor pressure (e.g., equilibrium pressure of vapor above its solid, liquid, or gaseous phase); therefore, were never discussed in literature (Entrop et al., 2016). Despite having a wide variety of PCMs with different melting temperature ranges available in market, solid-liquid PCMs is the most used one in previous literature (Su et al., 2015); and can be categorised into three types namely as (1) Organic; (2) Inorganic; and (3) Eutectic mixtures (see Figure 2.3). The advantages and disadvantages of organic, inorganic, and eutectic mixtures PCMs are summarised in Table 2.2; and thus, they lead to various processing, formulations, and end-user requirements. Compiled results from previous literature suggests that organic PCMs are more desirable than inorganic and eutectic mixture PCMs.
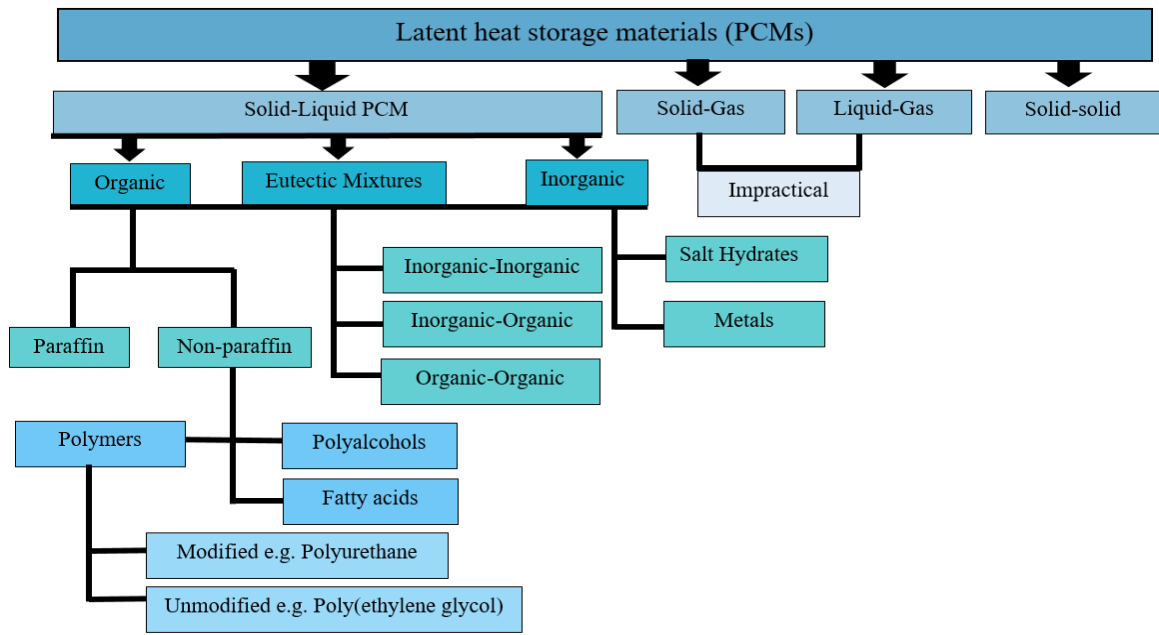
Figure 2. 3 Classification of Phase Change Materials (PCMs)

Table 2. 2 The advantages and disadvantages of Organic, Inorganic and Eutectic Mixtures PCMs.

PCM class	Advantages	Disadvantages	References
Organic	High latent heat capacity	Low thermal conductivity	(Amaral et al., 2017; Huang et al., 2017; Silva et al., 2016; Wahid et al., 2017)
	No supercooling behaviour	Expensive	
	No phase segregation	High flammability	
	No toxicity	High volatility	
	High corrosion resistance		
	Available in wide range of T_m		
	Low vapor pressure		
	High thermal stability		
	Congruent melting		
Inorganic	High latent heat capacity	Prone to corrosion	(Amaral et al., 2017; Silva et al., 2016; Wahid et al., 2017)
	High thermal conductivity	Supercooling behaviour	
	Low cost	Phase segregation	
	Non-flammable	Poor thermal stability	
		Incongruent melting	
		Poor nucleating properties	
		Available in low temperature range	
Eutectic mixtures	Sharp melting points	Supercooling behaviour	(Amaral et al., 2017; Silva et al., 2016; Wahid et al., 2017)
	High volumetric storage density	Low latent heat capacity	

	No phase segregation	Strong odours	
	Congruent melting	High cost	

2.5.3 Principal selection criteria of PCMs

The selection procedure of PCM is reported as a highly complex and time-consuming process because unlimited number of PCMs are available in market; and new PCMs are being developed continuously. When selecting a PCM for the intended application key parameters including availability, cost, product safety, adaptability, and reliability are initially considered. Thereafter, the principal characteristics of the PCMs are studied well before making the final decision since they have a major impact on their final performance. In general, PCMs are expected to have desirable thermal, physical, chemical, and kinetic properties since they impact their thermal performance greatly (Vadhera et al., 2018). The important criteria which should be considered when selecting a PCM for building applications are listed and explained below:

2.5.3.1 Physical criteria

➢ Should experience small volume changes during the phase transition process to avoid containment problems because large volume changes generate very high vapor pressure.

➢ Should have high storage density so that compact energy storage systems can be designed; thereby, less material will be used.

2.5.3.2 Chemical criteria

➢ Should have good chemical stability; thus, experience no decomposition because this impacts its durability.

➢ Should be non-corrosive for enhanced durability.

➢ Should be non-flammable and non-explosive for safety reasons.

➢ Should have good insulating properties since this will prevent short circuit if leakage occurs.

➢ Should have good compatibility with the chosen building material; otherwise, it is likely to experience phase segregation problems over time which affects its durability significantly.

2.5.3.3 Thermal criteria

➢ Should have a phase transition temperature within the operating temperature of building applications. The defined human comport level is between 23 and 27 °C in summertime; and therefore, the melting temperature of PCM should be between 19 and 24 °C (Sari et al., 2015). For sufficient heat transfer, the temperature

difference between air temperature and the melting temperature of PCM can be within the range of 3 to 5 °C (Butala and Stritih, 2009).

➢ Should have a high latent heat capacity to ensure the attainment of a compact heat storage system with good heat transfer capabilities.

➢ Should have a high thermal conductivity value to ensure that charging and discharging occurs at an adequate rate; otherwise, it will be too slow.

2.5.3.4 Kinetic criteria

➢ Should show no supercooling behaviour since this will cause energy extraction problems. Hence, the PCM will solidify at a lower temperature than its normal solidification point; and therefore, stored energy cannot be extracted fully. However, supercooling temperature in the range 5 to 10 °C will not lead to extraction issues.

➢ Should have a suitable crystallisation rate which can be defined as the time taken for the formation of crystals during the crystallisation process.

2.5.3.5 Economic criteria

➢ Should be available abundantly (e.g., large-scale availability)

➢ Should be available at a relatively low cost.

Table 2.3 summarises the ideal intrinsic characteristics a PCM is expected to exhibit to perform exceptionally in building applications; however, none of the PCMs available in market will exhibit all these merits.

Table 2. 3 Summarises the required desirable characteristics of PCMs.

Characteristics	Criteria	Reference
Physical properties	High density	(Amaral et al., 2017; Wahid et al., 2017)
	No supercooling behaviour	
	Low vapor pressure	
	No phase segregation	
	Low volume change	
Chemical properties	High chemical stability	
	Good compatibility with building materials	
	Non-toxic	
	Non-corrosive	
	Non-explosive	
Thermal properties	Suitable phase transition temperature	
	High latent heat capacity	
	High thermal conductivity	
	High specific heat capacity	
Kinetic properties	No supercooling behaviour	
	High crystallisation rate	
Economic properties	Abundant availability	
	Low cost	

2.5.4 Solid-liquid PCMs

Solid-liquid PCMs are materials that experience a phase change between liquid and solid states at their operating temperature. Phase transition occurs because its molecules have gained internal energy which results in breaking its supramolecular bonds. As result, highly ordered molecular arrangement gets converted into an irregularly ordered arrangement (e.g., solid to liquid state). As temperature falls below the crystallisation point, the nucleation process initiates (e.g., solidification/ crystallisation), whereby the molecules are re-arranged to form a crystalline lattice with regularly arranged molecules. In general, these phase changes are accompanied by volume changes. As PCM converts from solid to liquid state its volume will increase.

Vast number of solid-liquid PCMs have been prepared in the past to develop highly effective storage systems at low costs. However, this has not been possible yet since solid-liquid PCMs have poor shape-stability; and therefore, faces leakage problem. However, can be overcome by employing the encapsulation technology which tends to increase the overall cost slightly. In addition, they face other operational problems such as supercooling and corrosion (Bayon et al., 2019). Figure 2.4 illustrates the concept of how a solid-liquid PCM works during daytime and night to induce a cooling and warming effect to the surrounding environment to enhance the thermal comfort of indoor environment of buildings.
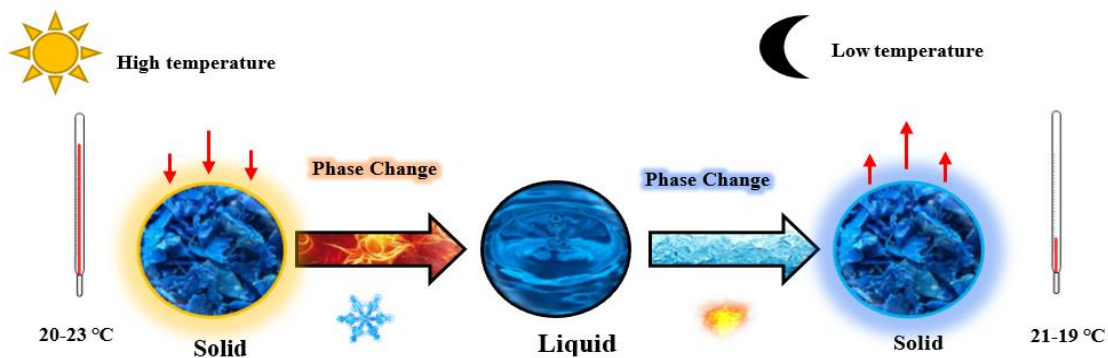
Figure 2. 4 Schematic representation of how solid-liquid PCMs function during day and night.

2.5.5 Organic solid-liquid PCMs

Paraffins and non-paraffins are two types of organic PCMs available. Paraffins are comprised of saturated linear and branched hydrocarbon chains while examples of non-paraffins includes fatty acids, fatty acid esters, polymers and polyalcohols. They can undergo congruent melting over many thermal cycles without experiencing phase segregation and supercooling. Paraffins are derivatives of fossils while non-paraffins are petroleum-free. Thus, non-paraffins are better than paraffins because they are stable, non-flammable and have good compatibility with building materials.

2.5.5.1 Paraffins

Organic paraffins or paraffin waxes are derivatives of fossils (e.g., hydrocarbons), and are usually found in natural gas, petroleum or can be produced synthetically from coal. They are comprised of straight propane chain (e.g., chain contains three carbon atoms) and other short chain hydrocarbon molecules (e.g., volatile compounds). The molecular formula of paraffins can be determined using the general formula C_nH_{2n+2}, where n represents the number of carbon atoms in the compound.

The melting temperature of paraffin is a function of the number of carbon atoms in the chain. Increasing the number of carbon atoms in the chain results in increasing its melting temperature because numerous intermolecular forces of attraction exist between the chain which needs to be overcome to break the long chains. Alkane mixtures which exist as wax-like solids at room temperature are preferred for most applications because they contain high number of carbon atoms usually in the range $20 \leq n \leq 40$. The latent heat capacity of paraffin is dictated by the ability of its alkyl chain (e.g., methyl chain) to crystalise (e.g., form crystals) because this process is responsible for releasing energy in form of latent heat during the crystallisation process.

Paraffins and their waxes with melting temperature in the range -12 to 71 °C, corresponding to a latent heat storage capacity in the range 128 kJ/kg to 198 kJ/kg (Akeiber et al., 2016), have been studied for commercialisation purposes. Blends are more commonly used over pure paraffins due to their lower costs; and also, because their transition temperatures can be tailored easily for a given application by mixing alkanes of different chain lengths together.

The thermal reliability of paraffins influence their long-term durability. In general, the thermal reliability of paraffins and paraffin waxes are dictated by their specific gravity (e.g., density of paraffin relative to the density of water); hence, they will have good thermal reliability if their specific gravity is low (Sarier and Onder, 2012). Paraffins are soft waxes; and therefore, will not generate large expansion forces. Hence, low vapor pressure will therefore be generated during the phase transition process. Hydrophobic nature (e.g., remains insoluble in water and solvents) of paraffins makes them suitable for physical and chemical encapsulation processes (Arpagaus et al., 2018; Onder et al., 2007). Exposing them to elevated temperatures causes evaporation of short chain hydrocarbon molecules as result of paraffin bond breakage.

2.5.5.2 Non-paraffins

Non-paraffin PCMs, namely fatty acids and fatty acid esters, are the most numerous PCMs existing with highly varied properties, unlike the different paraffin and paraffin waxes that exhibits very similar properties. The general formula $CH_3(CH_2)_{2n}COOH$, where n represents the number of carbon atoms (Shafigh et al., 2018) can be used to determine the molecular formula of non-paraffins. They can maintain long term thermal stability when exposed to elevated temperatures above their melting point because they have lower vapor pressure than paraffins; and therefore, they are thermally more stable and less volatile. Moreover, they are environmentally friendly and non-flammable.

Behzadi and Farid (2014) (Behzadi and Farid, 2014) investigated the potential changes experienced by organic PCMs namely Rubitherm 21 (RT21) (e.g., paraffin) and esters (e.g., non-paraffin) with time when exposed to elevated temperature conditions. Results suggested that paraffin based PCMs had experienced irreversible physical changes, which consequently destructed its intrinsic thermal characteristics. Mainly because paraffin waxes have higher vapor pressure than esters; and therefore, they were observed to experience greater weight loss attributed to the evaporation of its lightweight compounds. Ester mixtures were observed to exhibit good stability since no changes in its mass occurred, and it remained thermally stable throughout the heating period.

Previous literature considers fatty acids like stearic acid, palmitic acid, myristic acid and lauric acids as most promising PCMs for latent heat storage applications because

they have high latent heat capacity, along with major desirable thermal properties including little or no supercooling behaviour, low vapor pressure, good thermal and chemical stability, and shows self-nucleating behaviour (Tang et al., 2016).

Alkan et al. (2008) (Alkan and Sari, 2008) prepared fatty acids/ poly(methyl methacrylate) (PMMA) blends using PMMA, a commercially available acrylic resin, via a simple solution-cast approach, for latent heat thermal energy storage (LHTES) applications. Fatty acids used were stearic acid (SA), palmitic acid (PA), myristic acid (MA), and lauric acid (LA). Results confirmed the presence of strong interaction between the fatty acid and the supporting material (e.g., PMMA).

Palmitic acid (PA) (e.g., fatty acid) is one of the most investigated PCM since it consists of a suitable phase change temperature range for solar passive application (e.g., 58 to 64 °C), along with a high latent capacity usually in the range 190 to 220 J/g (Sari and Karaipekli, 2009). Also, it experiences little or no supercooling effect; and has no corrosion effect on metal construction material; however, its inherently low thermal conductivity tends to limit its potential application. Previous literature has solved this problem in several ways through the utilisation of heat-transfer promoters: (1) using finned configurations; (2) disperse particles of high thermal conductivity; and (3) dispersing metal matrix into the PCM. Hence, these approaches will enhance the thermal conductivity of the chosen PCM; however, it also results in increasing the overall weight and volume of the latent heat thermal energy storage (LHTES) system undesirably.

Number of studies have used porous graphite matrices for the enhancement of thermal conductivity of PCM. Sari et al. (2009) (Sari and Karaipekli, 2009) prepared palmitic acid (PA)/ expanded graphite (EG) composite PCM containing 80 wt.% of PA and 30 wt.% of EG. Results indicated PA and EG had good chemical compatibility; thus, composites had enhanced thermal conductivity of 0.60 W/m·K which was 2.5 times that of pure PA. Fang et al. (2011) (Fang et al., 2011) prepared palmitic acid/silicon dioxide (SiO_2) composites containing melamine which is a well-known non-corrosive flame retardant via the sol-gel method. Resulting composites were reported to have enhanced thermal stability and good fire-retardant property.

Despite having number of advantages such as shown no supercooling behaviour, non-paraffin PCMs have limited usage due to their major drawbacks including material

availability for large-scale production and their high costs. The cost of non-paraffins is approximately 2-2.5 times greater than conventionally used paraffin waxes (Abhat, 1983), and three times that of paraffin PCMs (Shafigh et al., 2018). Moreover, it is impossible to match the phase transition temperature of most fatty acids completely with the operating temperature of the intended application (Ma et al., 2019).

2.5.5.3 PEGs and their derivatives as PCMs

Poly(ethylene glycols) (PEGs) are solid-liquid polymeric PCMs comprised mainly of linear dimethyl ether chains with hydroxyl ending groups. They are defined as polymers with the general formula of $H-(O-CH_2-CH_2)_n-OH$ where n represents the number of oxyethylene repeating monomer units. They are polar substances due to the electronegativity difference between the oxygen and hydrogen atoms of the terminal hydroxyl groups (Wilhelm et al., 2018); and therefore, are miscible with water and other chemical solvents like alcohols, ketones, esters and vice versa (Krieghoff et al., 2021). PEG have number of desirable characteristics such as non-toxicity, good biodegradability, hydrophilicity, and ease of chemical modification. The width to height ratio (e.g., aspect ratio) of PEG particles are dictated by the molecular weight of PEG. PEG with molecular weight less than 600 g/mol are liquids at room temperature (Lucht et al., 2021).

PEG has proven to be suitable in several fields including cosmetics, food, biomedical and many more due to its inert nature (Deng and Yang, 2017). Currently, they are reported as the most versatile environmentally friendly polymeric PCM due to its high latent heat capacity, and availability in a wide range of phase transition temperatures (e.g.,-55 to 100 °C) (Sarı et al., 2018), along with other desirable characteristics including congruent melting, non-toxicity, no super-cooling behaviours, low vapor pressure in the melted state, high corrosion resistance and high chemical stability (Yang et al., 2016).

Melting temperatures of PEG varies with its molecular weight as shown in Table 2.5; therefore, PEG is being investigated for various applications including industrial heat utilisation, electronic device management and protection. In addition, they can be used in both active and passive heating and cooling systems of buildings. Adjustment of melting temperature and heat absorption capacity can be done by the means of mixing

two or more PEG of different molecular weights (Tanpichai et al., 2019; H. Wang et al., 2009).

Table 2. 4 Relationship between Molecular weight of PEG and its phase change properties (Sarier and Onder, 2012).

Molecular weight (g/mol)	T_m (°C)	T_c (°C)	H_m (J/g)
400	3.2	-24	91.4
600	22.2	-7	108.4
1000	32.0	28	149.5
1500	46.5	39	176.3
2000	51.0	35	181.4
3400	56.6	29	174.1
4000	59.7	22	189.7
6000	64.8	33	189.0
10000	66.0	38	189.6
20000	68.7	38	187.8

2.5.6 Inorganic PCMs

Inorganic PCMs includes salt hydrates, alloy of inorganic anhydrous salts with water, metals and alloys. They consist of several remarkable characteristics compared to organic PCMs, such as high latent heat capacity, high thermal conductivity, non-toxicity, and non-flammability. Therefore, they are considered having high potential in several applications including building, concentrated solar plants (CSP) and thermal management of lithium-ion battery.

2.5.6.1 Salt hydrate PCMs

Salt hydrates are usually composed of an alloy of inorganic anhydrous salts, and few water molecules (e.g., H_2O). The general formula $M.nH_2O$ can be used to determine the molecular formula of the different salt hydrates, where n represents the number of water molecules present in the compound. Examples of salt hydrates includes fluoride, chloride, and carbonate salts. Hence, Table 2.5 shows the thermal properties of common salt hydrates. Literature reports that salt hydrates experience changes in in the stoichiometric composition when exposed to elevated temperatures during the

heating process which may be attributed to the loss of water molecules (Kenisarin and Mahkamov, 2016).

The very high energy storage density of salt hydrates (e.g., 350 MJ/m^3) and their relatively low cost makes them suitable for high temperature applications (Farid et al., 2004; Mondal, 2008); however, the major disadvantages of salt hydrates including inherently low thermal conductivity, poor thermal stability, susceptibility to phase segregation, poor corrosion resistance and supercooling behaviours outweighs their advantages (Fashandi and Leung, 2017). Previous studies have reported that microencapsulating salt hydrates is difficult; however, Huang et al. (2013) (Huang et al., 2013) demonstrated the possibility of microencapsulating disodium hydrogen phosphate heptahydrate ($Na_2HPO_4.7H_2O$) via the suspension copolymerisation-solvent volatile method using modified PMMA as the shell material to produce microcapsules of smooth and compact surface with an average diameter in the range 650 to 740 µm.

Table 2. 5 The melting point, latent heat, and supercooling degree of some selected salt hydrates (Beaupere et al., 2018).

PCM name	H$_m$ (J/g)	T$_m$ (°C)	Supercooling degree (K)
Lithium chlrorate trihydrate ($LiClO_3.3H_2O$)	253	281	6.0
Potassium fluoride tetrahydrate ($KF.4H_2O$)	231	291.5	33.0
Calcium nitrate tetrahydrate ($Ca(NO_3)_2.4H_2O$)	153	320	65.0
Sodium thiosulfate pentahydrate ($Na_2S_2O_3.5H_2O$)	201	321	65.0
Tetrasodium diphosphate decahydrate ($Na_4P_2O_7.10H_2O$)	184	343	70.0
Zinc ammonium sulfate hexahydrate (($NH4)_2Zn(SO_4)_2.6H_2O$)	396	222	85.0

2.5.6.2 Metal-based PCMs

Metals and alloys with low melting points have the potential to be used as latent heat energy storage materials. Metals possess number of desirable properties including high thermal conductivity, good electrical conductivity, low vapor pressure, and they undergo small volume changes during the phase transition process. Compared to traditional PCMs both metal and metal alloy PCMs have higher thermal conductivity; therefore, they are suitable for high temperature applications (G. Wang et al., 2019). Examples of metals used as PCMs includes copper (Cu), zinc (Zn), aluminium (Al), magnesium (Mg), silicon (Si) and tin (Sn).

One major drawback limiting the potential application of both metals and metal alloys is their susceptibility to corrosion. This problem can be overcome by employing the encapsulation technology; however, the durability of the encapsulated metal PCMs are reported to decrease after long-term elevated temperature exposures. Tremendous efforts have been made in the past to prepare metal based PCMs via the encapsulation technology. Metal and metal alloy PCMs investigated in the past includes aluminium (Al)-silicon (Si), Al-Si-magnesium (Mg) and Al-Si-copper (Cu) for high temperature applications.

Maruoka et al. (2002) (Maruoka et al., 2002) prepared copper based PCM coated by a nickel film by the electroplating method for high temperature (e.g., T > 1200 K) application. Results suggested that producing a film with a two-layer structure using either carbon or ruthenium was beneficial because it appeared to prevent the formation of solution between copper and nickel (e.g., no reaction occurred to initiate the corrosion process). Wang et al. (2014) (Wang et al., 2014) prepared durable copper (Cu) based PCMs by encapsulating copper within a chromium-nickel bimetallic layer through an innovative approach called electroplating, for high temperature applications. Results demonstrated that the copper capsules experienced no leakage even after being subjected to 1000 charge-discharge cycles which was attributed to the presence of the chromium layer between nickel and copper.

An investigation on copper-magnesium metallic alloys as intermediate/ high temperature PCM was carried out for latent heat storage at concentrated solar power plants (CSP) (Karim et al., 2019). Results suggested that the formation of a corrosive layer was governed by the diffusion of both magnesium and nickel from the base

metal. They reported that this can be abided by selecting a construction material of proper composition (Blanco-Rodríguez et al., 2015). Dindi et al. (2020) used a Boron nitride (BN) based coating material to avoid corrosion of steel containers while preparing Al-Si PCMs (Dindi et al., 2020). Overall, the major drawbacks of metal and metal alloys PCMs includes high cost and poor corrosion resistance which is known to limit their potential application significantly.

2.5.7 Eutectic Mixtures

Eutectic mixtures PCMs are made by mixing two or more PCMs of similar chemical compositions to produce a PCM that solidifies at a lower melting temperature than its constituent PCMs; therefore, eutectic mixture PCMs experiences incongruent melting during the phase transition process. In general, eutectic mixture PCMs can be made by combining an inorganic material with an inorganic material or an organic material with an inorganic material or an organic material with an organic material. The existence of many individual salt species and mixtures means the combination space available for eutectic mixture PCMs is unlimited. Table 2.6 shows the melting point and latent heat capacity of various eutectic mixture PCMs investigated in previous literature.

Major advantage of eutectic mixture PCMs is that their melting points can easily be adjusted by combining different weight percentages of components, which means for every temperature range several potential eutectic PCM mixtures can be obtained which encourages optimal selection for the intended application. For instance, tetradecane with melting temperature in the range 1.5-5.6 °C can be obtained by combining octadecane, docasane and hexadecane (Su et al., 2015). Moreover, eutectic mixtures have other desirable characteristics such as high thermal conductivity, density and experiences no segregation and supercooling effect; however, their specific heat capacity is smaller than the ones of salt hydrates and paraffin which limits their potential application.

Table 2. 6 Combination of eutectic mixtures used in previous studies (Akeiber et al., 2016).

PCM/ material combination	T_m (°C)	H_m (J/g)
Capric/ lauric acid	21.0	143.0
Capric/ myrstic	21.4	152.0
Capric/ palmitate	22.1	153.0
Mehyl stearate/ cetyl stearate	22.2	180.0
Capric acid/ myristic acid	22.6	154.8
Methyl stearate/ methyl palmitate	23.9	220.0
$C_{14}H_{28}O_2$/ $C_{10}H_{20}O_2$	24.0	147.7
$C_{14}H_{28}O_2$/ $C_{10}H_{20}O_2$	24.0	147.7
Tetradodecanol/ lauric acid	24.5	90.0
Capric acid/ stearic acid	24.7	178.6
$CaCl_2$/ $MgCl_2 \cdot 6H_2O$	25.0	95.0
$CaCl_2 \cdot 6H_2O$/ nucleat/ $MgCl_2 \cdot 6H_2O$	25.0	127.0
Capric/ stearate	26.8	160.0
CH_3CONH_2/ NH_2CONH_2	27.0	163.0
Methyl stearate/ cetyl palmitate	28.2	189.0
Triethylolethane/ urea	29.8	218.0
$Ca(NO_3) \cdot 4H_2O$/ $Mg(NO_3)_3 \cdot 6H_2O$	30.0	136.0
$CH_3COONa \cdot 3H_2O$/NH_2CONH_2	30.0	200.5
$CaCl_2$/ NaCl/ KCl/ H_2O	26-28	188.0

2.6 Shape stabilisation of solid-liquid PCMs

Two main shortcomings that limits the potential application of solid-liquid PCMs includes the leakage problem and their inherently low thermal conductivity. Previous studies have demonstrated the possibility of overcoming these issues through the implementation of the encapsulation technology and shape stabilisation technology.

2.6.1 Encapsulation technology
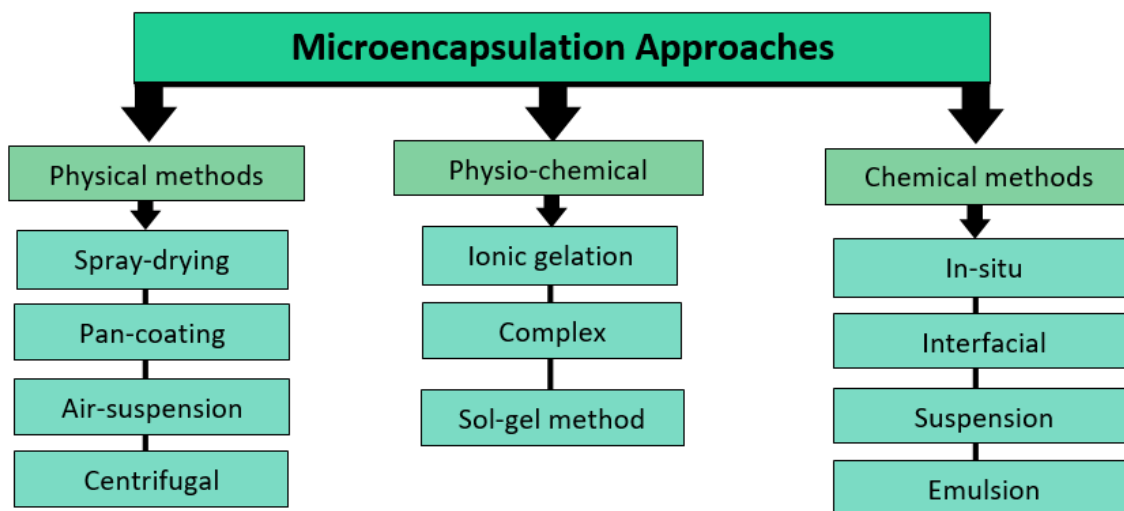
Figure 2. 5 Shows the different encapsulation methods available.

The encapsulation technology was first introduced in the 1940s and 1950s by BK Green to overcome the leakage problem of solid-liquid PCMs (Madene and Jacquot, 2006); and it can be defined as a process by which a PCM core comprised of one or more compounds gets surrounded by a polymeric film composed by one or more material regarded as the supporting material which results in the formation of a core-shell structure, mainly to isolate and protect the PCM core from the surrounding (Comunian and Favaro-Trindade, 2016; Huo et al., 2018). The different encapsulation approaches available for the synthesis of encapsulated particles are illustrated schematically in Figure 2.5.

Capsules resulting from the different encapsulation approaches are classified according to their size, namely as nanocapsules, microcapsules and macrocapsules as shown in Figure 2.6 (Chen et al., 2018; Z. Liu et al., 2018; Magdalena et al., 2018; Zangabad et al., 2018). The size of capsules produced depends entirely upon the synthesis approach employed and the type of shell material used (Chanda and Bajwa,

36

2021; Jamekhorshid et al., 2014; Martins et al., 2014; Tyagi et al., 2011). In general, capsules of reduced particle size are more advantageous since they have better structural stability and enhanced fracture resistance (J. Li et al., 2018).

Key: **d =** diameter of capsule

Nanocapsule	Microcapsule	Macrocapsule
0 nm < d < 1000nm	d < 1mm	d > 1cm
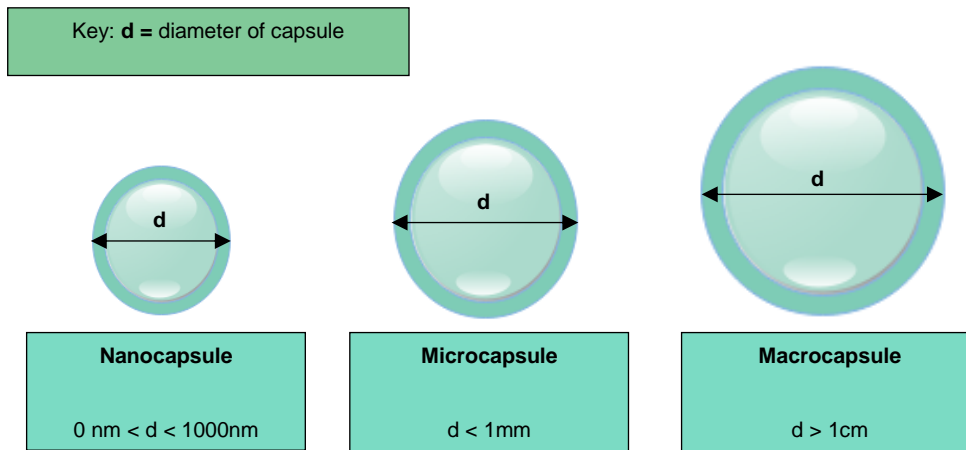
Figure 2. 6 The appearance of a typical capsule and its classification according to its size.

The encapsulation technology has evolved further in the recent times; and thus, has become the most researched and implemented technology in various fields, including chemistry, biology, and medicine (Huo et al., 2018). Overall, value-added end products can be obtained via this encapsulation technology provided correct design parameters are selected from previous literature. To produce encapsulated PCMs of exceptional performance correct PCM and shell material needs to be selected by following a standard selection procedure (Ng et al., 2017).

2.6.2 Supporting materials for encapsulation

The characteristic and performance of microencapsulated PCMs are influenced significantly by the physical and chemical properties of the supporting material (e.g., shell material). Therefore, selecting the correct shell material is crucial. In general, the three different types of supporting materials used includes organic, inorganic, and organic-inorganic hybrid shell.

Organic shell materials including melamine-formaldehyde (MF) resins, urea-formaldehyde (UF) resin, poly(urea-urethane), polyurea and acrylic resins have been used in previous studies mainly because they offer exceptional structural stability to the microcapsules; thus, resulting microcapsules were found to have good durability even after being subjected to numerous repeated heating and cooling cycles; however, major drawbacks of mentioned shell materials include poor chemical and thermal stability. Acrylic resins (e.g., methacrylate-based copolymers) are considered as the most promising organic supporting material available compared to the others due to the numerous advantageous characteristics they exhibit including non-toxicity, easy handling, high mechanical strength, and good chemical resistance (Lashgari et al., 2018).

In the recent times inorganic support materials like silica, titania, calcium carbonate, polystyrene and zinc oxide have gained more attention due its desirable intrinsic characteristics they possess including relatively high thermal conductivity, enhanced mechanical strength and durability, chemically inert and non-toxic (Alva et al., 2017). Encapsulating organic PCMs like paraffins/ paraffin waxes of high flammability within an inorganic shell material tends to reduce its flammability drastically.

Organic-inorganic shell materials do result in producing microcapsules of improved intrinsic characteristics including superior thermal conductivity, good chemical stability, and mechanical robustness through the superficial attachment of inorganic additives including silver nanoparticles, iron nanoparticles and silicon nitride. Detachment of inorganic additives from the surface of the microcapsule is the major shortcoming of this approach; however, this can be overcome through the employment of the chemical hybridisation approach (Umair et al., 2019).

2.6.3 Physical approaches of encapsulation

The first and one of the oldest physical encapsulation techniques called spray-drying was developed in the 1930s, and since then it has attracted much attention (Methaapanon et al., 2020) attributed to its simplicity, convenience, reproducibility, and scalability (Bhat et al., 2021). The spray-drying method is a well-established approach in the food industry. This method is usually comparable with the 'one stage drying operation' (Arpagaus et al., 2018) and is comprised of simple steps of high feasibility including choosing the drying gas, producing the droplets, drying the droplets, and collecting the isolated microcapsules as shown in Figure 2.7 (Rajabi et al., 2015; Samantha et al., 2015; Sivanathan et al., 2020); however, the spray drying equipment is bulky and expensive.

Hawlader et al. (2003) (Hawlader et al., 2003) encapsulated paraffin-wax within gelatine/ acacia shell material. Observation indicated that the microencapsulation efficiency reduced with increasing core-to-shell ratio; thus, results suggested that sufficient shell material was required for complete encapsulation. Also, incorporating crosslinking agents in the range 6 to 8 ml was observed to enhance the microencapsulation efficiency significantly. Borreguero et al. (2011) (Borreguero et al., 2011) encapsulated paraffin with and without carbon nanofibers (CNFs) within a low-density polyethylene ethylvinylacetate (LDPE-EVA) shell material. Experimental results demonstrated that particles of better size and shape were obtained from the collection vessel; thus, microcapsules collected from the inside of the drying vessel were bound together attributed to the melting of polymer. Fei et al. (2008) (Fei et al., 2008) encapsulated n-octadecane (C18) (e.g., paraffin) within a titania shell material via the rapid aerosol process; and concluded that microcapsules of two structures namely dense and hollow with diameters in the range 0.1 to 5.0 μm were produced successfully.

Step 1: Formation of oil-in-water emulsion
The core and shell material gets stirred until complete dissolution, and this results in the formation of an oil-in-water emulsion.

Step 2: Formation of isolated microcapsules
The emulsion prepared earlier gets sprayed in small droplets, by the means of an atomiser. Placing dispersion in contact with the hot air at relevant temperature results in evaporation of solvent. The solid dried particles produced are then separated by the means of cyclones.

Figure 2. 7 Schematic representation of spray drying method employed for the synthesis of isolated microcapsules (Sivanathan et al., 2020).

Pan-coating method is one of the most widely used approach in the pharmaceutical industry for the synthesis of small, coated capsules through the mixing of coating material with the solid particles followed by melting of coating material then cooling to encourage solidification. This method has not demonstrated the possibility of encapsulating PCM core within a chosen polymeric film. Another unsuitable approach for the synthesis of microencapsulated PCM is called air suspension coating; and this is one of the most used method in the pharmaceutical, food and cosmetic industry.

2.6.4 Physio-chemical approaches of encapsulation

Three physio-chemical approaches available include ionic-gelation, complex coacervation and sol-gel method; however, complex coacervation is the conventionally used approach for the synthesis of microencapsulated PCM. Initiation of complex coacervation occurs through the interaction between oppositely charged polymers. In the first step, the emulsion is prepared by dispersing the chosen core material into an aqueous polymer solution, followed by the addition of second polymer solution and salt to alter the pH temperature. Microcapsules are normally stabilised via crosslinking, desolvation or thermal treatment; and are collected by centrifugation as shown Figure 2.8 (Sivanathan et al., 2020).

Increasing paraffin wax-to-shell mass ratio while encapsulating paraffin wax within a gelatin/gum acacia shell through the complex coacervation approach resulted in enhancing the encapsulation efficiency (Hawlader et al., 2000). Encapsulating paraffin within two different shell materials including sterilised gelatine (SG) and arabic gum (AG) or agar-agar (AA)/arabic gum (AG) resulted in producing encapsulated particles of high encapsulation efficiency ratios (e.g., 49% and 48%) (Bayés-García et al., 2010). Maleikipirbazari at al. (2014) (Malekipirbazari et al., 2014) microencapsulated paraffin wax within a shell material composed of gelatin/ acacia for thermal energy storage (TES) applications. This technique is inexpensive and utilises environmentally friendly solvents only; however, it requires the use of large volume of solvents which is considered as a major drawback limiting its potential use (Rai et al., 2015).
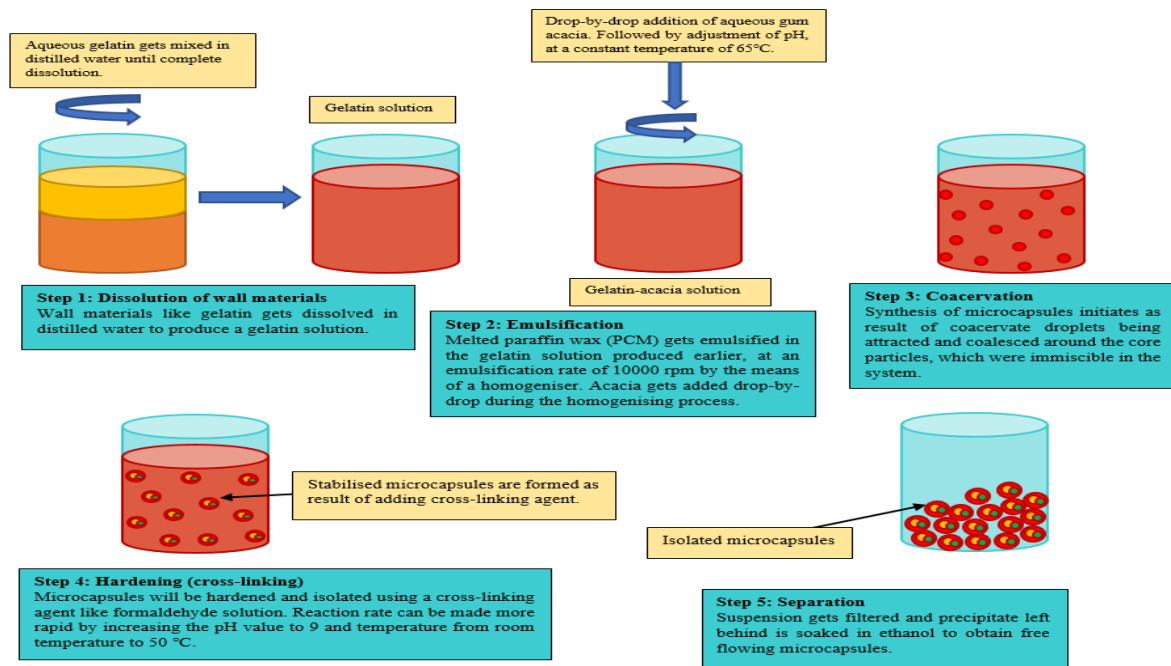
Figure 2. 8 Schematic representation of the fundamental steps involved in a complex coacervation process (Sivanathan et al., 2020).

2.6.5 Chemical approaches of encapsulation

Suspension polymerisation is one of the most used methods by several researchers for the encapsulation of PCMs because it is simple, cheap, robust, and environmentally friendly. In this chemical encapsulation approach, dissolution of polymer monomer into chosen organic phase occurs followed by formation of the oil/water emulsion, and separation and precipitation of monomer molecules from the core material. Hence, the process is governed by multiple simultaneous mechanisms including (1) coalescence of particles followed by break-up, (2) secondary nucleation; and (3) monomer gets diffused towards the interface (Sivanathan et al., 2020). The performance of microencapsulated PCMs prepared in previous literature via the suspension polymerisation approach is summarised in Table 2.7. This suggested that this approach was the commonly used one in practice.

Table 2. 7 Summarises the results from previous studies on encapsulation of PCMs via the different polymerisation approaches.

PCM/ core material	Encapsulation method	Shell material	Properties of microcapsules	Reference
PRS® Paraffin wax	Suspension polymerisation	Polystyrene (PSt)	➢ Particle diameter ~ 30 μm.	(Sánchez et al., 2008)
Paraffin wax	Suspension polymerisation	Styrene (St)and methyl methacrylate (MMA)	➢ Energy storage capacity of 41.65 J/g. ➢ Latent heat per mass (at MMA/ St Proportion of 4) ~ 84.04 J/g. ➢ Enhanced thermal conductivity and mechanical strength.	(Sánchez et al., 2010)
PRS® Paraffin wax	Suspension polymerisation	Styrene (St)	➢ Latent heat ~ 41.65 J/g (lower than pure paraffin). ➢ Optimum melting heat (nonadecane) was 119.80 J/g. ➢ Mean diameter of Rubitherm® R20 was the smallest.	(Sánchez et al., 2007)
Tetradecane	Suspension polymerisation			
Rubitherm® R27	Suspension polymerisation			
Rubitherm® R20	Suspension polymerisation			
Nonadecane	Suspension polymerisation			
Paraffin	Suspension polymerisation	Methyl methacrylate (MMA) and triethoxyvinylsilane (TEVS)	➢ Enhanced thermal stability, thermal conductivity, and heat transfer rate i.e., thermal conductivity was reported to reach an increment of 116%.	(Ng et al., 2017)

			➤ Electrical resistance of PCM greater than 10^{10} Ω/sq.	
n-octadecane	Suspension polymerisation	Styrene (St)-divnylbenzene (DVB)	➤ Thermal decomposition temperature ~ 230 ℃. ➤ N-octadecane content (at monomers/n-octadecane mass ratio 1:1) ~ 56.8 %. ➤ Optimum enthalpy of 57 J/g (at monomers/n-octadecane mass ratio of 5:2). ➤ Average particle size ~71 μm (at stirring rate of 1200 rpm).	(You et al., 2011)
Paraffin wax	Suspension polymerisation	Polystyrene	➤ Average particle size was 4.53 μm. ➤ Average storage capacity (latent heat) was 104.7 J/g.	(Sánchez et al., 2010)
Butyl stearate	Interfacial polymerisation	Polyurea	➤ Heat of fusion ~ 80 J/g. ➤ Melting point ~ 28.7 ℃ ➤ Particle diameter~ 20-35 μm. ➤ Good property of thermal periodicity. ➤ Good thermal stability after subjection to 400 repetitive heating and cooling cycling.	(Liang et al., 2009)
n-octadecane	Interfacial polymerisation	Silica	➤ Particle size 17.0 μm. ➤ Good thermal stability ➤ Enhanced thermal conductivity due to the presence of silica.	(Zhang et al., 2011)

			➤ Optimum thermal conductivity (at core/shell weight ratio of 50/50) ~ 0.6547 $Wm^{-1}K^{-1}$.	
Octadecane	Interfacial polymerisation	Polyurea	➤ Particle size 0.1-1 µm. ➤ Melting point 28-30 °C. ➤ Latent heat of fusion ~62.6-112 J/g. ➤ Heat of crystallization 20.9-22.7 °C.	(Cho et al., 2002)
Paraffin RT21	Interfacial polymerisation	Polyurea (IPDI and EDA as wall monomer)	➤ Mean particle diameter was 2.40 µm. ➤ Latent heat was 92.5 J/g. ➤ Good anti-osmosis property. ➤ Good anti-permeability and high stability.	(Zhan et al., 2016)
n-octadecane	Interfacial polymerisation	Polyurea	➤ Mean particle size 5-20 µm. ➤ Jeffamine based microcapsules exhibited better phase change properties, anti-osmosis property but poorer thermal stabilities.	(Zhang and Wang, 2009a)
Butyl stearate	Interfacial polymerisation	Cross-linked network polyurethane with pentaerythritol used as crosslinking agent.	➤ Diameter of microcapsule in the range 10-35 µm. ➤ Enthalpy was in the range 77-81 J/g. Thus, microcapsules have good latent heat storage performance. ➤ Enhanced thermal stability due to the presence of network polyurethane shell.	(Lu et al., 2018)

Styrene	In-situ polymerisation	Melamine-formaldehyde resin	➤ Particle size was in the range 20-71 µm. ➤ Core material content was ~ 60%.	(Zhang and Wang, 2009b)
n-octadecane	In-situ polymerisation	Melamine-formaldehyde	➤ Average diameter of 2.2 µm. ➤ Average content of 59 wt%. ➤ Latent heat of 144 J/g.	(Li et al., 2007)
n-octadecane	In-situ polymerisation	Melamine-formaldehyde	➤ Average diameter of 9.2 µm at stirring rate of 4000 rpm. ➤ Average content of 70 wt%. ➤ Latent heat of melting 169 J/g.	(Zhang et al., 2004)
n-octadecane	In-situ polymerisation	Urea-melamine-formaldehyde	➤ Average PCM content of 72 wt%. ➤ Latent heat of ~164 J/g. ➤ Average diameter of 0.8 µm.	(Zhang et al., 2005)
n-nonadecane	In-situ polymerisation	Urea-melamine-formaldehyde	➤ Average PCM content of 69 wt%. ➤ Latent heat of ~233 J/g.	
n-eicosane	In-situ polymerisation	Urea-melamine-formaldehyde	➤ Average PCM content of 71 wt%. ➤ Latent heat of ~172 J/g.	

2.6.5 Shape stabilisation technology

Shape stabilisation technology consists of both physical and chemical methods like the microencapsulation technology as shown in Figure 2.9; however, physical impregnation and chemical crosslinking reactions are much simpler, easier and requires no expensive equipment making this technology more feasible.

```
              ┌─────────────────────────────────────┐
              │   Shape Stabilisation Approaches    │
              └─────────────────────────────────────┘
                             │
             ┌───────────────┴───────────────┐
             ▼                               ▼
   ┌──────────────────┐            ┌──────────────────┐
   │ Physical methods │            │ Chemical methods │
   └──────────────────┘            └──────────────────┘
             │                               │
   ┌──────────────────┐            ┌──────────────────┐
   │ Physical blending│            │ Chemical grafting│
   └──────────────────┘            └──────────────────┘
             │                               │
   ┌──────────────────────┐        ┌──────────────────────┐
   │ Impregnation/Adsorption│      │ Chemical cross-linking│
   └──────────────────────┘        └──────────────────────┘
```
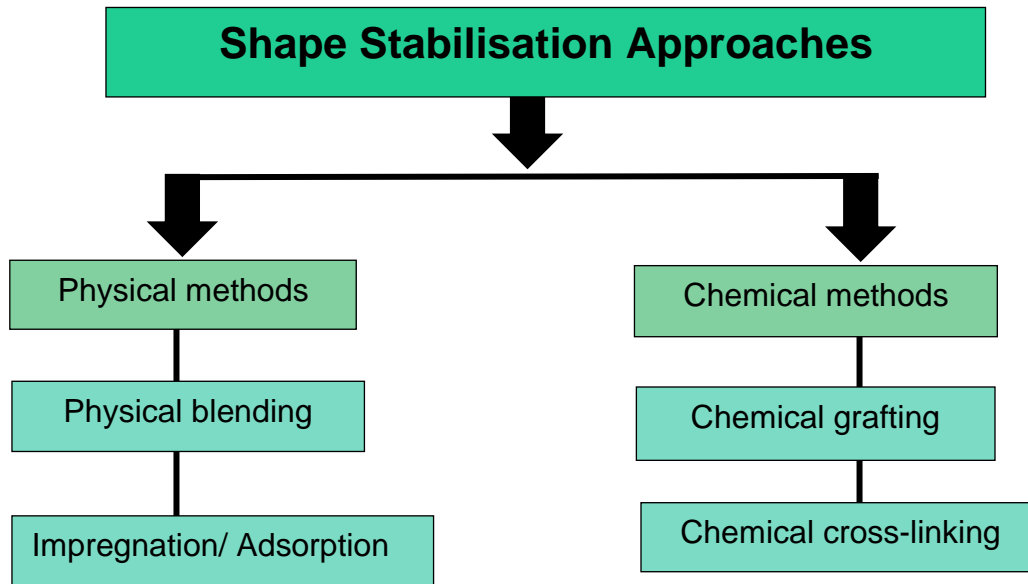
Figure 2. 9 Physical and chemical shape stabilisation approaches of PCMs.

Shape stabilisation process involves the confinement of PCMs such as fatty acids, polyalcohols, poly(ethylene glycol) (PEG) and others (e.g. soft segment) in the chosen polymer matrix (e.g. solid framework which acts as the hard segment). Thereby, the PCM can retain its original solid state during the phase transition process attributed to the force of capillary. A wide range of materials have been used (e.g., polymers, porous and nanomaterials) (Nor Azlan et al., 2021) as the supporting material in the past with a limited number of references discussing about the benefits using biopolymers including cellulose, chitosan and many more as supporting material to promote green chemistry (Ranu et al., 2021). The final product resulting from the shape stabilisation technology is known as a composite PCM (e.g., form stable PCM) PCM is the working substance; and thus, functions by storing or releasing latent heat during the phase transformation process, while the supporting material prevents leakage of PCM during this process; therefore, makes no contribution to latent heat storage (e.g., impurity).

In physical shape stabilisation approaches, composite PCMs are prepared by dispersing the PCM into the polymeric material of higher melting point. Hence, it

47

involves filling in the cavities of the chosen supporting material, usually porous manmade materials like concrete, plasterboards, wallboards, and aerogels with the chosen PCM in liquid state without any chemical reactions taking place. Resulting products are less durable since they are prone to phase segregation mainly because leakage of PCM is prevented by weak physical interactions namely capillary and surface tension forces due to the presence of physical interactions between the functional groups of both PCM and the supporting material (Meints et al., 2018; Strassburg et al., 2020). Chemical methods are preferable over the physical methods since final products have longer durability attributed to the formation of covalent bonds between the functional group of the PCM and the supporting material. In the recent times this technology has become the key interest of many researchers due to the drawbacks of the encapsulation technology including high processing cost, difficulty in choosing and designing the correct materials according to the intended application (Lai et al., 2020). Thus, composite PCMs resulting from shape stabilisation technology tends to exhibit better thermal properties making them suitable for different applications such as thermal management (e.g., in solar heating systems); thermal regulation in dwellings; and in commercial buildings (Wijesena et al., 2020).

Researchers are currently focusing on the utilisation of polymeric solid-solid PCMs due to the numerous advantages including they require no encapsulation, can be processed into arbitrary shape (i.e., desired shape) (C. Chen et al., 2011) and can be incorporated with building materials directly, e.g., in concrete or gypsum without the need of encapsulation (Fallahi et al., 2017). Solid-solid PCMs function by absorbing, storing, and releasing energy with the only difference lying in terms of phase transitions they experience. Hence, during phase change process, particles are likely to change from highly crystalline phase to another phase such as amorphous or semi-crystalline. The well-known drawbacks of solid-solid PCMs are the smaller latent heat capacity and supercooling behaviour. Among the various solid-solid PCMs available, such as polyhydric alcohol (polyalcohol), crosslinked polyethylene, polymers and hydrated inorganic salts are a few of many recently developed functional PCMs. Furthermore, using solid-solid PCMs will reduce preparation steps involved; and thereby cut down the overall cost significantly. Common defects of solid-solid PCMs are high transition temperature, low transition enthalpy and unstable thermal property, which tends to limit their applications greatly. Therefore, researchers have

endeavoured to fabricate novel materials (e.g., polymeric solid-solid PCMs) to overcome these shortcomings, because they consist of excellent integrated performances (Li and Ding, 2007). Hence, shape stabilisation technology is not limited to the preparation of solid-solid PCMs, but it is used to enhance the shape stability of the chosen PCM; thereby, overcoming the leakage problem of solid-liquid PCMs.

Developing materials from natural polymers for different applications is desirable; and thus, has been a hot topic for several years, mainly to avoid the use of petroleum-based materials due to their increasing costs and environmental concerns (Ernest Ravindran et al., 2020). Also, biopolymers are available in abundant quantities. Currently, petroleum based PCMs (e.g., paraffins and paraffin waxes) are commonly used in many sectors; however, it is more desirable to utilise environmentally friendly PCMs in building construction applications since they are available abundantly at relatively low costs.

PEG is used in many other fields including cosmetics, food, biomedical applications, and pharmaceutical industry due to its inert nature; and it is readily soluble in most solvents due to its hydrophilic nature which is the major drawback limiting its application as PCMs; therefore, encapsulation of PEG has not been established till date. One study reported that encapsulation of PEG is impossible based on experimental results obtained (Sánchez et al., 2007). Previous studies have all demonstrated the possibility of overcoming this short coming of PEG through the employment of both physical and chemical shape stabilisation approaches.

2.6.5.1 Supporting materials for shape stabilisation of PCMs

The two major drawbacks of solid-liquid PCMs are their poor shape stability which causes leakage problems during phase change, and their inherently low thermal conductivity. However, they can be overcome by selecting a suitable supporting material. In cases where the leakage problem needs to be overcome, a porous material will be selected as the supporting material but if composite PCM is expected to have improved thermal conductivity, the porous material will be combined with the chosen nanomaterial since such materials have very high thermal conductivity. It is important to ensure that nanomaterial is not incorporated in excess since high contents of nanomaterial will reduce the latent heat capacity of resulting composite PCM.

Vast number of papers have mainly utilised porous materials as supporting material due to the desirable characteristics they exhibit which includes increased surface area, high thermal conductivity, and enhanced chemical compatibility. The interaction existing between PCM and porous materials which arises due to Van der Waals, hydrogen bonds, surface tension and capillary force tend to prevent leakage of PCM. In general, the choice of supporting material used in the shape stabilisation process has great impact on the final properties of the prepared composite PCM. The different types of supporting materials used in previous literature to stabilise the chosen solid-liquid PCM is presented in Table 2.8 with a summary of its intrinsic characteristics (Li et al., 2016; Rathore and Shukla, 2021).

Table 2. 8 Characteristics of supporting materials used the shape stabilisation technology.

Supporting material	Advantages		Disadvantages	Examples
Porous carbon	Available abundantly		Expensive	➢ Tin tetrachloride reacted with sodium polyacrylate to produce porous carbon (Z. Liu et al., 2020). ➢ Eggplant porous carbon (C. Zhang et al., 2021). ➢ Mesoporous N-doped porous carbon (Atinafu et al., 2018).
	Non-toxic			
	Low density		Complex preparation protocol	
	Good capillarity			
Graphite	High thermal conductivity		Expensive	➢ Expanded graphite
	High porosity			
	Good thermal stability		Complex preparation protocol	
	Low density			
	Non-flammable			
Polyurethane	Good insulator		High flammability	➢ Polyurethane foam resulting from the crosslinking reaction
	Light weight			
	Good corrosion resistance		Toxic	
Silica	Good mechanical properties		Expensive	➢ Mesoporous silica (J. Li et al., 2021) ➢ Silicon dioxide ➢ Monolithic silica (P. Liu et al., 2020)
	Available abundantly			
	High porosity			
	Good chemical stability			
	Good thermal stability			
	Excellent insulation properties			
Clay	Good thermal stability		Poor mechanical strength	➢ Diatomite ➢ Expanded perlite ➢ Expanded vermiculite ➢ Bentonite ➢ Kaolin ➢ Sepiolite
	Low cost		Hygroscopic nature	
	High porosity			
Cellulosic material	Available abundantly		None	➢ Wood powder ➢ Cellulose diacetate (CDA) ➢ Microcrystalline cellulose ➢ Cardboard ➢ Plant fibres
	Good mechanical properties			
	Non-toxic			

2.6.5.2 PEG composite through physical blending

Physical blending (e.g., polymer blending) is the contemporary method used for the development of new polymeric materials; and thus, the ideal technique for the synthesis of materials with desired characteristics. It is mainly comprised of simple three steps including the dissolution of PCM and supporting material in the chosen solvent at 70 °C followed by pouring the solution into a glass dish (e.g., petri dish) and allowing evaporation of solvent at room temperature. Major advantage of this approach is that the synthesised composite PCM tends to exhibit properties superior to its individual constituent polymer as shown in Table 2.9.

The final properties of synthesised polymers are influenced mainly by the miscibility of the composite blend (Ernest Ravindran et al., 2020). Wang et al. (2009) (W. Wang et al., 2009) attempted PEG-expanded graphite (EG) composite PCM of mass ratio in the range 50-90 wt.%. Sundararajan et al. (2017) (Sundararajan et al., 2017a) prepared PEG-cellulose acetate composites via a microwave assisted blending approach; and reported that composite PCMs containing an optimum PEG content of 60 wt.% was produced. Li et al. (2018) (S. Li et al., 2018) developed a novel graphene oxide (GO)-PEG composite (e.g., photo-thermal conversion material), with a latent heat capacity higher than 180 J/g and a corresponding phase transition temperature of 50.5 °C via the ultrasonic assisted physical blending approach.

A novel PEG/poly(L-lactic acid) (PLLA) composite PCM was formulated by Lai et al. (2004) (Lai et al., 2004). Results suggested that PLLA content caused no significant impact on the crystalline properties of PEG which was attributed to the partial miscibility of PEG and PLLA (Lai et al., 2004); however, increasing PLLA content above 30 wt.% reduced the crystallinity of PEG in the composite from 80 to 70%. This consequently reduced the latent heat capacity insignificantly. Overall, experimental results suggested that PEG/PPLA blends containing PLLA content less than 35 wt.% were suitable for thermal energy storage purposes because they had latent heat capacity values greater than 100 J/g; and they were able to remain intact even after being subjected to 100 thermal cycles (e.g., good thermal reliability).

Table 2. 9 Properties of composite PCMs from previous literature.

Composite PCM	Technique	PEG		PEG composite		Reference
		T_m (°C)	H_m (J/g)	T_m (°C)	H_m (J/g)	
PEG6000-bone char composite	Impregnation	59.87	162.07	59.36	71.17	(Wen et al., 2018)
PEG8000-cellulose acetate blend (with microwave)	Blend	63	189.5	46-61	23-155	(Sundararajan et al., 2017a)
Cellulose-graft-PEG1100	Synthesis in ionic liquid	46.2	140.3	42.8	94.7	(Li et al., 2009)
Cellulose-graft-PEG2000		53.2	183.3	51.0	129.9	
Cellulose-graft-PEG5000		60.1	204.7	58.9	153.1	
PEG-MCS	Blending/ impregnation	58.95	183.10	57.03	122.10	(Zhang et al., 2016)
PEG10000-PGMA	Ring open crosslink	63.40	166.70	55.9	73.20	(Chen et al., 2011b)
PEG-CDA	Blending	-	186.7	-	104.5	(Jiang et al., 2001)
PEG-CDA	Chemical crosslink	-	186.7	-	73.6	

2.6.5.3 Thermal properties of composite PCMs prepared via physical shape stabilisation approaches

Vacuum impregnation is the most used physical approach for the stabilisation of PCMs because it is simple, yet highly effective (Barreneche et al., 2017; Ding et al., 2008a, 2008b; Mathis et al., 2018). Vacuum conditions are usually used to enhance the impregnation efficiency by forcing the liquid PCM into the pore system of the supporting material, and the conventional set-up used in previous literature is shown in Figure 2.10.

Step 1: Melted PCM is stirred vigorously at 80℃, followed by addition of supporting material. mixture is stirred for required amount of time.

Step 2: PCM-supporting material mixture is placed in a vacuum oven at 80℃ for 24h at selected pressure to encourage adsorption of PCM.

Step 3: PCM/supporting material solid-solid PCM is obtained.
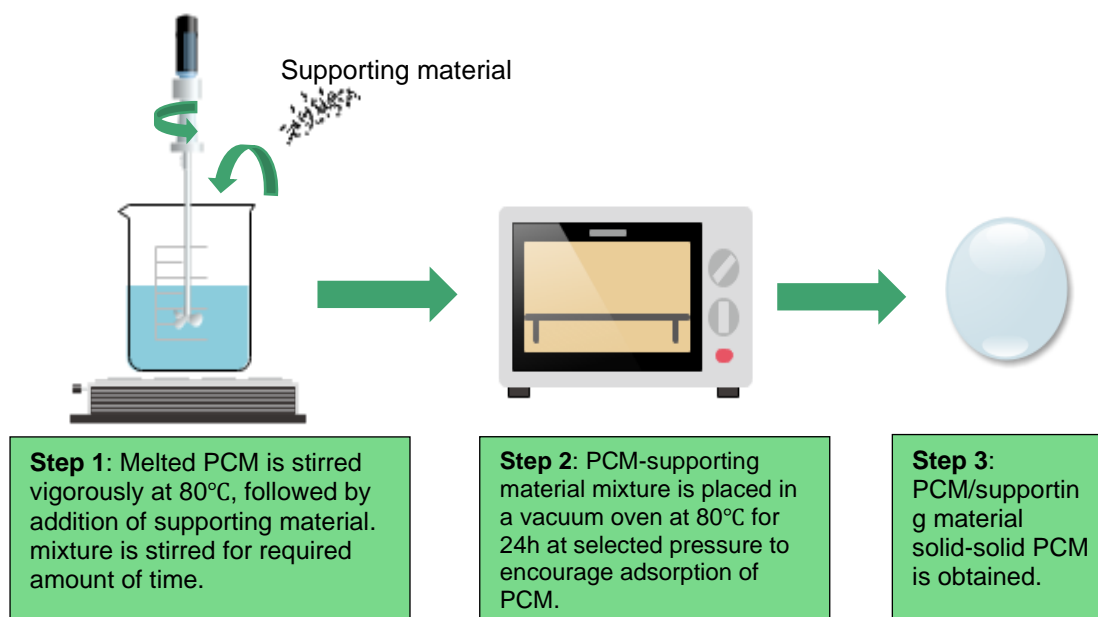
Figure 2. 10 Schematic illustration of the vacuum impregnation approach employed in previous literature.

The physical shape stabilisation processes are very simple, easy, and flexible (e.g., highly feasible); and thus, any PCM and supporting material can be selected and used. Majority of previous studies have prepared numerous composite PCMs using variety of PCMs and supporting material via this approach. Therefore, unlimited combination of PCM and supporting material are available in literature as shown in Table 2.10. Extensive research has not been carried out in previous literature to study and evaluate changes in the intrinsic properties of the chosen PCM after the shape stabilisation process.

Nomura et al. (Nomura et al., 2009) prepared Erythritol/ Expanded perlite (EP) composite PCM with latent heat capacity of 332.2 J/g which was lower than pure Erythritol which had a latent heat capacity of 354.7 J/g. This phenomenon was predicted to occur due to the existence of an unusual interaction between the PCM

and the nano-sized pores of EP. Lee et al, (Lee et al., 2014) prepared Erythritol/ Expanded graphite composite PCMs via a simple melting method with latent heat capacities of 317.5 J/g, 322.1 J/g, 327.7 J/g, 334.3 J/g, 38.5 J/g and 351.2 J/g, respectively. The difference in latent heat capacity of the composite PCMs was reported to be attributed to the variation in the interlayer distance of expanded graphite. They concluded that incorporation of impurity in form of EG resulted in reducing the latent heat capacity of Erythritol significantly.

Jeong et al. (2013) (Jeong et al., 2013) prepared n-hexadecane/diatomite composite PCMs with a melting temperature and latent heat capacity of 23.68 °C and 120.1 J/g using pure hexadecane with melting temperature and latent heat capacity of 20.84°C and 254.7 J/g. Significant changes had occurred to the melting temperature and latent heat capacity but was not addressed anywhere is this study. The reduction in the crystallisation temperature from 16.78 °C to 13.17 °C was reported to be attributed to the existence of poor intermolecular forces between n-hexadecane molecule and pore walls of diatomite. Li et al, (Li et al., 2014) prepared paraffin/ diatomite composite PCMs via a simple mixing/ surface absorption approach. Reduction in phase transition temperature of paraffin from 26.1°C to 25.2°C was reported to be due to the presence of weak interactions between paraffin and diatomite; and, due to the confinement of paraffin within the pores of diatomite. The latent heat capacity of pure paraffin had reduced from 133.7 J/g to 45.96 J/g after the shape stabilisation process; however, this was not discussed anywhere is the study. Zhang and Fang (2006) (Zhang and Fang, 2006) prepared paraffin/ expanded graphite composite PCMs via the melting approach with melting temperature and latent heat of 48.93 °C and 161.45 J/g. The melting temperature and latent heat of pure paraffin was 57.99 °C and 188.69 J/g. Sari and Karaipekli (2007) (Sari and Karaipekli, 2007) prepared paraffin/ expanded graphite composite PCMs and investigated the influence of expanded graphite (EG) content on the thermal properties of paraffin. Mass fraction of 2, 4, 7 and 10% of EG led to the production of composite PCMs with melting temperatures of 41.10 °C, 41.00 °C, 40.70 °C, and 40.20 °C and corresponding latent heat capacities of 192.6 J/g, 188.0 J/g, 181.9 J/g, and 178.3 J/g, respectively. Results demonstrated that increasing the amount of supporting material in the composite PCM resulted in suppressing the latent heat capacity of the chosen PCM (e.g., undesirable effect). Hence, the thermal

performance of composite PCM became very poor when the EG content in the composite PCM was very high.

Mehrali et al, (2013) (Mehrali et al., 2013b) prepared paraffin/ graphene oxide (GO) composite PCMs via vacuum impregnation using paraffin with a melting temperature and latent heat capacity of 53.46 °C and 130.92 J/g. The composite PCM containing the highest paraffin content (e.g.,48.3%) had melting and crystallisation temperatures of 53.57 °C and 42.25 °C. Observations indicated that no significant changes occurred to the melting temperature, but the crystallisation temperature increased due to an unknown reason. The latent heat of the composite PCM seemed to have a positive correlation with the paraffin content because composite PCMs with 44.3 wt.%, 47.39 wt.%, 47.80 wt.% and 48.30 wt.% had latent heats of 59.12 J/g, 62.53 J/g, 63.11 J/g, and 63.77 J/g; however, the enhancement in latent heat capacity was not significant. Pure paraffin had a latent heat capacity of 131.92 J/g. The percentage difference between the latent heat capacity of pure PCM and the composite PCM with optimum PCM content was 51.7%. This suggested that the thermal properties of paraffin had been destructed greatly by the elevated temperature exposure during the vacuum impregnation process. Karaman et al, (2011) (Karaman et al., 2011) prepared PEG/ diatomite composite PCMs via the vacuum impregnation. The melting temperature of pure PEG reduced from 33.32 °C to 27.7°C. The insignificant reduction in the phase transition temperature was reported to be due to the presence of weak physical interactions between PEG and diatomite. Reduction in latent heat capacity of PEG from 143.16 J/g to 87.09 J/g was not addressed in the study. Leakage of the melted PEG from composite PCM was reported to be prevented by the physical interactions (e.g., capillary and surface tension forces). Results from thermal cycling test indicated that the composite PCM exhibited very good thermal reliability and chemical stability, even after being subjected to 1000 repeated thermal cycles. Sari (2014) (Sari, 2014) prepared PEG600/gypsum and PEG600/natural clay composite PCMs with maximum absorption ratio of 18 and 22 wt.% via the vacuum impregnation approach. They reported that changes in the phase transition and latent heat of pure PEG600 after impregnation was attributed to the confinement of PEG600 into the pores of gypsum or natural clay by capillary and surface tension forces. The cubicles of PEG600/gypsum and PEG600/natural clay composites, constructed at small scale,

exhibited very good thermal properties including thermal reliability and chemical stability, even after being subjected to a lengthy thermal cycling test.

Y. Li et al (2016) prepared paraffin/TiO$_2$ foam composite PCMs of three-dimensional interpenetrating structures (Li et al., 2016). The composite PCMs had enhanced melting and freezing temperatures with a difference of no more than 3 °C. This was reported to be attributed to the surface tension forces and the capillary effect present between paraffin and the TiO$_2$ foam. Reduction in latent heat capacity of melting and freezing from 184.3 J/g and 182.67 J/g to 97.27 J/g and 99.05 J/g suggested that the thermal properties of paraffin had changed after vacuum impregnation although no chemical reactions had occurred between paraffin and the foam. Hence, calculated percentage difference of 47% and 46% indicated major changes in the phase change properties of paraffin. The porosity and the pore size of the supporting material was reported as the two influential factors likely to impact the thermal properties of paraffin compared to the surface tension forces and capillary forces. The composite PCMs were observed to undergo thermal degradation when exposed to an elevated temperature of 150 °C. Results indicated that the thermal stability of composite PCM was higher than pure paraffin since its onset degradation temperature was higher than the one of paraffin.

Y. Zhang et al. (2018) (Zhang et al., 2018) prepared paraffin/ silica composite PCMs containing 30 wt.%, 50 wt.%, 55 wt.% and 60 wt.% of paraffin via the blending/ impregnation approach. The melting temperature and latent heat capacity of composite PCM with optimum paraffin content was 25 °C and 95 J/g. The latent heat of paraffin was observed to have reduced from 168 J/g to 95 J/g which was attributed to the accommodation of paraffin in the pores of silica. Kim et al (2021) (Kim et al., 2021) prepared paraffin/ light weight sand composite PCMs through a simple blending/ impregnation approach with a melting temperature in the range 19.67 to 25.36 °C and latent heat capacity in the range 19.01 to 19.11 J/g. Sarı et al., (2018) (Sarı et al., 2018) impregnated PEG within a binary composite consisting of raw diatomite (RD)/ carbon nanotubes (CNTs) to prepare composite PCMs with latent heat capacity and melting temperature in the range 51.4 to 62.9 J/g and 7-8 °C. The leakage test results showed that the skeleton of RD/CNTs pre-composite was able to absorb an optimum PEG content of 51.0 wt.% without sacrificing its structural stability. Presence of carbon nanotubes (CNTs) in the composite PCM was observed to have enhanced the thermal

durability significantly. Yang et al. (2018) (Yang et al., 2018) prepared the PEG/EG composite, by filling the pores of EG was filled up with liquid PEG under vacuum by air pressure and pore syphoning. Cheng et al (2020) (Cheng et al., 2020) prepared PEG10000/carbon nanotubes (CNTs)/ PVA/ chitosan (CPC) composite PCMs via a blending/ impregnation approach. They reported that 8% increase in the latent heat capacity of the resulting composite PCMs was attributed to the existence of hydrogen bonding between the PCM and the supporting material.

Liu et al (2022) (Liu et al., 2022) prepared novel PCM/ carbon composite PCMs using carbon foam derived from insulation materials polyisocyanurate (PIR) foam. Pure PCM was reported to have a supercooling temperature of 4.10 °C while the composite PCMs only had a supercooling temperature in the range 1.90 to 2.50 °C. This was reported to be due to the presence of carbon foam in the composite PCM which resulted in enhancing its thermal conductivity. Observations indicated that with increasing PCM content the supercooling temperature increased undesirably; however, increasing PCM content had a positive impact on latent heat capacity since increasing PCM content from 76 to 90.8 wt.% resulted in increasing the latent heat capacity from 80.5 to 105.2 J/g.

Literature review and results summarised in Table 2.11 shows that numerous design parameters including PCM, supporting material, processing temperature influence the thermal properties including the phase transition temperatures and latent heat capacities (e.g., phase change properties); however, further research needs to be carried out to evaluate the effects of the identified influential parameters on the intrinsic properties of the designated PCM.

Table 2. 10 Summarises the design parameters and thermal properties of composite PCMs synthesised via the physical shape stabilisation approaches.

Composite PCM (PCM/support material)	Design parameters	Thermal properties				Reference
		T_m (°C)	T_c (°C)	H_m (J/g)	H_c (J/g)	
n-hexadecane/ diatomite via vacuum impregnation	➢ 80 g PCM and 50g diatomite ➢ Oven drying at 80 °C for 24h. ➢ Removal of excess PCM through filtration.	23.68	13.17	120.1	118.0	(Jeong et al., 2013)
n-octadecane/diatomite via vacuum impregnation	➢ 80 g PCM and 50g diatomite ➢ Oven drying at 80 °C for 24h. ➢ Removal of excess PCM through filtration.	31.29	23.65	116.8	112.9	
Paraffin wax/ diatomite via vacuum impregnation	➢ 80 g PCM and 50g diatomite ➢ Oven drying at 80 °C for 24h. ➢ Removal of excess PCM through filtration.	54.24	50.23	61.96	59.74	
Erythritol/ Expanded perlite (EP) via vacuum impregnation	➢ Melting solid erythritol at 150 °C using furnace.	-	-	332.2	-	(Nomura et al., 2009)
Erythritol/ Expanded graphite via the melting method	➢ Melting process took place at 120 °C.	-	-	317.5	-	(Lee et al., 2014)
		-	-	322.1	-	
		-	-	327.7	-	

	➤ 10g of Erythritol was melted followed by the addition of 0.25g EG.	-	-	334.3	-	
		-	-	338.5	-	
		-	-	348.5	-	
	➤ The reaction mixture was stirred under heating for 5 minutes.	-	-	351.2	-	
Paraffin/ Diatomite via simple mixing and surface absorption	➤ Heating diatomite at 105 °C for 24 hours to remove moisture.	22.3	-	63.93	-	(Li et al., 2014)
	➤ Melting paraffin at 60 °C before mixing.	23.6	-	47.93	-	
	➤ Unknown amounts of PCM and support material was added and mixed in a mixing vessel.	23.3	-	45.96	-	
PEG/ diatomite via vacuum impregnation	➤ Vacuum impregnation was carried out at an unknown temperature and vacuum pressure of 65 kPa for 90 minutes.	27.7	32.19	87.09	82.22	(Karaman et al., 2011)
Paraffin/ Expanded graphite (EG) via the vacuum impregnation	➤ Unknown amount of paraffin was melted, and impregnated in expanded graphite with mass fraction 2%, 4%, 7% and 10% in a duration of 60 minutes to reach optimum saturation.	41.10	-	192.6	-	(Sari and Karaipekli, 2007)
		41.00	-	188.0	-	
		40.70	-	181.9	-	
	➤ Temperature used to melt paraffin was not reported.	40.20	-	178.3	-	

Paraffin/ graphene oxide (GO) via vacuum impregnation	➢ Paraffin and GO was placed in a vacuum furnace at 100 kPa for 2h to remove any entrapped air of GO. ➢ Temperature was increased to 90 °C to melt down paraffin followed by immersing GO sheets in liquid paraffin for 3h. ➢ To remove excess paraffin, which was not impregnated in the pores of GO, furnace temperature was increased to 120 °C.	54.60	44.78	63.11	64.45	(Mehrali et al., 2013b)
		51.48	45.76	62.53	63.34	
		52.33	44.63	59.12	60.73	
		53.57	44.59	63.76	64.89	
Paraffin/ silica via vacuum impregnation	➢ Paraffin wax and liquid paraffin was blended via the fusion approach. ➢ Silica spheres immerged into the liquid paraffin mixture and allowed to impregnate. Hence, no vacuum was used. ➢ Temperature used to melt paraffin and duration of impregnation is unknown.	26	20	68	50	(Zhang et al., 2018)
		26.5	23	80	71	
		25.5	22	95	70	
PEG600/ gypsum through impregnation	➢ Unknown amount of PEG600 was melted and poured into the flask containing gypsum.	10.55	10.85	24.18	21.64	(Sari, 2014)

	➤ The flask was heated at 25 °C and shaken at 150 rpm to produce a homogeneous mixture.					
PEG600/ natural clay through impregnation	➤ Unknown amount of PEG600 was melted and poured into the flask containing natural clay. ➤ The flask was heated at 25 °C and shaken at 150 rpm to produce a homogeneous mixture.	15.79	16.28	28.79	26.02	(Sari, 2014)
n-octadecane/ light weight sand via vacuum impregnation	➤ Oven dried light weight sand was poured into container containing melted PCM. ➤ The composite PCM was then vacuum oven dried at 80 °C for 24h to remove excess PCM present on surface.	19.67 to 25.36°C	24.10 to 31.54	19.011 to 19.114	-	(Kim et al., 2021)
Paraffin/ porous TiO2 foam via vacuum impregnation	➤ After removing air from the enclosed container containing unknown amount of solid paraffin and foam, the container was heated at 80 °C under vacuum to facilitate the impregnation of liquid paraffin into the pores of the foam.	49.27	50.65	97.27	99.05	(Li et al., 2016)

	➤ For the removal of excess of excess paraffin, the synthesised composite PCMs were heated in an oven at 80 °C for an unknown duration of time.				
PEG10000/carbon nanotube (CNT)/poly(vinyl alcohol) (PVC)/ chitosan (C) via blending/ impregnation	➤ Unknown amount of PEG10000 was melted and dissolved in absolute alcohol for 0.5h at 80 °C. ➤ Prepared CNT/PVC/C (CPC) supporting material was evenly distributed in the PEG solution formed, and the mixture was dissolved at 80 °C for 2h to produce the monolithic composite PCM.	36.80	68.40	150.90	152.00	(Cheng et al., 2020)
PCM/ carbon foam via vacuum impregnation	➤ Beaker containing 50g of solid PCM and 0.5g of carbon foam was heated at 60 °C for 2h. ➤ The prepared composite PCM was heated for another 4h at 60 °C to remove excess PCM.	26.10	24.20	85.60	91.00	(Liu et al., 2022)
		24.90	23.10	80.50	84.90	
		26.20	24.00	95.00	91.80	
		26.60	24.10	105.20	105.40	

2.6.5.4 Thermal properties of composite PCMs prepared via chemical shape stabilisation approaches

In chemical shape stabilisation processes covalent bonds are formed between the functional groups of the designated solid-liquid PCM and the supporting material with the help of a suitable crosslinking agent. Therefore, it is important that both the PCM and the supporting material contains suitable functional groups to encourage chemical crosslinking reaction. Preparation of chemically bonded composite PCMs via chemical approaches like chemical crosslinking is preferred over non-covalently bonded composite PCMs prepared via physical approaches since the latter exhibit drawbacks including poor mechanical performance and solvent resistance (Cabane et al., 2014). Also, if supporting material gets damaged by external forces or solvent, the PCM will suffer from leakage in addition to phase segregation due to poor compatibility between the PCM and the supporting material. In general, covalently bonded composite PCMs acquire better mechanical performance and solvent resistance along with enhanced anti-leakage properties.

Jiang et al (2001) (Jiang et al., 2001) prepared a series of PEG/cellulose acetate (CDA) composite PCMs via the chemical crosslinking reaction; and discussed in their study the phenomenon behind the reduction in latent heat capacity of pristine PEG after the crosslinking reaction. Firstly, the crosslinked composite PCM consisted of CDA impurity which resulted in destructing the perfection of the crystallisation course. Secondly, end hydroxyl groups of PEG (e.g., terminal hydroxyl groups) were attached onto the backbone of CDA which consequently restricted the mobility of the PEG chain during the phase transition process. Results also suggested that composite PCMs containing very low PEG content had very low latent heat capacity attributed to the inability of PEG chain to crystallise.

Li W (2007) (Li and Ding, 2007) prepared PEG10000/4,4'-diphenylmethane diisocyanate (MDI)/ pentaerythritol (PE) composite PCM via the chemical crosslinking reaction. The latent heat capacity of pristine PEG10000 was observed to reduce from 189.45J/g to 152.97 J/g after the chemical crosslinking reaction. This was attributed to the presence of the rigid benzene ring in the composite PCM structure formed which consequently resulted in reducing the number of crystallisable segments (e.g., PEG chain become less crystallisable). The crystalline regions were reported to have become smaller (e.g., reduced lamellae thickness); and thus, this was reflected by a

decrease in phase transition temperature from 59.43 to 58.68 °C. Li et al. (2008) (Li et al., 2008) prepared copolymers using poly(ethylene glycol) monomethyl ether iodide (mPEGI) and MMTritylcellulose via chemical grafting under nitrogen atmosphere. Results suggested that there is a relationship between the crystal lamellae thickness and the phase transition temperature of the polymer crystals. After reaction the phase transition temperature was observed to reduce which was attributed to the decrease in thickness of PEG crystal lamellae. The molecular weight of PEG influenced both phase transition temperature and latent heat capacity significantly. Hence, composite PCM prepared with PEG molecular weight of 1100 g/mol had lower phase transition and latent heat capacity than the one prepared with 2000 g/mol molecular weight, mainly because PEG1100 had more end groups, and lower crystallinity (e.g., imperfect crystal lattice structure) than PEG2000.

Chen et al (2009) (Chen et al., 2009) prepared PEG10000/ cellulose acetate (CA) composite PCMs via the electrospinning/ crosslinking reaction with melting temperature and latent heat capacity of 52.14 °C and 36.72 J/g. The latent heat of PEG10000 was observed to reduce by more than 50% after the chemical crosslinking reaction. This was attributed to the restricted mobility of the flexible PEG chain due to the presence of interchain crosslinks within the molecules. Results suggested that that composite PCMs had good thermal reliability because the composite PCM experienced insignificant changes in phase transition temperature and latent heat capacity even after being subjected to 100 repeated thermal cycles. Thus, the melting temperature and latent heat capacity changed from 52.14 to 52.12 °C (e.g., 0.038% decrease) and 36.79 to 36.72 J/g (e.g.,0.19% decrease).

Xi et al (2009) (Xi et al., 2009) prepared novel polymeric solid-solid PCMs and reported that the latent heat capacity of the corresponding composite PCMs were lower than the one of pure PCM due to the incorporation of the support materials (e.g., impurity). Chen et al. (2009) (Chen et al., 2009) prepared PEG/cellulose acetate (AC) composite PCMs with latent heat capacity of 36.79 J/g. Chen et al (2011) (Chen et al., 2011b) prepared PEG10000/ poly(glycidyl methacrylate) (PGMA). The latent heat of melting and crystallisation of pure PEG was observed to reduce after the chemical crosslinking reaction from 166.7 and 161.8 J/g to 69.8 to 73.2 J/g; and its melting temperature and freezing temperature reduced from 63.4 °C and 39.20 °C to 55.9 °C and 31.1 °C. This was attributed to the confinement of PEG molecular chain by PGMA skeleton which

resulted in suppressing and partially restricting the orientation of the PEG molecules due to the steric effect (e.g., reduced crystallinity). Overall, the number of crystallisable segments and crystalline regions had reduced after the chemical crosslinking reaction.

Chen et al, (2014) (Chen et al., 2014) prepared paraffin/ polyurethane (PU) composite PCMs containing PEG as soft segment via the bulk polymerisation approach. The phase transition temperature of the composite PCMs were observed to increase with increasing PEG content which was attributed to the attainment of a more ordered polymer. Thus, this resulted in enhancing the crystalline properties of the resulting composite PCMs. Three different paraffins namely n-octadecane, n-eicosane, and paraffin were used to prepare the composite PCM. Observation of the DSC curves produced suggested that no chemical reactions had occurred between the PCM and the supporting material since two dips appeared in the heating curve at 36.93°C and 53.96°C. This was attributed to the existence of weak intermolecular forces of attraction between the PCM and the supporting material. The synthesised composite PCMs were reported to be susceptible to thermal degradation when exposed to an elevated temperature of 300 °C. Polarised optical microscopy (POM) analysis confirmed changes in crystallinity of PEG in the composite PCM. The spherulite size were observed to have reduced with increasing TDI and BDO (e.g., hard segment) content. As result, the characteristic spherulite shape was not evident in the crosslinked structure.

Yanshan et al (2014) (Yanshan et al., 2014) prepared series of PEG/melamine/formaldehyde composite PCMs using PEG with different molecular weights (e.g.,1000, 2000, 4000, 6000 and 10000) via the condensation/ crosslinking reaction. The latent heat capacity of pure PEG reduced in the composite PCMs and was reported to be due to the following two reasons: (1) the covalently crosslinked network structure had fewer crystallisable segments due to the fixation of nitrogen atoms in the end groups of PEG (e.g., steric hindrance effect); and (2) the mobility of the PEG chain had reduced after chemical crosslinking; and therefore, the crystal lattice was unable to arrange regularly to form perfect crystals (e.g., became less crystallisable). The melting temperature of pure PEG10000 and its composite PCM were 61.46 °C and 54.84 °C. Reduction in melting temperature was associated with the formation of covalent linkages near the end groups of PEG e.g., bonds between

PEG and nitrogen atoms from amino in melamine, which resulted in reducing the number of crystallisable segments of PEG available near the end groups of PEG.

Yanshan et al (2014) (Yanshan et al., 2014) reported that the degree of crystallinity of PEG6000 based composite PCMs was lower than pristine PEG6000. The presence of supporting material in small amount made no changes to the crystallinity of PEG. Polarised optical microscopy (POM) analysis confirmed changes in crystallinity since the characteristic cross petal shaped spherulites of PEG appearing at room temperature became less apparent in the composite PCM.

Sundararajan et al (2017) (Sundararajan et al., 2017b) prepared PEG8000/ hyperbranched composite PCMs via the chemical crosslinking reaction. They reported that the reduction in latent heat capacity of PEG was attributed to the interference of the hard polyurethane segment with PEG during the crystallisation process. Results suggested that increasing PEG content had a positive effect on the thermal properties of the resulting composite PCMs since the number of crystallisable segments were observed to increase. Sari et al. (2017) (Sarı et al., 2017) synthesised novel polystyrene-co-maleic anhydride (SMA)-graft-PEG copolymers as solid-solid PCMs (S-SPCMs) for solar passive thermal energy storage (TES) applications. The phase transition temperature was in the range 39 to 45 °C with latent heat capacity in the range 107 to 155 J/g. The resulting copolymers were reported to exhibit good thermal reliability and chemical stability even after being subjected to 5000 thermal cycles.

Zhou et al. (2020) (Zhou et al., 2020) prepared a novel PEG/cellulose nanocrystal (CNC) PCM via a UV-induced thiol-ene click chemistry and solvent exchange. Results showed that the loading capacity of PEG could be as high as 97% with latent heat capacity of 150 J/g. The phase transition of pristine PEG was observed to reduce from 40.1 °C to 33.5 °C which was attributed to high specific area of CNC network, and due to the presence of strong intermolecular hydrogen bonds between PEG and CNC.

Zhou et al (2021) (Zhou et al., 2021) prepared PCM/ PVA composite PCMs. They reported that changes in the latent heat capacity of PCM was attributed to the incorporation of supporting material and crosslinking agents since both make no contribution to latent heat. Also, increasing GA content (e.g., crosslinker content) was observed to have no desirable impacts on the phase change properties of the resulting

composite PCMs. Subjecting the crosslinked composites to 100 repeated heating and cooling cycles resulted in reducing the latent heat capacity by 2 J/g and 1 J/g.

Yin et al (2021) (Yin et al., 2021) prepared PEG6000/ Poly(glycerol-itaconic acid) (PGI) composite PCMs with optimum PCM content of 72.67% corresponding to a latent heat capacity of 86.93 J/g. The crystallinity of the prepared composite PCMs was observed to be lower than the one of pure PEG6000. This was attributed to the incorporation of PGI (e.g., impurity) which suppressed the crystallinity of PEG undesirably. Increasing PCM content in the composite PCMs from 62.76% to 68.70% to 72.67% resulted in increasing the crystallinity from 50.15% to 60.78% to 60.95% which indicated increased mobility of PEG chain with increased PEG content. Hence, composite PCM containing an optimum PCM content of 72.67% had the highest latent heat of melting of 86.93 J/g. This suggested that composite PCMs with high crystallinity have higher number of crystallisable segments (e.g., better crystallinity).

Table 2.12 outlines the characteristic properties and performance of PEG/cellulosic material based composite PCMs prepared in previous literature.

Table 2. 11 Summary of highlights of PEG-cellulose composite PCMs from previous literature

Composite PCM (PCM/support material)	Design parameters	Thermal properties				Reference
		T_m (°C)	T_c (°C)	H_m (J/g)	H_c (J/g)	
PEG/cellulose diacetate (CDA) via crosslinking with PEG with molecular weight in the range 2000 to 20000 g/mol.	➤ 1/3 and 1/10 weight of dried PEG and CDA was dissolved in acetone separately. ➤ In PEG solution containing di-n-butyl tin dilaurate catalyst, toluene-2,4-diisocyanate (TDI) crosslinking agent was added dropwise and resulting mixture was heated at 313 K for 4h which resulted in producing a gel-like substance. ➤ Complete desiccation of gel resulted in the formation of hard/solid product.	-	-	-	-	(Jiang et al., 2001)
PEG10000/ poly(glycidyl methacrylate) (PGMA)	➤ Unknown amount of PEG was dissolved in dichloromethane (DCM) followed by the addition of succinic anhydride (SA) and pyridine solution under heating at 90 °C under reflux for 24h. ➤ Final product was precipitated using ether and filtered off, washed with ether and dried in vacuum.	55.90	31.10	73.20	69.80	(Chen et al., 2011b)

Paraffin/ polyurethane (PU) via crosslinking	• 25 g of PEG6000 and 1g of PDMS-b-PPO were placed in an oven at 100 °C to prepare the melt. • 3.78g of 4,4'-diphenylmethane diisocyanate (L-MDI), 0.64g of 1,4-butanediol (BDO) and required amount of n-octadecane was added and reaction mixture was stirred for 1 min at 1000 rpm. • The mixture was poured into a mould and placed in an oven at 100 °C for 4 to 6h.	37.99; 58.91	-	46.25; 77.66	-	(Chen et al., 2014)
		27.81; 58.52	-	18.60; 104.2	-	
		28.57; 57.81	-	34.56; 95.36	-	
		28.12; 57.18	-	40.52; 89.11	-	
		28.60; 58.14	-	30.83; 92.42	-	
PEG/melamine/ formaldehyde via crosslinking with PEG1000, PEG2000, PEG4000, PEG6000 and PEG 10000 via condensation/ crosslinking	• 36 wt.% of melamine and formaldehyde and unknown amount of PEG was added into a three necked round bottomed flask containing water with an overhead stirrer. • Reaction temperature was in the range 30 to 70 °C. • To obtain solid the composite PCM, the reaction mixture was oven dried at 110 °C until all water had evaporated.	46.56	25.96	89.70	92.70	(Yanshan et al., 2014)
		49.13	28.30	91.10	85.30	
		55.50	35.31	103.10	97.90	

		57.75	36.88	109.40	103.90	
		54.84	32.30	95.60	96.20	
Solid-solid polymeric PCM via crosslinking	➤ Polyethylene glycol monomethyl ether (MPEG) phase change unit was firstly reacted with 2,4-toluene diisocyanate (TDI) and N-hydroxymethylacrylamide (NMA) at 40 ℃ for 6 hours to form a copolymer (PD) by modifying the hydrogen group present in MPEG. ➤ The copolymerisation of PD and phenyl ethylene then took place at 70 ℃ for 24 h to produce polymeric based solid-solid PCM (PD)	57.70	18.30	108.5	81.60	(Xi et al., 2009)
		55.80	11.70	90.30	63.40	
		55.40	8.40	75.90	49.60	
		54.00	4.30	53.40	44.0	
		53.20	1.50	47.20	33.90	
PEG10000/cellulose acetate (CA) via electrospinning/ crosslinking	➤ 15 wt.% of cellulose acetate (CA) was added into acetone/ dimethyl acetamide solution. 15wt.% of PEG10000 was added into this solution.	52.14	40.99	36.72	25.92	(Chen et al., 2009)

Material / method	Procedure					Reference
	➢ PEG/CA composites of thickness around 0.1mm was immersed in 10 wt.% of TDI/ toluene solution at 40 °C followed dropwise addition of dibutyltin dilaurate (e.g., catalyst). ➢ The resulting composites were oven dried at 30 °C for 24h.					
Dodecanol dodecanoate/ polyvinyl alcohol (PVA) via electrospinning/ crosslinking	➢ To prepared PVA solution, 20g of PVA was dissolved in 120 ml of deionised water at 90 °C for 3h. ➢ In 60 ml of deionised water, 0.88g of SDS and 0.22g of span-80 (e.g., emulsifiers) were added and stirred, followed by the addition of 10g of PCM. ➢ The final reaction mixture was stirred at 10000 rpm for 35 minutes.	28.53	24.04	63.78	64.89	(Zhou et al., 2021)
		28.60	24.36	65.32	64.89	
		28.38	24.10	64.68	64.52	
		29.24	24.02	65.40	65.39	
PEG6000/ poly(glycerol-itaconic acid) (PGI) via solvent free crosslinking	➢ Unknown amounts of glycerol, Itaconic acid and PEG6000 was mixed under heating at 180 °C for 6h. ➢ This resulted in producing a light-yellow viscous oil.	-	-	86.93	83.65	(Yin et al., 2021)

PEG10000/4,4'-diphenylmethane diisocyanate (MDI)/ pentaerythritol (PE) via crosslinking	➤ Required amount of MDI was dissolved in dimethyl formamide (DMF) and added into a four-necked equipped with an agitator, immersed in an oil bath at 65 °C. ➤ Temperature of oil bath was increased to 90 °C followed by the dropwise addition of PA-DMF within 2h and continuing reaction for another 4h afterwards. ➤ PEG10000-DMF solution within two hours, and reaction was allowed to continue for another 4 h and then 24h. ➤ Reaction mixture was washed with deionised water and dried in an oven at 70 °C for 30 min to obtain the composite PCMs.	58.68	-	152.97	-	(Li and Ding, 2007)
PEG8000/hyperbranched via crosslinking	➤ 0.001mol of dried PEG8000 was melted and combined with slightly excess IPDI (crosslinking agent) in the presence of a catalyst, and reaction was carried out for 3h at 70 °C. ➤ Trimethylolpropane was added into the reaction mixture to promote the formation of the hyperbranched polymer.	50.01	-	119.60	-	(Sundararajan et al., 2017b)

	➢ Product was vacuum oven dried.					

2.6.6 Conclusions and outlooks

Paraffins based composite PCMs are most developed PCM for building applications but are highly flammable and available at relatively high costs. Therefore, it is crucial to identify a potential replacement PCM which is non-flammable and cheaper. Compiled information suggested that PEG may be a promising replacement of the conventionally used organic solid-liquid PCMs like paraffins (e.g., petroleum based PCMs). PEG PCM possesses merits including no need of encapsulation, non-flammable and it is cheaper. The performance of encapsulated PCMs is influenced by numerous factors ranging from material selection to processing parameters, making the synthesis of the encapsulated PCMs the most challenging. By contrast, the shape stabilisation of PEG is comprised of simpler steps which are easy to follow and requires no sophisticated/ expensive equipment. The materials used in this technique can also be environmentally friendly unlike the encapsulation technique which solely depends on the utilisation of toxic chemicals/solvents and non-environmentally friendly materials. For the innovation of the shape stabilisation technology, it is critical for researchers to focus on preparing composite PCMs for building applications and to understand factors that influence their final performance.

Following recommendations are made to enable further growth and development of environmentally friendly composite PCMs for practical implementation in building applications:

➢ Shape stabilisation technology is an effective and efficient technology for the stabilisation of solid-liquid PCMs. Furthermore, this technology enables the utilisation of polymeric PCMs PEG and their derivatives which are environmentally friendly PCMs. The production of solid-solid PEG PCMs requires no encapsulation, since no liquid or gas gets generated during the phase transition process; therefore, the overall cost can be reduced significantly.

➢ Numerous studies have managed to convert PEG into a solid-solid PCM for thermal energy storage (TES) applications only. However, understanding the factors influencing the intrinsic phase change properties of PCM is crucial to promote the development of composite PCMs of exceptional performance. To widen the potential application of composite PCMs in building applications, it is essential to determine a synthesis route which enables the development of composite PCMs operating at room temperature.

- Physical approaches are commonly used for the stabilisation of PEG, but the resulting products have poor durability since they are susceptible to phase segregation; therefore, current research should be focusing more on the synthesis of PEG-based composite PCMs via chemical approaches including chemical crosslinking reaction.

- Both encapsulation and shape stabilisation technologies rely mainly on using petroleum based synthetic supporting materials; however, to promote the green industry biopolymers like cellulose, nanocellulose or chitosan (Y. Li et al., 2021) should be utilised instead, since they are available abundantly at low costs.

- Only a limited number of publications have demonstrated the possibility of synthesising PEG-cellulose composite PCMs for TES applications. The formulation used is not clear and the properties of resulting composite PCMs varied significantly; therefore, an extensive investigation must be performed to get a thorough understanding of the interaction exiting between PEG and the cellulose chain to produce composite PCMs of enhanced durability.

- Majority of previous studies have used the toxic isocyanate based crosslinking agent for the preparation of PEG-cellulose based composite PCMs via the chemical crosslinking reaction (L. Zhang et al., 2021); however, it is highly desirable to replace them with environmentally friendly crosslinking agents like Citric Acid (CA) (Meißner and Jutzi, 2009) for the production of environmentally friendly composite PCMs for building applications.

Chapter 3: Materials and methodologies

Abstract

This Chapter provides the complete specifications of all raw materials used in current research. Furthermore, the synthesis approaches investigated and implemented for the stabilisation of PEG is discussed in detail. Then, the analytical techniques used for the characterisation of PEG and the resulting composites PCMs including FTIR, XRD, DSC, TGA, SEM and POM are presented. Methodology implemented to analyse the data obtained from the different analytical techniques are explained in detail.

3.1 Research materials

The main materials used in the current research includes polymeric PCMs of different molecular weights (Mw), supporting material, crosslinking agent, and solvent. The steps involved in the preparation of PEG based composite PCMs via PU and CA crosslinking reactions are explained, and characterisation approaches employed are discussed comprehensively.

3.2 Phase change materials (PCMs)

Organic solid-liquid polymeric PCM called Poly(ethylene glycol) (PEG) with linear formula $H(OCH_2CH_2)_nOH$ as presented in Figure 3.1 of different molecular weights namely 600 g/mol (CAS number 25322-68-3), 1000 g/mol (CAS number 25322-68-3), 4000 g/mol (CAS number 25322-68-3) and 8000 g/mol (CAS number 25322-68-3) was purchased from Sigma Aldrich and used as PCMs in current study.
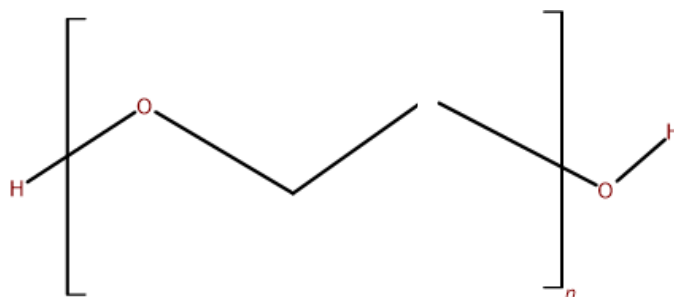
Figure 3. 1 Skeletal formula of Poly(ethylene glycol) (PEG).

3.2.1 Poly(ethylene glycol) (PEG)

Table 3.1 shows the properties of the different PEG PCMs used in current study, and the appearance of PEG8000 and PEG4000 are shown in Figure 3.2.

Table 3. 1 Properties of PEG used in the current study.

Name	Molecular weight (g/mol)	Melting temperature (°C)	Physical state at room temperature
PEG600	600	17-22	Liquid
PEG1000	1000	33-40	Liquid
PEG4000	4000	58-61	Solid pellets
PEG8000	8000	61-64	Solid powder

Figure 3. 2 Appearance of (a) PEG8000; and (b) PEG4000 at room temperature.

3.3 Supporting material

Cellulosic materials namely Microcrystalline cellulose (MCC) and carboxymethyl cellulose (e.g., cellulose fibre) are both biopolymers, and was used as supporting material in current study for the stabilisation of PEG.

3.3.1 MCC

Microcrystalline cellulose (MCC) with particle size of 20 μm and molecular formula $(C_6H_{10}O_5)_n$ (CAS number 9004-34-6) was purchased from Sigma Aldrich and used as received as supporting material in the PU crosslinking reaction. Figure 3.3 (a) and (b) shows the appearance of MCC and its skeletal formula.
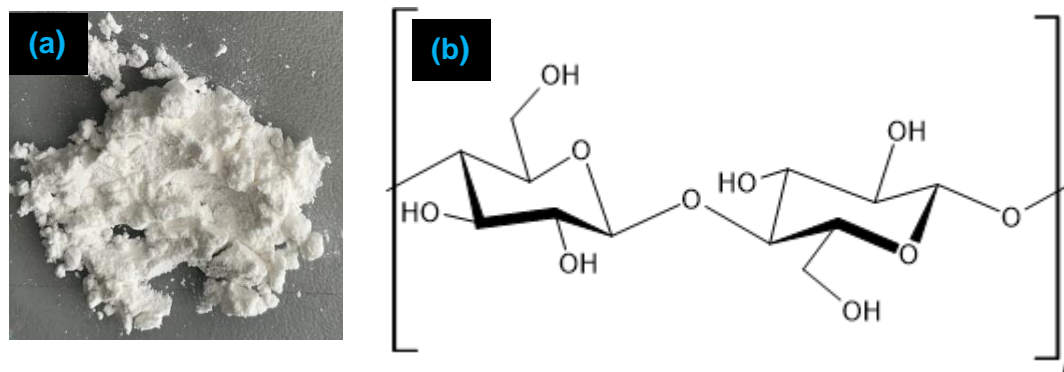
Figure 3. 3 (a) Appearance of MCC; and (b) skeletal formula of MC cellulose.

3.3.2 CMC/ cellulose fibre (CF)

Carboxymethyl cellulose (CMC) of technical grade regarded as 'cellulose fibre' throughout the current study with a polymerisation degree (e.g., the number of monomer units a polymer is made up of) of 1566 was supplied by Craigowl Services Ltd. (UK). Before use, cellulose was heated in an oven at 104±3°C for 24 hours to ensure entrapped moisture was removed completely since this will influence the water content of the reaction mixture during CA crosslinking reaction. Figure 3.4 shows the appearance of the oven dried cellulose fibre along with its chemical formula.
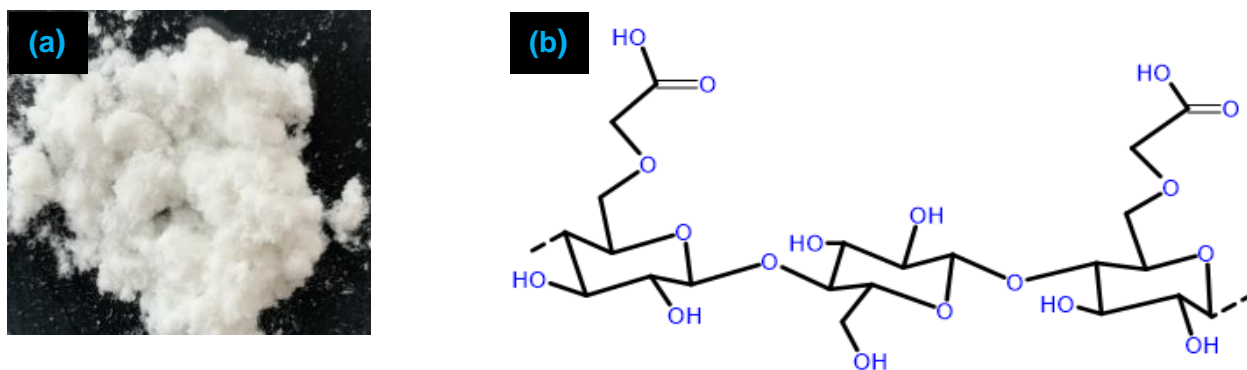
Figure 3. 4 Appearance of (a) oven-dried cellulose fibre; and (b) skeletal formula of cellulose fibre e.g., CMC.

3.4 Crosslinking agents

3.4.1 Diisocyanate based crosslinking agent

Tolyene-2,4-diisocyanate (TDI) of 95% purity (CAS number 584-84-9) with molecular formula $CH_3C_6H_3(NCO)_2$ was purchased from Sigma Aldrich with molecular weight and melting temperature range of 174.16 g/mol and 20-22 °C. Figure 3.5 shows the structural skeletal formula of TDI.
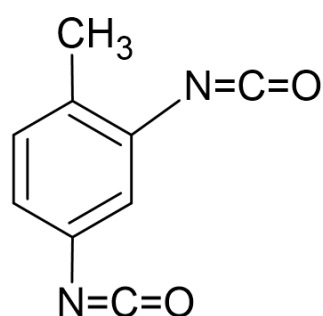
Figure 3. 5 Skeletal formula of TDI crosslinker.

3.4.2 Tricarboxylic acid (TCA) as crosslinking agent

Anhydrous Citric acid (CA) of purity greater than or equal to 99.5% (CAS number 77-92-9) with molecular formula $HOC(COOH)(CH_2COOH)_2$ was purchased from Sigma Aldrich with molecular weight and melting temperature range of 192.12 g/mol and 153-
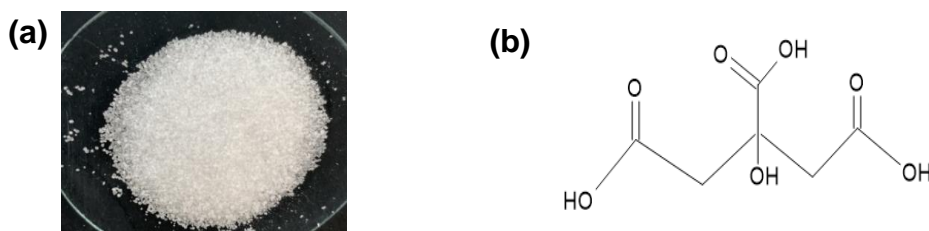
Figure 3. 6 (a) Physical state appearance; and (b) Skeletal formula of Citric acid (CA).

159 °C. Figure 3.6 (a) and (b) shows the physical appearance at room temperature and skeletal formula of CA.

3.5 Solvents

In general, dissolution of reactants is encouraged by dissolving chosen reactants in relevant solvents. Chemical solvents like dimethyl formamide (DMF) and acetone are commonly used solvents for the stabilisation of PEG through chemical crosslinking with cellulose and its derivatives. However, current study uses deionised (DI) water as solvent to encourage chemical reactions between chosen reactants.

3.5.1 *N,N*-Dimethylformamide (DMF)

N,N-Dimethylformamide (DMF) (CAS number 68-12-2) of 99.9% purity with molecular formula of $HCON(CH_3)_2$ was purchased from Sigma Aldrich with molecular weight and boiling point of 73.09 g/mol and 153 °C. Figure 3.7 shows the structural formula of DMF.
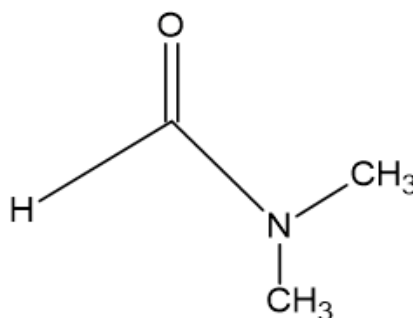
Figure 3. 7 Skeletal formula of DMF.

3.5.2 Deionised (DI) water

Deionised (DI) water (H_2O) (product code 553771620) with boiling point of 100 °C was purchased from Eurocarparts.com and used as solvent to carry out crosslinking reactions; and to rinse beakers and equipment before use to avoid contaminating reaction mixtures. Thus, tap water also known as hard water was not used to carry out the chemical reactions since it contains cations and anions mainly calcium (Ca^{2+}) and magnesium (Mg^{2+}) ions; and therefore, its ions are likely to interfere with the reactants which will result in the formation of undesired final products or reducing the total yield of desired product.

3.6 Moulds

Plastic petri dishes of good chemical and heat resistance was used as moulds to prepare test samples via the TCA crosslinking reaction in two different shapes and dimensions.

3.6.1 Circular petri dishes

Sterilisable circular polystyrene disposable petri dishes (Product number: P5731) of high quality and acceptable heat and chemical resistance with dimensions 100 mm x 15 mm was purchased from Sigma Aldrich.

3.6.2 Square petri dishes

Sterilisable square polystyrene disposable petri dishes (Product number: Z617679) of high quality and acceptable heat and chemical resistance with dimensions 120 mm x 120 mmx 16 mm was purchased from Sigma Aldrich.

3.7 Stabilisation of PEG through crosslinking

Crosslinking reactions are conventionally used to enhance the physical property of soft polymers by combining it with the chosen hard segment in the presence of a suitable crosslinking agent which results in the formation of covalent linkages between the polymer chain (e.g., soft segment) and the hard segment. Previous literature has demonstrated the possibility of crosslinking PEG with chosen supporting material; and therefore, this concept was employed in the current study. Two different crosslinking reactions namely PU and TCA crosslinking were carried out to investigate the influence of reaction routes and chemical composition on the thermal and crystalline properties of the resulting PEG-based composite PCMs.

3.7.1 Polyurethane (PU) crosslinking

Required amount of DMF solvent was heated at 80 °C under continuous stirring using a mechanical stirrer at moderate speed followed by the addition of the required amount of PEG. After complete dissolution of PEG in DMF solvent, required amount of MC cellulose (MCC) was added gradually to prevent agglomeration under constant heat and continuous stirring which led to the formation of a cloudy solution. Into a separate beaker, required amount of melted TDI was dissolved in DMF solvent in the absence of heating to obtain a homogenous TDI-DMF reaction mixture, and this beaker was covered in cling film to prevent TDI interacting with the moisture present in the air since this may lead to the formation of unwanted by products because TDI is sensitive to

moisture. TDI-DMF solvent was added dropwise using a transfer pipette over 10 minutes into the PEG-DMF solvent with constant heating and continuous stirring. The final reaction mixture was covered with cling film to ensure that no heat escaped during reaction, and to prevent evaporation of solvent. It was further allowed to stir for another 3 hours which eventually led to the formation of a solid 'gel-like' final product (e.g., composite PCM). The proposed synthesis route for this reaction is illustrated schematically in Figure 3.8.

Step 1: PEG-DMF-MC solution preparation
Adding PEG powder gradually in the DMF solvent under heating at 80 °C with continuous stirring followed by the addition of microcrystalline (MC) cellulose.

Step 2: Initiation of crosslinking reaction
Required amount of liquid TDI was added and mixed in DMF solvent to produce TDI-DMF solution. This was added dropwise over a time of 15 minutes into the PEG-DMF-MC reaction mixture with constant heating and stirring.

Step 3: Formation of a crosslinked product
The reaction mixture was allowed to stir under heating and continuous stirring after adding the TDI (e.g., crosslinking agent). As reaction proceeds, the viscosity of reaction mixture is observed to increase. Eventually, completion of reaction results in the formation of a gel-like material (e.g., PEG-MC-TDI composite PCM).

Figure 3. 8 Schematic representation of polyurethane crosslinking reaction for the synthesis of shape stabilised composite PCMs.

3.7.2 TCA crosslinking

Required amount of CA was added into the beaker containing the measured amount of DI water under heating at 80 °C with continuous stirring. The concentration of CA solution required to encourage complete crosslinking reaction between PEG and cellulose fibre has not been reported anywhere in previous literature, and the information available regarding crosslinking agent content is very unclear; thus, no synthesis route is available for the development of PEG-cellulose composite PCMs via TCA crosslinking reaction using CA as the crosslinking agent for building applications. In the current study several CA concentrations were investigated (see Table 3.2) and equation (4) was used to determine the mass ratio of CA to DI water. Four different citric acid concentrations in weight/volume (w/v) percentage including 30, 50, 75 and 100 w/v% were selected from trial-and-error results; and used throughout this study. Results suggested that concentrations lower than 30 w/v% resulted in forming no solid composites which indicated that low concentration of CA is unable to aid the formation of covalent bonds between PEG and CF. Thus, unstable soft composite films which broke apart during the demoulding process were formed.

The concentration of citric acid in w/v% was determined using equation (4).

$$Concentration \left(\frac{w}{v}\%\right) = \frac{\left(solute\ mass\ (g)\right)}{\left(solution\ volume\ (ml)\right)} \times 100\%$$

(4)

Table 3. 2 Concentration of citric acid solutions investigated.

Citric acid solute (g)	Deionised water (g)	Citric acid concentration (w/v%)
3	10	30
5	10	50
7.5	10	75
10	10	100

Required amount of PEG was measured and poured gradually into the beaker containing the CA solution under constant heating with continuous stirring to avoid agglomeration of PEG since this will affect the homogeneity of reaction mixture

formed. Resulting reaction mixture was allowed to mix for 10 minutes because by that time all PEG particles were observed to have dissolved completely in the CA solution which resulted in the formation of a clear viscous solution. The viscosity of the solution was observed to increase with increasing concentration of both citric acid and PEG. Into this reaction mixture, the required amount of cellulose fibre (CF) was gradually added with high shearing since a stronger force was required to form a homogenous blend. The final viscous reaction mixture was poured into the designated mould and mould was placed in an oven at 80 °C for 24 hours to encourage chemical crosslinking by the 'slow evaporation' approach; thus, a simple solution casting method was used to crosslink PEG and CF in the presence of CA. The oven dried samples were stored in resealable plastic bags until testing. The proposed synthesis route for this reaction is illustrated schematically in Figure 3.9.
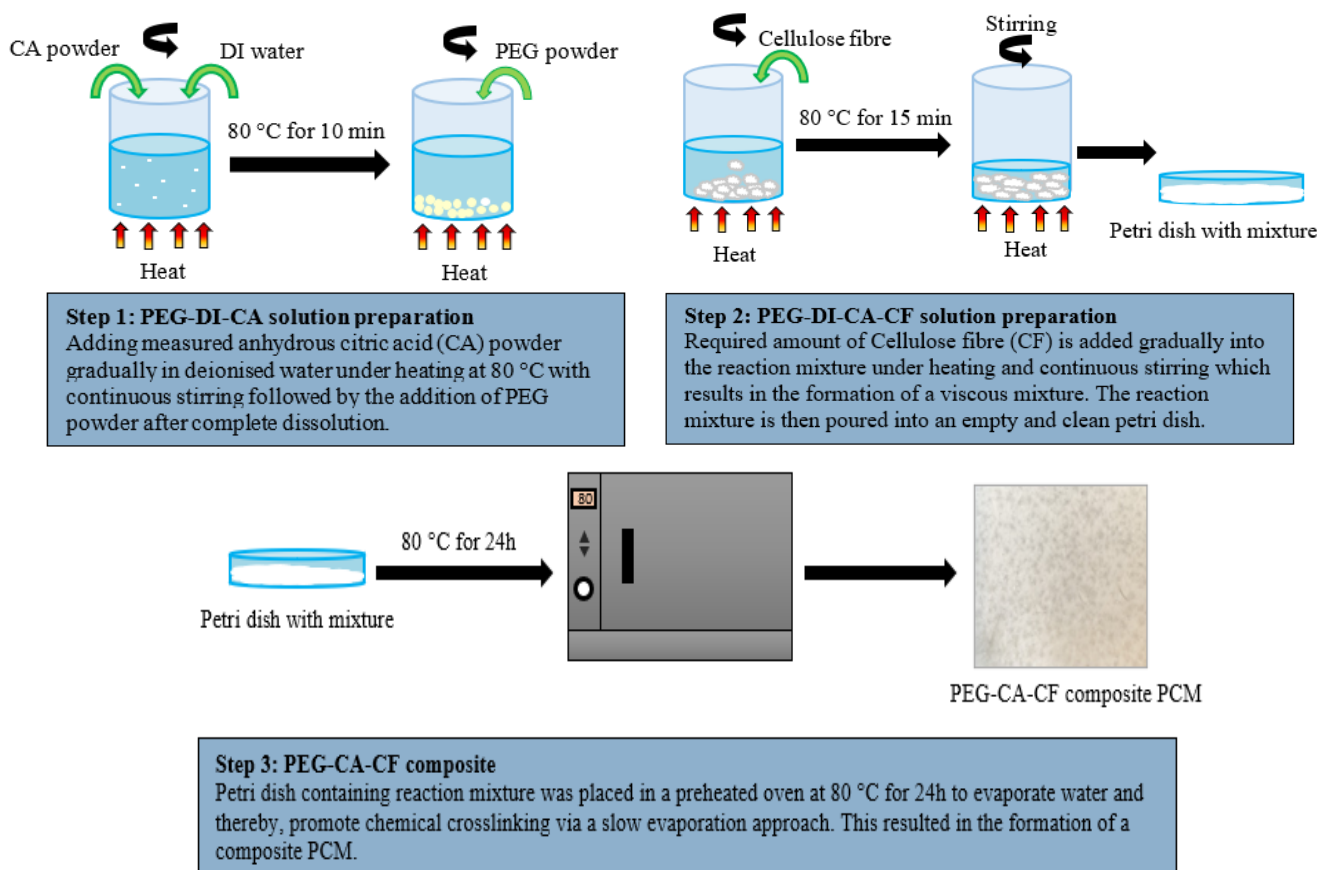
Figure 3. 9 Schematic illustration of TCA crosslinking reaction using CA as crosslinking agent.

3.8 Curing approaches for TCA crosslinking

In general, enhancing the degree of crosslinking is very important to form final composite PCMs of acceptable durability. To evaluate an effective curing approach for the synthesis of shape stabilised composite PCMs via TCA crosslinking reaction, different heating approaches as shown in Figure 3.10 were developed and used. Also, changes in thermal properties of PEG after MW irradiation during the chemical crosslinking process were studied and reported since this was never discussed in previous literature.
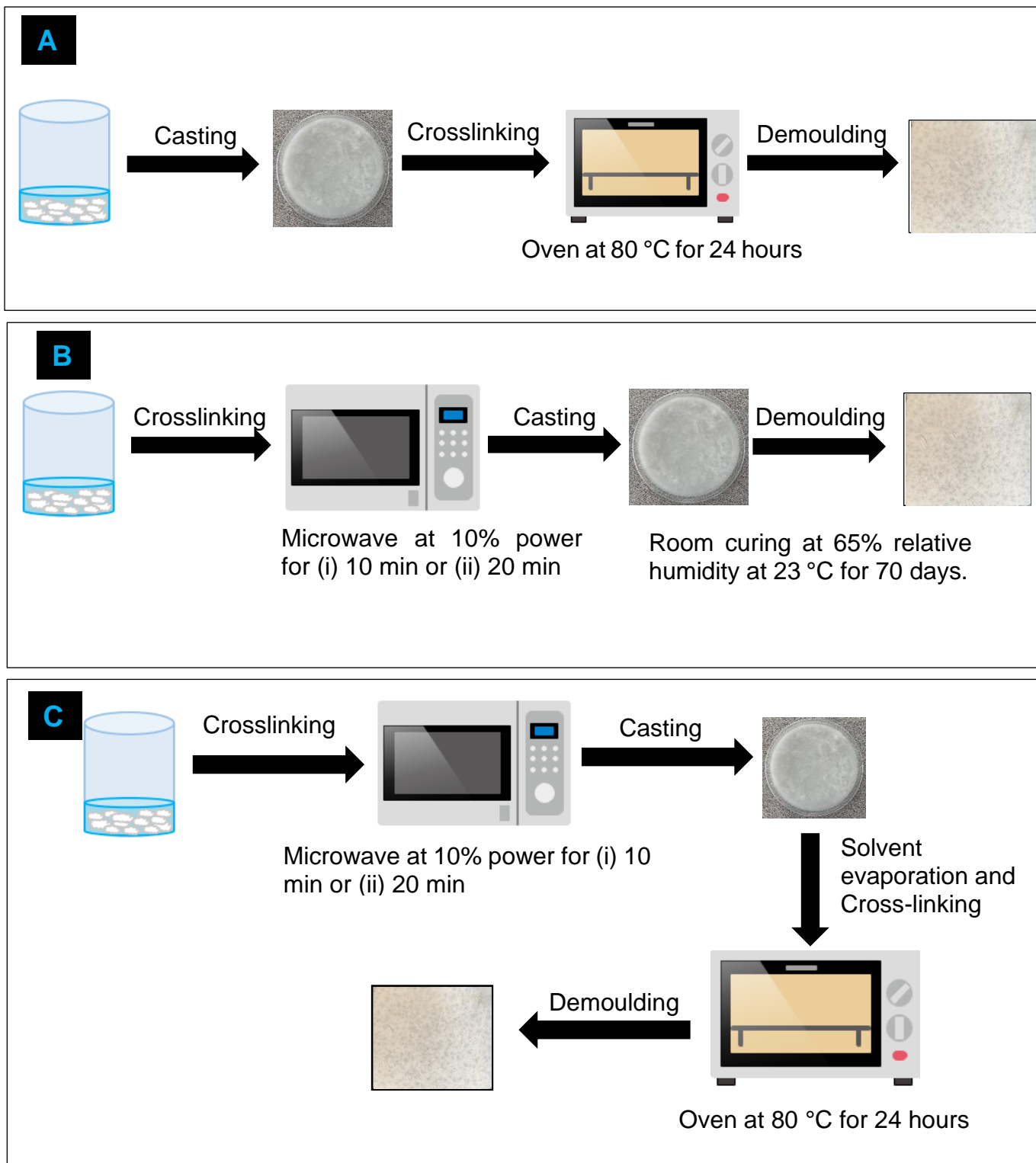
Figure 3. 10 (A) Solution casting/slow evaporation; (B) MW irradiation/ room curing; and (C) MW irradiation/ slow evaporation.

3.10 FTIR spectroscopy

Fourier transform infrared (FTIR) spectroscopy is an easy non-destructive technique conventionally used infrared spectroscopy in previous literature (Hospodarova et al., 2018; Oh et al., 2005) to examine the chemical structure, to evaluate the interaction existing between PCM and supporting material. Moreover, to confirm the formation of a covalently bonded network after the chemical crosslinking reaction. During the analysis, infrared radiation (IR) passes through the chosen material while some IR gets absorbed by the material and the IR that manages to pass through the material gets recorded in form of FTIR spectrum.

Percentage transmittance gives information regarding how strongly light was absorbed. The peaks are observed to be pointing downwards because the vibrational energy of bonds present in the molecules changes as result of absorbing IR of specific wavelengths. It induces a type of vibration which depends upon the atoms of the bonds since the absorption frequency is a function of the chemical bonds and functional groups. In general, the chemical bonds of organic molecules are in motion at room temperature, and they behave like springs. The vibrational motion of the molecules can be divided into different vibrational modes as illustrated in Figure 3.11.

The IR bands in the FTIR spectrum can be classified as strong, medium, or weak, and depending on their shape they are defined as either narrow or broad. Strongly polar bonds tend to produce strong bands and medium bands indicates that the bond has medium polarity and is asymmetric while weak bands usually result from symmetric bonds of weak polarity. Figure 3.11 shows the typical type of bond vibrations, and Table 3.3 provides useful information regarding the IR frequencies.

Table 3. 3 Assignment of FTIR spectra.

Peak assignment (cm^{-1})	Description	Reference
2871	O-H and C-H stretching vibration	(Kong et al., 2017)
1467	C-H stretching vibration -CH$_2$ scissoring	(Kong et al., 2017; Sundararajan et al., 2017a)
1342	C-H stretching vibration -CH$_2$ wagging Crystalline phase of polymer	(Capanema et al., 2018; Kong et al., 2017)
1280	C-H stretching vibration	(Kong et al., 2017)
1242	C-H stretching vibration C-O and C-O-C	(Capanema et al., 2018; Kaewprachu et al., 2022)
1099	Sharp peak C-O-C symmetrical stretching vibration	(Kong et al., 2017; Sundararajan et al., 2017a)
960	Sharp peak C-O-C symmetrical stretching vibration	(Kong et al., 2017; Qin et al., 2019a)
842	C-H stretching vibration	(Kong et al., 2017)
3445	Stretching vibration of the hydroxyl (-OH) groups and may indicate the presence of water	(Qin et al., 2019a)
2885	Stretching vibration of -CH group of CH$_2$	(Qin et al., 2019a)
1724	Due to the stretching vibration of the C=O groups	(Qin et al., 2019a)
Blue shift if wavenumber changes from 1724 to 1733	It indicates the disappearance of the C=C group adjacent to the C=O group better known as the conjugation effect which normally occurs after polymerisation reaction.	(Qin et al., 2019a)

94
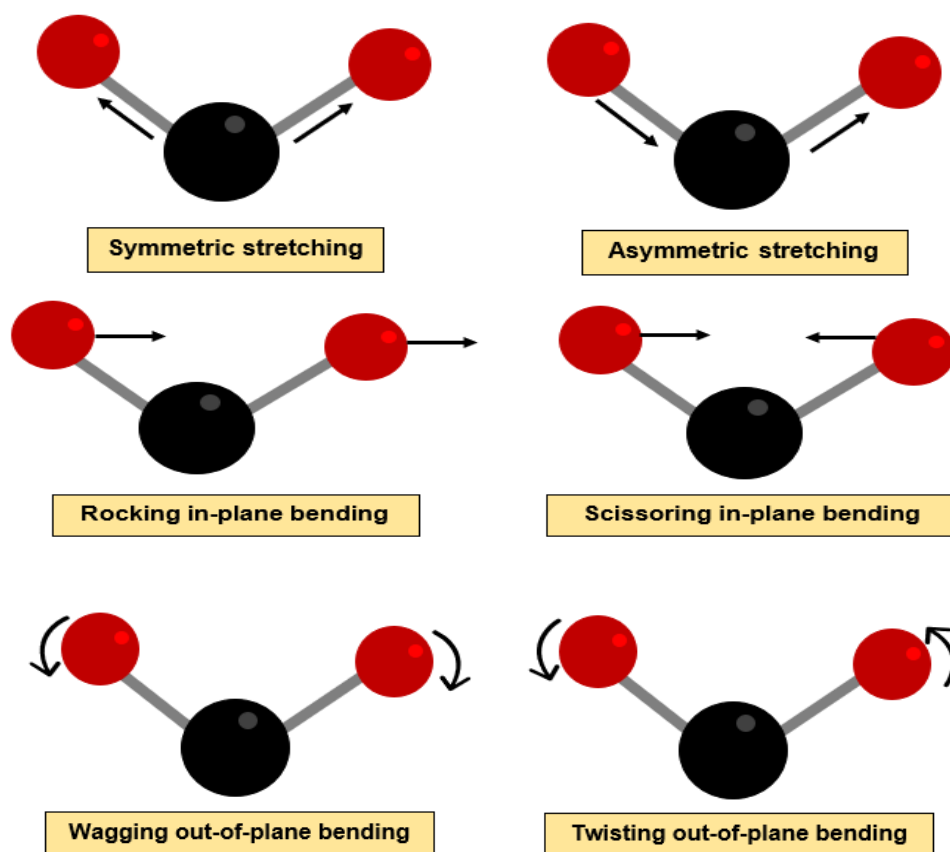
Figure 3. 11 The different types of bond vibrations.

3.10.1 FTIR analysis

The infrared spectroscopy analysis was performed at the Experimental Technique Centre (ETC), Brunel University London, using the Perkin Elmer Attenuated Total Reflectance Fourier Transform Infrared (ATR-FTIR) spectroscopy equipped with a 3x bounce diamond crystal with an incident angle at 45° (see Figure 3.12). The FTIR spectra was recorded over a range of 4000 to 500 cm^{-1} by averaging 32 scans with a resolution of 4 cm^{-1} for every spectrum to ensure FTIR spectra patterns with full details were produced. The powder sample was placed on the stage to carry out the FTIR analysis.
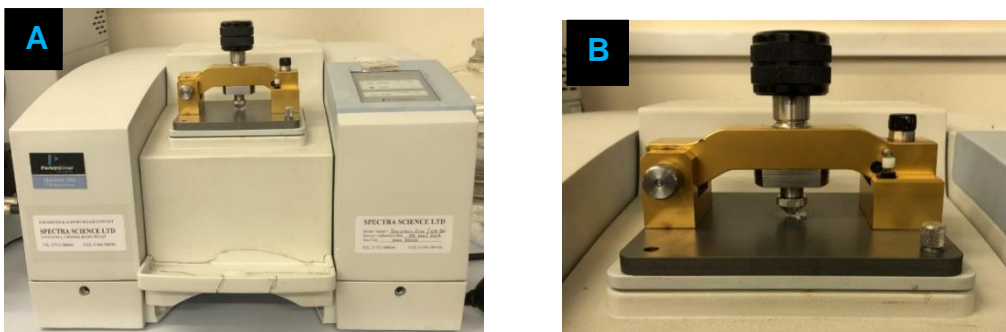
Figure 3. 12 (A) Perkin Elmer ATR-FTIR instrument; and (B) Diamond tipped ATR-FTIR stage.

3.11 Scanning electron microscopy (SEM)

It is the conventionally used analytical tool which utilises an electron ejecting probe for the formation of an electron beam which is used to produce SEM images as result of electron reflection during scanning. SEM analysis was performed at the Experimental Technique Centre (ETC), Brunel University London.

3.11.1 Scanning electron microscopy (SEM) sample preparation

To enhance the clarity of the SEM images produced the non-conductive polymeric test samples were gold coated using the Polaron range sputter coater shown in Figure 3.13 (A). Firstly, the sample mounted onto an aluminium stud using carbon tape was placed inside the chamber (depicted in Figure 3.13 (B)) and were gold sputtered for a duration of 135s. The physical appearance of a gold coated sample is shown in Figure 3.13 (C).
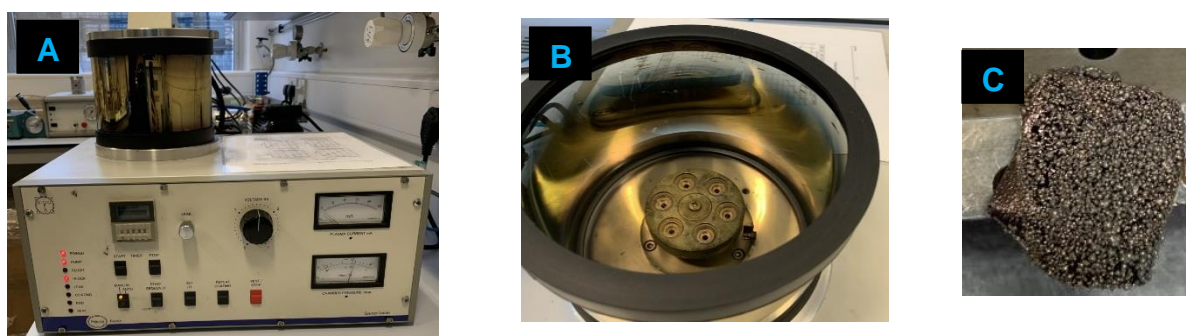
Figure 3. 13 (A) Polaron Gold sputter coater; (B) chamber; and (C) appearance of gold coated sample.

3.11.2 Scanning electron microscopy (SEM) analysis

The scanning electron microscopy (SEM) images of raw materials and the crosslinked composite PCMs were obtained with a LEO-1455VP SEM (see Figure 3.14) mainly to investigate, and study changes in the surface morphology and microstructure with chemical composition. Also, to evaluate the homogeneity of the crosslinked composite PCMs. The SEM was initially vented to allow air into the system to open the vacuum chamber door. The sample holder was then placed inside the SEM chamber (see Figure 3.14(C)) and the system was pumped which took couple of minutes to reach completion. A secondary electron (e.g., S2) detector was selected, and the accelerating voltage also known as the electron high tension (EHT) was set at 3kV to avoid burning the polymeric samples. Hence, using 5kV EHT resulted in degrading the sample within couple of minutes. The probe current was set to 50 pA. Lower magnification in the range 100x to 300x was used for imaging because at higher magnifications it was impossible observe any features such as voids and cracks.

To obtain images of high resolution the following steps were followed: (1) adjusting stage height using the joysticks to 14mm after getting a focused image on the screen at a high magnification (3000x); (2) adjusting the focus and magnification to get a well-defined image; (3) turn on the 'wobble' and align the apertures at a low scanning speed using the adjusters found above the chamber door; (3) correcting the stigmatism and adjusting the focus; and (4) setting the scanning speed to 9 and saving the SEM images. Several locations of each sample were imaged and surfaces containing interesting features were reported.
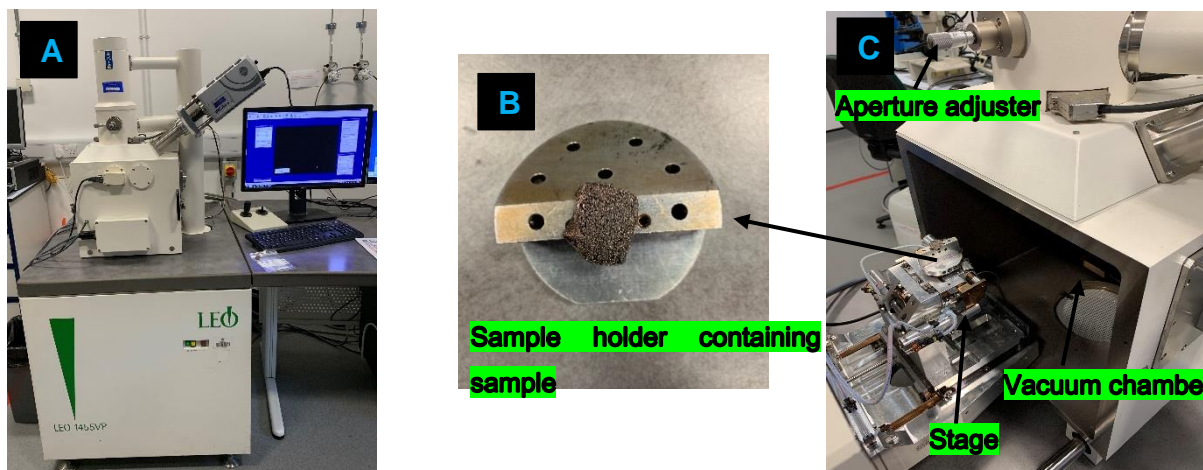
Figure 3. 14 (A) LEO-1455VP SEM; (B) Gold coated sample mounted on the sample holder; and (C) the vacuum chamber and stage of the SEM.

3.12 Polarised optical microscopy (POM)

The fundamental working principle of POM is based on the object's illumination, and a microscopic image usually results from either scattering or transmittance of light by the system of lenses. POM analysis was performed at University of Strathclyde, Glasgow.

3.12.1 Polarised optical microscopy (POM) analysis

POM analysis was performed by placing the glass slide containing the test sample under the optical microscope mainly to determine the crystal morphology and structure of PEG8000 and its crosslinked composite PCMs at room temperature using an OLYMPUS-BX60 optical microscope with a polarising filter equipped with a camera on top to project the visuals observed under the microscope to the monitor screen and later capture relevant POM images. Low magnifications, namely 100x and 200x, were only used since at higher magnifications crystals and particles of PEG were not fully visible, and no interesting features were observed at higher magnifications.

3.12.2 POM equipped with a hot stage analysis

To make in-situ observations of changes in the crystal morphology and crystal behaviour during the phase transition process, an Olympus BX51 POM equipped with a Mettler Toledo FP90 hot stage was used (see Figure 3.16 (A)). The test sample was sandwiched between two cover slips (e.g., glass slides), and inserted inside the furnace of the Mettler Toledo FP90 hot stage (see Figure 3.16 (B)). To improve the clarity of images produced, one side of the glass slide was coloured black using a permanent marker because the visibility of colourless/ white samples under the

microscope was very poor. Pristine PEG8000 and its composite PCMs were heated from 25 °C at a heating rate of 3°C/min up to 70 °C and 80 °C (e.g., ending temperatures), and kept at this temperature for 10 min to ensure the attainment of a complete melt without any liquid-liquid phase separation. The samples were cooled at a cooling rate of -3°C/min until reaching room temperature (19 °C). The temperature protocol employed to perform POM observations are illustrated schematically in Figure 3.15. Numerous high and low magnification (e.g., 200x and 100x) images were captured with 30 seconds intervals using the Nikon Coolpix P5100 digital camera mounted on top of the microscope, and relevant images are reported within this thesis.
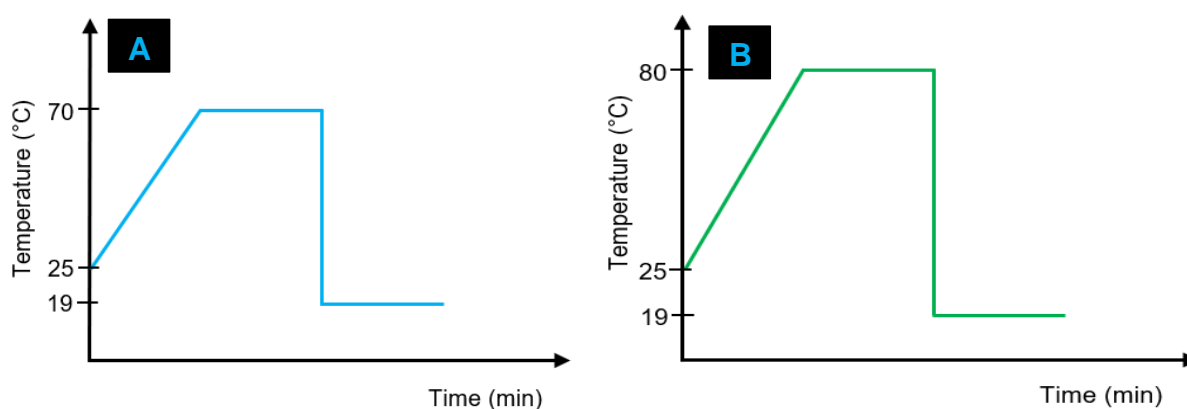
Figure 3. 15 Temperature protocol used for (A) pristine PEG8000; and (B) PEG8000 based composite PCMs.
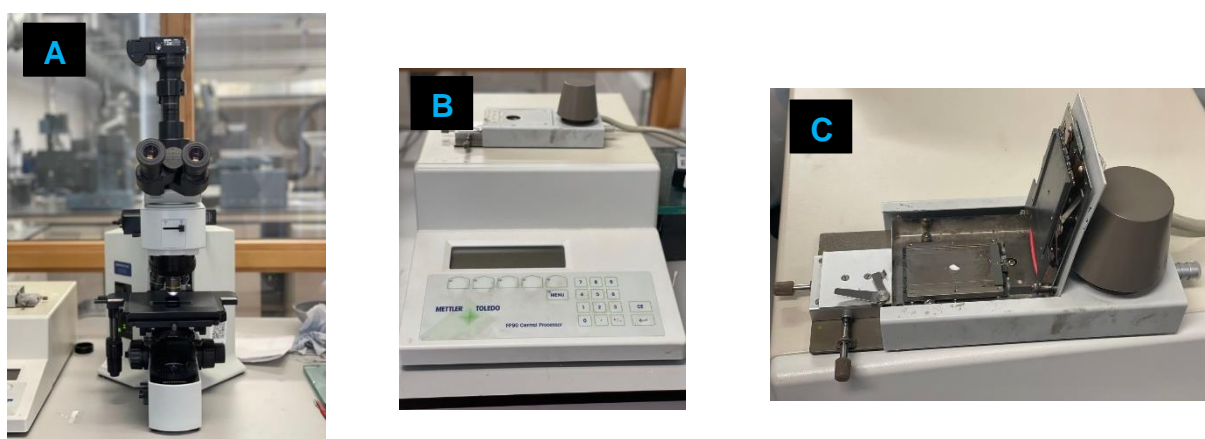
Figure 3. 16 (A) Olympus BX51 equipped with the Mettler Toledo FP90 hot stage; (B) Mettler Toledo FP90 hot stage; and (C) furnace of the Mettler Toledo FP90 hot stage.

3.13 Differential scanning calorimetry (DSC)

In current study DSC analysis was used to investigate and study the behaviour of pristine PEG and PEG based composites exposed to heating. Thus, using data obtained the melting and crystallisation temperatures or glass transition temperature along with the corresponding latent heat will be determined. In this technique the difference between heat flow rate of the pan containing the sample and the empty reference pan is derived as a function of temperature and/ or time. It usually results in producing a DSC curve containing an endothermic (heating) and exothermic (cooling) curve as shown in Figure 3.17.
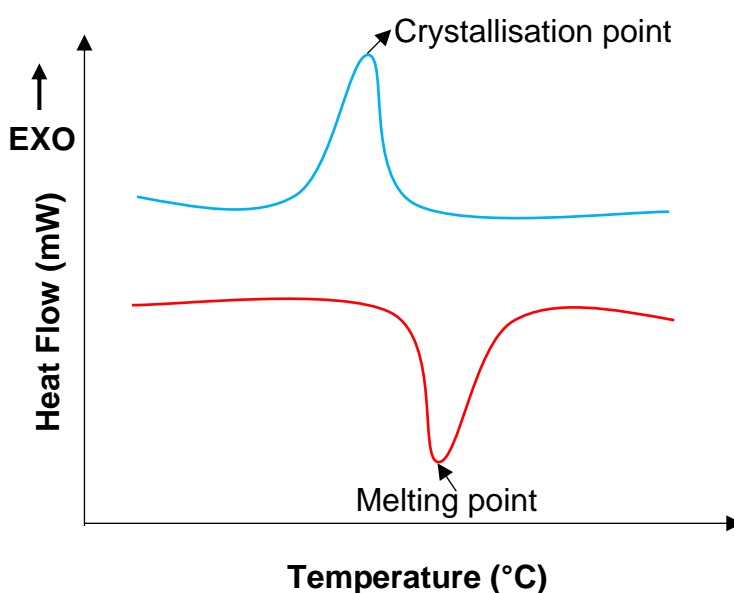
Figure 3. 17 Appearance of a typical DSC curve.

The odd cycles (e.g., first, third, fifth etc.) are regarded as the heating cycles throughout the thesis since material was in solid state initially; and was forced to undergo a phase change by subjecting it to a gradual temperature change over time and eventually its melting temperature was reached which caused it to undergo a phase change under isothermal conditions. The peak of the heating cycle points in the endothermic direction (e.g., dips are produced) which shows that the reaction is endothermic. Hence, melting process involves breaking existing bonds and therefore, this process tends to absorb energy from the surrounding because they are endothermic reactions. While the even cycles are regarded as cooling cycles in this study, and they are comprised of one or more peaks pointing towards the exothermic

direction which indicates that the cooling process in exothermic which means energy will be released into the surrounding as the process proceeds.

3.13.1 Differential scanning calorimetry (DSC) analysis

DSC analysis was performed at the Experimental Technique Centre (ETC), Brunel University London, on pristine PEG and its composites using the DSC Q2000 instrument shown in Figure 3.18. It comprised of a measurement chamber and a computer. The DSC chamber shown in Figure 3.18 (B) consisted of two pans; however, sample in form of solid or powder usually with mass ranging from 5 to 20 mg was added into the 'sample pan' while the 'reference pan' was left empty according to ISO 11357 to obtain accurate results. Computer was used during test to monitor the temperature, and to regulate the heating/ cooling rate (e.g., the temperature at which the pans changed). The heating and cooling rate was set at 10 °C/min under nitrogen (N2) atmosphere to prevent thermo-oxidative decomposition of the polymeric test samples.
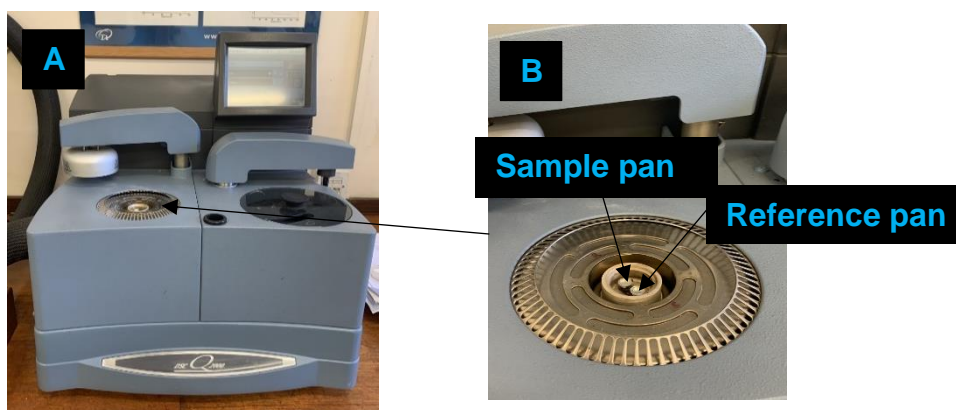
Figure 3. 18 (A) DSC instrument; and (B) DSC chamber.

3.13.2 DSC data analysis

DSC curves were plotted using Origin Lab software. The melting and crystallisation temperature of pristine PEG and its composite PCMs was determined from the heat flow (mW) against temperature (°C) curve. To determine the latent heat capacity of melting and crystallisation, a graph of heat flow (mW) divided by weight (mg) against time (s) was plotted and integrated using Origin Lab software since the area under this graph represented the latent heat capacity in J/g. Hence to determine the latent heat capacity of melting, the heating curve was integrated vice versa.

3.14 Thermogravimetric analysis (TGA)

TGA is a type of thermal analysis technique which can be used to evaluate changes in chemical and physical properties as well as other physical phenomena including vaporisation and desorption. They are usually performed either as a function of temperature increase with a constant heating rate or as a function of time with a constant temperature accompanied by mass loss. The test sample is subjected to a gradual temperature increase in a furnace and the change in its weight is measured using a highly sensitive scale (e.g., analytical balance) located above the furnace. Common reasons for mass loss or gain includes decomposition, dehydration, oxidation, or evaporation of volatile compounds. The change in weight of polymeric materials like PEG is usually attributed to the decomposition and oxidation reactions. In the current study, TGA was used to determine the thermal stability of the PEG and its crosslinked composite PCMs.

TGA measurements were performed at the Experimental Technique Centre (ETC), Brunel University London, on powder samples using the TA instrument (SDT Q600 model) shown in Figure 3.19 (A) by heating the test sample of mass in the range 8-10 mg under nitrogen atmosphere from 25 °C to 600 °C at a heating rate of 10 °C/min.
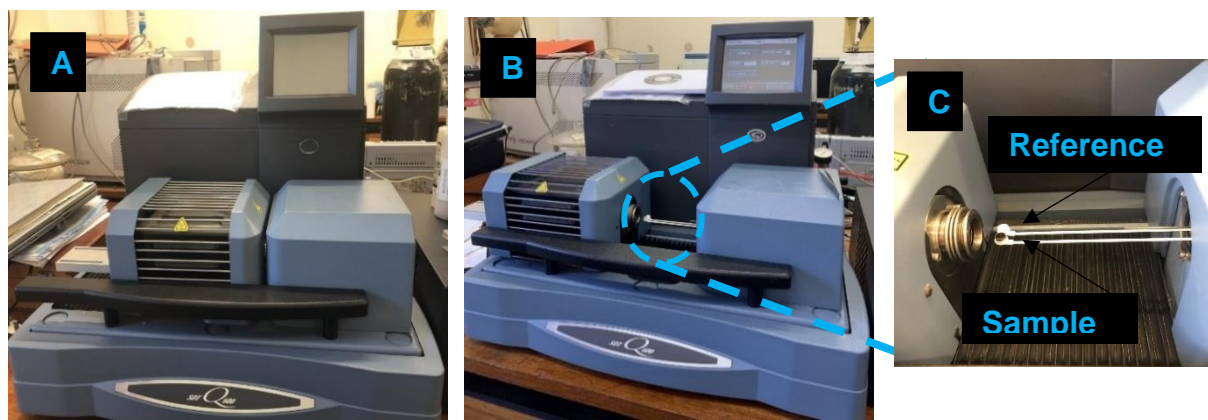
Figure 3. 19 (A) TA instrument (SDT Q600); (B) Furnace.

3.15 X-ray powder diffraction (XRD)

Powder X-ray diffraction (XRD) analysis is classified as a non-destructive technique since it causes no damage to the sample during analysis, and it is conventionally used in material science to evaluate the crystallographic structure of materials which can be defined as the underlying crystal structure of the chosen material. Moreover, using the XRD data obtained it is possible to derive information regarding the crystalline composition e.g., whether material contains crystalline, semi-crystalline or amorphous phases from the calculated crystallinity index (CI) value.

3.15.1 XRD sample preparation

Powder samples were prepared using the Laarman Wizz 320 Micro ball mill shown in Figure 3.20. The solid sample pieces were placed inside the metal jar (see Figure 3.20 (A)) and time was set to 2 mins. The appearance of the final product is shown in Figure 3.20 (B). The powder was evenly distributed over the sample holder as shown in Figure 3.20 (C) for the XRD analysis.

Figure 3. 20 Laarman Wizz 320 Micro ball mill.

Figure 3. 21 (A) Metal jar containing ball and solid sample pieces; (B) Powder sample; and (C) XRD sample holder containing test sample.

3.15.2 XRD analysis

Powder XRD analysis is a technique was performed at the Experimental Technique Centre (ETC), Brunel University London, on the Bruker D8 advanced diffractometer with CuKα radiation (shown in Figure 3.22) to examine the phase characteristics such as the crystallinity of PEG and its composite PCMs using XRD measurements obtained. During analysis the surface of the test samples were irradiated with incident X-rays and measurements of intensities and angle scattering of X-rays were measured and recorded. Diffraction angles were measured from 5 to 100°. A full angle range were selected in the current study for the characterisation of the crosslinked PEG based composite PCMs since this information is unavailable in literature for the chemical compositions investigated. Data obtained from XRD analysis in form of an XRD pattern was used to determine the crystallinity of the composite PCM samples.
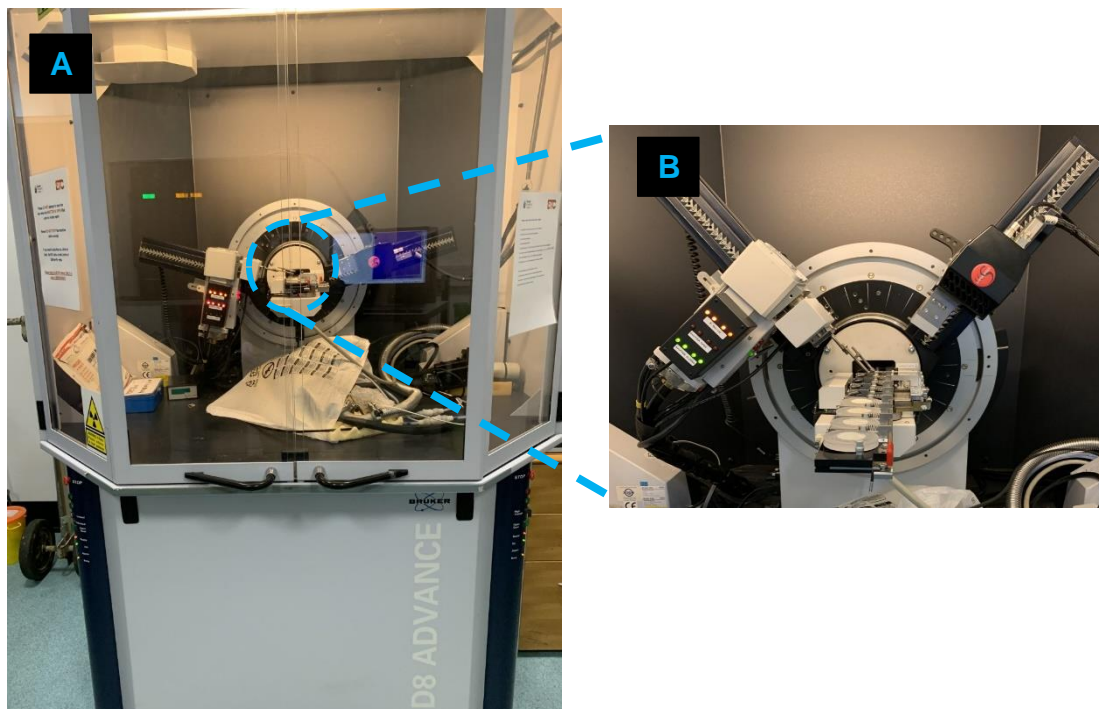
Figure 3. 22 (A) Bruker D8 advanced diffractometer; and (B) shows zoomed in view of test samples.

3.15.3 XRD data analysis

The XRD patterns were first plotted using the Origin Lab software, and the area under the crystalline peaks and amorphous peaks were determined through integration and values were recorded. The crystallinity index was calculated using equation (5) and this value is considered as a quantitative indicator of the crystallinity of a chosen material. From the determined CI value, it is possible to determine whether the chosen material is crystalline, semicrystalline, or amorphous. In general, for PCMs like PEG its crystallinity index dictates its thermal properties and may indicate changes in the crystalline properties.

$$CI\ (\%) = \frac{area\ of\ crystalline\ peaks}{area\ of\ crystalline\ and\ amorphous\ peaks} \times 100\% \qquad (5)$$

3.16 Interim Conclusions

This Chapter has provided the details of the materials used and methodologies employed for the preparation of the different crosslinked composite PCMs reported in Chapters 5,6 and 7. The approaches followed to perform the different characterisation analysis namely FTIR, SEM, POM, DSC, TGA and XRD for the attainment of accurate experimental results, and methodologies employed for the interpretation of data obtained are thoroughly explained in this Chapter.

Chapter 4: Characterisation of raw materials

Abstract

This chapter presents the intrinsic characteristics of PEG, supporting material and crosslinkers used in current study. The analytical results provide useful information regarding the chemical, physical, thermal, and crystalline properties of pristine PEG, the polymeric PCM used in current study, since these properties are known to affect the latent heat and phase transition temperature of PEG.

4.1 Introduction

The raw materials used for the stabilisation of solid-liquid PCM like PEG plays a major role in dictating the final properties of the resulting composite PCMs. Therefore, it is critical to investigate, study and understand the chemical structure, surface morphology, crystal morphology, crystalline properties and thermal properties of raw materials used in the current study for the preparation of PEG-cellulose based composite PCMs.

This chapter aims to characterise in detail the raw materials namely PEG, MC cellulose/ cellulose fibre and citric acid individually through analytical techniques including FTIR, SEM, XRD, DSC, TGA and POM. There is a need to compile all relevant information available to produce PEG based composite PCMs of optimised thermal performance and to find convenient ways of tailoring the phase transition temperature to match the operating temperature of the intended application e.g., building. Therefore, information provided in this study will serve as a useful database to better understand the formulation mechanism of stabilised PEG composite PCMs.

4.2 Methods

4.2.1 Visual examination

This was performed by observing the digital photographs captured to determine the suitable reaction temperature, MW radiation exposure and CA concentration.

4.2.2 ATR-FTIR

This was performed to determine the chemical composition and structure of all raw materials used in this thesis and results obtained was used to understand the experimental results presented in the other chapters. Also, to confirm whether chosen materials contain the required functional groups to participate in the relevant crosslinking reactions studied in current study.

4.2.3 Powder XRD

This was performed to determine the degree of crystallinity of all materials used in the study because this will be useful when studying the changes caused to the crystalline properties of PEG after chemical crosslinking. Mainly because crystalline properties of polymeric PCMs like PEG influences the phase change properties like latent heat greatly, and by studying the crystallinity using the XRD results allows the identification of material(s) that impacts the phase change properties of PEG negatively.

4.2.4 DSC

This was performed to determine the thermal properties of all materials used; thus, to determine the latent heat and melting temperature of PEG used in current study before chemical crosslinking since this allows the changes in thermal properties to be evaluated after chemical crosslinking. The thermal properties of other materials were also determined to confirm that they make no contribution to latent heat.

4.2.5 TGA

TGA was performed to determine the thermal stability of PEG, CA and CF by studying their thermal degradation process in nitrogen atmosphere at a heating rate of 10 °C/min from 30 to 650°C.

4.2.6 SEM analysis

This was performed to study the surface morphology of raw materials since this will allow predictions regarding its behaviour during chemical reactions to be made. Hence, the SEM images was used to plot histograms and thus to determine the particle size of all materials used in current study.

4.2.7 POM/ hot stage analysis

Changes in the spherulitic crystal structure of pristine PEG (e.g., crystal morphology) after chemical crosslinking reaction was studied and evaluated using polarised optical microscopy analysis.

4.3 Results and discussion

4.3.1 Determination of suitable curing temperature

In general, chemical reactions like crosslinking are influenced greatly by the reaction temperature. Therefore, it is important to ensure that sufficient temperature is used otherwise no reaction will occur which is attributed to the availability of insufficient energy to break the existing bonds of the reactants and as result no new bonds will form. However, current thesis works on studying PEG as functional PCMs and therefore, it was critical to ensure that very high temperatures were avoided since they have high chances of degrading the intrinsic thermal properties of PEG because elevated temperature exposure causes thermal degradation of PEG resulting in colour changes from white to yellow. To evaluate the suitable curing temperature to encourage chemical crosslinking of composite PCMs prepared via TCA crosslinking reaction two different temperatures were selected and used including (I) 50 °C (e.g., lower than T_m of PEG8000); and (II) 80 °C (e.g., higher than T_m of PEG8000). For the determination of the suitable curing temperature reaction mixture were poured into two moulds (e.g., petri dish). One mould was cured at 50 °C while the other mould was cured at 80 °C for 24 hours. Based on the physical property of the resulting composite PCM the suitable curing temperature was selected.

The purpose of the slow evaporation method was to cause complete evaporation of water which should consequently result in producing a solid material with a homogenous surface. This was only achieved with 80 °C oven curing for 24 h while

Figure 4. 1 Appearance of TCA samples cured at 50 °C for 24h.

108

50 °C curing for 24 h resulted in producing non-homogenous wet samples as shown Figure 4.1 which demonstrated that this temperature was too low to encourage chemical crosslinking reaction; therefore, was not selected as suitable curing temperature in the current study.

Allowing these wet samples to dry/ cure at room temperature for three weeks led to the formation of radial structures as shown in Figure 4.3 (a) and (b). They appeared as typical spherulites which are usually comprised of nanocrystals arranged radically resulting in the production of a cross-extinction pattern. The possible cause for this may be attributed to the presence of PEG8000 which a semicrystalline polymer consisting of spherulitic crystals. This suggested that this temperature was not sufficient to cause water evaporation and did not encourage bond formation between PEG and CF via TCA crosslinking. Therefore, 80 °C was selected as the suitable curing temperature in throughout this thesis.
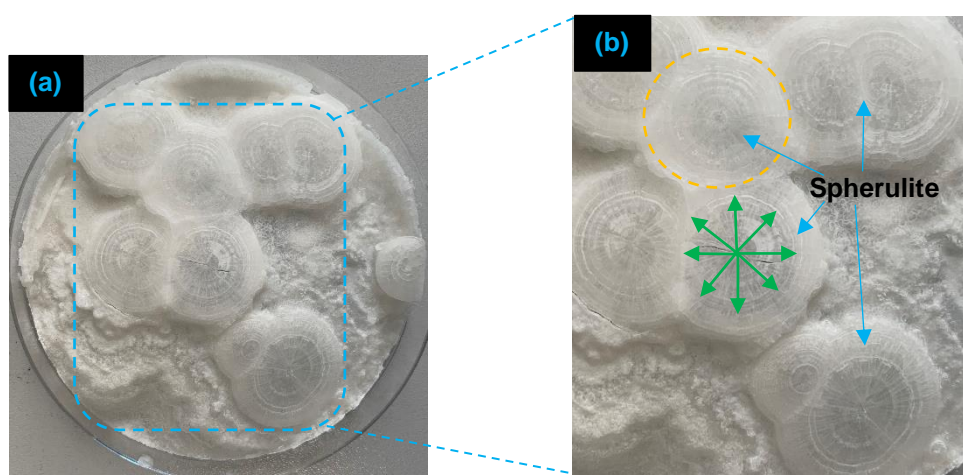
Figure 4. 2 (a) Appearance of TCA composite PCMs formed at 50 °C; and (b) close-up view of the spherulites.

4.3.2 Determination of suitable MW radiation intensity and duration

The purpose of MW irradiation was to evaluate its influence on the crystalline properties of PEG. Excess MW irradiation will cause thermal degradation of the crystalline and thermal properties of PEG; therefore, it was critical to evaluate the suitable powder intensity (e.g., function of the temperature) and duration to minimise undesirable changes in its intrinsic characteristics. The power intensity of the domestic MW oven used was 10, 30, 50 and 100%; however, using power intensity greater than 10% resulted in burning the polymeric reaction mixture which was confirmed by a colour change from white to yellowish brown due to thermal degradation of PEG. Also,

at increased MW duration the reaction mixture became almost dry, and volume of mixture reduced drastically due to complete evaporation of water. This consequently resulted in affecting the homogeneity of the final composite PCMs produced because the reaction mixture became extremely adhesive and could hardly be spread out to form a film of even surface.

4.3.3 Determination of suitable CA concentration

In the current study CA was used as the crosslinker; and therefore, its concentration was believed to play a major role in determining the degree of crosslinking which impacts the three-dimensional covalently bonded network formed after the chemical reaction. Selected combinations along with their appearance are presented in Figure 4.3.

Combination	1	2	3	4
Appearance				
Combination	5	6	7	8
Appearance				
Combination	9	10	11	12
Appearance				
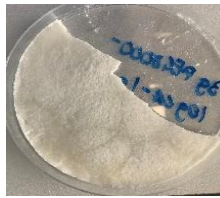
Figure 4. 3 Appearance of PEG-CF composite PCMs produced using different CA concentrations.

Observations indicated that combinations 1,5 and 9 produced samples of poor physical property since they were very soft and adhesive. Therefore, they got damaged during the demoulding process while the remaining combinations produced

composite PCMs of adequate physical property. Hence, they were selected as suitable combinations for further investigation in the current study. Overall, composite PCMs prepared using low concentrations were highly adhesive while increasing the concentration from 30 wt./v% to 50 wt./v% resulted in producing samples of reduced opacity and enhanced flexibility. Further increase in CA concentration resulted in producing rigid samples of brittle nature with a rough surface which indicated obvious changes in the crystalline properties of PEG. Also, results showed that the crystalline properties of TCA crosslinked composite PCMs varied with the chemical composition; therefore, the thermal properties were also expected to change accordingly, and this was studied extensively, and results were reported in Chapters 6 and 7.

4.3.4 Chemical characterisation analysis of raw materials

4.3.4.1 Chemical composition of PEG with different M_w

To evaluate the relationship between the molecular weight (Mw) of PEG and its chemical structure, FTIR spectra of PEG8000, PEG4000 and PEG1000 presented in Figure 4.5 were compared.

Observations indicated that all had very similar FTIR spectra patterns despite having different chain lengths mainly because they were all made up of the same monomer unit. The FTIR spectra pattern of PEG8000, PEG4000 and PEG1000 in the fingerprint region (e.g., 500 to 1500 cm^{-1}) all had very similar patterns which suggested that the chemical structure and composition of PEG was not dictated by the molecular weight of the chain.

The characteristic peaks of PEG8000, PEG4000 and PEG1000 appeared at wavenumbers 3480 cm^{-1}, 2800 cm^{-1} and 1960 cm^{-1} which are ascribed to the stretching vibration of the OH and CH groups in the skeletal of PEG. The intensity of peak corresponding to the presence of OH group varied with Mw. Thus, PEG1000 contained higher number of OH group attributed to the presence of a more intense broad peak at 3480 cm^{-1} which suggested that PEG1000 is more hydrophilic than PEG4000 and PEG8000; and therefore, is more likely to produce unstable composite PCMs.
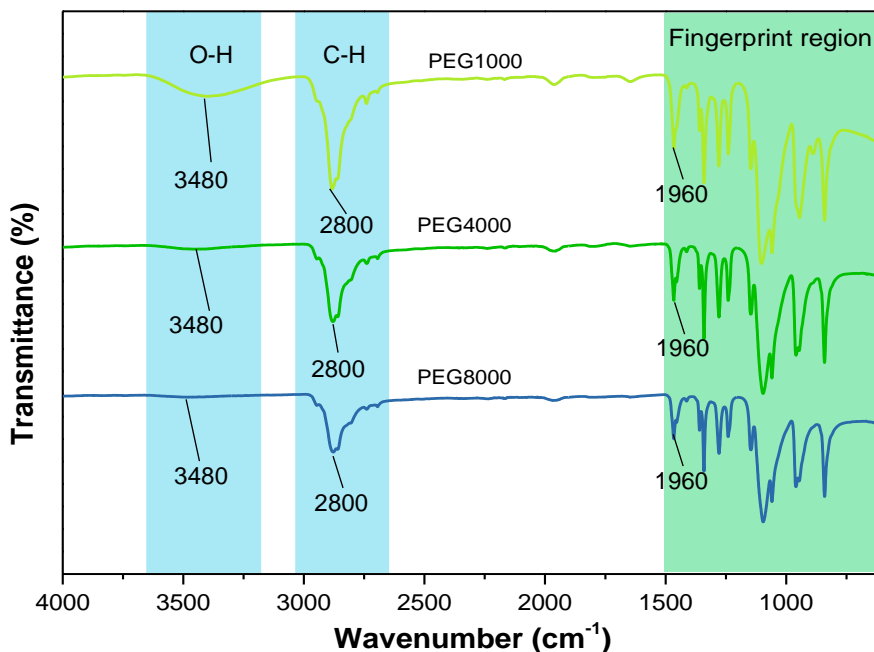
Figure 4. 4 FTIR spectra of PEG1000, PEG4000 and PEG8000.

4.3.4.2 Effects of MW irradiation on chemical structure of PEG

To study the effects of MW irradiation on chemical structure of PEG8000 after 10 min and 20 min MW radiation exposure, the FTIR spectra of both unirradiated and MW irradiated PEG8000 presented in Figure 4.5 were compared. Observation showed that no significant changes occurred to the absorption peak positions and obvious changes in intensity of the characteristic peaks were not observed; however, results indicated that the intensity of characterisation peak at 2800 cm^{-1} increased from 90.86% to 146.18% and 209.97% after 10 min and 20 min MW exposure which indicated that some changes may have occurred to the content of OH groups or to the polarity of the O-H bond. Overall results demonstrated that no chemical structure changes had occurred after MW radiation exposure.
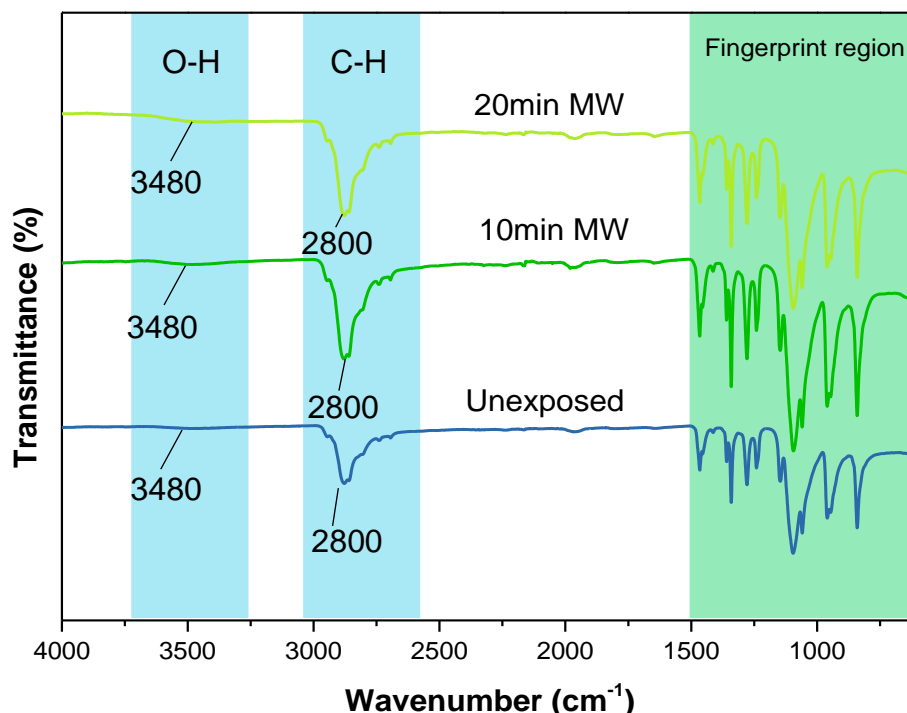
Figure 4. 5 FTIR spectra of unirradiated and MW irradiation PEG8000.

4.3.4.3 Functional groups of cellulose and its derivatives

To determine the chemical composition and structure of both MCC and CF the FTIR spectra of both supporting materials presented in Figure 4.6 were compared.
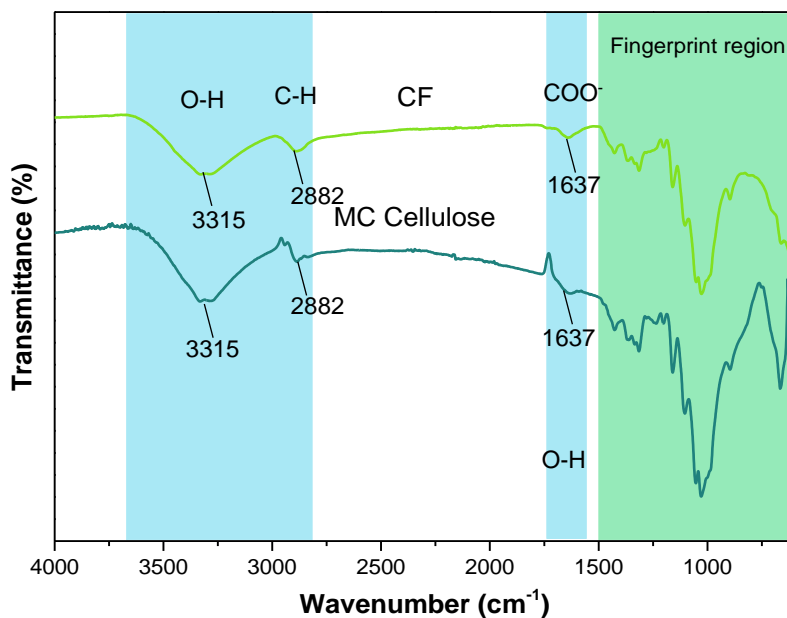
Figure 4. 6 FTIR spectra of CF and MCC.

Results indicated that MCC and CF both exhibited very similar FTIR pattern. The spectra pattern in the fingerprint region (500 to 1500 cm^{-1}) appeared to be identical which confirmed the fact that both MCC and CF had very similar chemical structures. The characteristic peaks of CF and MCC appeared at 3315 cm^{-1}, 2882 cm^{-1} and 1637 cm^{-1} which were ascribed to the stretching vibration of O-H bonds, stretching vibration of C-H bond, and O-H bending of absorbed water (Oh et al., 2005). Presence of broad wide peak at 3315 cm^{-1} corresponding to the OH stretching vibration indicated that both MCC and CF will participate readily in PU and TCA crosslinking reaction as OH donors.

4.3.4.4 Chemical structure of MW irradiated CF

The FTIR spectra of unirradiated and MW irradiated CF are presented in Figure 4.7. The characteristic peaks of CF appearing at 3324 cm-1, 2887 cm-1 and 1641 cm-1 corresponding to the stretching vibration of the OH group, C-H and carboxyl asymmetric stretching vibration undergoes no significant changes in position after MW irradiation; however, intensity of peak at 3324 cm-1 appears to have reduced which indicated that the OH group content had reduced after MW irradiation exposure attributed to the evaporation of water molecules from its chemical structure (Rahimi Kord Sofla et al., 2016). Also, changes in peak intensity suggested that the polarity
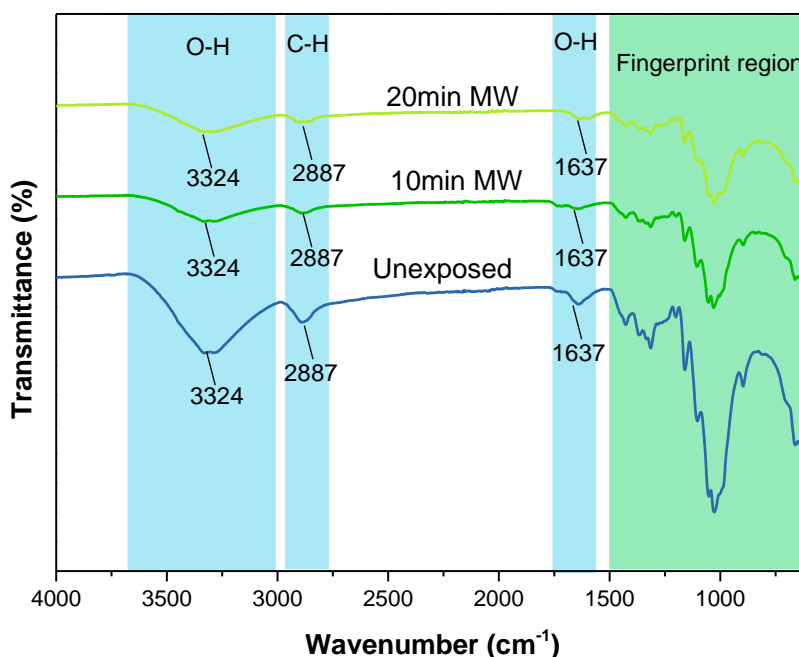
Figure 4. 7 FTIR spectra of unirradiated and MW irradiated CF.

strength of the O-H bond appearing at 3324 cm-1 had changed. Hence, OH bonds

became weaker after MW radiation exposure confirmed by the reduction in peak intensity. Table 4.1 summarises the assignment of the characteristic peak positions of the unirradiated and MW irradiated CF.

Table 4. 1 Assignment of ATR-FTIR spectra of both unirradiated and MW irradiated CF.

Wavenumber (cm⁻¹)	Assignment	Reference
3324	Stretching of -OH group	(Capanema et al., 2018; Kaewprachu et al., 2022; Tangthuam et al., 2020)
2887	C-H stretching vibration	
1641	Carboxyl groups (COO-) asymmetric stretching	
1429	Carboxyl groups (COO-) and CH_2 scissoring	
1314	O-H bending	
1026	$CH-O-CH_2$ bending	

4.3.4.5 Functional groups of CA and TDI

Figure 4.8 compares the FTIR spectra of CA and TDI (e.g., crosslinkers used in the current study).
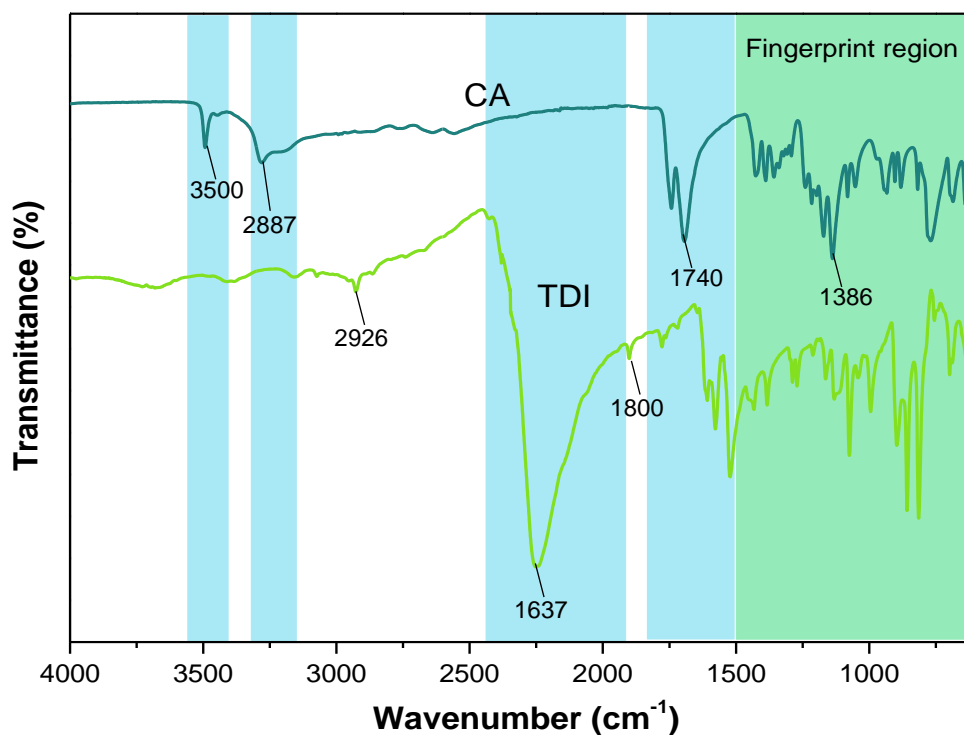
Figure 4. 8 FTIR spectra of CA and TDI.

115

The intense peak at 2256 cm^{-1} attributed to the presence of plentiful of isocyanate groups (-NCO). This suggested that TDI will readily react with PEG and MCC since both polymers comprised of plentiful of -OH groups. The medium band appearing at 1612 cm^{-1} is attributed to the imine stretching vibration of C=N group. The weak absorption peaks appearing at 1800 cm^{-1} and 1496 cm^{-1} are attributed to the C=C stretching vibration of the benzene ring (C$_6$H$_6$). Weak band at 2926 cm^{-1} is attributed to the aliphatic stretching vibration of the C-H bond. The strong peak at 1522 cm^{-1} indicated the aromatic stretching vibration of the C=C bond.

The characteristic peaks of CA at 3492 cm^{-1} to 3283 cm^{-1}, 1740 cm^{-1} to 1693 cm^{-1}, 1386 cm^{-1} to 1139 cm^{-1} was ascribed to the O-H stretching vibration, C=O stretching vibration and C-O stretching vibration. Assignment of characteristic peak positions of TDI crosslinker is summarised in Table 4.2.

Table 4. 2 ATR-FTIR assignment of TDI.

Wavenumber (cm^{-1})	Transmittance (%)	Assignment	Reference
3688	81.6	O-H stretching vibration	(Alemdar et al., 2005; Gök et al., 2019; Shetty et al., 2019)
3071	84.3	C-H group stretching vibration	
2926	80.5		
2236	15.5	Isocyanate (N=C=O) group	
1607	54.7	Aromatic C=C stretching	
1576	48.1	C-C group in the benzene ring stretching vibration	
1524	36.6		
1433	52.3	Aromatic C=C stretching	
1384	53.5	C-H group stretching vibration	

4.3.4.6 Chemical structure of unirradiated and MW irradiated CA

Figure 4.9 presents the FTIR spectra of unirradiated and MW irradiated CA. The main characteristic peaks are observed at 3492 cm^{-1} to 3283 cm^{-1}, 1740 cm^{-1} to 1693 cm^{-1}, 1386 cm^{-1} to 1139 cm^{-1} which corresponds to the O-H stretching vibration, C=O stretching vibration and C-O stretching vibration. Observations indicated that no changes occurred to the peak positions after MW irradiation exposure; however,

changes in the intensity of the peaks occurred which indicated changes in the polarity of the existing polar bonds.
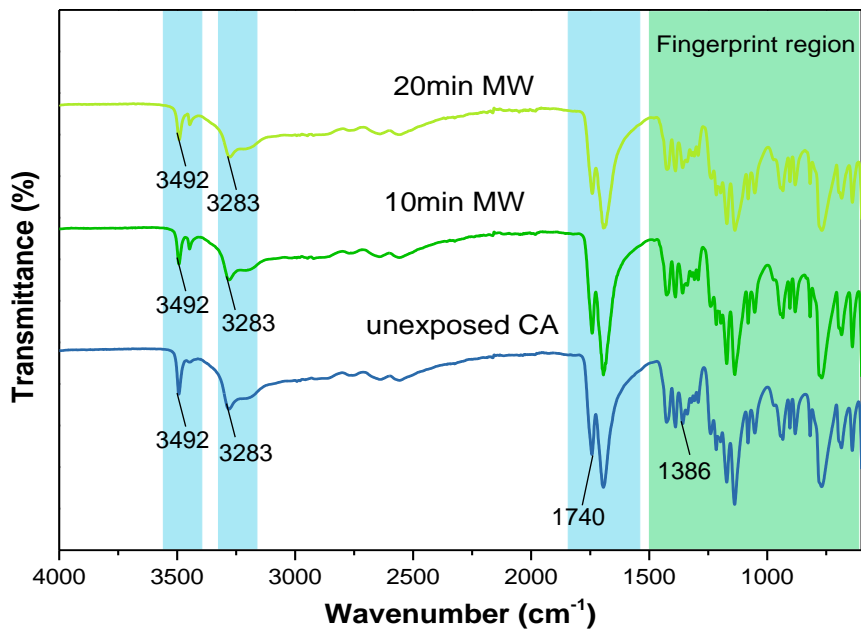
Figure 4. 9 FTIR spectra of unirradiated and MW irradiated CA.

Assignment of characteristics peak positions unexposed and MW radiation exposed CA crosslinker is summarised in Table 4.3.

Table 4. 3 Assignment of ATR-FTIR spectra of unirradiated and MW irradiated CA.

Name	Wavenumber (cm⁻¹)	Intensity (%)	Description	Reference
CA	3492	87.6	O-H stretching	(Capanema et al., 2018; Qin et al., 2019a)
	3283	84.0		
	1740	73.8	-C=O stretching vibration of ester	
	1693	65.2		
	1386	80.5	C-O stretching vibration	
	1169	67.1		
	1139	61.1		
10 min MW CA	3492	90.7	O-H stretching	
	3448	94.3		
	1742	78.3	-C=O stretching vibration of ester	
	1691	70.1		
20 min MW CA	3492	91.2	O-H stretching	
	3447	94.8		
	1740	74.4	-C=O stretching vibration of ester	
	1695	64.2		

4.3.5 XRD analysis of raw materials

4.3.5.1 Crystalline properties of pristine PEG

The XRD patterns of pristine PEG8000 and PEG4000 are presented in Figure 4.10. They were used to determine the crystallinity of PEG8000 and PEG4000. Observations indicated that both PEG8000 and PEG4000 had similar XRD patterns, since they both exhibited characteristic crystalline peaks at 2θ = 19.10° and 23.23° which is consistent with their crystalline nature (Shah et al., 2018). The two sharp peaks appearing at mentioned positions represent the highly ordered crystalline phases of PEG and corresponds to the crystal lattice planes (1 2 0) and (0 3 2) of its crystals (Deshpande et al., 2021; Jing et al., 2022). Observations suggested that PEG8000 and PEG4000 is comprised of both crystalline and amorphous phases since their XRD patterns only contain two sharp crystalline. Hence, a crystalline material will

contain numerous crystalline peaks. Also, presence of minor humps corresponds to the existence of amorphous phases in PEG8000 and PEG4000.
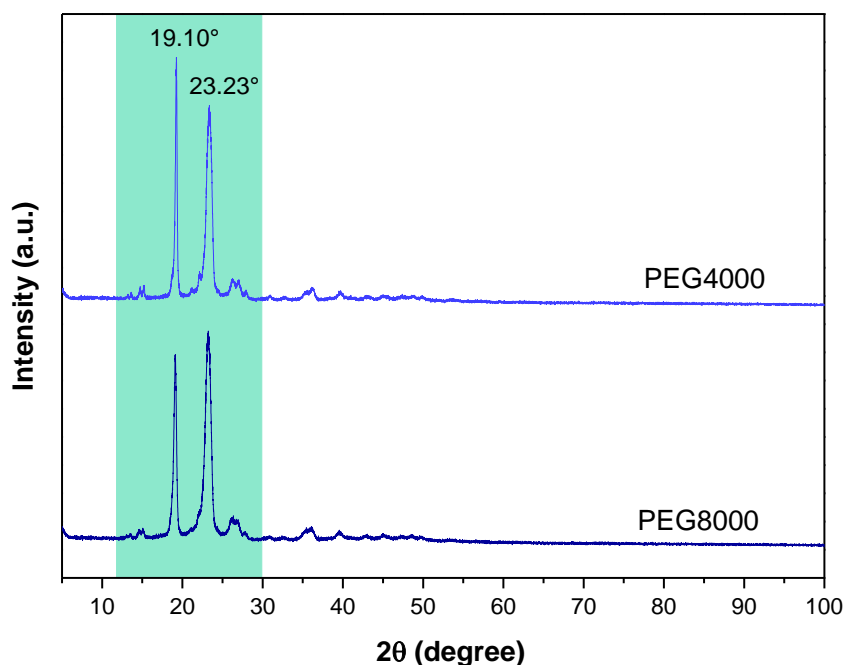
Figure 4. 10 XRD patterns of PEG4000 and PEG8000.

4.3.5.2 Changes caused to crystallinity of PEG8000 by MW irradiation

The XRD patterns of unirradiated and MW irradiated PEG8000 are presented in Figures 4.11. Observations showed that no new peaks had formed after MW irradiation. Also, no significant changes had occurred to the crystalline peak positions and intensities after MW irradiation which indicated that the crystallinity of PEG was unaffected by MW irradiation (Deshpande et al., 2021). However, the XRD results showed that 20 min MW irradiation caused the peak at $2\theta= 19.10°$ of intensity 3367% to shift to the right to become $2\theta= 19.15°$, and the intensity changed from 3367% to 3702%. The crystalline peak at $2\theta= 23.23°$ with relative peak intensity of 3772% became 23.30° and 23.34° after 10 min and 20 min MW irradiation. Overall, results indicated that MW irradiation had induced changes in the crystalline properties of PEG8000 which was attributed to the formation of crystal defects, and the reduction of crystal size. Therefore, the crystalline properties of PEG8000 were impacted negatively by MW irradiation (Qin et al., 2019a).
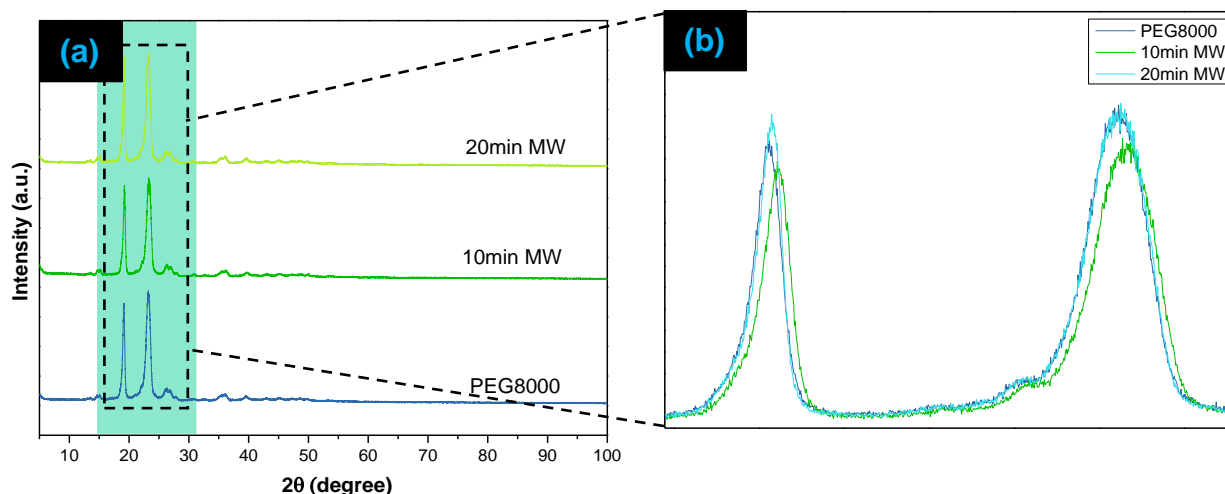
Figure 4. 11 (a) XRD patterns of the unirradiated and MW irradiated PEG8000; and (b) compares the crystalline peaks.

4.3.5.3 Crystalline properties of unexposed and MW exposed CA

The XRD patterns of the unirradiated and MW irradiated CA are presented in Figure 4.12. Observations showed that CA is a highly crystalline material. MW irradiation resulted in forming no new peaks. However, changes in the crystalline peak intensities were observed after ten and twenty minutes of MW irradiation which suggested changes in the crystalline properties (Jing et al., 2022).
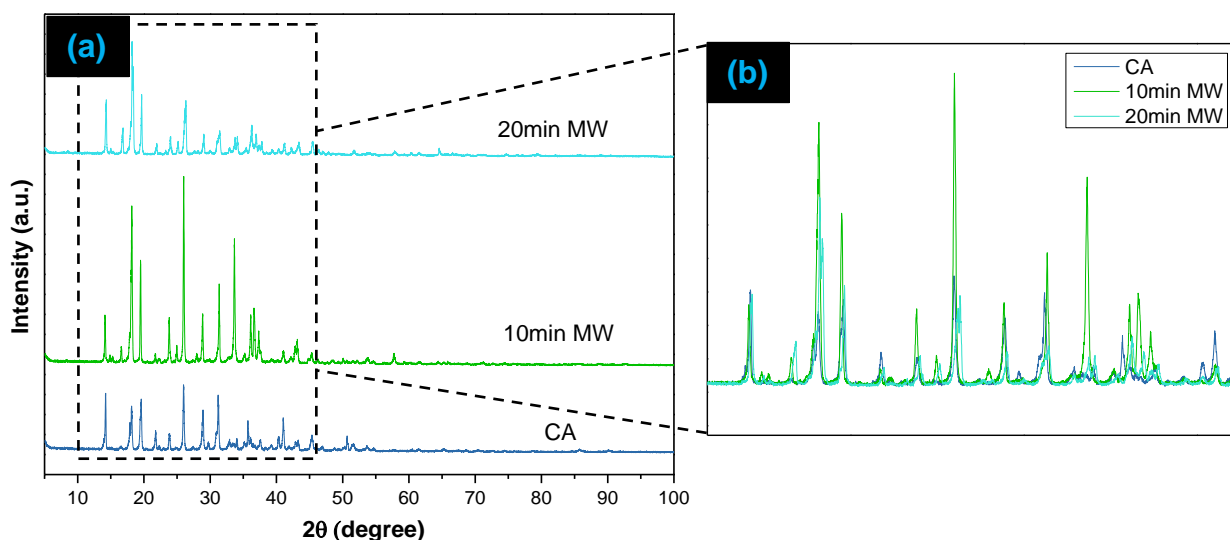
Figure 4. 12 (a) XRD pattern of unirradiated and MW irradiated CA; and (b) characteristics peaks comparison.

4.3.5.4 Crystalline properties of unexposed and MW exposed CF

Figure 4.13 presents the XRD patterns of unirradiated and MW irradiated CF. XRD pattern of CF has one broad peak appearing as a hump at 2θ= 15.50° and a peak at 2θ= 22.40° with a broad underlying feature indicating the presence of highly amorphous structures in CF (Sundararajan et al., 2017a). Absence of sharp crystalline peak suggested that CF was mainly comprised of amorphous phases. Observations show that no significant changes had occurred to the XRD pattern of CF after MW irradiation which means the crystallinity of CF was unaffected by MW irradiation. However, Figure 4.13 (a) shows that the relative intensity of peaks at 2θ= 15.50° reduced from 623% to 560% after MW irradiation while the peak 2θ= 22.40° reduced from 1244% to 994% and then increased to 1106% after 10 min and 20 min MW irradiation which confirmed changes in crystallinity of CF due to the disruption caused by MW irradiation to its the crystalline structure (Kaewprachu et al., 2022). Increase in crystallinity usually occurs due to the removal of hemicellulose and lignin. The crystallinity of CF is likely to increase if the number of amorphous phases decrease. The amorphous regions are known to contain higher number of free hydroxyl groups compared to the crystalline region (Song et al., 2021); and therefore, results suggested that CF contained a plentiful of OH groups since it appeared to be an amorphous polymer.
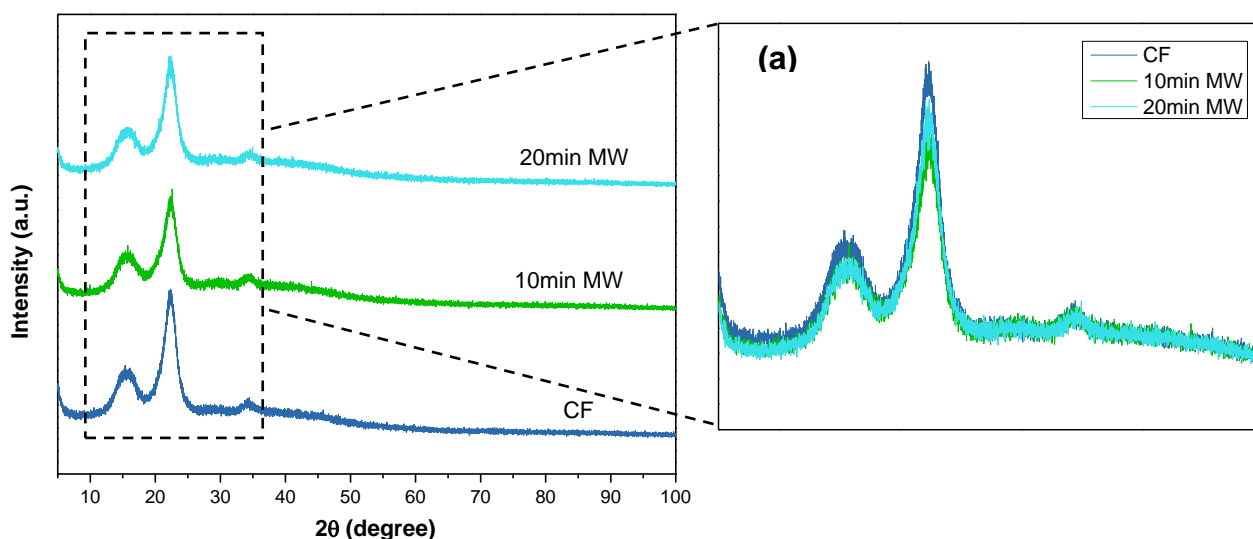
Figure 4. 13 XRD patterns of the unirradiated and MW irradiated CF; and (a) compares the main characteristics peaks.

4.3.5.5 Crystallinity indices of PEG, CF, and CA

The crystallinity index (CI) values of the unirradiated and MW irradiated PEG, CF and CA are presented in Figure 4.14 and Table 4.4. Results indicated that PEG8000 and PEG4000 were both semicrystalline polymers in which crystalline and amorphous phases coexist; therefore, they are crystallisable (e.g., can form crystals) (Pielichowska et al., 2008). The CI of pristine PEG8000 was observed to increase from 51.51% to 52.24% and then returned close to its original CI value after 10 min and 20 min MW irradiation which demonstrated that MW irradiation could rearrange the crystalline phases of PEG; and thereby, change its crystalline properties. The CI value of PEG4000 increased from 49.41% to 58.52% after 10 min MW irradiation, and the value dropped to 51.50% after 20 min MW irradiation. Overall, results suggested that MW irradiation caused a degree of destruction to the crystal lattice structure of PEG8000 and PEG4000; however, the impact of MW irradiation on the crystalline properties of PEG in the crosslinked composite PCMs is still unknown. This in good agreement with the XRD analysis results. Results indicated that CF is an amorphous polymer because it comprised of 60. 02% of amorphous phases; and therefore, is a non-crystallisable polymer. Ten min MW irradiation resulted in increasing its CI value from 39.98% to 51.59% but twenty min MW irradiation reduced it back close to its original CI value (e.g., 38.98%).
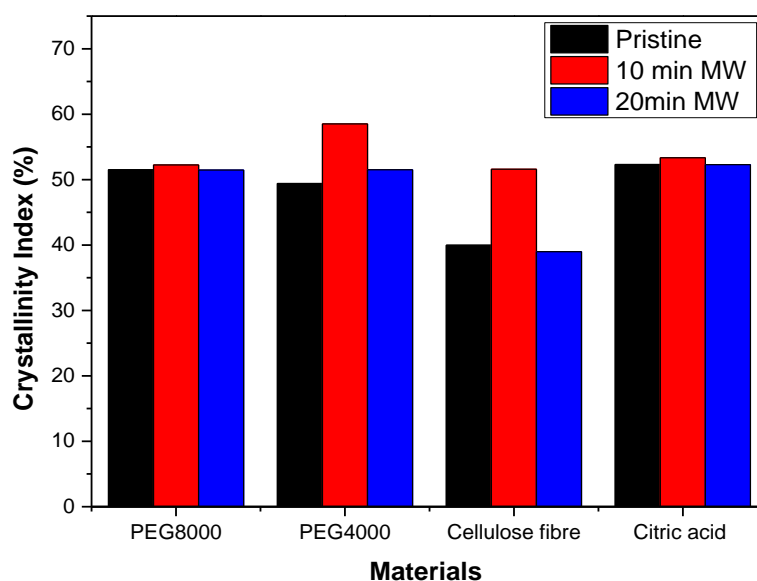
Figure 4. 14 CI of unirradiated and MW irradiated PEG, CF, and CA.

Table 4. 4 CI values of unirradiated and MW irradiated PEG, CF, and CA.

Material	Crystalline phases (%)	Amorphous phases (%)	CI (%)
PEG8000	52.94	48.49	51.51
10 min MW PEG8000	52.24	47.76	52.24
20 min MW PEG8000	51.47	48.53	51.47
PEG4000	49.41	50.59	49.41
10 min MW PEG4000	58.52	41.48	58.52
20 min MW PEG4000	51.50	48.50	51.50
CA	52.30	47.70	52.30
10 min MW CA	53.34	46.66	53.34
20 min MW CA	52.28	47.72	52.28
CF	39.98	60.02	39.98
10 min MW CF	51.59	48.41	51.59
20 min MW CF	38.98	61.02	38.98

4.3.6 Thermal property and stability characterisation

DSC analysis was performed on PEG8000, CF and CA to determine their thermal properties since this will influence the thermal performance of the crosslinked products prepared in the current study. The thermal properties were determined using procedure explained in Chapter 3.

4.3.6.1 The phase change properties of PEG8000

Figure 4.15 presents the DSC heating and cooling curves of the unirradiated and MW irradiated PEG8000; and Table 4.5 summarises its thermal properties. Observation indicated that unirradiated and MW irradiated PEG8000 exhibited the typical single endothermic and exothermic peak during the heating and cooling process which was attributed to the presence of a single type of crystal in PEG (e.g., spherulite crystals). Due to its relatively high molecular weight, PEG8000 was observed to have a very high melting temperature of 63.12 °C with a corresponding latent heat capacity of 181.5 J/g along with a crystallisation temperature of 43.78 °C with a corresponding latent heat capacity of crystallisation of 182.1 J/g, respectively. Results from Table 4.5 indicated that PEG8000 shows a degree of supercooling which is a phenomenon by

which it is unable to crystallise under its normal crystallisation point instead it starts to crystallise at a much lower temperature. This is reported to cause energy extraction issues since energy stored by PEG in form of latent heat cannot be extracted completely. The supercooling temperature (ST) of unirradiated PEG8000 used in the current study was 19.34 °C. Results demonstrated that ten and twenty min MW irradiation of PEG resulted in enhancing the H_m from 181.5 J/g to 236.6 and 247.2 J/g; and H_c from 182.1 to 237.5 and 235.8 J/g. This suggested that MW irradiation had a desirable effect on the crystalline properties of PEG and was attributed to the melting of the amorphous phases (e.g., non-crystallisable component) which consequently resulted in increasing the number of crystalline phases (e.g., crystallisable component). Also, 10 min MW irradiation was observed to reduce the ST from 19.34 to 15.71 °C (e.g.,3.63% decrease) which was attributed to the enhanced nucleation due to the increased number of nucleating sites. However, 20min MW irradiation was observed to reduce the number of nucleating site because the ST was increased from 19.34 to 21.15 °C (e.g.,9.36% increase) (Cabaleiro et al., 2020, 2019). Overall, it can be concluded that MW irradiation had a desirable effect on the crystalline properties of PEG8000.

Table 4. 5 Thermal properties of unirradiated and MW irradiated PEG8000.

Material	Phase transition temperature		ST (°C)	Latent heat	
	T_m (°C)	T_c (°C)		H_m (J/g)	H_c (J/g)
PEG8000	63.12	43.78	19.34	181.5	182.1
PEG8000 10min MW irradiation	60.46	44.75	15.71	236.6	237.5
PEG8000 20min MW irradiation	63.32	42.17	21.15	247.2	235.8
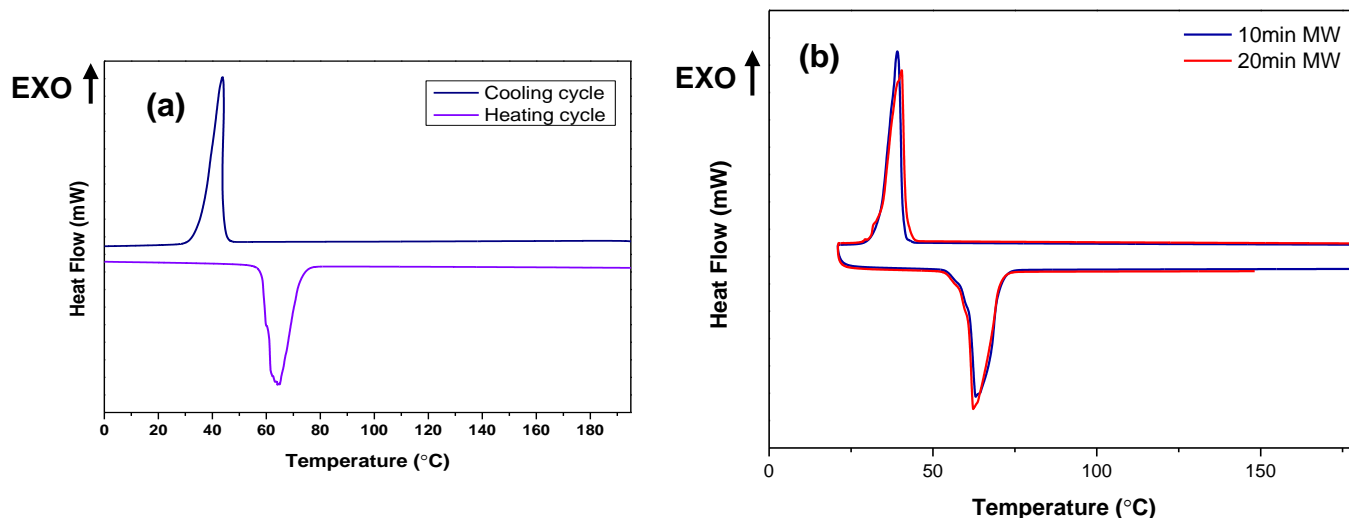
Figure 4. 15 The DSC heating and cooling curve of (a) unirradiated; and (b) MW irradiated PEG8000.

4.3.6.2 Thermal properties of MCC and CF

Figure 4.16 presents the DSC heating and cooling curves of CF and MCC; and their thermal properties are summarised in Table 4.6. DSC analysis was used to evaluate the thermal properties of CF and MCC (e.g., supporting material) to determine whether the supporting materials used in the current study makes contribution to latent heat. Observations indicated that CF and MCC exhibited very poor thermal properties which is in good agreement with previous literature which reports that supporting materials make no contribution to latent heat. During the melting process at 88.96 °C and 91.05 °C both materials appeared to have stored 109.1 J/g and 118.5 J/g of energy in form of sensible heat as result of experiencing a temperature change during the heating process. During the cooling process CF appeared to show almost no PCM behaviour because it produced a single exothermic peak at 46.27 °C with a corresponding latent heat of crystallisation of 1.63 J/g, and during the third heating cycle it produced an endothermic peak at 59.62 °C with a corresponding latent of melting of 1.67 J/g. Overall, the values of latent heat capacity of melting and crystallisation of CF were insignificant which means CF used as supporting material in the current study was a non-crystallisable material.
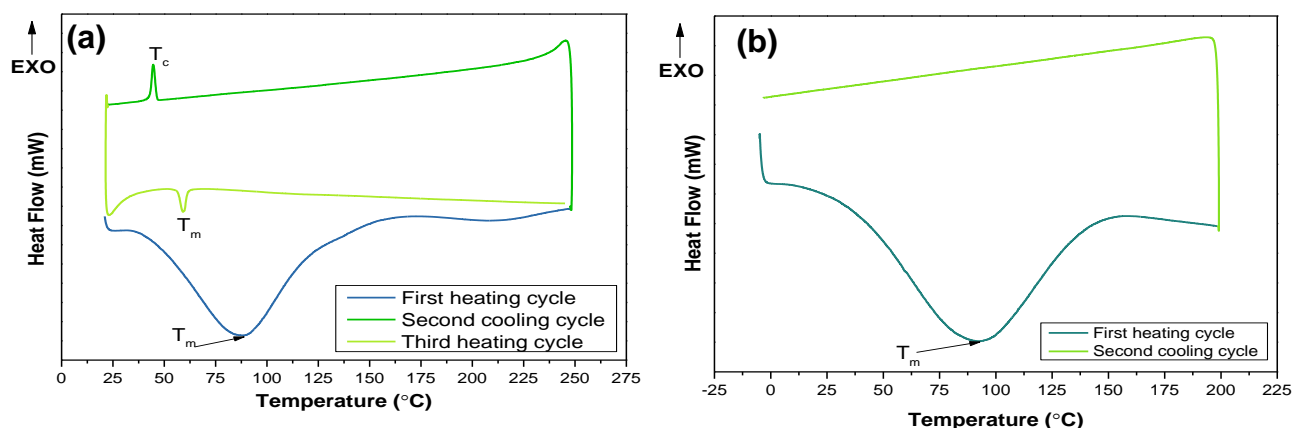
Figure 4. 16 The DSC heating and cooling curves of (a) CF and (b) MCC.

Table 4. 6 Thermal properties of CF and MCC.

Material	Phase transition temperature (°C)		ST (°C)	Latent heat (J/g)	
	T_m	T_c		H_m	H_c
MCC	91.05		NA	NA	118.5	NA
CF	88.96	59.62	46.27	13.35	109.1	1.67	1.63

4.3.6.3 Thermal properties of CA

Figure 4.17 shows the DSC heating and cooling curve of pristine CA while Table 4.7 summarises its thermal properties. Observations indicated that CA undergoes melting at 157.98°C which demonstrated the requirement of a significant amount of energy to overcome the strong covalent bonds existing in the CA structure. This suggested that enough energy was required to carry out the crosslinking reaction using CA as crosslinker. Therefore, in the current study 80 °C was used during the dissolution process which was more than enough since CA dissolves completely in water at 20 °C. Results showed that CA makes no contribution to latent heat because latent heat of melting was determined to be 7.29 J/g which is insignificant.
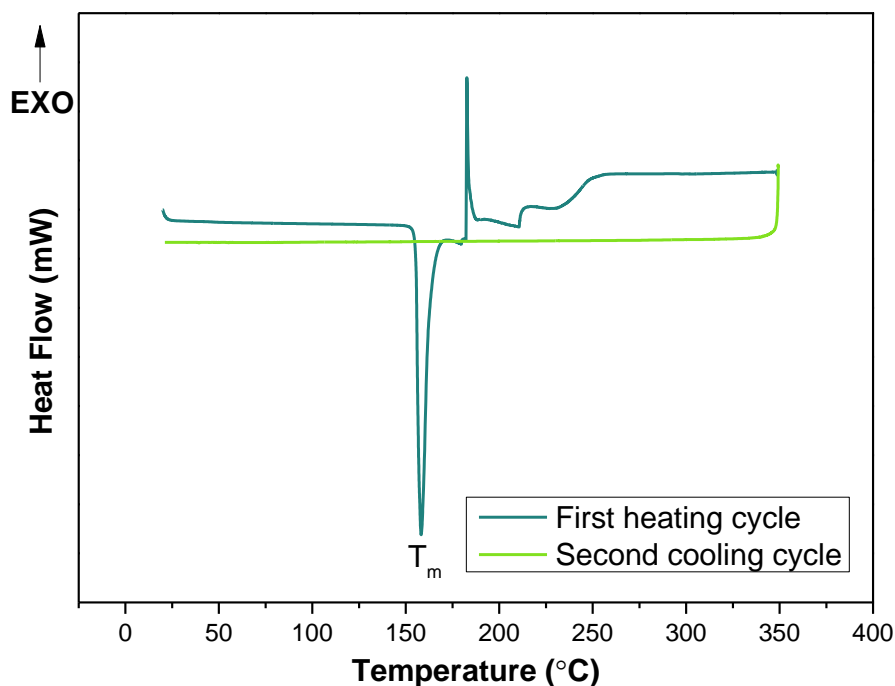
Figure 4. 17 DSC heating and cooling curves of CA.

Table 4. 7 The thermal properties of CA.

Material	Phase transition temperature		ST (°C)	Latent heat	
	T_m (°C)	T_c (°C)		H_m (J/g)	H_c (J/g)
CA	157.98	NA	NA	7.29	NA

4.3.6.4 Thermal stability of PEG8000, CA and CF

TGA was used to measure the thermal stability of PEG, CA, and CF by monitoring the change in mass experienced by the material as result of subjecting it to a temperature increase until reaching the maximum temperature (e.g., 600 °C). TGA curves of pristine PEG8000, CA and CF are presented in Figure 4.18. Observations indicated that PEG, CA, and CF experienced a two-stage mass loss. The TGA properties of PEG, CA and CF are summarised in Table 4.8. Results indicated that PEG8000 had the lowest onset temperature of 189.90 °C while CF had the highest onset temperature of 392.72 °C which indicated that PEG had the lowest thermal stability because it is a semicrystalline polymer; and therefore, could undergo thermal decomposition easily. CF had the highest thermal stability, which means combining PEG with cellulose via chemical crosslinking reaction is expected to enhance the thermal stability of PEG.

127

The first stage of mass loss of PEG, CA and CF was observed to occur in the temperature range of 170 to 270 °C; 215 to 253 °C; and 392 to 474 °C. This mass loss was attributed to the thermal decomposition of PEG, CA, and CF since major mass loss in the range 84.78 to 88.56 % occurred in the first stage. Results indicated that the total weight loss of pristine PEG8000 was 99.41% with a negligible amount of PEG8000 remaining undecomposed (e.g.,0.59%) which may be attributed to the presence of impurities in PEG8000.
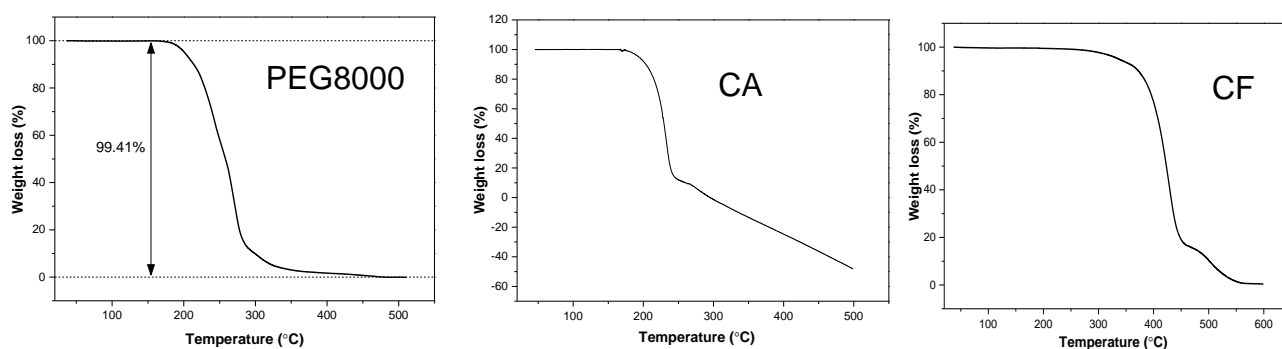
Figure 4. 18 TGA curves of PEG8000, CA and CF.

Table 4. 8 TGA results of PEG8000, CA and CF.

Name	Mass loss (%)		T_{onset} (°C)	T_{max} (°C)
	Stage 1	Stage 2		
PEG8000	85.92	13.99	189.90	479.60
CA	88.56	9.60	215.50	288.96
CF	84.78	14.71	392.72	585.03

4.3.7 Morphology characterisation of PEG8000

4.3.7.1 Surface morphology of unirradiated and MW irradiated PEG8000

Figures 4.19 presents the SEM images of unirradiated and MW irradiated PEG8000 particles. The particle shape of polymers like PEG depends entirely upon the preparation method. The synthesis of polymer particles via the spray drying method and the solvent precipitation methods results in producing spherical and nearly spherical particles (Vehring et al., 2020). The temperature used during the preparation also tends to affect the particle shape. For instance, preparing particles via low temperature pulverisation method results in producing irregularly shaped particles.

Observation indicated that pristine PEG8000 used in the current study comprised mainly of individual spherical to near-spherical particles of varying size with a very smooth surface which suggested that they were either prepared via the spray drying or solvent precipitation method. Presence of large clusters of granules and elongated particles may be attributed to the high M_w of PEG because during the synthesis process of PEG8000 high concentration of PEG solution (e.g., highly viscous solution) will be used which tend to produce large droplets which consequently leads to the formation of PEG8000 particles of increased particle size (Wu et al., 2019). Figure 4.19 indicated that MW irradiation caused no apparent changes to the particle structure and size of the PEG particles; however, it appeared that the number of individual spherical particles had decreased which was ascribed to the formation of large clusters due to the thermal effect of MW irradiation. Increasing the MW irradiation duration from 10 to 20 min resulted in increasing the size of clusters which was attributed to the melting of the amorphous phases, and some particles were observed to become elongated.
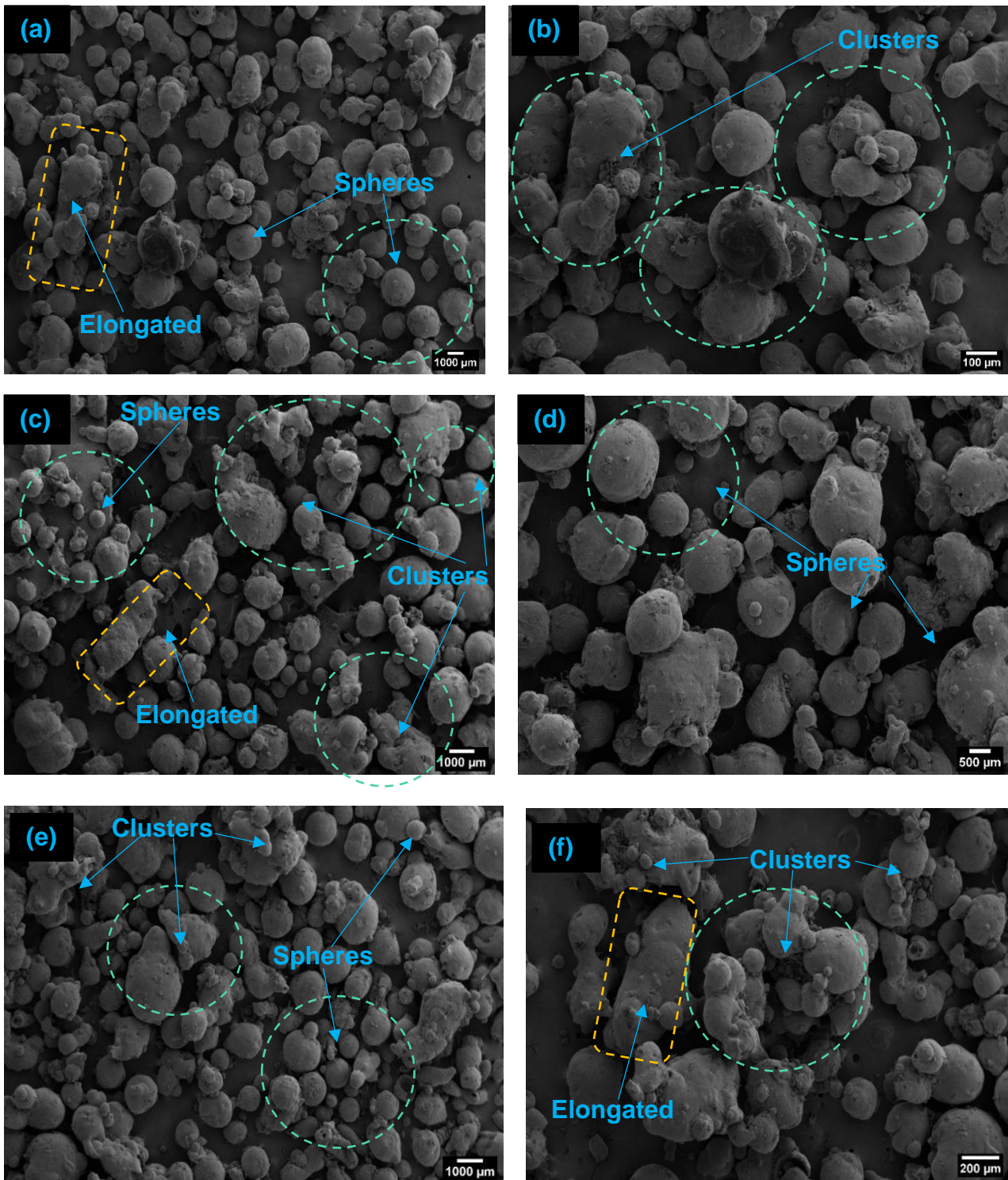
Figure 4. 19 SEM images of (a) Unexposed; (c) 10min MW exposed; (e) 20min MW exposed PEG particles; and (b), (d) and (f) shows the close-up view of the unexposed, 10min and 20min MW exposed particles.

4.3.7.2 Crystal morphology and structure of unirradiated and MW irradiated PEG8000

Figure 4.20 presents a series of POM images of pristine PEG8000 powder taken at room temperature to study its crystal morphology at room temperature. These images were compared with the SEM images mainly to determine the variation in crystal morphology with particle shape of PEG8000. It was observed that large clusters exhibited amorphous structures while the spheres appeared to contain the crystalline regions. The typical spherulite structures were observed to be surrounded with an amorphous layer. This indicated that visibility of PEG8000 crystals in large clusters will be poor. Therefore, it was quite challenging to observe the crystalline phases of PEG8000 through the optical microscope (see Figure 4.20) since amorphous structures were dominating the crystalline phases; and they appeared to exist between the crystalline regions due to its very high molecular weight. PEG8000 is a semicrystalline polymer; therefore, it comprised of both crystalline and amorphous phases in unequal proportions. Figure 4.20 (d) shows that PEG8000 exhibited a spherulite crystal structure which was demonstrated by its obvious cross-extinction pattern (Fang et al., 2010). Figure 4.21 shows that MW radiation exposure resulted in destructing the crystal lattice of the spherulite crystals (e.g., smudged effect on crystals).
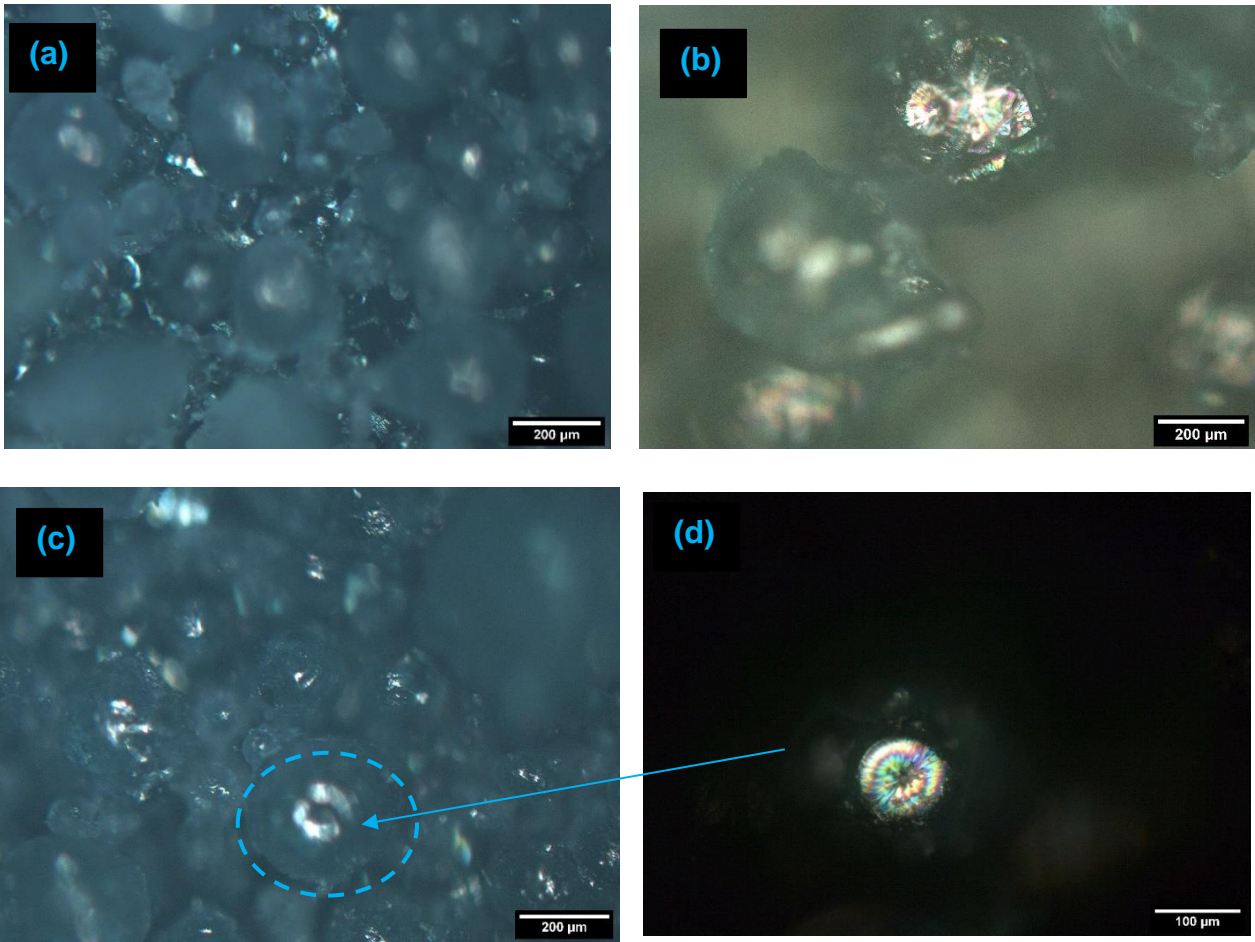
Figure 4. 20 POM images taken at room temperature shows (a) PEG8000 particles; (b) Crystals of PEG8000; (d) particle containing a visible crystal and (d) close-up view of PEG8000 crystal.
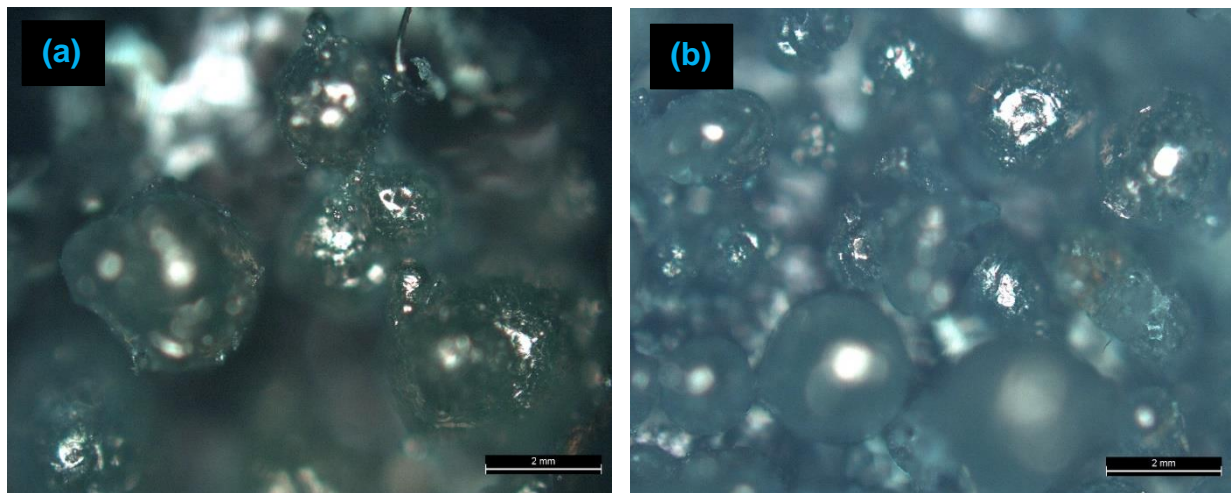
Figure 4. 21 POM images of (a) 10min; and 20min MW irradiated PEG8000 particles.

4.3.7.2 Crystal Morphology changes of PEG8000 during phase change

Figures 4.22 and 4.23 show the changes in the crystal morphology of PEG8000 during the melting process, and they indicated that with increasing temperature pristine PEG8000 particles were observed melt resulting in causing the crystalline phases to
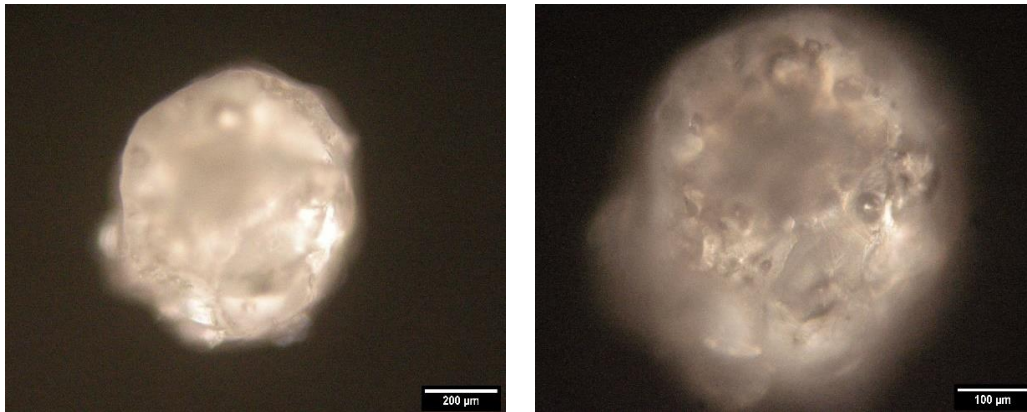
Figure 4. 23 PEG particle undergoing melting as result of elevated temperature exposure.
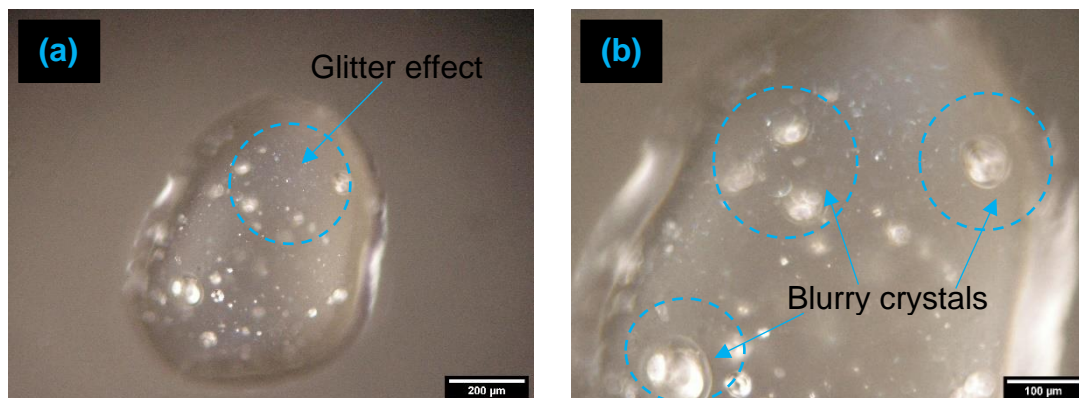
Figure 4. 22 POM images of (a) PEG8000 melt; and (b) close-up view of the melt containing tiny crystals and blurry crystals.

melt. The visibility of the characteristic spherulite crystals reduced significantly because they were observed to have blended well with the amorphous phases. Approaching the melting temperature of PEG8000 resulted in reducing the opacity of the melt formed. Thus, it was observed to become transparent, and it contained fewer crystals of reduced size which appeared as 'blurred crystals' as shown in Figure 4.23 (b) which suggested that PEG melt is an amorphous material since it contained no crystals.

Figures 4.24 and 4.25 show the crystal morphology of PEG8000 during the crystallisation process (e.g., cooling process) from the melt state, and it can be observed that spherulitic crystals which are crystalline lamellae with 3D superstructures. In general, the spherulite crystal formation occurs in three stages: (1) formation of the nuclei, (2) growth of crystal; and (3) secondary crystal growth which

involves increment of the crystallinity and thickness of the lamellar crystals (Yazdani et al., 2021).

It can be observed that after the formation of new crystals in the nucleation step from a clear PEG melt, followed by growth of the crystal size with reducing temperature in the crystal growth step. Figure 4.25 indicates that crystals formed exhibits a cross-extinction pattern.

Figure 4.25 illustrates the crystal morphology of PEG during the crystallisation (e.g., cooling) process from the melt state.
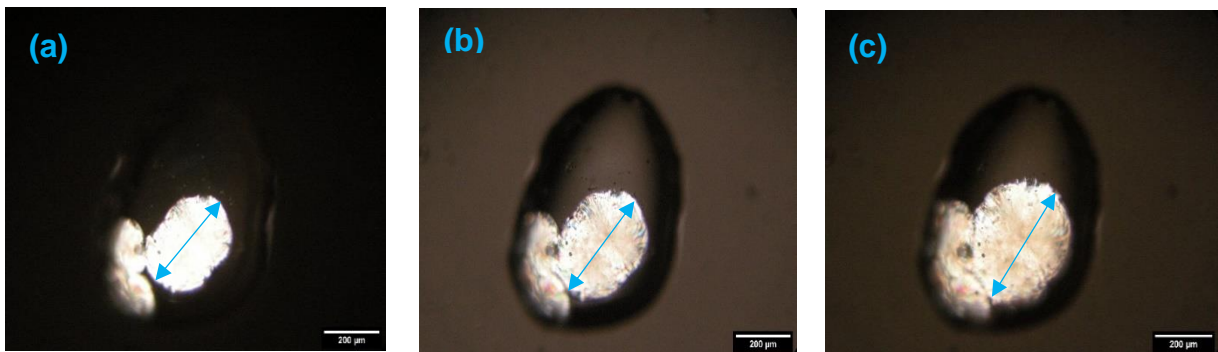
Figure 4. 25 Illustrates crystal growth after the nucleation step.
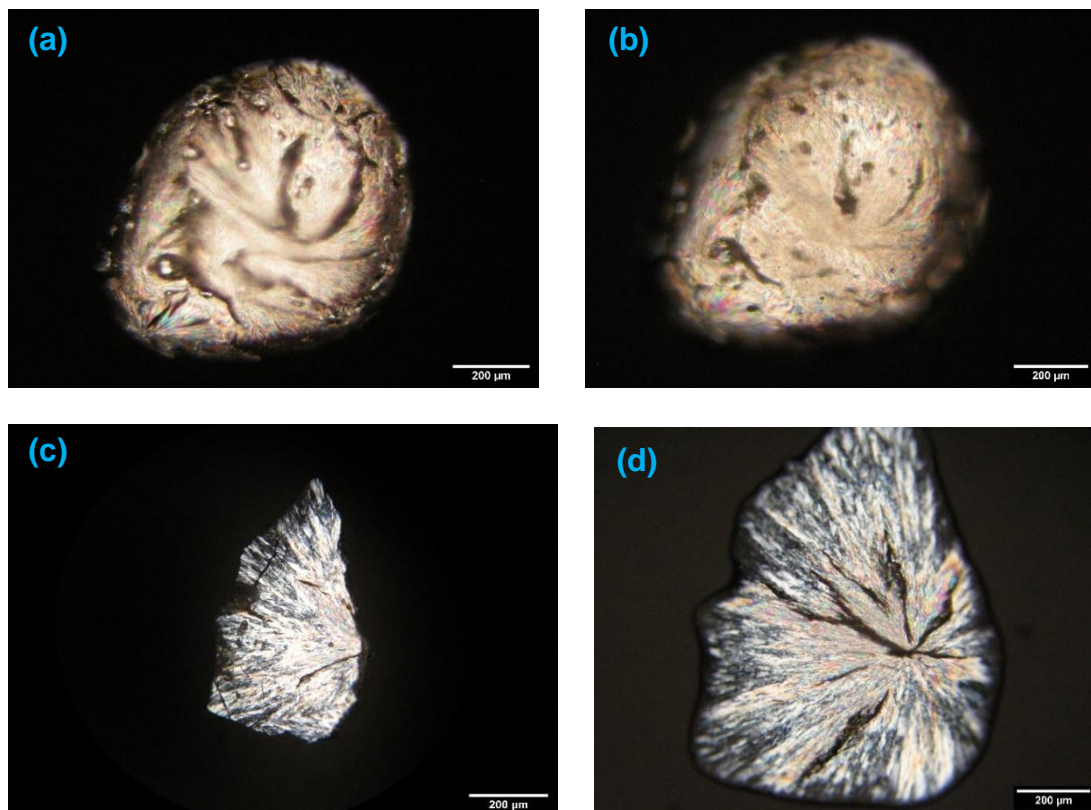
Figure 4. 24 Illustrates the crystallisation process of PEG8000: (a) and (b) PEG melt with no crystals; (b) PEG crystal formation; and (d) spherulite crystal of PEG.

4.4 Interim Conclusions

This Chapter has successfully studied the chemical structure, crystalline properties, thermal properties, thermal stability, surface morphology, crystal morphology of raw materials used in the current study using FTIR, XRD, DSC, TGA, POM and SEM analysis.

4.4.1 Outcomes

➢ DSC results showed that PEG8000 had a very high latent heat of melting and crystallisation of 181.5 and 182.1 J/g, but it was observed to exhibit the undesirable supercooling behaviour. The supercooling temperature of PEG8000 was determined to be 19.34 °C.

➢ DSC results showed that cellulose (supporting material) and citric acid (the crosslinker) exhibited poor thermal properties; and therefore, results indicated that they make no contribution to latent heat.

➢ The TGA results indicated that PEG had poor thermal stability compared to both CF and CA.

➢ XRD results confirmed that PEG was a semicrystalline polymer and cellulose was an amorphous polymer. Microwave radiation exposure resulted in changing the crystalline properties of PEG.

4.4.2 Outlooks

➢ The influence of incorporating both supporting material and crosslinker on the thermal properties and crystalline properties of pristine PEG needs to be examined and understood.

➢ The effects of chemical crosslinking reaction on the crystalline and thermal properties of PEG need to be evaluated.

➢ Changes in supercooling temperature of PEG after chemical crosslinking reaction need to be determined.

➢ The changes in the thermal stability of PEG after the chemical crosslinking reaction need to be evaluated.

➢ The changes in the crystal morphology and structure of PEG after chemical crosslinking reaction need to be evaluated since this may influence its thermal performance.

Chapter 5: Influence of chemical compositions on the thermal properties of PEG in the PU crosslinked composite PCMs

Abstract

This chapter describes the preliminary experimental work conducted to investigate and evaluate the influence of chemical compositions e.g., the mass ratio of PCM to supporting material, crosslinking agent content, and type of solvent on the thermal properties of PEG and its composite PCMs. Overall, intrinsic property changes experienced by PEG after the shape stabilisation process via the conventionally used polyurethane (PU) crosslinking reaction using TDI crosslinker was examined via analytical techniques namely FTIR, XRD and DSC analysis. This Chapter aims at meeting specific objectives 2 and 3 listed in section 1.4.

5.1 Introduction

Poly(ethylene glycol) (PEG) of different molecular weights (M_w) is a biodegradable, biocompatible and an environmentally friendly synthetic polymer used conventionally in several biomedical applications for the preparation of crosslinked hydrogels. In the recent years it has been considered as the most versatile organic solid-liquid PCM with major desirable characteristics including high latent heat capacity, availability at a wide range of transition temperatures, non-toxic, non-corrosive and available at relatively low costs, which has drawn significant attention of researchers in the field of TES for the synthesis of novel and advanced PEG based composite PCMs. Focus of most studies was usually on combining PEG of different M_w with different supporting materials via physical or chemical processes for the synthesis of composite PCMs of enhanced thermal performance. However, the factors affecting the intrinsic thermal properties of PEG, and the influence of chemical compositions were never addressed but should be investigated since this affects the durability and determines the phase change properties of the prepared composite PCMs.

Physical processing techniques like vacuum impregnation was commonly employed for the shape stabilisation of PEG because it is comprised of easy and simple steps even though the resulting composite PCMs suffer from phase segregation problems. In contrast, chemical processes like chemical crosslinking are considered as promising routes to produce durable composite PCMs since they involve the formation of crosslinked structures between PEG and the chosen supporting material. In the latter approach it is critical to ensure that the degree of crosslinking it not optimised since this will result in affecting the crystalline properties of PEG which subsequently reduces its latent heat capacity.

PEG is reported to have good to partial miscibility with numerous synthetic polymers of different chemical structures including poly(acrylic acid), poly(methacrylic acid), poly(hydroxyether of bisphenol A), poly(vinyl alcohol), carboxylated poly(phenylene oxide) and poly(p-vinyl phenol) (Alberdi et al., 1994; Pedrosa et al., 1995; Pielichowska et al., 2008) but to promote the sustainability of the shape stabilisation technology it would be ideal to utilise biopolymers like cellulose and/ or their derivatives which are available abundantly in different forms at relatively low costs. Thus, PEG are comprised of plentiful of hydroxyl groups which makes them susceptible to chemical modifications, and since each monomer unit of cellulose and their derivatives contain two or more hydroxyl groups it means they can easily participate in chemical reactions like esterification (TCA) or polyurethane (PU) reaction which involves reaction between hydroxyl and carboxyl or isocyanate functional groups.

Results indicated that a limited number of studies have showed some interest on utilising cellulose and/ or their derivatives as supporting material for the synthesis of PEG based composite PCMs using a standard mass ratio of PEG to MCC of 5:1 and unknown amount of crosslinking agent for thermal energy storage (TES) applications. Therefore, in the current study number of unique formulations were developed by varying the mass ratio of PEG to MCC and TDI content (see Tables 5.1 to 5.5) for the synthesis of PEG-MCC based composite PCMs via the PU crosslinking reaction using TDI as the crosslinking agent mainly to study and evaluate the effect of chemical compositions on the final intrinsic properties of the PU crosslinked composite PCMs. Also, sufficient information is not available regarding the changes caused to the phase change properties of PEG when its crystallinity changes which must be thoroughly understood to optimise the thermal and crystalline properties of PEG in the composite

PCMs. The particle size of cellulose was limited to 90 μm in the previous studies and justification regarding its suitability was never provided. Therefore, current study will also investigate the impacts caused by reducing the particle size of microcrystalline cellulose from 90 to 20 μm. The characteristics of the final products were evaluated using relevant analytical techniques and reported.

5.2 Experiments

5.2.1 Studying the impact caused to the thermal properties of PEG by the solvent

To get a fundamental understanding of PEG behaviour in both deionised (DI) water and DMF solvent, and to study the resulting impacts on its intrinsic thermal properties, two control aqueous solvents were prepared by dissolving PEG and MCC in DI water and DMF solvent separately and stirred until complete dissolution in the absence of heat. The formulations used for the preparation of these aqueous solutions are presented in Table 5.1.

Table 5. 1 Formulations to study the effects of PEG-solvent interactions on the phase change properties.

Sample name	PEG8000 (g)	Cellulose (g)	DI water (ml)	DMF (ml)
PEG-MC-DI water	5	1	10	0
PEG-MC-DMF	5	1	0	10

5.2.2 Formulations for the preparation of PU composite PCMs

To study the changes in the thermal properties of PEG after PU crosslinking; and to evaluate the influence of MCC content and TDI content on its phase change properties a series of unique reaction formulations were developed and investigated. However, only a selected number of formulations are presented in this Chapter.

5.2.2.1 Interaction between PEG and MC cellulose with TDI crosslinker

Table 5. 2 Synthesis of MCC/TDI and PEG8000/TDI composites via PU crosslinking reaction.

Name	PEG8000 (wt.%)	MCC (wt.%)	TDI (wt.%)
1:5 MCC/TDI	45.5	9.09	45.5
1:1 PEG8000/TDI	47.6	4.76	47.6

5.2.2.2 Influence of TDI crosslinker content on the degree of crosslinking

Table 5. 3 Synthesis of PEG/MCC/TDI composite PCMs via PU crosslinking reaction using different blend ratios.

Blend ratio PEG:MCC:TDI	PEG8000 (wt.%)	MCC (wt.%)	TDI (wt.%)
5:1:5	45.5	9.09	45.5
5:0.5:5	47.6	4.76	47.6
5:1:3	55.6	11.1	33.3
5:0.5:3	58.8	5.88	35.3

5.2.2.3 Influence of MC cellulose content on thermal properties of PU crosslinked composite PCMs

Table 5. 4 Studying the impacts of MCC content the thermal properties of PU crosslinked composite PCMs.

Blend ratio PEG:MCC:TDI	PEG8000 (wt.%)	MCC (wt.%)	TDI (wt.%)
5:1.75:5	42.6	14.9	42.6
5:1.5:5	43.5	13.0	43.5
5:1.25:5	44.4	11.1	44.4
5:1:5	45.5	9.09	45.5
5:0.5:5	47.6	4.76	47.6

5.2.2.4 Influence of Mw of PEG on the degree of crosslinking

Table 5. 5 Studying the impacts of Mw on the thermal properties of the PU crosslinked composite PCMs.

Blend ratio	PEG (wt%)			MCC (wt.%)	TDI (wt.%)
M_w (g/mol)	600	1000	8000		
50:50PEG8000/PEG600	22.7	0	22.7	9.09	45.5
25:75PEG8000/PEG600	34.1	0	11.4	9.09	45.5
50:50PEG8000/PEG1000	0	22.7	22.7	9.09	45.5
25:50PEG8000/PEG1000	0	34.1	11.4	9.09	45.5

5.3 Methods

5.3.1 Visual examination

To perform visual examination, high resolution images of the newly prepared PU crosslinked composite PCMs were taken using a camera phone. To study the chemical stability of these composite PCMs, photos of the composite PCMs were taken after 3 months, and comparison was made.

5.3.2 ATR-FTIR analysis

ATR-FTIR was performed to study the chemical structure of the PU composite PCMs, and to confirm the formation of covalent bonds between the functional groups of PEG, MCC and TDI.

5.3.3 DSC analysis

DSC analysis was performed to study the thermal properties of the PU crosslinked composite PCMs; and to determine the impact of the PU crosslinking reaction on the intrinsic thermal properties of pristine PEG.

5.3.4 XRD analysis

XRD analysis was performed to determine changes in the crystalline properties of pristine PEG after PU crosslinking. The influence of chemical compositions on crystalline properties was also determined.

5.4 Results and discussion

5.4.1 Visual examination of PU composite PCMs

Figure 5.1 shows the appearance of the PU crosslinked composite PCMs, and observations indicated that changing the chemical composition resulted in producing
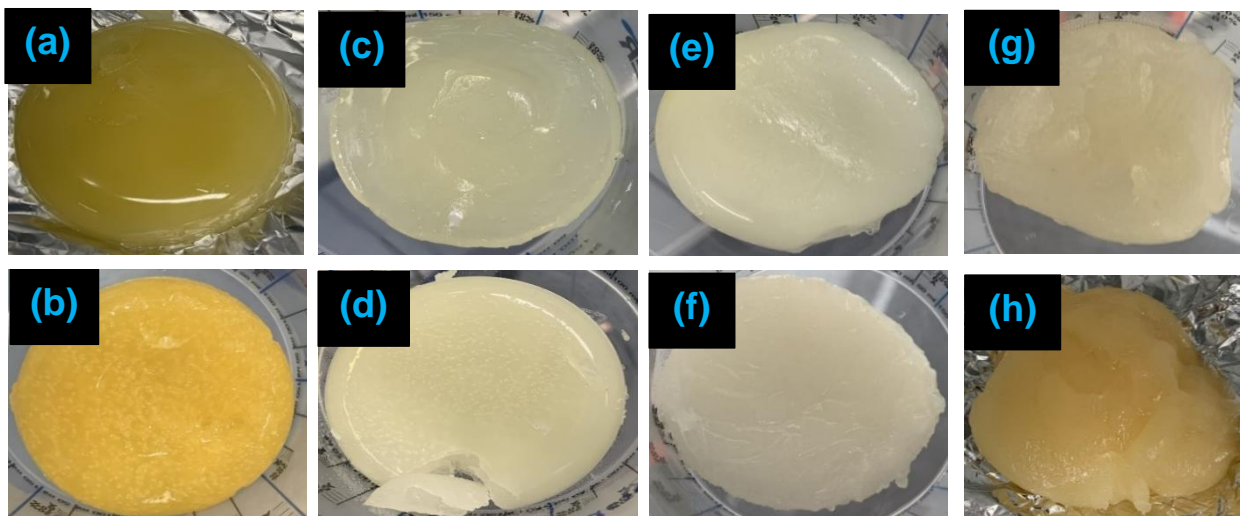
Figure 5. 1 Appearance of PU crosslinked composite PCMs resulting from different formulations.

composite PCMs of varying colour and opaqueness. The yellow colour was attributed to the thermal degradation (e.g., thermo-oxidative degradation) of PEG due to prolonged exposure to elevated temperatures during processing. Whereas samples that appear white (see Figure 5.1 (c), (d) (e) and (f)) had experienced no to negligible thermal degradation during processing. However, this gives no information regarding the extent of degradation experienced by PEG after PU crosslinking reaction. The flexibility of the samples was observed to reduce with increasing MCC content which was attributed to the reduction in the number of crystalline domains as result of incorporating an amorphous polymer in higher content (e.g., MCC).

5.4.2 Visual examination of decomposed PU composite PCMs

PEG was observed to be successfully shape stabilised via the PU crosslinking reaction according to Figure 5.1. However, Figure 5.2 shows that the PU crosslinked composite PCMs experienced severe degradation when left at standard laboratory conditions (e.g.,65% RH and 23 °C) for 3 months which was attributed to the formation of weak intermolecular forces between PEG and MCC.
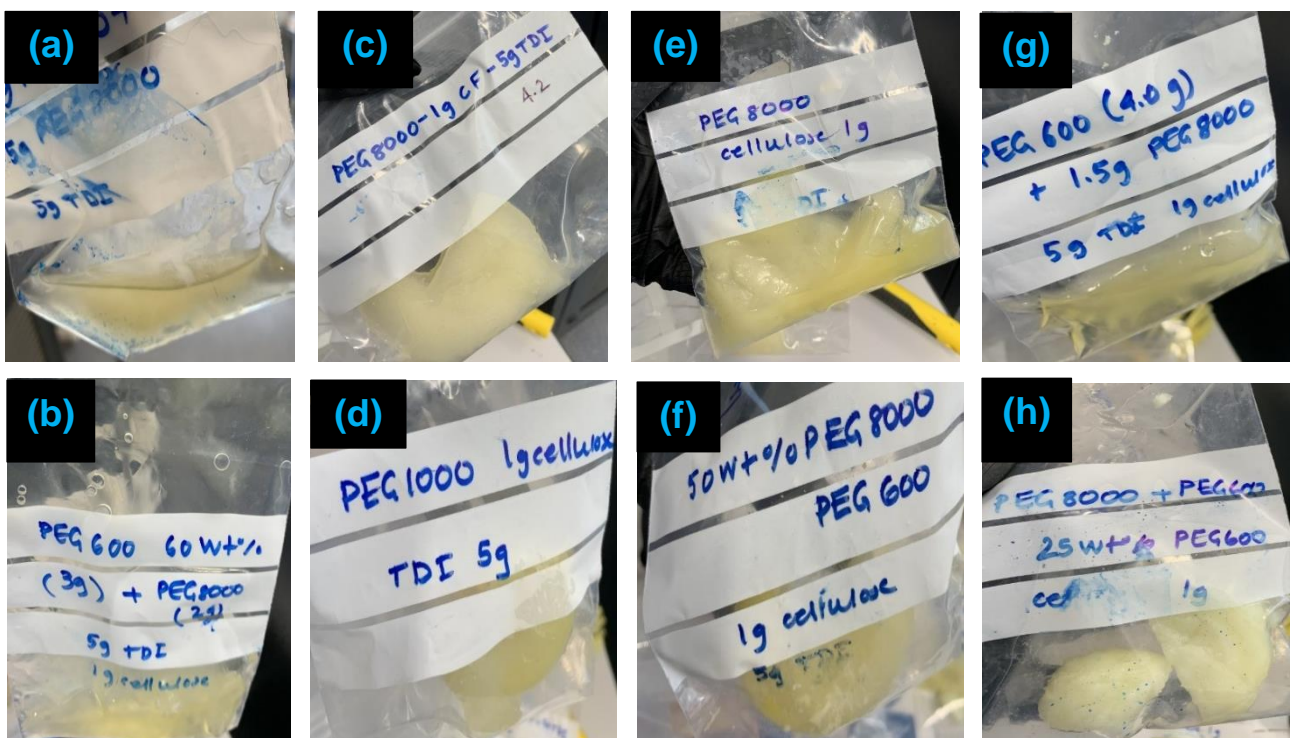
Figure 5. 2 Appearance of decomposed PU crosslinked composite PCMs.

5.4.3 PU crosslinking reaction

In general, PU crosslinking reaction can be defined as a reaction that occurs between two or more hydroxyl (OH) groups and isocyanate (NCO) groups. PEG and MCC are comprised of similar chemical compositions; and they both contain plentiful of hydroxyl groups in their chemical structure. Therefore, it is quite challenging to determine the actual reaction routes since three chemical routes are possible including reaction between (a) MCC and TDI; (b) PEG and TDI; and (c) PEG, MCC and TDI; however, according to the synthesis route employed in the current study reaction (c) was expected to occur since TDI was only added to the reaction mixture after the addition of both PEG and MCC.

5.4.4 Formation mechanism of PU composite PCMs

Figure 5.3 illustrates the proposed reaction mechanism for the formation of the PU crosslinked composite PCMs of the current study.
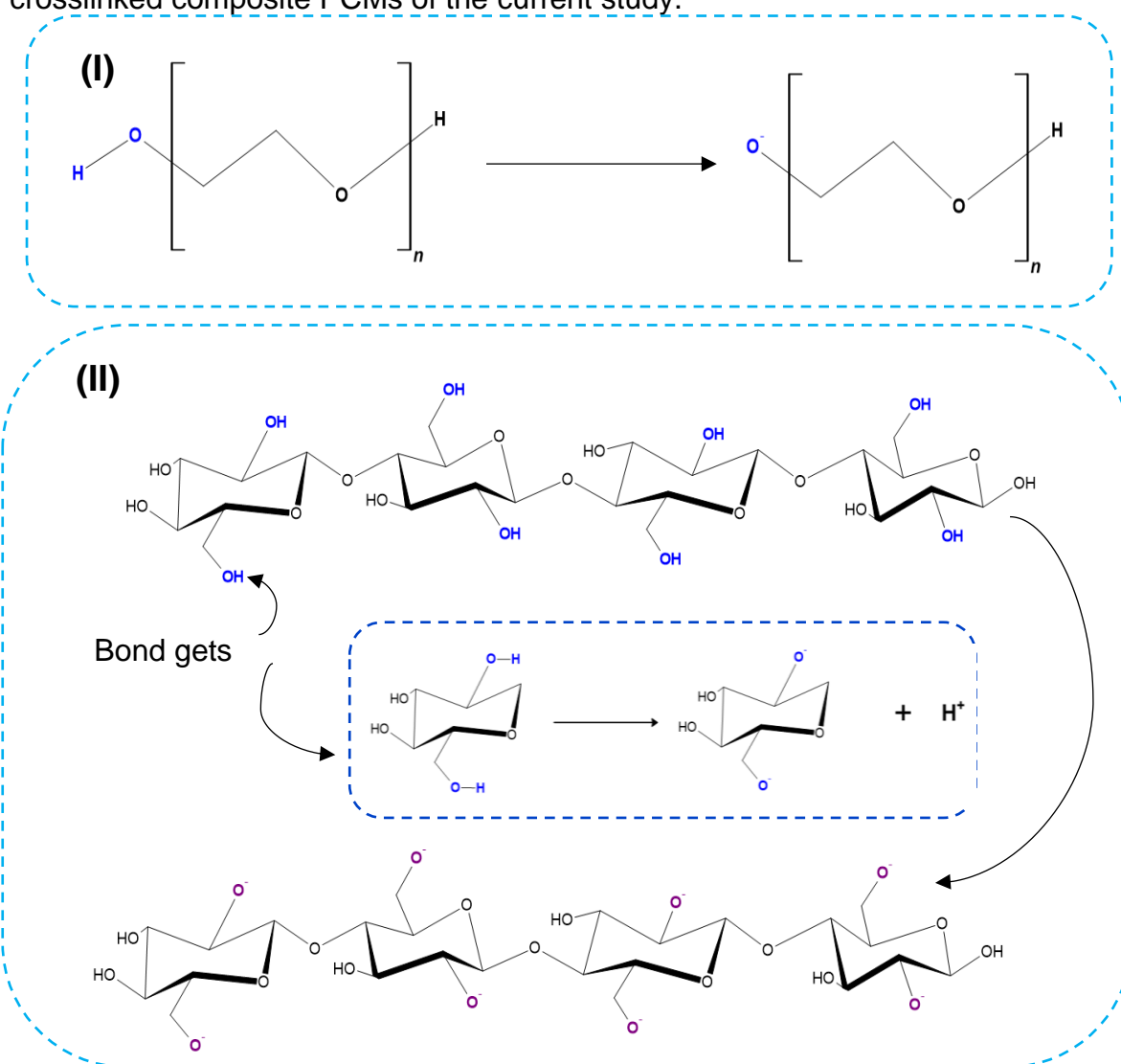
Figure 5. 3 Schematic illustration of the dissolution mechanism of (I) PEG and (II) MCC in any solvent.

In the first step PEG was dissolved in DMF under heating at 80 °C mainly because at ambient temperature it will be difficult to dissolve PEG of very high molecular weight (e.g.,8000 g/mol) due to the existence of a strong network of hydrogen bonding. Addition of DMF solvent will facilitate the bond breaking process thereby encourage PEG dissolution as illustrated in Figure 5.3 (I). In this process the OH group of PEG gets attacked which consequently results in bond disruption which involves the removal of the H+ ion. This leads to the formation of a reactive deprotonated groups (O-) as shown in Figure 5.3 (II) which is susceptible to chemical attacks. MCC gets attacked in a very similar way since both PEG and MCC belong to the alcohol family

since they contain plentiful of OH groups in their structure. This results in producing deprotonated (O⁻) groups as result of O-H bond breakage. Figure 5.4 illustrates schematically the dissolution of TDI in DMF solvent. During the dissolution of TDI in
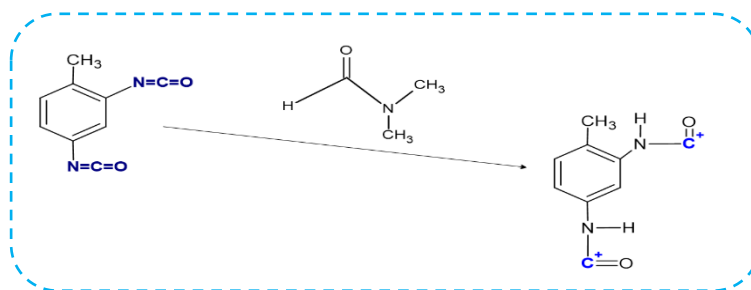
Figure 5. 6 Schematic illustration of TDI dissolution in DMF solvent.
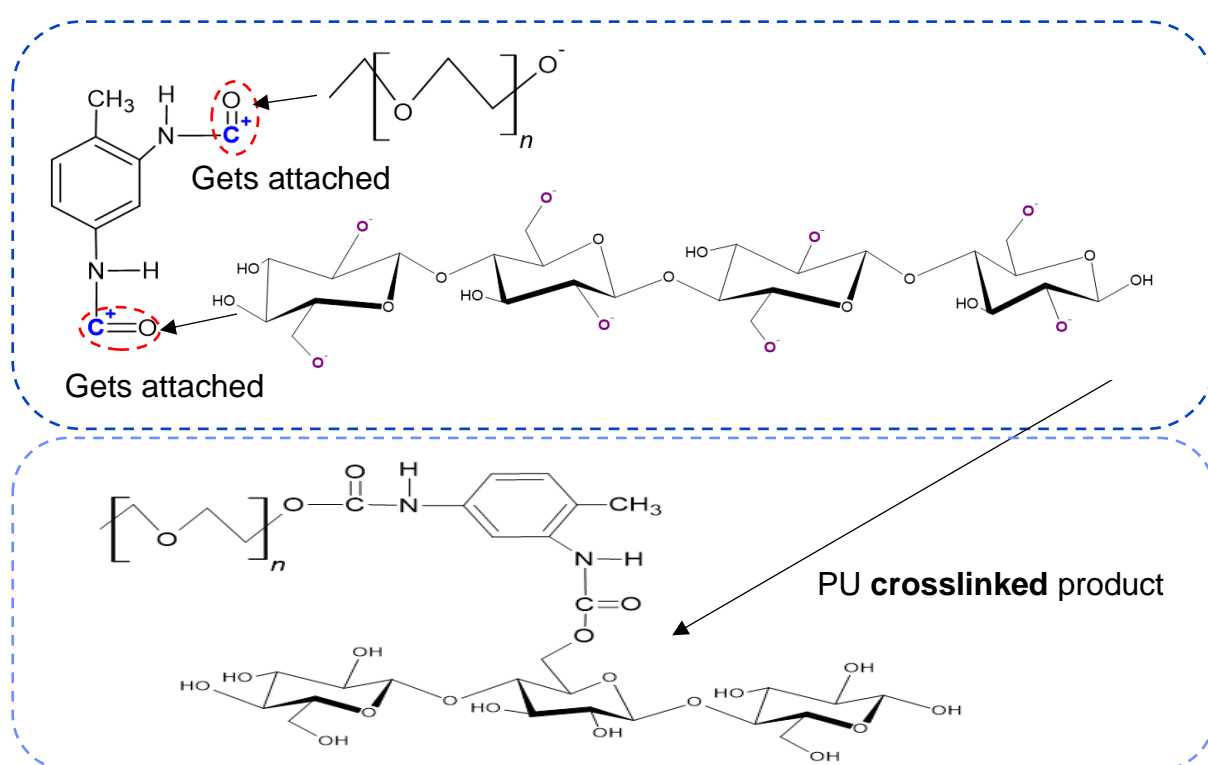
Figure 5. 4 Reaction mechanism for the formation of PEG-MCC composite PCM via PU crosslinking.

DMF solvent the N-C double bond of the isocyanate group (NCO) group breaks which results in the formation of a reactive compound as shown in Figure 5.4. This compound can readily react with the deprotonated compounds formed in step 1. Therefore, adding TDI-DMF solution dropwise leads to the formation of a crosslinked product shown in Figures 5.5.

5.4.5 FTIR analysis for PU crosslinked composite PCMs

5.4.5.1 Functional groups of PU crosslinked composite PCMs

Figure 5.7 presents the FTIR spectra of PEG, MCC, TDI and the PU crosslinked composite PCMs. The spectra of the PEG and its crosslinked structures look different and the peaks in the fingerprint region (e.g., 500 to 1500 cm^{-1}) of PEG8000 has changed pattern in the composite which confirms that reaction has taken place between PEG and TDI. Peak of TDI spectra at 1612 cm^{-1} attributed to the imine stretching vibration of the C=N group disappears after reaction, and new bands are formed at 3347 cm^{-1} to 3353 cm^{-1} attributed to N-H stretching vibration and 1666 cm^{-1} to 1652 cm^{-1} indicating the presence of carbonyl (C=O) groups in the crosslinked structures.
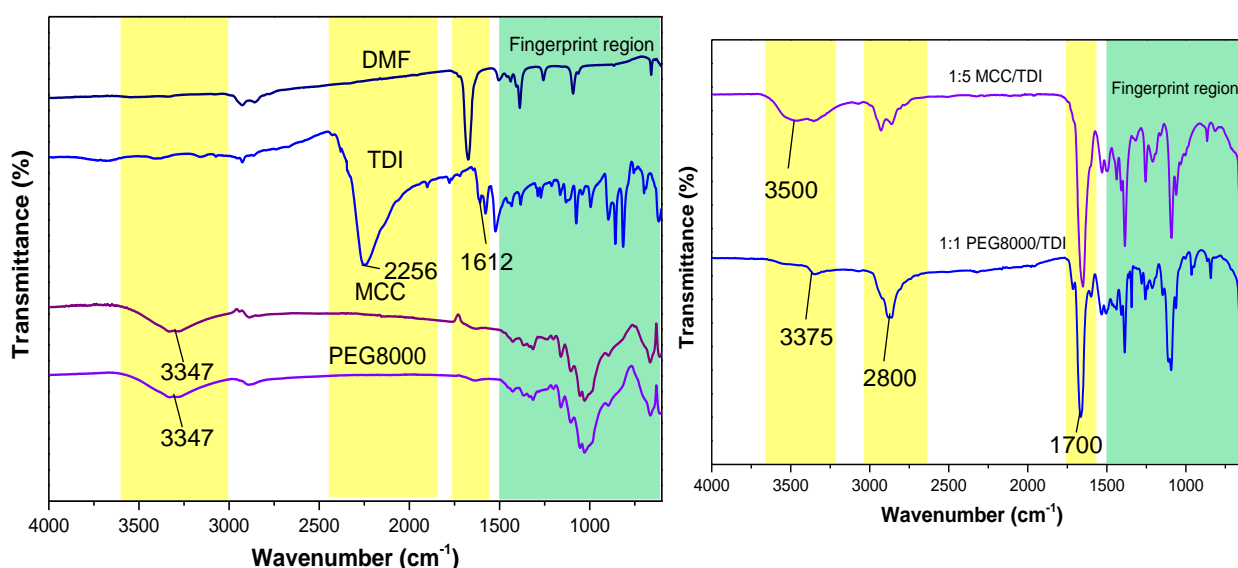
Figure 5. 7 FTIR spectra of PEG, MCC, TDI and the PU crosslinked composite PCMs.

Disappearance of peak at 1612 cm^{-1} after chemical reaction confirms changes in TDI chemical structure which is in good agreement with the proposed formulation mechanism presented in Figures 5.3 to 5.5. The peak at 1700 cm^{-1} indicates the presence of -NCO group. The new peak formed at 1700 cm^{-1} was attributed to the stretching vibration of C=O groups. Narrow peak at 3375 cm^{-1} is attributed to the N-H group which appears to be replaced by the OH group in the spectra of 1:5 MCC/TDI composite PCM.

Figure 5.8 shows the FTIR spectra of PU crosslinked composite PCMs. All four FTIR spectra of the composite PCMs exhibits a weak broad peak at 3436 cm^{-1} to 3462 cm^{-1} which may be attributed to the -OH stretching vibration from either water, MCC or PEG8000. In the spectra of the composites the peak corresponding to the presence

of OH group had merged with the peak corresponding to N-H group (Li and Ding, 2007).

According to the formulation mechanism presented in Figure 5.5, the crosslinked structure contains fewer OH groups since OH groups have participated in the PU crosslinking reaction; however, Figure 5.8 shows that the peak attributed to the presence of OH group was also present in the final structure which indicates that not all OH groups had participated in the chemical crosslinking reaction. Thus, a crosslinked structure may not have formed. The peak at 2866 cm^{-1} to 2886 cm^{-1} is attributed to the C-H stretching vibration while the peak appearing at 1386 cm^{-1} to 1389 cm^{-1} indicates the deformation of the C-H groups and the peak at 1091 cm^{-1} to 1093 cm^{-1} corresponds to the stretching vibration of the C-O-C group (Alemdar et al., 2005; Shetty et al., 2019). The peaks appearing at 1653 cm^{-1} to 1661 cm^{-1} indicates the presence of the carbonyl (C=O) group. The peak at 2256 cm^{-1} appearing in the TDI spectra attributed to the N=C=O group disappears in the FTIR spectra of the composite PCMs which confirms that crosslinking reaction has taken place. However, this does not demonstrate the formation of a crosslinked structure because no new peaks had formed at 3400 cm^{-1} corresponding to the presence N-H group to confirm the formation of linkages (Yang et al., 2010). Therefore, results may suggest that weak intermolecular forces of attraction existed between PEG and MCC in the composite PCMs formed via PU crosslinking reaction.
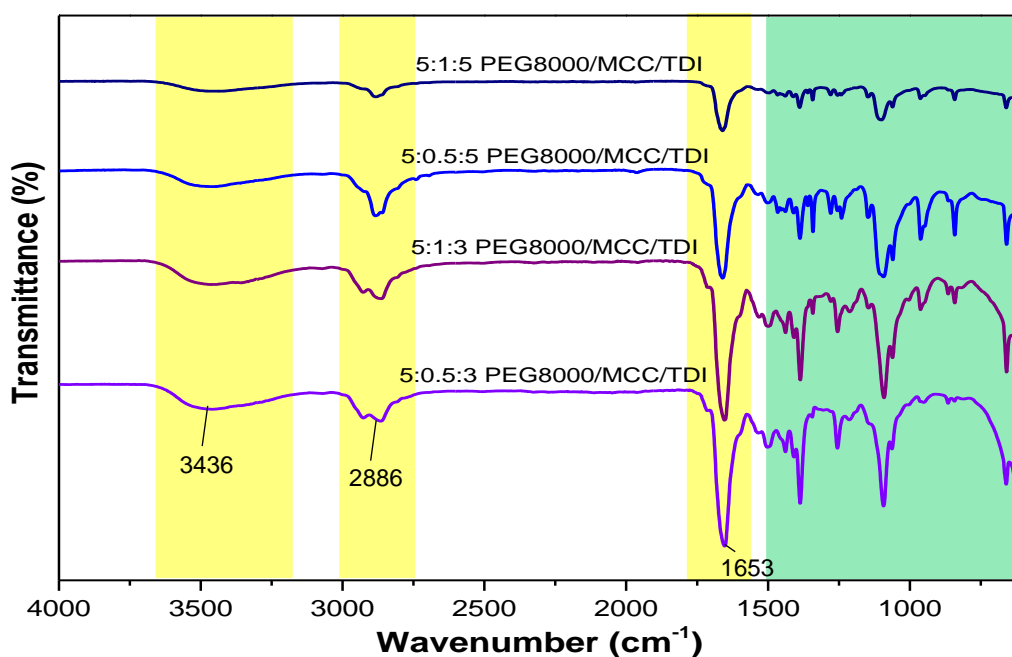
Figure 5. 8 The ATR-FTIR spectra of PU crosslinked composite PCMs.

5.4.5.3 Influence of MCC content on degree of crosslinking

Figure 5.9 shows that with increasing MCC content from 4.76% to 9.09%, the peak position at 3453 cm^{-1} attributed to the OH stretching vibration from MCC is observed to be shifted to 3436 cm^{-1} (e.g., lower wavenumber) which indicated that the hydrogen bonding interaction of OH group had become stronger in the PU crosslinked composite PCM (Kuru and Aksoy, 2014). Increasing MCC content from 4.76% to 9.09%, 11.1%, 13.0% and 14.9% resulted in changing the wavenumber from 3453 cm^{-1} to 3436 cm^{-1} to 3479 cm^{-1} and to 3379 cm^{-1}, respectively. The peak intensities were observed to change from 90.0% to 93.7%, 90.6%, 77.3% and 79.6%, respectively. This indicated that the strength of the hydrogen bond of OH group became weaker when MCC content exceeded 13.0%. The intensity of the new peak appearing at 1651 cm^{-1} to 1661 cm^{-1} corresponding to the stretching vibration of the C=N groups was observed to change from 72.7% to 21.2%, 25.05% and 35.0% which is due to the 'electron withdrawing' effect of the urethane groups that resulted in changing the relative vibration of the C=N group. The peak at 2879 cm^{-1} to 2884 cm^{-1} is attributed to the C-H group. The peak at 2256 cm^{-1} indicating the presence of the isocyanate group (N=C=O) had disappeared after reaction.
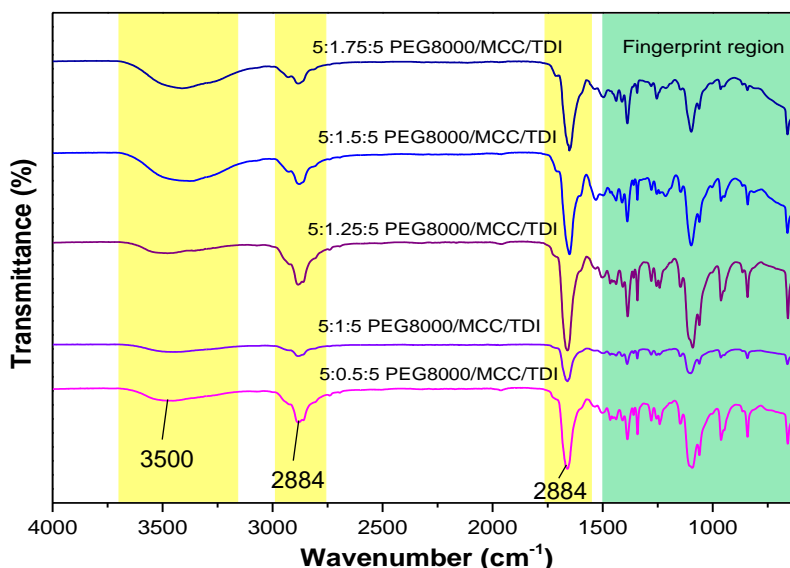
Figure 5. 9 FTIR spectra of PU crosslinked composite PCMs with different MCC content.

5.4.5.4 Influence of chemical composition and MW of PEG on PU crosslinked products

Figure 5.10 presents the FTIR spectra of PEG600, PEG8000 and the corresponding PU crosslinked composites PCMs. The results are in good agreement with previous literature which states that the chemical composition of PEG is not a function of its molecular weight (M_w). Increasing the M_w of PEG resulted in increasing the chain length and reduced its crystallinity due to an increase the number of amorphous phases. PEG600 and PEG8000 were compared due to the significant difference in their M_W values, and major difference was not observed in the FTIR spectra pattern which shows that both PCMs are likely to react in a similar manner.
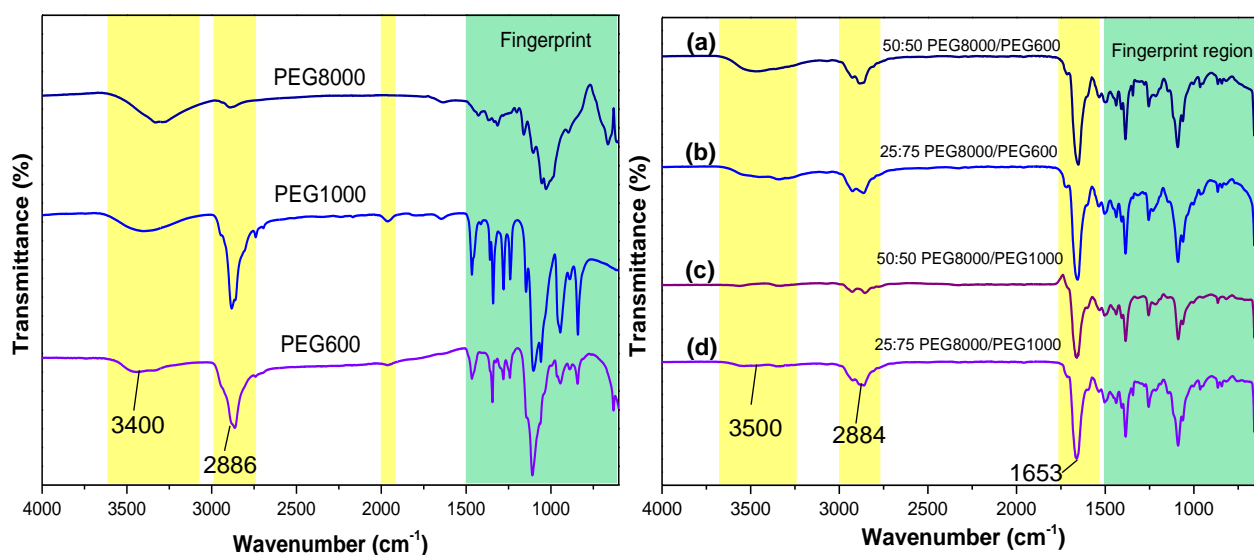
Figure 5. 10 FTIR spectra of PEG of different Mw and the corresponding PU crosslinked composite PCMs.

All crosslinked composites seemed to possess adequate shape stability initially since reaction had managed to convert the solid-liquid PCM into a 'gel-like' solid-solid PCM; however, visual examination results indicated that weak interactions only existed between PEG and MCC. The FTIR spectra presented in Figure 5.10 indicated that same since main peaks confirming the formation of a crosslinked structure did not exist. Hence, if a crosslinked structure had formed, a peak should have appeared at 1725 cm^{-1} to indicate the presence of the urethane group. Peak in the range 1649 cm^{-1} to 1661 cm^{-1} was present in the FTIR spectra of all the PU composite PCMs indicating the presence of the C=O group. Also, peak indicating the presence of the amide group (N-H group) should technically be appearing at 3500 cm^{-1} as an intense narrow peak but was absent in the FTIR spectra of all composites. At this wavenumber a weak broad peak indicating the presence of OH groups were observed; and this confirms

the fact that not all OH groups had participated in the PU crosslinking reaction to form shape stabilised composite PCMs. Overall, results indicated that PU crosslinking reaction did not lead to the formation of a crosslinked structure.

5.5 Impact of PEG and cellulose interaction on thermal properties dissolved in a solvent

The DSC heating and cooling curves of PEG dissolved in DI water and DMF solvent are presented in Figure 5.11 (a) and (b). The thermal properties determined using DSC measurements are presented in Table 5.6 which demonstrates changes in intrinsic thermal properties of pristine PEG8000 after dissolution in both DI water and DMF solvent.
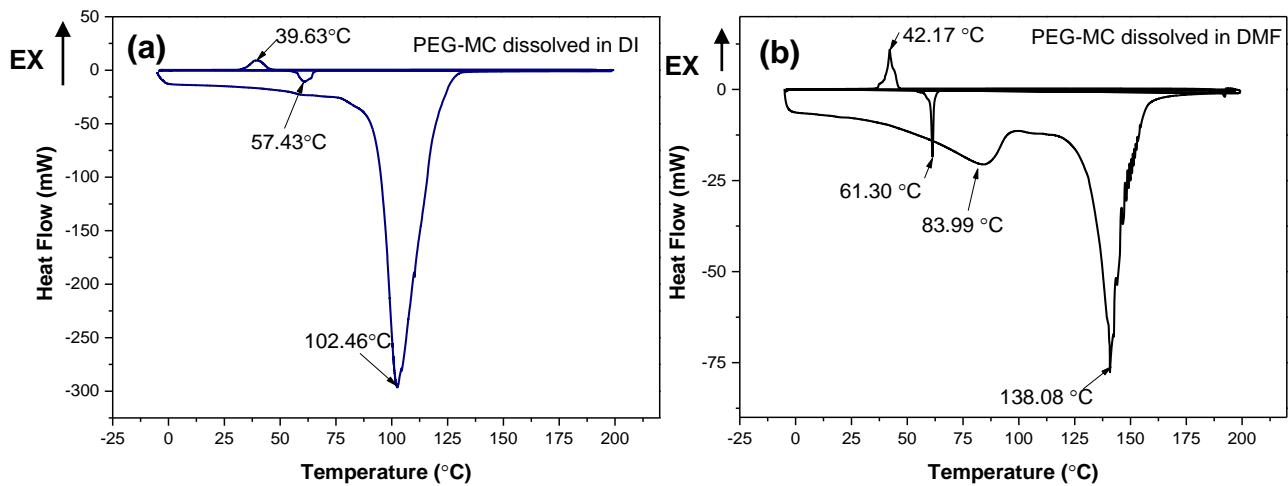
Figure 5. 11 DSC curves of PEG-MCC dissolved in (a) deionised (DI) water; and (b) DMF solvent.

Table 5. 6 Thermal properties of PEG-MCC dissolved in DI water and DMF solvent.

Sample name	Phase transition temperatures		Latent heats	
	T_m (°C)	T_c (°C)	H_m (J/g)	H_c (J/g)
PEG8000	63.12	43.78	181.5	182.1
MC cellulose	91.05	-	118.5	-
Heating cycle 1				
5PEG:1MC:10DI	102.46	-	1674	-
5PEG:1MC:10DMF	83.99 138.08	-	17.23 124.0	-
Cooling cycle 2				
5PEG:1MC:10DI	-	39.63	-	18.84
5PEG:1MC:10DMF	-	42.17	-	7.09
Heating cycle 3				
5PEG:1MC:10DI	57.43	-	18.39	-
5PEG:1MC:10DMF	61.30	-	6.39	-

5.5.1 Studying influence of DI on thermal properties of PEG

Figure 5.11 (a) shows that the first and third heating cycles consisted of one dip each at 102.46 °C and 57.43 °C while the second cooling cycle consisted of a single peak at 39.63 °C. Results indicated that subjecting the solution containing PEG-MCC dissolved in DI water to elevated temperatures initially caused complete evaporation of DI water. The solution experienced a phase change from liquid to gaseous phase as result of reaching and exceeding the boiling temperature of pure water (100 °C); and its latent heat was 1674 J/g. The very high latent heat capacity was attributed to the significant volume changes that occurred during phase transition process. Also, in the first heating cycle PEG experienced no phase changes which could be due to the presence of PEG in a relatively smaller proportion in the solution. Moreover, dissolving PEG and MCC in DI water resulted in the formation of strong intermolecular hydrogen bonds and weak Van der Waals forces between PEG, MCC and the water molecules since both PEG and MCC consisted of hydroxyl groups in their structure. They are both hydrophilic polymers. Therefore, the generated interactions had an adverse effect on the intrinsic thermal and crystalline properties of PEG since its phase change properties were observed to have changed (Chami Khazraji and Robert, 2013). In general, amorphous regions of PEG are reported to become unstable during the interaction with water molecules; thus, PEG8000 is comprised of higher amorphous regions which means stronger interactions had formed between PEG and water due

150

to the presence of higher number of unstable regions which was the main cause for the significant reduction in its latent heat capacity.

The third heating cycle had a dip at 57.43°C with a latent heat of 18.39 J/g. The melting point is close to the one of pristine PEG8000 because calculated percentage difference was 4.59%; however, the latent heat capacity appears to have reduced drastically from 181.5 J/g to 18.39 J/g (e.g.,89.9% decrease) which is attributed to the formation of strong hydrogen bonds between PEG and water molecules which has impacted the crystalline properties of PEG significantly. The crystallisation of PEG occurs at 39.63 °C and latent heat of crystallisation was 18.84 J/g. The supercooling temperature of pristine PEG had increased from 16.41°C to 17.80 °C (e.g., 8.47% increase). Therefore, it can be concluded that in composite PCMs prepared via chemical crosslinking reaction it is essential to ensure that the moisture content is minimised provided water was used as solvent during the chemical reaction since interactions between PEG, MCC and water was observed to have an undesirable effect on both the thermal and crystalline properties of PEG.

Figure 5.11 (b) shows that the first heating cycles consists of two endothermic peaks/dips: one at 83.99 °C and the other at 140.79 °C with corresponding latent heats of 17.23 J/g and 124.0 J/g which suggested the formation of an immiscible aqueous solution resulting from micro-mixing a soft and hard segment (e.g., PEG and MCC) (Yahiaoui et al., 2014). Dissolution of PEG in the DMF solvent may have caused it to aggregate, mainly due to two reasons namely the temperature effect and due to the nature of the solvent. Once clusters of PEG had formed it becomes very difficult to break them. Results indicated that MCC and DMF experienced a phase change initially but in the third heating cycle PEG was observed to undergo a phase change at 61.30 °C with latent heat of 7.44 J/g which confirms that MCC dissolved in DMF solvent makes no contribution to latent heat.

The second heating cycle indicates that PEG crystallises at 42.17 °C with a latent heat of crystallisation of 7.06 J/g. The results shows that the interactions generated between PEG and DMF solvent resulted in affecting the thermal properties of the PEG negatively. Therefore, it would be essential to minimise the amount of DMF solvent present in the PU crosslinked network to avoid destructing the crystalline properties of PEG.

5.6 Studying the thermal properties of PU composite PCMs

The DSC heating and cooling curves of the PU crosslinked composite PCMs with blend ratios of 5.0:0.5:3, 5.0:0.5:5, 5.0:1:3, 5.0:1:5, and 5.0:1.5:5 is presented in Figure 5.12, and their thermal properties are summarised in Table 5.7.
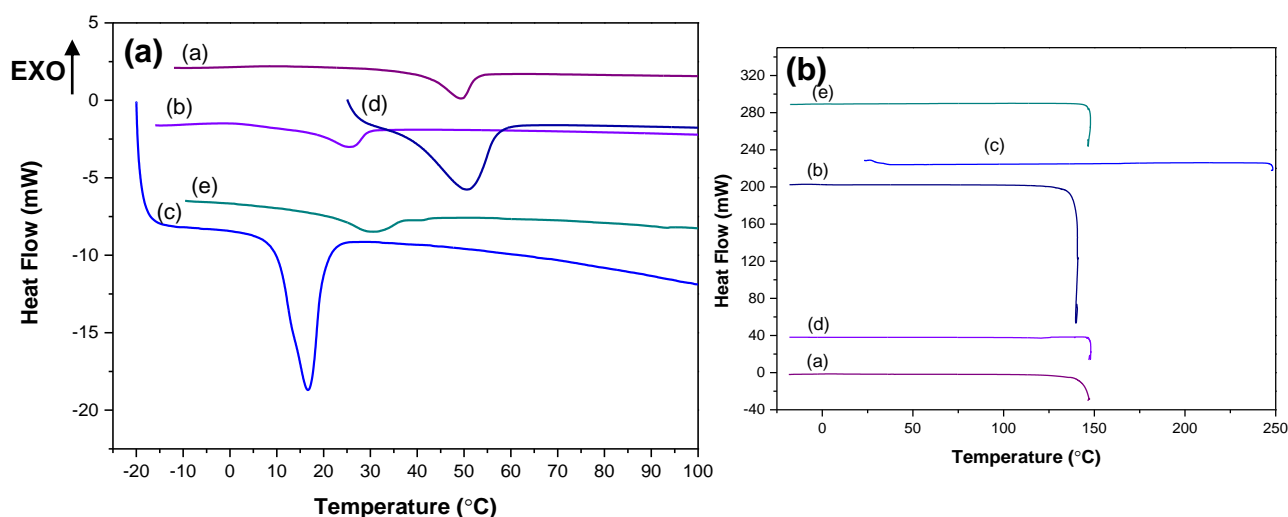
Figure 5. 12 The DSC (a) heating and (b) cooling curves of the PU crosslinked composite PCMs.

Observations indicated that the PU crosslinked composite PCMs all exhibited a single endothermic peak which was attributed to the presence of a single type of crystal (e.g., spherulite crystal). Also, no exothermic peaks were generated during the cooling process which is an indication that no liquid phases were generated during the phase transition process. Therefore, results showed that the solid-liquid PCM had been converted into a solid-solid PCM after the PU crosslinking reaction. This was one of the main reasons why the latent heat of melting of PEG8000 had reduced drastically after chemical reaction.

The melting enthalpy of the PU crosslinked composite PCMs lied in the range 5.86 to 16.57 J/g while pristine PEG8000 had a melting enthalpy of 181.5 J/g because PU crosslinking reaction resulted in restricting the mobility of the PEG chain during phase change. Hence, significant reduction in the latent heat of melting value shows that the crystalline properties of PEG was destructed greatly. This was attributed to the formation of an increased number of crystal defects which resulted in increasing the number of amorphous phases accompanied by a decrease in the number of crystallisable segments. The melting temperature of the composite PCMs were all observed to be shifted to a lower temperature; and lied in the range 16.98 to 50.62 °C

while the T_m of PEG8000 was 60.19 °C. This was due to the reduced thickness of the crystal lamellae after the chemical crosslinking reaction.

Table 5. 7 Thermal properties of the PU crosslinked composite PCMs.

Sample name		Phase transition temperatures		Latent heats	
		T_m (°C)	T_c (°C)	H_m (J/g)	H_c (J/g)
PEG8000		60.19	43.78	181.5	182.1
(a)	5PEG8000:0.5MC:3TDI	49.36	Not available	10.67	Not available
(b)	5PEG8000:0.5MC:5TDI	25.50	Not available	7.52	Not available
(c)	5PEG8000:1MC:3TDI	16.98	Not available	16.57	Not available
(d)	5PEG8000:1MC:5TDI	50.62	Not available	12.29	Not available
(e)	5PEG8000:1. 5MC:5TDI	30.53	Not available	5.86	Not available

5.7 Studying the crystalline properties of PU crosslinked composite PCMs

The XRD patterns of pristine PEG8000, MCC and the PU crosslinked composite PCMs with blend ratios 5.0:1:5, 5.0:1.25:5, 5.0:1.50:5 and 5.0:1.75:5 is presented in Figures 5.13 and 5.14 to study the changes in the crystalline properties of PEG8000 after the PU crosslinking reaction. The XRD patterns of the PU crosslinked composite PCMs appears to be completely different compared to the one of PEG8000, MCC and TDI which suggested that the crystalline properties of PEG8000 had experienced significant destruction. Hence the major two distinctive peaks of PEG8000 appearing at 2θ = 19.10° and 23.23° representing the highly crystalline phases of PEG8000 had disappeared completely in the XRD patterns of the PU crosslinked composite PCMs due to the incorporation of MCC (e.g., amorphous polymer). Also, the XRD pattern of the composite PCMs are observed to contain a single broad hump which confirms the presence of amorphous structures.

MCC is considered as an impurity, and therefore resulted in reducing the ability of the crystalline regions to reorganise which consequently resulted in producing non-crystallisable composite PCMs containing very few crystalline phases (Sundararajan et al., 2019). Reduction of the crystalline peak intensities of PEG8000 in the composite

PCM indicated that the crystal size and the perfection of the crystal lattice of PEG had reduced (Chen et al., 2015) due to the breaking of PEG8000 crystallinity which led to the loss of crystallites. This resulted in increasing the number of crystal defects and amorphous phases since crystal defects are concentrated in the amorphous regions (St-Onge et al., 2021). Increasing the MCC content from 9.09% to 11.1% (e.g.,22.1% increase) caused no significant changes in the appearance of the broad hump at 2θ= 20.44°; however, the intensity was observed to reduce from 1328% to 1180% (e.g.,11.14% decrease) due to the decreased crystallinity with increasing MCC content. Increasing the MCC content further to 13.0% caused a drastic reduction in the peak intensity; and the peak position got shifted from 2θ= 20.44° to 22.74° due to the reduced size of PEG crystals.

Increasing the MCC content to 14.9% was observed to convert the weak broad peak to a sharper peak; and intensity increased from 1328% to 1783% which may suggest that the crystallinity of PEG8000 had improved significantly. Therefore, results indicated that the crystallinity of PEG8000 was influenced mainly by the type of chemical crosslinking reaction and the chemical composition. Overall, it can be concluded that amorphous polymers were prepared in the current study as result of shape stabilising PEG8000 via the PU crosslinking reaction. Therefore, the PU crosslinked composite PCMs had very poor thermal properties (e.g., latent heat of melting) which was in good agreement with the DSC results.
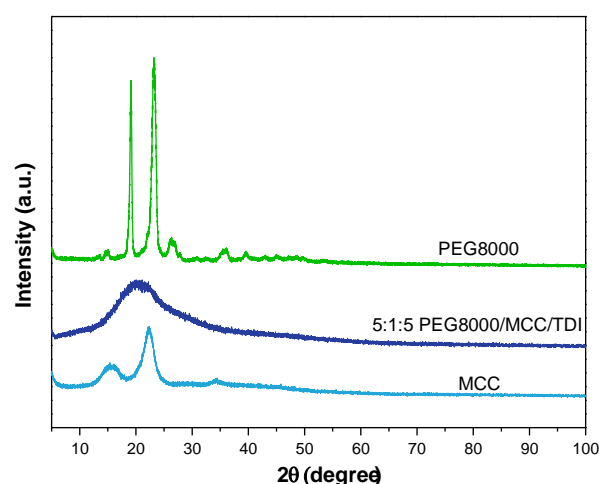
Figure 5. 13 XRD patterns of the raw materials and the PU crosslinked composite PCMs.
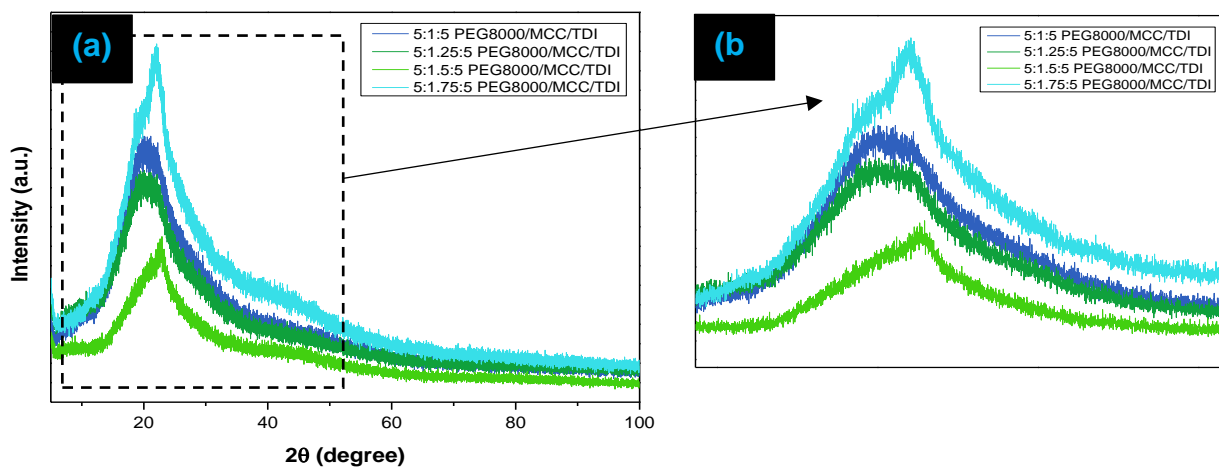
Figure 5. 14 (a) XRD pattern of the PU crosslinked composite PCMs containing different MCC content; and (b) zoomed-in view of the humps.

5.8 Interim Conclusions

In this Chapter the leakage problem of PEG was successfully overcome through the employment of the PU chemical crosslinking reaction under normal laboratory conditions in the absence of nitrogen (N_2) atmosphere. Results demonstrated that the thermal and crystalline properties of PEG was influenced greatly by the type of chemical crosslinking reaction and the chemical composition of the PU crosslinked composite PCMs. The conclusions and outcomes of current research are summarised below.

5.8.1 Outcomes

➢ Results indicated that the existence of weak intermolecular forces between PEG and DMF solvent resulted in affecting the latent heat capacity of PEG greatly.

➢ Drastic reduction was caused to the latent heat capacity of PEG after the PU crosslinking reaction attributed to the weak interactions that existed between PEG and MCC along with the destruction caused by the PU crosslinking reaction on the thermal and crystalline properties.

➢ The PU crosslinking reaction prepared using different formulations resulted in producing non-crystallisable composite PCMs with poor thermal properties since they contained higher number of amorphous phases and very few crystalline phases.

➢ The durability of the PU crosslinked composite PCMs were very poor since they were observed to undergo degradation in less than 3 months which was attributed to the formation of weak intermolecular forces in the gel-like composite PCMs due to the existence of solvent in the crosslinked network.

5.8.2 Outlooks

➢ Formation of covalent bonds between PEG and the supporting material is necessary to enhance the durability of the resulting composite PCMs; however, forming a highly crosslinked network is not ideal according to the results from current study since this had an undesirable effect on the latent heat capacity of PEG which consequently resulted in preparing non-crystallisable composite PCMs with poor thermal performance. Therefore, need to determine suitable formulations for the preparation of composite PCMs of enhanced thermal performance.

➢ Sufficient reaction temperature is necessary to initiate and proceed chemical reactions; however, when it comes to dealing with chemical reactions involving

PCMs like PEG which are known to be 'temperature sensitive' it is crucial to ensure that PEG is not subjected to elevated temperatures for a long duration since this would degrade its thermal properties which most studies rarely paid attention to. Therefore, need to develop a synthesis route which causes minimal thermal degradation of PEG during the shape stabilisation process.

➢ Previous studies mainly rely on utilising toxic solvents and chemical crosslinking agents like DMF and TDI in excess for the shape stabilisation of PEG. However, it is crucial to avoid the use of toxic materials/ chemicals to encourage green chemistry. Therefore, need to replace the toxic solvent and crosslinking agent with promising environmentally friendly materials like deionised water and citric acid.

➢ Changes in crystalline properties were demonstrated using the XRD data; however, it is essential to visualise the changes caused to the crystal morphology and structure of PEG after the chemical crosslinking reaction. Therefore, need to perform POM analysis to determine the changes in crystal morphology and structure of PEG after the shape stabilisation process.

Chapter 6: Development and characterisation of TCA crosslinked composite PCMs

Abstract

In this Chapter the leakage problem of PEG was overcome through the employment of the facile and feasible TCA crosslinking reaction using citric acid (CA) as the crosslinking agent and cellulose fibre (CF) as the supporting material. A series of composite PCMs with different PEG loadings were successfully prepared. Its chemical structure, crystalline properties, thermal properties, and surface morphology were investigated and studied using FTIR, XRD, DSC, POM and SEM analysis. Supercooling temperature of PEG was observed to have decreased after the TCA crosslinking reaction. SEM images suggested that the compatibility between PEG and CF was influenced mainly by the chemical composition of the composite PCM. This Chapter aims at meeting specific objectives 3, 4 and 6 listed in section 1.4.

6.1 Introduction

Majority of the previous literature aimed at preparing environmentally friendly PEG based composite PCMs by focusing solely on replacing the synthetic supporting material with an environmentally friendly biopolymer like cellulose/ and or their derivatives but always avoided addressing the issues of utilising organic solvents and toxic crosslinking agents in excess during the chemical crosslinking reaction. Hence, incorporating toxic solvents or crosslinking agent will result in producing toxic PEG-cellulose based composite PCMs which are unsuitable for most applications including buildings since resulting materials will release toxic fumes over service life which may cause health problems to occupants after prolonged exposure. Therefore, it is critical to utilise environmentally friendly materials (e.g., green materials) while stabilising PEG through chemical crosslinking reactions.

PEG is susceptible to chemical reactions since it is comprised of a plentiful of hydroxyl groups which means its reactions are not limited to the PU crosslinking in which reactions occur between the hydroxyl and isocyanate groups but can also participate in other reactions namely with tricarboxylic acid (TCA) crosslinking better known as

chemical esterification reaction which occurs between the hydroxyl and carboxyl functional groups. TCA crosslinking reaction utilises citric acid (CA) which is commonly utilised in the food, pharmaceutical and cosmetic industries, as the crosslinking agent. Moreover, in this reaction deionised (DI) water can be utilised as the solvent which is a promising replacement for the conventionally utilised toxic organic solvents like N,N-Dimethylformamide (DMF). Therefore, in the current study DI water and CA was used as solvent and crosslinking agent during the TCA crosslinking reaction to encourage green chemistry by avoiding the use of toxic chemicals; and solely relying on the use of environmentally friendly materials.

Overall, a facile and highly feasible solution casting and slow evaporation method (discussed in Chapter 3) was employed to develop a series of PEG-CF composite PCMs of different thermal performance by varying the mass ratio of PEG:CF and CA content since results from Chapter 5 demonstrated that the chemical composition plays a major role in dictating the thermal and crystalline properties which subsequently affects the thermal performance of the resulting composite PCMs. Unique formulations were developed and investigated in the current study. Chemical composition of the different blend ratios developed and investigated are presented in Tables 6.1 to 6.4.

Changes in thermal and crystalline properties of PEG in the TCA crosslinked composite PCMs resulting from the different formulations was studied extensively in the current study for the first time since PEG based composites using CF as supporting materials have only been prepared as hydrogels in biomedical applications; and therefore, the thermal and crystalline properties were of least interest. The interfacial compatibility between PEG and CF in the TCA crosslinked composite PCM is yet to be studied.

6.2 Experiments

6.2.1 Studying the crystalline properties of the TCA crosslinked composite PCMs

Table 6. 1 Formulation table

Name	PEG8000 (wt.%)	CF (wt.%)	CA (wt.%)
2.5:1:3	38.46	15.38	46.15
2.5:1:5	29.41	11.76	58.82
2.5:1:7.5	22.73	9.09	68.18
3.0:1:3	42.86	14.29	42.86
3.0:1:5	33.33	11.11	55.56
3.0:1:7.5	26.09	8.69	65.22

6.2.2 Influence of PEG8000 content on the crystalline properties of the TCA crosslinked composite PCMs

Table 6. 2 Formulation table

Name	PEG8000 (wt.%)	CF (wt.%)	CA (wt.%)
2.5:1:5	29.41	11.76	58.82
3.0:1:5	33.33	11.11	55.56
3.5:1:5	36.84	10.53	52.63
4.0:1:5	40.00	10.00	50.00
2.5:1:10	18.52	7.41	74.07
3.0:1:10	21.43	7.14	71.43
3.5:1:10	24.14	6.90	68.96
4.0:1:10	26.67	6.67	66.66

6.2.3 Impact of CA and CF content on the crystalline properties of PEG8000 in the TCA crosslinked composite PCMs

Table 6. 3 Formulation table

Name	PEG8000 (wt.%)	CF (wt.%)	CA (wt.%)
2.5:1:3	38.46	15.38	46.15
2.5:1:5	29.41	11.76	58.82
2.5:1:7.5	22.73	9.09	68.18
2.5:1:10	18.52	7.41	74.07
4.0:1:5	40.00	10.00	50.00
4.0:1:7.5	32.00	8.00	60.00
4.0:1:10	26.67	6.67	66.66
4.5:1:5	42.86	9.52	47.62
4.5:1:7.5	34.62	7.69	57.69
4.5:1:10	29.03	6.45	64.52
4.0:0.80:5	40.82	8.16	51.02
4.0:0.85:5	40.61	8.63	50.76
4.0:0.90:5	40.40	9.09	50.51
4.0:0.95:5	40.20	9.55	50.25
4.0:0.80:10	27.03	5.40	67.57
4.0:0.85:10	26.94	5.72	67.34
4.0:0.90:10	26.85	6.04	67.11
4.0:0.95:10	26.76	6.35	66.89
4.0:1:10	26.67	6.67	66.66

6.2.4 Influence of CF and CA content on the thermal properties of PEG8000 in the TCA composite PCMs

Table 6. 4 Formulation table

Name	PEG8000 (wt.%)	CF (wt.%)	CA (wt.%)
3.5:0.85:7.5	29.54	7.17	63.29
3.5:1:7.5	29.17	8.33	62.50
3.5:0.85:10	24.39	5.92	69.69
3.5:1:10	24.14	6.90	68.96

6.3 Methods

6.3.2 ATR-FTIR analysis

ATR-FTIR was performed in the wavenumber range 500 to 4000 cm^{-1} on powder samples to confirm the formation of a crosslinked structure.

6.3.3 XRD analysis

Powder XRD was performed on powder TCA crosslinked composite PCM samples to study the crystalline properties of the TCA crosslinked composite PCMs (see Chapter 3 for a detailed explanation regarding the procedure followed).

6.3.4 DSC analysis

DSC analysis was performed under nitrogen (N$_2$) atmosphere to determine the latent heat of melting and crystallisation with the corresponding melting and crystallisation temperatures (e.g., phase transition temperatures). Using the DSC data, relevant heating and cooling curves were plotted. By calculating the area under the peaks/ dips the latent heat of melting and crystallisation was calculated in J/g (see Chapter 3 for detailed explanation regarding the procedure followed to calculate the latent heat capacities).

6.3.6 POM/ hot stage analysis

POM analysis was performed to study the changes in the crystal morphology and crystal structure of pristine PEG8000 after TCA crosslinking. The POM images (e.g., digital images) of the TCA crosslinked composite PCMs were taken at room temperature. While hot stage analysis was performed to evaluate changes in crystal morphology of the crosslinked composite PCMs during the phase transition process by capturing digital photos during the melting and crystallisation processes (see Chapter 3 for a detailed explanation regarding the procedure followed).

6.3.7 SEM analysis

SEM analysis was performed to study the surface morphology and the microstructure of the TCA crosslinked composite PCMs. The test samples were coated with a thin layer of gold to enhance the clarity of the SEM images produced (see Chapter 3 for a detailed explanation regarding procedure followed).

6.4 Results and discussion

6.4.1 Formation mechanism of composite PCM via the TCA crosslinking

Firstly, anhydrous CA was dissolved in DI water under heating at 80 °C; and as result of exposing CA to an elevated temperature a highly reactive anhydride CA compound had formed (see Figure 6.1) due to dehydration; thus, water (H_2O) molecule leaves the compound; however, the degree of conversion from CA to anhydride was not known but it is a function of the reaction temperature which was one of the main reasons why reaction had to be performed at an elevated temperature (e.g., 80 °C). Dissolution of PEG in CA solution resulted in initiating the partial esterification reaction since the reaction mixture contained both OH groups and COOH groups which is the main driving force of this reaction; and because PEG was deprotonated during the dissolution process (as shown in Figure 6.2) it became susceptible to chemical attacks; however, it was unknown whether PEG reacted with CA or the anhydride CA.
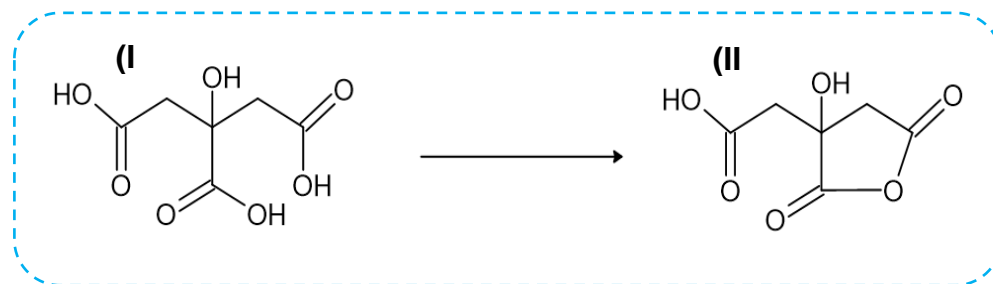
Figure 6. 1 (I) CA; and (II) CA Anhydride.
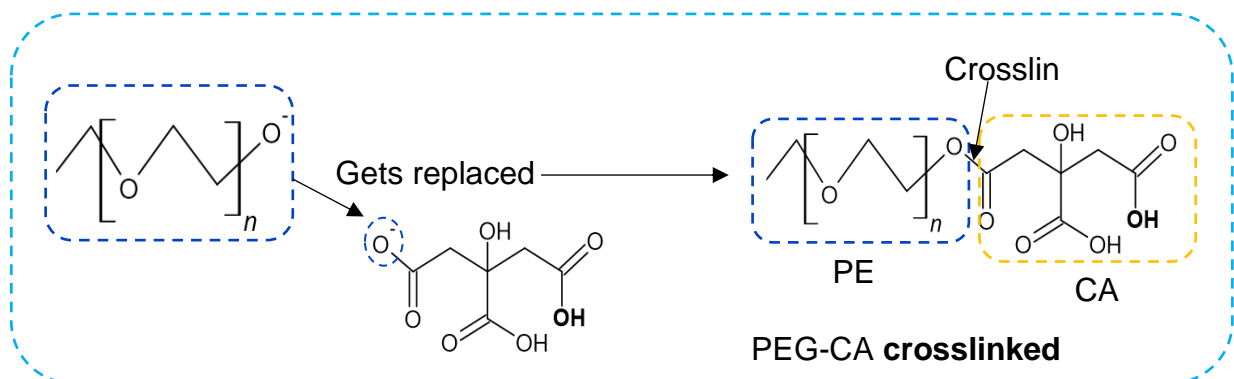
Figure 6. 2 Reaction between PEG and CA solution.

6.4.2 Functional groups of the TCA crosslinked composite PCMs

Figure 6.3 shows the FTIR spectra of PEG8000, CF and CA along with the TCA crosslinked composite PCMs. Observations indicated that the absorption bands of the FTIR spectra of the TCA crosslinked composite PCMs all appear in three wavenumber regions of 3600 to 2900 cm^{-1}, 2700 to 2900 cm^{-1} and 1800 to 1500 cm^{-1}.

The FTIR spectra of the CF/CA composites with blend ratios 1:3 and 1:5 containing 25 and 16.67 wt.% of CF prepared with 75 and 83.33 wt.% of CA appears to exhibit a different FTIR spectra pattern compared to both CF and CA which indicated that a chemical reaction had taken place between both CF and CA. The FTIR spectrum of CF consisted of the characteristic weak broad peak at 3310 cm^{-1} which is ascribed to the stretching vibration of the OH group while the peak appearing at 2885 cm^{-1} corresponded to the stretching vibration of the C-H bands. Observations indicated that the OH group content had reduced after chemical crosslinking because the broad peak at 3310 cm^{-1} appeared to have become weaker which demonstrated the participation of the OH groups in the chemical reaction to form covalent bonds with CA. Peak of CA at 1638 cm^{-1} attributed to the stretching vibration of COOH had disappeared in the crosslinked composites which confirmed the bond breakage of the COOH group during chemical crosslinking reaction. Also, reducing the CF/CA ratio from 0.33 to 0.20 was observed to cause no significant changes to the intensity of this weak band. The weak bands appearing at 1413 cm^{-1} and 1342 cm^{-1} are attributed to the symmetric COO^{-}. Peak appearing at 1744 cm^{-1} and 1698 cm^{-1} indicates the presence of C=O group which confirms the formation of ester linkages during the chemical crosslinking reaction. Reducing the mass ratio of CF to CA from 0.33 to 0.20 resulted in increasing the peak intensity which suggested that sufficient CA was required to produce crosslinked composite PCM. The peak appearing at 2885 to 2878 cm^{-1} attributed to the stretching vibration of the C=O group (e.g., ester bond) confirms the formation of ester linkages via the TCA crosslinking reaction. The intensity of this peak was observed to increase from 69.7 to 87.2% (e.g., 25.11% increase) with increasing CA content which suggested that more linkages had formed in 1:5 CF:CA composite (Chen et al., 2011b).

The characteristics IR peaks of PEG8000 observed at 3480, 2800 and 1960 cm^{-1} were attributed to the O-H and C-H stretching vibrations. The characteristics peaks of CF appearing at 3600-3200, 2900, 1638 and 1053 cm^{-1} were attributed to the stretching

vibration of the OH, CH, COOH and CO groups (Uyanga and Daoud, 2021). These peaks were also present in the FTIR spectra of the TCA crosslinked composites which confirms the presence of PEG in the TCA crosslinked composite PCMs; however, the relative intensities of peaks at 1146, 1098 and 1059 cm^{-1} had reduced from 71.84, 40.38 and 48.84% to 66.83, 22.95 and 32.28% after chemical reaction which confirms the existence of weak interactions between PEG8000 and CF in the crosslinked product. Overall, observations indicated that the FTIR spectra patterns of the TCA crosslinked composite PCMs all appear to exhibit a similar pattern despite having different chemical compositions; and noticeable changes in peak intensity are observed to occur in the bands indicating the presence of the O-H and C=O group.

In the FTIR spectra of the composite PCMs with blend ratios 3.5:1:3 and 3.5:1:5 the weak broad characteristic band of PEG8000 and CF appearing in the range 3500-3400cm^{-1} ascribed to the stretching vibration of the O-H group appears in both composite PCMs which is attributed to the stretching vibration of O-H; however, the peak intensity had reduced from 90.7% to 40.7 and 72.1% after the crosslinking reaction due to the formation of ester linkages during the crosslinking reaction between PEG8000 and CF which resulted in reducing the number of OH groups (Capanema et al., 2018). Reduction in OH group content confirms the formation of a crosslinked structure. The peak at 1113 cm^{-1} of PEG8000 is attributed to the stretching vibration of the -C-O-C- groups (Qin et al., 2019b).

Peaks appearing in the fingerprint region at 1146, 1098 and 1059 cm^{-1} are ascribed to the C-O-C stretching vibration. The peaks appearing at 1341 and 1360 cm^{-1} are attributed to the CH$_2$ bending vibrations and indicated the existence of the crystalline phases in pristine PEG8000 (Polu and Rhee, 2015). The band at 1426 cm^{-1} of the composite PCM is associated with the number of crystalline phases of PEG8000 in the crosslinked composite PCMs (Capanema et al., 2018; Hospodarova et al., 2018). Intensity reduction of band at 1426 cm^{-1} confirms changes in the crystalline properties of PEG8000 due to the formation of a crosslinked structure where the PEG chain was less crystallisable which was in good agreement with the XRD results. The intense peak observed at 2880 cm^{-1} with 70.96% intensity was ascribed to the CH$_2$ stretching vibration while the other less intense peaks appearing at 841 and 960 cm^{-1} were attributed to the CH$_2$ wagging and twisting vibrations (Polu and Rhee, 2015; Sari, 2014). The peak at 1638 cm^{-1} attributed to the stretching vibration of COOH had

disappeared in the crosslinked composites PCMs which confirms the bond breakage of the COOH group during chemical crosslinking reaction. This peak had shifted to 1468 cm^{-1} (e.g., lower wavenumber) in the composite PCMs due to the weak intermolecular interactions during chemical crosslinking and hydrogen bonding. Therefore, results suggested that intermolecular forces of attraction co-existed in the crosslinked composite PCMs between the unreacted PEG and CF (Uyanga and Daoud, 2021).

In the composite PCMs with blend ratios 2.5:1:5, 3.5:1:5 and 4.5:1:5, increasing the PEG content from 29.41 to 36.84 and 42.86 wt.% and decreasing the CF content from 11.76 to 10.53 and 9.52 wt.% resulted in altering intensity of the peak at 3450 cm^{-1} corresponding to the stretching vibration of the OH group. In the composite PCM with blend ratio 2.5:1:5 this peak appears to have become less visible which indicated that the OH groups had all participated in the chemical reaction while this peak appeared to be very intense in the composite PCM with blend ratio 3.5:1:5. This suggested that weak intermolecular forces also existed and led to the formation of a less crosslinked structure. However, in the composite PCM with blend ratio 4.5:1:5 the peak intensity had reduced which indicated that the density of the crosslinked network had improved due to the addition of PEG8000. Overall, FTIR analysis confirms the formation of a network of covalent bond and the presence of weak intermolecular forces of attraction between the unreacted PEG8000 and CF. Therefore, both physical and chemical interactions will allow PEG8000 to retain its original solid state; thereby, prevent leakage of PEG8000 during the phase transition process (Deshpande et al., 2021).
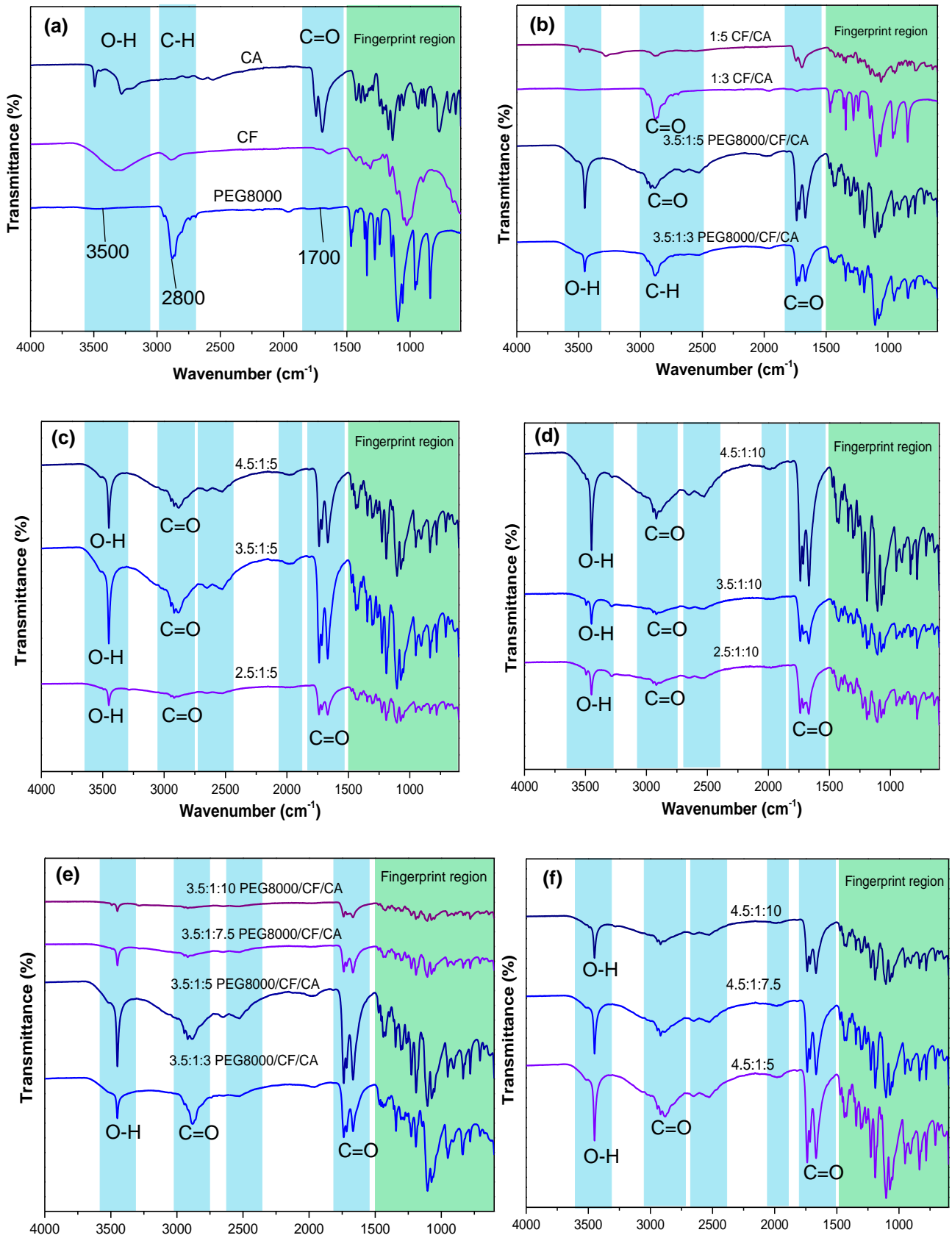
Figure 6. 3 FTIR spectra of (a) raw materials; and (b) to (f) TCA crosslinked composite PCMs.

6.4.3 Studying the crystalline properties of TCA crosslinked composite PCMs

The XRD patterns of TCA crosslinked composite PCMs with blend ratios 2.5:1:3, 2.5:1:5, 2.5:1:7.5, 3.0:1:3, 3.0:1:5 and 3.0:1:7.5 containing 38.46, 29.41, 22.73, 42.86, 33.33 and 26.09 wt.% of PEG8000 are presented in Figure 6.4 to study the changes in the crystalline properties of PEG8000 after the TCA crosslinking reaction. As discussed in Chapter 4 PEG8000 is a semicrystalline polymer since its CI value was 52.94% which means it is comprised of both crystalline and amorphous phases. Observations indicated that it exhibited two sharp, major diffraction peaks at 2θ = 19.10° and 23.23°. CF had a CI value of 39.98% which indicated that it an amorphous polymer since the amorphous phases appear to outweigh the crystalline phases while its XRD pattern demonstrated the same. Two broad humps are observed to appear at 2θ = 15.50° and 22.40° which confirms the presence of amorphous structures in CF (see Chapter 4 for more information regarding the crystalline properties of the raw materials used in the current study).

The XRD patterns of the TCA crosslinked composite PCMs appears to exhibit a different pattern compared to the one of PEG8000, CF and CA which suggested that the crystalline properties of PEG8000 had changed after the TCA crosslinking reaction because the major two distinctive peaks appearing at 2θ = 19.10° and 23.23° corresponding to the crystal lattice planes (1 2 0) and (0 3 2), representing the highly crystalline phases of pristine PEG8000 became less prominent in the XRD patterns of the composite PCMs. This was attributed to the destruction caused to the crystal structure of PEG after the shape stabilisation process due to the formation of a highly crosslinked structure; and due to the incorporation of impurities in form of CF and CA which resulted in reducing the ability of the crystalline regions of PEG to reorganise. This consequently made the resulting composite PCMs less crystallisable (Sundararajan et al., 2019).

Reduction of the crystalline peak intensities of PEG8000 in the composite PCM indicated that the crystal size and the perfection of the crystal lattice of PEG had reduced (Chen et al., 2015) attributed to the breaking of PEG8000 crystallinity which led to the loss of crystallites. This resulted in increasing the number of crystal defects and amorphous phases since crystal defects are concentrated in amorphous regions only (St-Onge et al., 2021). Moreover, results also indicated that crystallinity of the TCA crosslinked composite PCMs of the current study were much lower than pristine

PEG8000; and they were observed to vary with the blend ratio (see Figure 6.4 (c)). Provided that the PEG/CF mass ratio was 2.50, increasing PEG content from 22.73 wt.% to 29.41 wt.% (e.g., 29.39% increase), PEG/CA mass ratio from 0.33 to 0.50 (e.g., 51.52% increase) and CF content from 9.09 to 11.76 wt.% (e.g., 29.37% increase) resulted in increasing the CI from 40.17% to 43.69% (e.g., 8.76% increase) attributed to the increased number of crystalline phases in the composite PCM accompanied by the reduction in the number of amorphous domains and thus, crystal defects.

For the same PEG/CF mass ratio, increasing the PEG content from 29.41 to 38.46 wt.% (e.g.,30.77% increase), PEG/CA ratio from 0.50 to 0.83 and CF content from 11.76 to 15.38 wt.% (e.g.,30.78% increase) resulted in reducing the CI drastically from 43.69 to 8.92% (e.g., 79.58% reduction). This indicates that in the corresponding composite PCM the crystalline segments of PEG8000 were reduced significantly attributed to formation of a very tight crosslinked network structure in which the mobility of the PEG8000 chain was restricted. This is in good agreement with previous literature which reports that the content of PEG segments do not affect the crystallisation properties of the composite PCMs significantly (Peng et al., 2016).

The same trend was observed when the PEG/CF ratio was 3.00 and the PEG content was increased from 26.09 to 33.33 and 42.86 wt.% since the CI was observed to increase from 35.44 to 41.50 (e.g.,17.10% increase) followed by a decrease to 19.09% (e.g., 54.00% reduction). The degree of reduction was lower which indicated that the PEG segments in the crosslinked structure resulting from the blend ratio 3.0:1:3 had better mobility attributed to the formation of a less dense structure of covalent bonds.
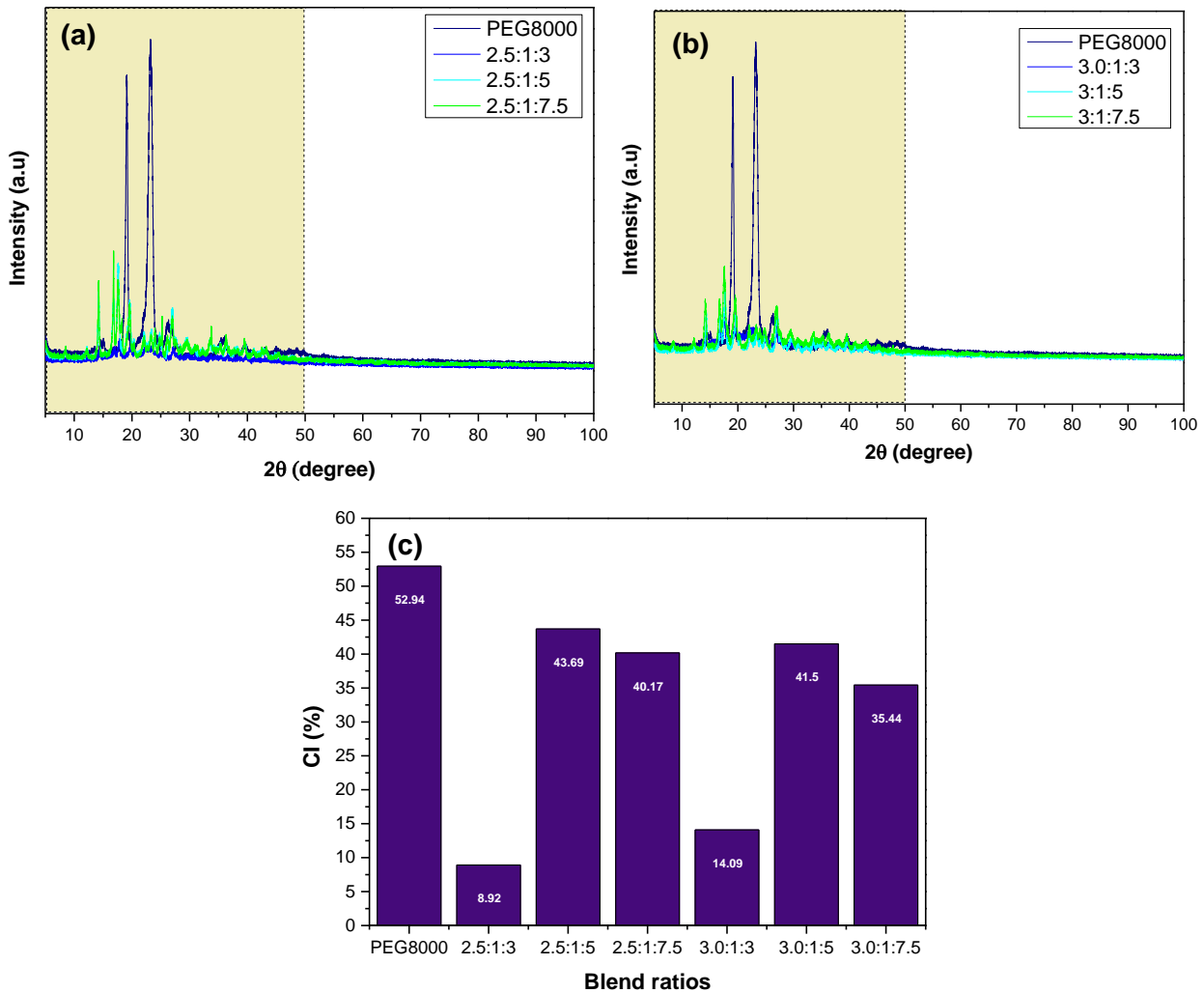
Figure 6. 4 (a) and (b) XRD patterns of TCA crosslinked composite PCMs; (c) CI values of the different TCA crosslinked composites.

6.4.3.1 Influence of PEG8000 content on the crystalline properties of composite PCMs

In general, previous literature reports that increase in crystallinity is attributed to the increased wt.% of PEG in the crosslinked composite PCM (Sundararajan et al., 2019). PEG is a semicrystalline polymer; therefore, it will contain both amorphous and crystalline phases. Therefore, increasing PEG content will not only increase the crystalline phases but will be accompanied by an increase in the number of amorphous phases. The experimental results demonstrated the same.

The XRD patterns of TCA crosslinked composite PCMs with blend ratios 2.5:1:5, 3.0:1:5, 3.5:1:5, and 4.0:1:5 containing 29.41, 33.33, 36.84, and 40 wt.% of PEG8000 is presented in Figure 6.5 mainly to evaluate the effects of PEG8000 content on the crystallinity of the TCA crosslinked composites PCMs. Results indicate that all crosslinked PCMs had lower crystallinities compared to pristine PEG8000 since their

170

CI values lied in the range 19.41 to 45.30% (see Figure 6.5 (c)) attributed to the formation of the crosslinked structure. Increasing PEG8000 content from 29.41 to 33.33, 36.84 and 40.00 wt.% resulted in decreasing the CI from 43.69 to 41.50, 23.65 and 19.41%. This suggested that optimisation of PEG content caused no enhancement of its crystallinity, but it was observed to increase the amorphous phases and the crystal defects. This was attributed to the density of the crosslinked structure formed since the higher the number of hydroxyl group participates in the TCA crosslinking reaction the higher the density of the crosslinked structure will be which will result in the formation of composite PCMs with higher number of amorphous domains.

In reactions where a limited number of hydroxyl groups take place the resulting final products will have higher crystallinity because the PEG chain had better mobility in the structure during the phase transition process. Results indicated that PEG8000 content was inversely proportional to the crystallinity. With increasing PEG8000 content the PEG/CF mass ratio was observed to increase from 2.50 to 3.00, 3.50 and 4.00 while the PEG/CA mass ratio increased from 0.50 to 0.60, 0.70, and 0.80 which suggested that the other reactants are more crucial in impacting the crystallisation properties of the composite PCMs since they determine the density of the crosslinked network formed, and thus, the mobility of the PEG8000 chains which is required to be free and flexible to facilitate crystallisation (Peng et al., 2016). The composite PCM with lowest CI of 19.41% had a PEG/CF and PEG/CA mass ratio of 4.0 and 0.80 while the one with an optimum CI of 43.69% had much lower PEG/CF and PEG/CA mass ratio of 2.50 and 0.50 which shows that incorporating impurities in form of CF and CA resulted in impacting the crystallinity.

The XRD patterns of TCA crosslinked composite PCMs with blend ratios 2.5:1:10, 3.0:1:10, 3.5:1:10, and 4.0:1:10 containing 18.52, 21.43, 24.14 and 26.67 wt.% of PEG8000 are presented in Figure 6.5 (b) mainly to evaluate the effects of PEG8000 content on the crystallinity of the TCA crosslinked composites PCMs prepared using the highest concentration of CA (e.g., 10 wt.%).
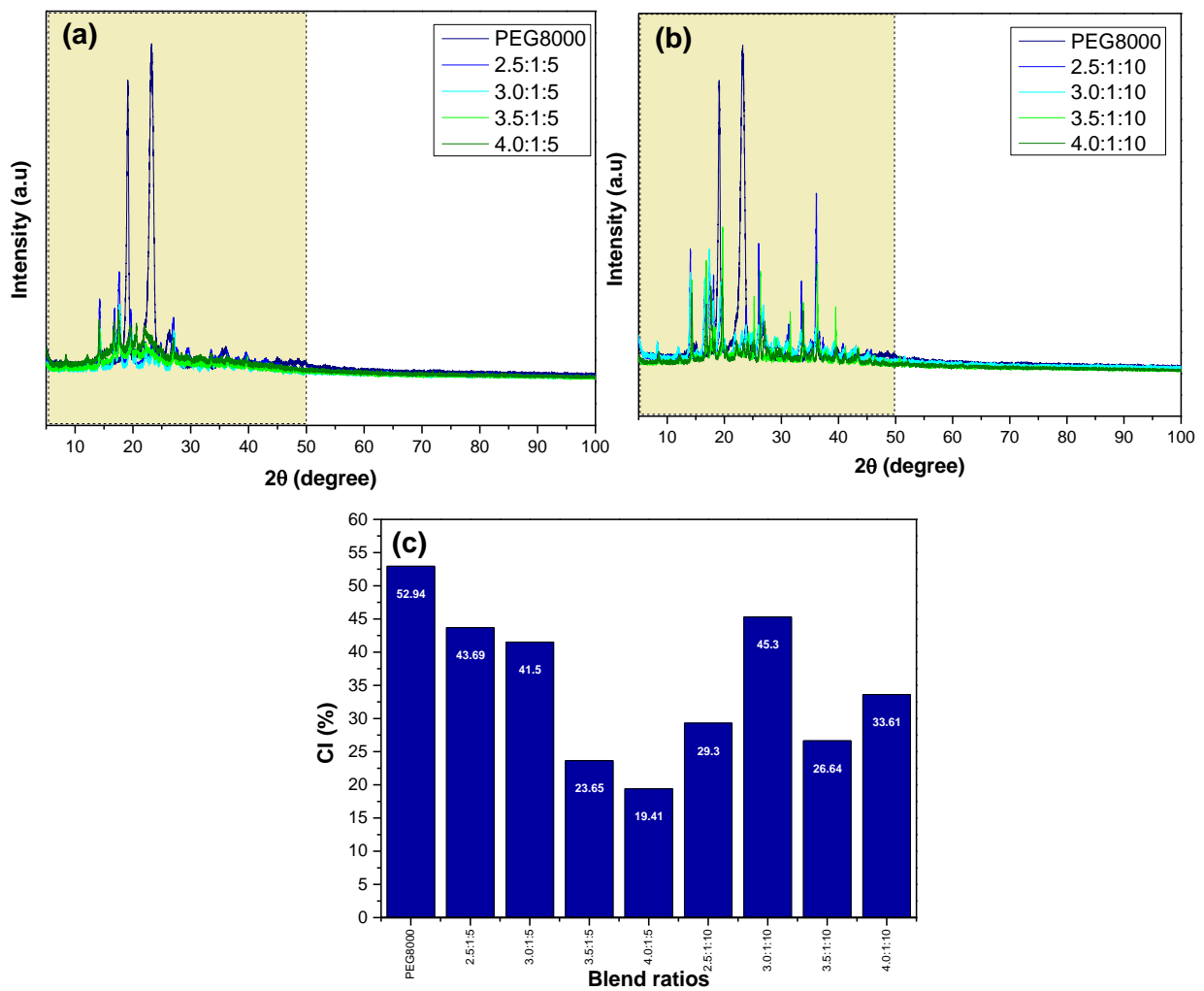
Figure 6. 5 (a) and (b) XRD patterns of TCA crosslinked composite PCMs; (c) CI values of the different TCA crosslinked composites.

6.4.3.2 Impact of CA and CF content on the crystalline properties of PEBG8000

The XRD patterns of composite PCMs prepared using the blend ratios 2.5:1:3, 2.5:1:5, 2.5:1:7.5 and 2.5:1:10 containing PEG8000 contents of 38.46, 29.41, 22.73 and 18.52 wt.% are presented in Figure 6.6(a). Provided that the PEG/CF mass ratio was 2.50, increasing the PEG8000 content from 18.52 wt.% to 22.73 and 29.41 wt.% resulted in increasing the CI from 29.30 % to 40.17 and 43.69%, respectively. Mainly because increasing PEG content resulted in increasing the soft segment in the crosslinked network. As result PEG chain had more freedom to move during the phase transition process, and therefore it became more crystallisable (Peng et al., 2016). Moreover, results suggested that composite PCM containing 29.41 wt.% had enhanced crystallisation properties since it had a high CI value compared to the other composite PCMs.

172

However, further increase of PEG8000 content from 29.41 to 38.46 wt.% had an adverse effect on the crystallinity since the CI value was observed to decrease drastically from 43.69 to 8.92% (e.g.,79.58%) which indicated that increasing PEG8000 content did not only increase the number of crystalline phases but was accompanied by an increase in the number of amorphous phases. Overall, it can be concluded that increasing the PEG/CA mass ratio from 0.25 to 0.33 and 0.50 seemed to have a desirable effect on the crystallinity of the final composite PCM; however, exceeding PEG/CA mass ratio of 0.50 and increasing it to 0.83 resulted in destructing the crystalline phases resulting in increasing the number of crystal defects and amorphous phases.

The XRD patterns of composite PCMs prepared using the blend ratios 4.0:1:5, 4.0:1:7.5 and 4.0:1:10 containing PEG8000 contents of 40.0, 32.00 and 26.67 wt.% are presented in Figure 6.6(b). Provided that the PEG/CF mass ratio was 4.00, increasing the PEG8000 content from 26.67 wt.% to 32.00 resulted in increasing the CI from 33.61 % to 35.65% (e.g., 6.07% increase) while increasing the PEG8000 content from 32.00 to 40.00 wt.% resulted in decreasing the CI to 19.41% (e.g.,45.55% decrease). This suggested that PEG/CA mass ratio influences the crystallinity of PEG8000 significantly because increasing the PEG/CA mass ratio from 0.40 to 0.53 (e.g., 32.5% increase) appeared to have increased the number of crystalline phases present in the composite PCM; however, doubling the PEG/CA mass ratio from 0.40 to 0.80 resulted in reducing the number of crystalline phases significantly since the CI value was observed to have reduced by 42.25%. Composite PCMs containing 40.00 wt.% of PEG8000 was considered undesirable because it was comprised mainly of amorphous phases (Polińska et al., 2021) which are structureless domains comprised of regions of different packing densities, and defects along the chain.

The XRD patterns of composite PCMs prepared using the blend ratios 4.5:1:5, 4.5:1:7.5 and 4.5:1:10 containing PEG8000 contents of 42.86, 34.62 and 29.03 wt.% are presented in Figure 6.6(b). Provided that the PEG/CF mass ratio was 4.50, increasing the PEG8000 content from 29.03 wt.% to 34.62 resulted in increasing the CI from 32.75 % to 36.00% (e.g.,9.92% increase) while increasing the PEG8000 content from 34.62 to 42.86 wt.% resulted in decreasing the CI from 36.00 to 25.17% (e.g., 30.08% reduction). This suggested that PEG/CA mass ratio influences the crystallinity of PEG8000 significantly. While increasing the PEG/CA mass ratio from

0.45 to 0.60 (e.g., 33.3% increase) appeared to have increased the number of crystalline phases present in the composite PCM; however, doubling the PEG/CA mass ratio from 0.45 to 0.90 resulting in reducing the number of crystalline phases significantly since the CI value was observed to have reduced by 23.15%.
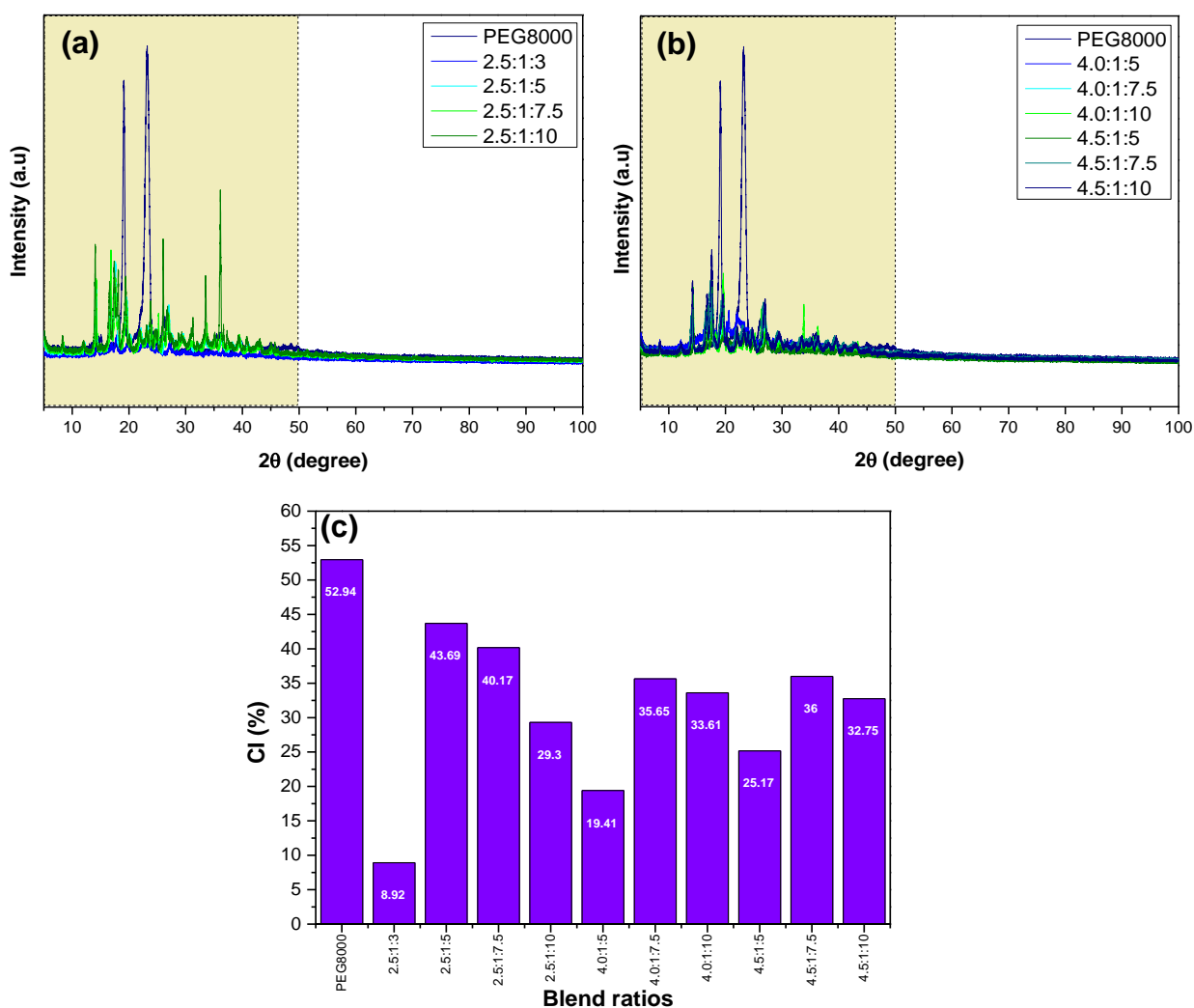
Figure 6. 6 (a) and (b) XRD patterns of TCA crosslinked composite PCMs; (c) CI values of the different TCA crosslinked composites.

The XRD patterns of composite PCMs prepared using the blend ratios 4.0:0.80:5, 4.0:0.85:5, 4.0:0.90:5 and 4.0:0.95:5 with CF contents of 8.16, 8.63, 9.09, 9.55 and 10 wt.% are presented in Figures 6.7(a) and 4.0:0.80:10, 4.0:0.85:10, 4.0:0.90:10, 4.0:0.95:10 and 4.0:1:10 with CF contents of 5.41, 5.72, 6.04, 6.35 and 6.67 wt.% in Figure 6.7(b). Results from Figure 6.7(c) indicated that incorporation of 8.16 wt.% of CF resulted in reducing the CI from 52.94% to 30.0% (e.g., 76.47% reduction) which

is in good agreement with previous literature which reports that presence of CF affects the crystal structure of PEG8000 in the composite PCM since CF is considered as an impurity. Therefore, it resulted in reducing the number of crystalline segments (Li et al., 2013; Sundararajan et al., 2017a). Increasing CF content from 8.16 to 8.63 wt.% made no significant changes in the crystallinity since CI was observed to increase from 30.00 to 30.68% (e.g., 2.27% increase). However, increasing the CF content from 8.63 to 9.09 wt.% (e.g., 5.33% increase) was observed to produce composite PCM of amorphous nature since the CI decreased significantly from 30.68 to 13.76 wt.% (e.g.,55.15% reduction) which suggests that incorporating 9.09 wt.% of CF had an adverse effect on the crystallinity. Moreover, increasing the CF content from 9.09 wt.% to 9.55 and 10wt.% was observed to increase the CI value from 13.67% to 16.67 and 19.41%, respectively. However, these CF contents are not suitable for the synthesis of composite PCMs of enhanced crystallisation properties since the CI values were comparatively lower compared to the other composite PCMs. Also, results suggested that the PEG/CF mass ratio had a major effect on the crystallinity.
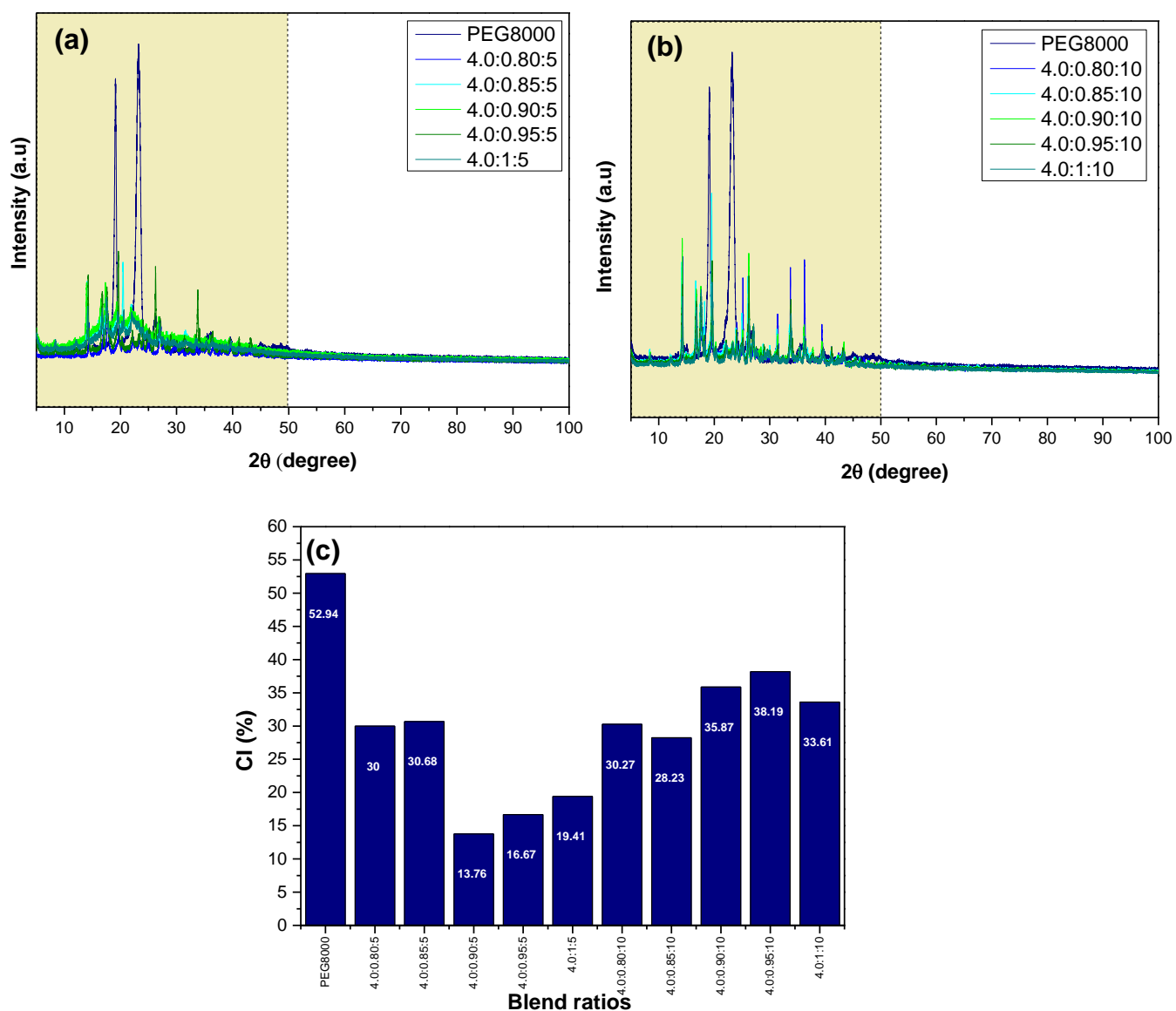
Figure 6. 7 (a) and (b) XRD patterns of TCA crosslinked composite PCMs; (c) CI values of the different TCA crosslinked composites.

6.4.4 Studying the thermal properties of composite PCMs prepared via TCA crosslinking reaction

6.4.4.1 Thermal behaviour of the TCA crosslinked composite PCMs during the first heating cycle

Figure 6.8 shows the thermal behaviour of composite PCMs with blend ratios 3:1:3, 3:1:5, 3:1:7.5 and 3:1:10 during their first heating cycle; and the thermal properties are summarised in Table 6.5. Two or three endothermic peaks appear at three different temperatures ranges of 21 to 73 °C, 114 to 173 °C and 185 to 265 °C. Two obvious endothermic peaks are observed in all the heating curves of the composite PCM samples which are attributed to melting of PEG8000 and the evaporation of residual water.

The first peak appears in the range 60.94 to 66.50 °C which is very close to the melting temperature of pristine PEG8000. Results suggested that the composite PCM containing low PEG content of 21.43 wt.% had a high latent heat capacity of 72.30 J/g. This demonstrates the possibility of producing composite PCMs of enhanced thermal performance using low PEG contents.

The second peak in the range 114 to 173 °C only appeared to be produced in composite PCMs containing high CA content, and the temperature was very close to the melting temperature of CA which is in the range 153 to 159 °C. This suggested that unreacted CA particles were present in the composite PCMs with blend ratio of 3:1:10 since it contained high CA content (e.g., 71.43 wt.%).

The third peak in the range 185 to 265 °C was attributed to the evaporation of water molecules. Hence, evaporation temperature of residual water present in the crosslinked structure was much higher than the one of bulk water (approximately 100 °C) because strong electrostatic force of attraction existed between the oxygen and hydrogen ions (e.g., strong hydrogen bonds) in the TCA crosslinked composite PCMs between the water and PEG8000 molecules compared to the one among the sole water molecules. Therefore, more energy was required to overcome these strong forces before the evaporation process (P. Liu et al., 2019). This behaviour was only observed during the first cycle and subjecting them to two or more heating/ cooling cycles resulted in producing typical DSC curves with single endothermic and exothermic peaks which suggested that the materials corresponding to the additional

endothermic peaks had decomposed or degraded as result of being exposed to an elevated temperature.
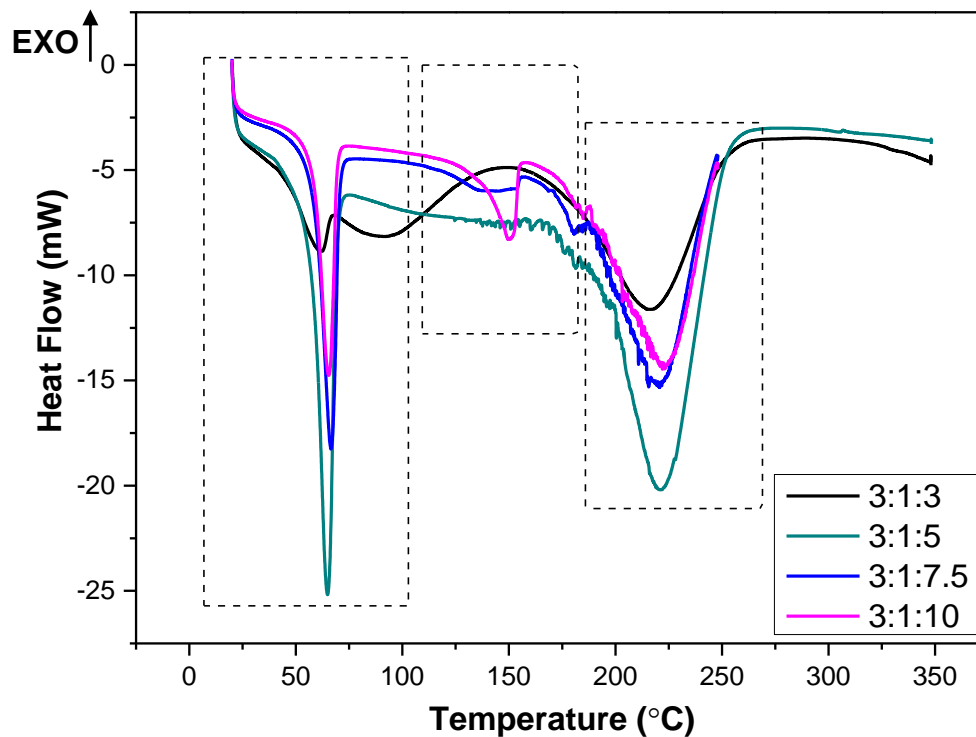
Figure 6. 8 DSC first heating cycles of the TCA crosslinked composite PCMs.

Table 6. 5 The thermal properties of the TCA crosslinked composite PCMs.

Sample name	T_m (°C)			H_m (J/g)		
PEG8000	63.12			181.5		
3.0:1:3	60.94		217.25	14.25		227.9
3.0:1:5	64.83		221.68	100.80		336.1
3.0:1:7.5	66.50		220.68	98.92		299.91
3.0:1:10	65.45	149.51	222.00	72.30	44.22	340.48

6.4.4.2 Thermal properties of the TCA crosslinked composite PCMs

In the prepared TCA composite PCMs PEG8000 is the working material since it is the only contributor to latent heat while CF is the supporting material since it makes no contribution to latent heat but is responsible for restricting the mobility of the PEG8000 chains during the phase transition process. It is supposed to ensure that the macro-fluidity of PEG8000 is lost even when it is in its amorphous state (e.g., melting process). The heating cycles are produced when the composite PCM undergoes melting as result of absorbing energy from the surrounding (e.g., endothermic process) and cooling cycles are produced when composite PCM undergoes crystallisation which involves release of stored energy into the surrounding (e.g., exothermic process).

Figure 6.9 (a), (b) and (c) shows the heating cycles since the peak points away from the exothermic direction, while Figure 6.9 (d), (e), and (f) shows the cooling cycles since peak points towards the exothermic direction of the TCA crosslinked composite PCMs with blend ratios 2.5:1:3, 3:1:3, 2.5:1:5 3:1:5, 2.5:1:7.5 and 3:1:7.5. They were produced as result of composite PCMs undergoing a phase change during the melting and cooling process. All curves appear to exhibit a single endothermic and exothermic peak which indicated the existence of one type of crystal structure in the TCA crosslinked composite PCMs. This was attributed to the melting and crystallisation of PEG8000 in the composite PCMs (Kong et al., 2017). The thermal properties are summarised in Table 6.6. The area under the exothermic and endothermic peaks of the crosslinked composite PCMs appears to be lower compared to the one of pristine PEG8000 which indicates reduction in latent heat of melting and crystallisation after chemical reaction.

The melting and crystallisation enthalpy of the TCA crosslinked composite PCMs lied in the range 24.93 to 47.35 J/g (e.g., 73.91 to 86.26% reduction) and 23.61 to 47.10 J/g (e.g., 74.19 to 87.03% reduction). PEG8000 had a melting and crystallisation enthalpy of 181.5 and 182.1 J/g, respectively. The very high latent heat of melting and crystallisation of PEG8000 indicates that the simple linear polymer chain which contains both $(CH_2-CH_2-O)_n$ and OH end groups is susceptible to crystallisation (e.g., can form crystals easily). Reduction in latent heat of melting and crystallisation is ascribed to the formation of a crosslinked structure in which the mobility and flexibly of the PEG8000 chain in restricted greatly.

179

The DSC results obtained from current study demonstrated that the TCA crosslinked composite PCMs prepared using different blend ratios all had latent heat of melting and crystallisation values lower than the one of pristine PEG8000. This suggested that the crystalline properties of PEG8000 had experienced a noticeable change since in the composite PCMs the stacks of lamellae were arranged randomly compared to pristine PEG8000 in which crystallisation occurred in a highly ordered lamellae arrangement (Golitsyn et al., 2019). Furthermore, the significant reduction in the latent heat of melting and crystallisation of PEG8000 in the crosslinked composite PCMs may be due to several reasons.

The addition of both CF and CA crosslinker resulted in reducing the total weight percentage of PEG8000 present in the TCA crosslinked composite PCMs since both CF and CA are known to make no contribution to latent heat in the composite PCMs. Therefore, both CF and CA are considered as impurities for PEG8000 since they affected the perfection of its crystal lattice structure. The formation of a network of covalent bonds between PEG8000 and CF had caused a significant reduction in the number of crystallisable segments available for crystallisation which was attributed to the confinement of the end OH groups of PEG8000 which resulted in restricting the mobility of the PEG chains during the phase change process. Another cause for the reduced crystallisation ability of PEG8000 is due to the formation of defects.

Previous literature reports that the wt.% of PEG8000 in the composite PCM plays are major role in dictating its final thermal performance (Jiang et al., 2001). Therefore, it is important to determine the suitable wt.% of PEG8000 required to encourage the aggregation of crystals for the formation of crystalline regions which is critical for the fabrication of TCA composite PCMs of enhanced thermal properties for the use in building applications. Increasing PEG content from 29.41 to 33.33 wt.% (e.g.,13.33% increase), increasing PEG/CF ratio from 2.50 to 3.00 and increasing PEG/CA ratio from 0.50 to 0.60 resulted in increasing the latent heat of melting from 33.18 J/g to 47.35 J/g (e.g.,42.71% increase); and latent heat of crystallisation from 33.31 J/g to 45.68 J/g (e.g., 36.15%). This suggested that the number of crystalline segments had increased with increased wt.% of PEG8000 provided this was accompanied by a reduction in CF content from 11.76 to 11.11 wt.% (e.g., 5.53% decrease) and CA content from 58.82 to 55.56 wt.% (e.g., 5.54 % decrease). These results are in good agreement with previous literature which states that increasing the PEG content in the

crosslinked composite PCM results in increasing the latent heat attributed to the increased crystallinity which encourages the crystal aggregation of the whole chain. The same phenomenon was observed when PEG8000 content increased from 22.73 to 26.09 wt.% (e.g.,14.78% increase) provided that the PEG/CF ratio increased from 2.50 to 3.00 (e.g., 20.00% increase) and PEG/CA ratio increased from 0.33 to 0.40 (e.g., 21.21%) since the latent heat of melting was observed to increase from 24.93 J/g to 30.97 J/g (e.g., 24.22% increase) while the latent heat of crystallisation increased from 26.61 J/g to 28.57 J/g (e.g.,7.37% increase).

However, increasing PEG content from 38.46 to 42.86 wt.% provided that the PEG/CF ratio increased from 2.50 to 3.00 (e.g., 20.0% increase) and PEG/CA ratio increased from 0.83 to 1.00 was observed to have an adverse effect on the latent heat of melting and crystallisation of the composite PCMs with blend ratios 2.5:1:3 and 3.0:1:3. The latent heat values were observed to reduce from 46.27 to 42.11 J/g (e.g.,8.99% decrease) and from 47.10 to 43.20 J/g (e.g., 8.28% decrease), respectively. This indicated that the thermal performance of the synthesised PEG based composite PCMs are solely not dictated by the PEG content as reported in previous literature, but the PEG/CF and PEG/CA seemed to have influenced the crystallinity by disturbing the intrinsic crystalline properties of PEG8000 (Sundararajan et al., 2017a); and thereby, made it less crystallisable. As result the latent heat capacity of the TCA crosslinked composite PCMs had therefore reduced significantly (Sundararajan et al., 2019). Also, the lamellae thickness of PEG8000 in the crosslinked composite PCMs appears to have reduced with increased impurity content incorporation which consequently reduced the crystallinity since lamellae of reduced thickness are comprised mainly of folded PEG chains; and therefore, consists of higher number of amorphous regions.

In general, the reduction in the phase transition temperature of PEG8000 is attributed to the destruction caused to the perfection of its crystalline lattice which leads to the formation of an increased number of defects. The crystals will therefore be susceptible to damage at much lower temperatures and this is believed to be influenced mainly by the CF content since literature reports that increasing CF content will increase the number of defects present in the crystal lattice which may be attributed to the greater degree of disruption caused to its crystalline lattice (Liang et al., 1995).
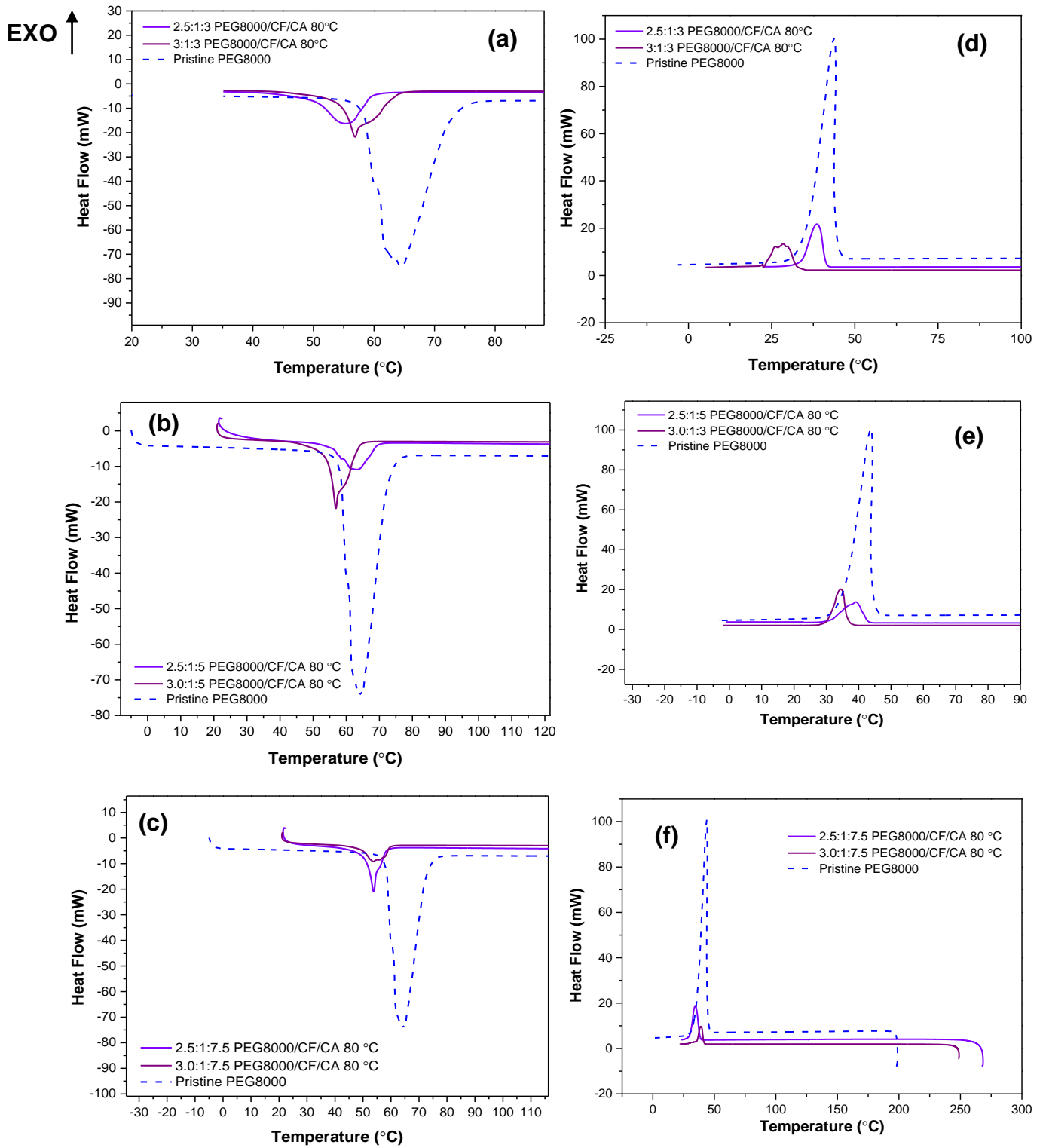
Figure 6. 9 DSC (a), (b) and (c) heating; and (d), (e) and (f) cooling curves of the TCA crosslinked composite PCMs.

Table 6. 6 Thermal properties of the TCA crosslinked composite PCMs.

Sample name	Phase transition temperature		Latent heats	
	T_m (°C)	T_c (°C)	H_m (J/g)	H_c (J/g)
PEG8000	63.12	43.78	181.5	182.1
2.5:1:3	49.27	41.01	46.27	47.10
2.5:1:5	63.13	42.29	33.18	33.31
2.5:1:7.5	53.78	38.50	24.93	23.61
3.0:1:3	55.87	32.40	42.11	43.20
3.0:1:5	56.87	36.35	47.35	45.68
3.0:1:7.5	53.70	41.36	30.97	28.57

6.4.4.3 Impact of PEG8000 content on the thermal properties of PEG8000 in the TCA crosslinked composite PCMs

The Figure 6.10 (a) and (b) shows the heating and cooling cycles of composite PCMs with blend ratios 2.5:1:5, 3.0:1:5, 3.5:1:5, 4.0:1:5 containing 29.41, 33.33, 36.84 and 40.0 wt.% of PEG8000. The thermograms presented indicates that all the curves obtained from the second and third heating and cooling cycles exhibited a single endothermic and exothermic peak. This indicated the existence of one crystal form in the composite PCMs and was attributed to the melting and crystallisation of PEG8000 in the composite PCMs. The thermal properties are summarised in Table 6.7. The latent heat of melting and crystallisation of the crosslinked composite PCMs lied in the range 33.18 to 58.09 J/g (e.g., 67.99 to 81.72% decrease) and 33.31 to 55.75 J/g (69.38 to 81.71% reduction) which was much lower than the one of pristine PEG8000 which had a melting and crystallisation enthalpy of 181.5 and 182.1 J/g.

Results indicated that increasing PEG content from 29.41 wt.% to 33.33 and 36.84 wt.% provided the PEG/CF and PEG/CA mass ratio increased from 2.50 to 3.0 and 3.50; and from 0.50 to 0.60 and 0.70 resulted in enhancing the thermal properties. Hence the latent heat of melting was observed to increase from 33.18 J/g to 47.35 and 58.09 J/g (e.g., 42.7% and 75.1% increase); and the latent heat of crystallisation increased from 33.31 J/g to 45.68 and 55.75 J/g (e.g., 37.1% and 67.4% increase). This was ascribed to the increased mobility of the PEG8000 chain, and the

acceleration of the crystallisation rate which resulted in reducing the energy required for the chain folding process during crystallisation which consequently resulted in producing crystallisable composite PCMs (Athanasoulia and Tarantili, 2017). This was in good agreement with previous literature which reports that increasing PEG content results in increasing the latent heat capacity due to enhanced crystallinity (Sundararajan et al., 2019).

However, optimisation of PEG content from 36.84 to 40 wt.% (e.g., 8.58% increase) provided the PEG/CF and PEG/CA mass ratio increased from 3.50 to 4.00; and from 0.70 to 0.80 had an adverse effect on the thermal properties. This resulted in decreasing both latent heat of melting and crystallisation from 58.09 to 50.78 J/g (e.g.,12.58% decrease) and 55.75 to 45.93 J/g (e.g.,17.61% decrease) which may be attributed to the hindrance of PEG8000 crystallisation due to the fact that both CF and CA (e.g., non-crystallisable component) were trapped in the intra-spherulitic region of PEG8000 (Athanasoulia and Tarantili, 2017; Lai et al., 2004). Also, due to the occurrence of the microphase separation of PEG8000 segments from CF attributed to the presence of PEG8000 in high content (Sundararajan et al., 2019). This suggested that the synthesis of PEG based composite PCMs of enhanced thermal performance is solely not dependent upon the PEG content as reported in previous literature but is also influenced by the CF content and crosslinker content (e.g., chemical composition).

Figure 6.10 (c) and (d) shows the heating and cooling cycles of composite PCMs with blend ratios 2.5:1:10, 3.0:1:10, 3.5:1:10, 4.0:1:10 and 4.5:1:10 containing 18.52, 21.43, 24.14, 26.67 and 29.03 wt.% of PEG8000. Increasing the PEG content from 18.52 to 21.43 wt.% (e.g., 15.71% increase) provided that the PEG/CF and PEG/CA mass ratios increased from 2.50 to 3.00; and from 0.25 to 0.30 resulted in increasing and decreasing the latent heat of melting and crystallisation from 18.19 and 18.96 J/g to 21.35 and 15.27 J/g (e.g.,17.34% increase and 19.46% decrease) which suggested that exceeding the optimum PEG content reduced the crystallinity. This was attributed to the formation of a highly crosslinked structure that resulted in confining the mobility and flexibility of the PEG chain (Sundararajan et al., 2016).

Further increase in PEG8000 content from 21.43 to 24.14 wt.% provided the PEG/CF and PEG/CA mass ratio increased from 3.00 to 3.50; and 0.30 to 0.35 resulting in

optimising the latent heat of melting and crystallisation from 21.35 and 15.27 J/g to 26.39 and 24.90 J/g (e.g., 23.61 and 63.06% increase). However, increasing the PEG content from 24.14 to 26.67 and 29.03 wt.% provided the PEG/CF and PEG/CA mass ratio increased from 3.50 to 4.00 and 4.50; and from 0.35 to 0.40 and 0.45 resulted in increasing the latent heat of melting and crystallisation significantly from 26.39 and 24.90 J/g to 43.28 and 43.79; and 38.51 and 36.29 J/g. This indicated that overloading the crosslinked composite PCMs with PEG resulted in reducing its crystallinity because the mobility of the PEG chain was restricted and the physical interaction in form of hydrogen bonding between PEG and CF was also reduced. Therefore, PEG8000 which was supposed to behave as the 'working substance' served as a plasticiser since it was observed to delay the crystal growth rate of the crystallisation process (Ali and Eisa, 2013). Also, decreasing the CF content from 7.14 to 6.90 wt.%; and CA content from 71.43 to 68.97 wt.% resulted in improving the crystallinity of the composite PCMs provided this was accompanied by PEG content increase from 21.43 to 24.14 wt.% (e.g., 12.65% increase). Overall, results suggested that both PEG/CF and PEG/CA ratio played a major role in dictating the latent heat capacity of the resulting composite PCMs since the density of the crosslinked network formed was influenced greatly by the chemical composition.
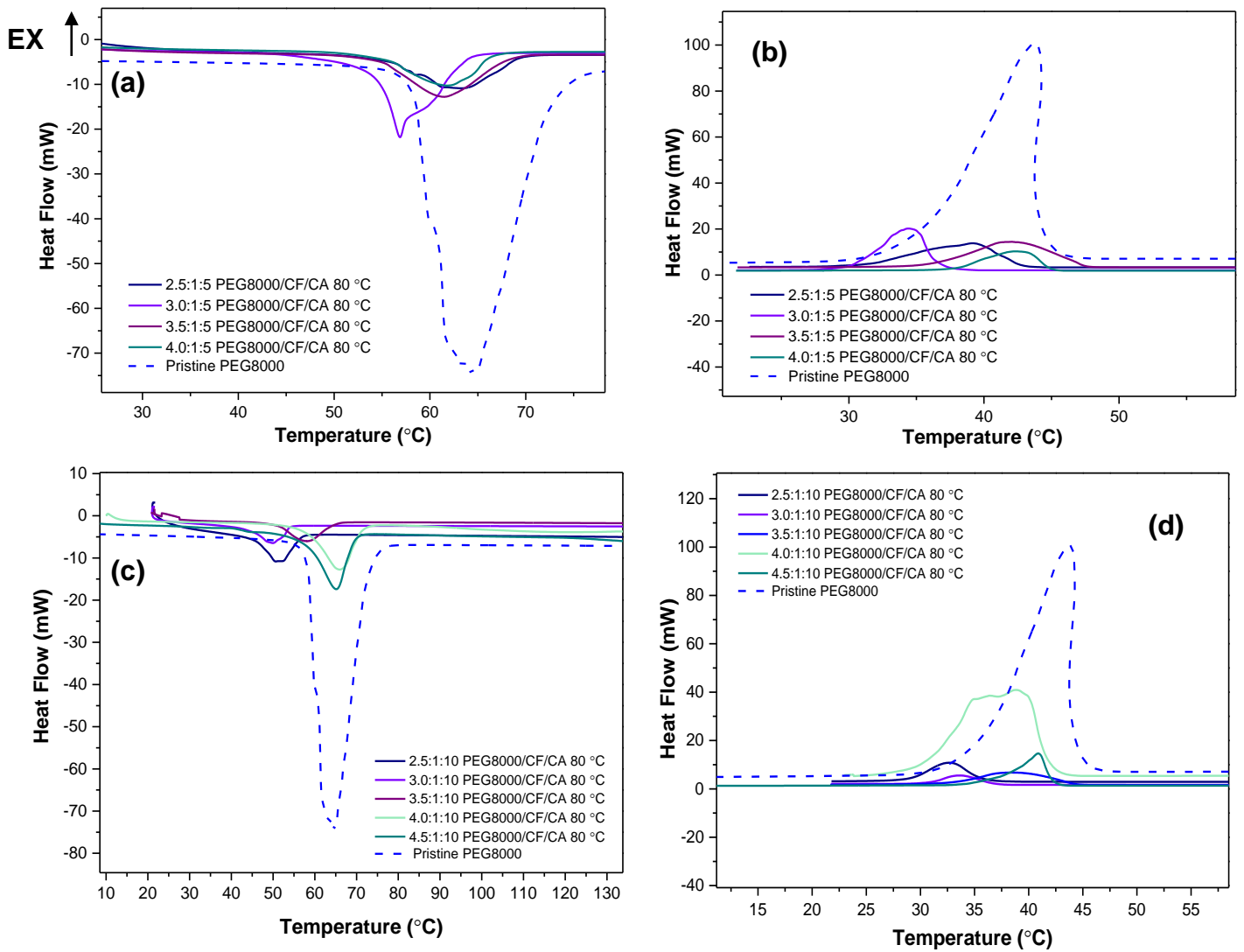
Figure 6. 10 DSC (a) and (c) heating; and (b) and (d) cooling curves of the TCA crosslinked composite PCMs.

Table 6. 7 Thermal properties of the TCA crosslinked composite PCMs.

Sample name	Phase transition temperatures		Latent heat	
	T_m (°C)	T_c (°C)	H_m (J/g)	H_c (J/g)
PEG8000	63.12	43.78	181.5	182.1
2.5:1:5	63.13	42.29	33.18	33.31
3.0:1:5	56.87	36.35	47.35	45.68
3.5:1:5	64.11	45.11	58.09	55.75
4.0:1:5	61.79	44.92	50.78	45.93
2.5:1:10	50.78	32.88	18.19	18.96
3.0:1:10	49.93	33.70	21.35	15.27
3.5:1:10	58.22	44.44	26.39	24.90
4.0:1:10	55.68	37.97	43.28	43.79
4.5:1:10	55.48	40.86	38.51	36.29

6.4.4.4 Impact of CF and CA content on thermal properties of PEG8000 in the TCA crosslinked composite PCMs

Figures 6.11 (a) and (b) shows the heating and cooling cycles of composite PCMs with blend ratios 3.5:0.85:7.5, 3.5:1:7.5, 3.5:0.85:10 and 3.5:1:10 containing 29.53, 29.17, 24.39 and 24.14 wt.% of PEG8000; and 7.17, 8.33, 5.92 and 6.90 wt.% of CF. The thermograms presented indicates that all the curves obtained from the second and third heating and cooling cycles exhibited a single endothermic and exothermic peak which indicates the existence of one crystal form in the composite PCMs. This was attributed to the melting and crystallisation of PEG8000 in the composite PCMs. The thermal properties are summarised in Table 6.8.

In general, previous literature considers supporting materials like CF as an impurity since it is integrated with PEG via chemical reactions with the aid of relevant crosslinkers. This results in disrupting the crystal arrangement, which consequently affects the growth habit of the spherulitic crystals of PEG8000 (Sangwal, 1996). Increasing the CF content from 7.17 to 8.33 wt.% (e.g., 16.18% increase) and decreasing the PEG8000 content from 29.53 to 29.17 wt.% (e.g., 1.22% decrease)

resulted in increasing the latent heat of melting and crystallisation from 32.03 and 31.12 J/g to 38.64 and 37.62 J/g (e.g., 20.64% and 20.89% increase) provided the PEG/CF ratio decreased from 4.11 to 3.50; and PEG/CA ratio remained constant at 0.47 which was attributed to the increased crystallinity which resulted in reducing the cooling rate; and therefore, the crystal growth rate was hindered (Urwin et al., 2021).

This shows that crystallinity of TCA crosslinked composite PCMs also depended upon the CF content. Hence, having sufficient CF in the crosslinked network was necessary to produce composite PCMs of enhanced phase change properties. Increasing the CF content from 5.92 to 6.90 wt.% (e.g., 16.55% increase) and decreasing the PEG8000 content insignificantly from 24.39 to 24.14 wt.% (e.g., 1.03% decrease) resulted in decreasing the latent heat of melting and crystallisation from 40.62 and 37.49 J/g to 26.39 and 24.90 J/g (e.g., 35.03% and 33.58% decrease) provided the PEG/CF ratio decreased from 4.12 to 3.50; and PEG/CA ratio was kept constant at 0.35 which suggested that incorporating high CA content and increasing the CF had a noticeable impact on the crystallinity since both impurities were incorporated in the crystal lattice structure of PEG8000; and therefore, had distorted its crystal lattice and caused crystal morphology changes which is good agreement with the POM images (Sangwal, 1996; Urwin et al., 2021).
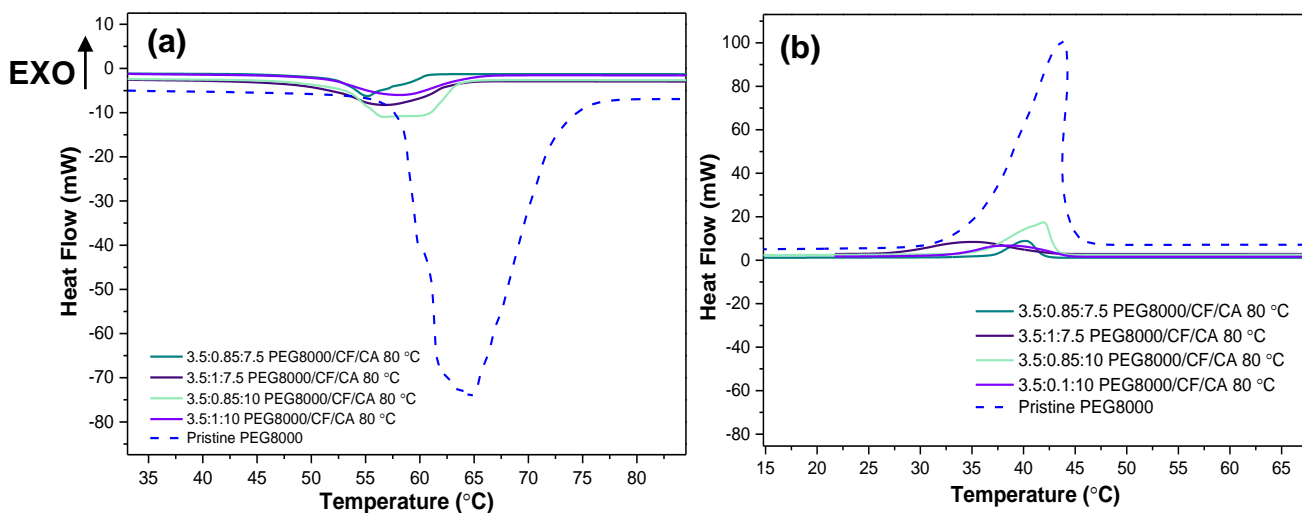
Figure 6. 11 DSC (a) heating; and (b) cooling curves of the TCA crosslinked composite PCMs.

Table 6. 8 Thermal properties of the TCA crosslinked composite PCMs.

Sample name	Phase transition temperature		Latent heats	
	T_m (°C)	T_c (°C)	H_m (J/g)	H_c (J/g)
PEG8000	63.12	43.78	181.5	182.1
3.5:0.85:7.5	55.27	40.19	32.03	31.12
3.5:1:7.5	50.69	41.60	38.64	37.62
3.5:0.85:10	56.53	41.90	40.62	37.49
3.5:1:10	58.22	44.44	26.39	24.90

Figure 6.12 (a) and (b) shows the heating and cooling cycles of composite PCMs with blend ratios 2.5:1:3, 2.5:1:5, 2.5:1:7.5 and 2.5:1:10 containing 38.46, 29.41, 22.73 and 18.52 wt.% of PEG8000 content and 46.15, 58.82, 68.18 and 74.04 wt.% of CA content. The thermal properties are summarised in Table 6.8. Increasing the CA content from 46.15 to 58.82, 68.18 and 74.04 wt.% which was accompanied by a reduction in the PEG content from 38.46 to 29.41, 22.73 and 18.52 wt.% resulted in decreasing the latent heat of melting from 46.27 to 33.18, 24.93 and 18.19 J/g and latent heat of crystallisation from 47.10 to 33.31, 23.61 and 18.96 J/g because CA is an impurity since it makes no contribution to latent heat. Therefore its incorporation resulted in increasing the number of crystal defects as result of distorting the crystal lattice of PEG8000. Results demonstrated that when the CA content exceeded 46.15 wt.% it resulted in decreasing the crystallinity due to increased impurity content which consequently reduced the latent heat of melting and crystallisation.

Figure 6.12 (c) and (d) shows the heating and cooling cycles of composite PCMs with blend ratios 4.0:1:5, 4.0:1:7.5 and 4.0:1:10 of PEG8000 content of 40.00, 32.00 and 26.67 wt.%; and CA content of 50.00, 60.00 and 66.67 wt.%. The thermal properties are summarised in Table 6.9. The same phenomenon was observed when increasing the CA content from 50.00 to 60.00 and 66.67 wt.% which was accompanied by a reduction in the PEG content from 40.00 to 32.00 and 26.67 wt.% since the latent heat of melting reduced from 50.78 to 41.94 and 43.28 J/g and latent heat of crystallisation reduced from 45.93 to 39.81 and 43.79 J/g. Therefore, results indicated that increasing CA content led to the formation of a highly crosslinked structure. The mobility of PEG

chain was restricted to a greater extent in the crosslinked network leading to the formation of higher number of crystal defects due to the distortion caused to the crystal lattice of PEG8000. Moreover, increasing CA content increased the hydrophilic nature of the resulting composite PCMs which had an adverse effect on the crystallinity since crystalline regions are known to have lower moisture content than the amorphous regions. This means increasing the moisture content resulted in decreasing the crystallinity which consequently reduced the latent heat capacity (Negoro et al., 2016).
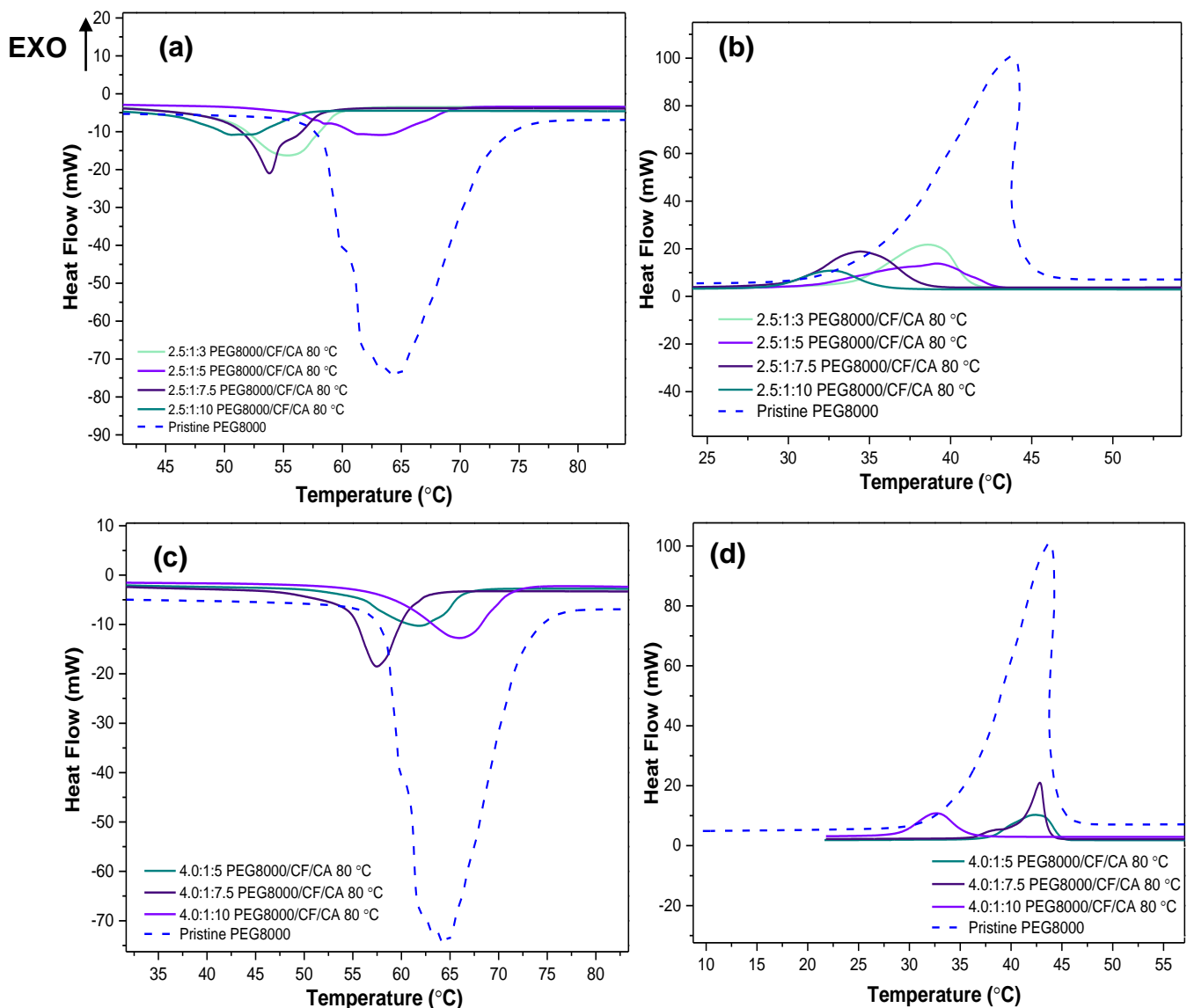
Figure 6. 12 DSC (a) and (c) heating; and (b) and (d) cooling cycles of the TCA crosslinked composite PCMs.

Sample name	Phase transition temperature		Latent heats	
	T_m (°C)	T_c (°C)	H_m (J/g)	H_c (J/g)
PEG8000	63.12	43.78	181.5	182.1
2.5:1:3	49.27	41.01	46.27	47.10
2.5:1:5	63.13	42.29	33.18	33.31
2.5:1:7.5	53.78	38.50	24.93	23.61
2.5:1:10	50.78	32.88	18.19	18.96
4.0:1:5	61.79	44.92	50.78	45.93
4.0:1:7.5	57.45	41.94	41.94	39.81
4.0:1:10	55.68	37.97	43.28	43.79

6.4.4.5 Changes in the phase transition and supercooling temperature of PEG8000 in the TCA crosslinked composite PCMs

Figure 6.13 shows the T_m and T_c of composite PCMs prepared using different blend ratios. Observations indicated that changes were caused to the initial phase transitions temperatures of pristine PEG8000 after chemical crosslinking reaction; thus, incorporation of CF and CA leads to the shifting of the phase transition temperature of pristine PEG8000 to lower temperatures because the T_m and T_c of the composite PCMs lied in the range 49.27 to 63.13 °C and 32.40 to 44.92 °C due to the changes in the thickness of the crystal lamellae which consequently resulted in restricting the mobility of the PEG chains. Hence it reduced ability of PEG chains to bend or fold, during the phase transition process due to the formation of crosslinked structures (Cabaleiro et al., 2020). Mainly because the thickness of the PEG crystals depends mainly upon the number of folds in the PEG8000 chain (Pielichowski and Flejtuch, 2002).

However, in composite PCMs with blend ratios 2.5:1:5 and 4.0:1:5 the thickness of crystal lamellae of PEG8000 was observed to remain unchanged since both T_m and T_c changed insignificantly from 63.12 and 43.78 °C to 63.13 and 42.29 °C; and to 61.79 and 44.92°C, respectively. In composite PCMs with blend ratio 2.5:1:3,

maximum reduction in T_m and T_c occurred from 63.12 and 43.78 °C to 49.27 and 41.01°C (e.g., 21.94 and 6.33% decrease) which indicated that the thickness of the crystal lamellae of PEG8000 formed during crystallisation had been reduced greatly. These thin PEG crystals present in the TCA composite PCMs will undergo relevant phase transitions at much lower temperatures (Golitsyn et al., 2019; Pielichowski and Flejtuch, 2002). Moreover, reduction in the phase transition temperature of PEG8000 indicated that the size of the spherulite crystals had reduced after the chemical crosslinking reaction since smaller crystals are reported to undergo melting at lower temperatures.

Results also suggested that the undesirable supercooling temperature of pristine PEG8000 was observed to have reduced in this composite PCM after chemical crosslinking from 19.34 to 8.26 °C (e.g., 57.29% decrease). This was attributed to the enhancement of the nucleation during the crystallisation process due to the formation of extra nucleation sites (Cabaleiro et al., 2020, 2019). The number of nucleating sites available varied with chemical composition; and was observed to depend mainly upon the mass ratio of PEG/CA provided the mass ratio of PEG/CF was kept constant at 2.50.

Results showed that PEG/CA mass ratio of 0.83 optimised the number of nucleating sites and as result the ST was reduced significantly. However, PEG/CA mass ratios of 0.25, 0.33 and 0.50 were observed to produce fewer nucleating sites since the STs were observed to be either higher or close to the one of pristine PEG8000. Overall, incorporating low CA content had a positive impact. Observations indicated that increasing CF content had an adverse effect on the thermal stability of the resulting composite PCM because T_m had decreased from 55.27 to 50.69 (e.g., 8.29% decrease) but the T_C had increased insignificantly from 40.19 to 41.60 (e.g., 3.51% increase). The supercooling temperature had reduced from 15.08 to 9.09 °C which indicated that CF appeared to provide more nucleating sites for the crystallisation and appears to have acted like a shield to prevent damages caused to the critical nuclei during synthesis because literature reports that crushing of the critical nuclei during chemical reaction may have been detrimental to the crystal nucleation. This would subsequently result in increasing the supercooling temperature (X. Liu et al., 2017). By comparing composite PCMs with blend ratios 4.0:1:10 and 4.5:1:10 increasing the PEG content insignificantly from 26.67 to 29.03 wt.% (e.g., 8.85% increase) provided

this was accompanied by a reduction in CF content from 6.67 to 6.45 wt.% (e.g.,3.30% decrease) resulted in decreasing the ST from 17.71 to 14.62 °C (e.g., 17.45% decrease). This indicates incorporating adequate amount of PEG in the composite PCM is necessary to suppress the undesirable supercooling behaviour which most PCMs exhibits since incorporating PEG content in excess was observed to increase the ST. Increasing PEG content from 26.09 to 32.0 wt.% (e.g., 22.65% increase) provided this was accompanied by a reduction in CF content from 8.70 to 8.00 wt.% (e.g.,8.05% decrease) resulted in increasing the ST from 12.34 to 25.69 °C (e.g., 25.69% increase). It can be concluded that both CF and CA acted as nucleating agents since most of the TCA crosslinked composite PCMs of current study had ST lower than the one of pristine PEG8000. However, results demonstrated that incorporating CF or CA in excess resulted in increasing the ST undesirably. For blend ratios 2.5:1:5, 3.0:1:3 and 3.0:1:5 ST increased from 19.34 to 20.84, 23.47 and 20.52 °C with increasing PEG, CF, and CA content from 29.41, 11.76 and 58.82 wt.% to 42.86, 14.29
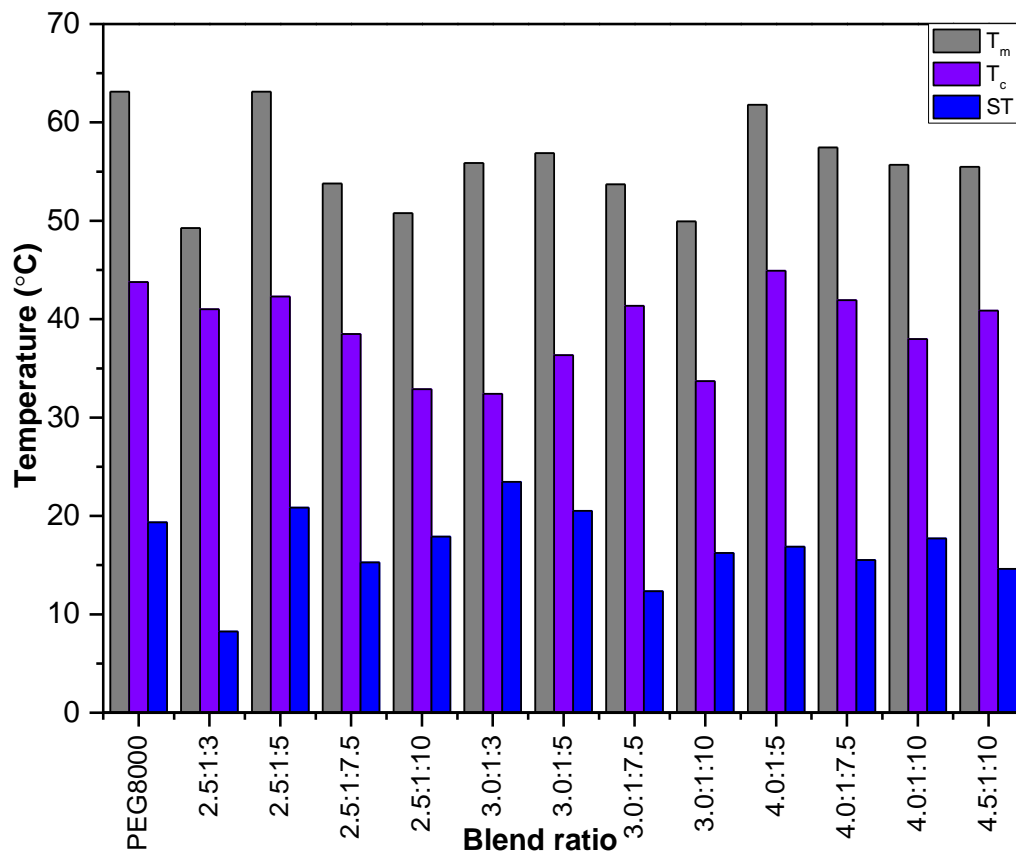
Figure 6. 13 The phase transition and supercooling temperature of the different TCA crosslinked composite PCMs.

and 42.86 wt.%; and 33.33, 11.11 and 55.56 wt.% which shows that incorporating the correct amount of CF and CA was necessary to speed up the crystallisation process, and thus, to reduce the ST (Shamseddine et al., 2022).

193

6.4.5 Studying the crystal morphology and structure of PEG8000 in the TCA crosslinked composite PCM

Figure 6.14 (a) clearly indicates that pristine PEG8000 film exhibited the typical spherulitic crystal morphology at room temperature since it was observed to be comprised of long fibrillar crystals radiating from the centre (see marked yellow arrows in the radial direction) (Shi et al., 2012). With increasing temperature, the spherulite structures are observed to disappear gradually (see Figure 6.14(b)); and thus, eventually in the melted state no crystals are visible. This was attributed to the transition of PEG crystal into an amorphous state (see Figure 6.14(c)) (Alkan et al., 2012).
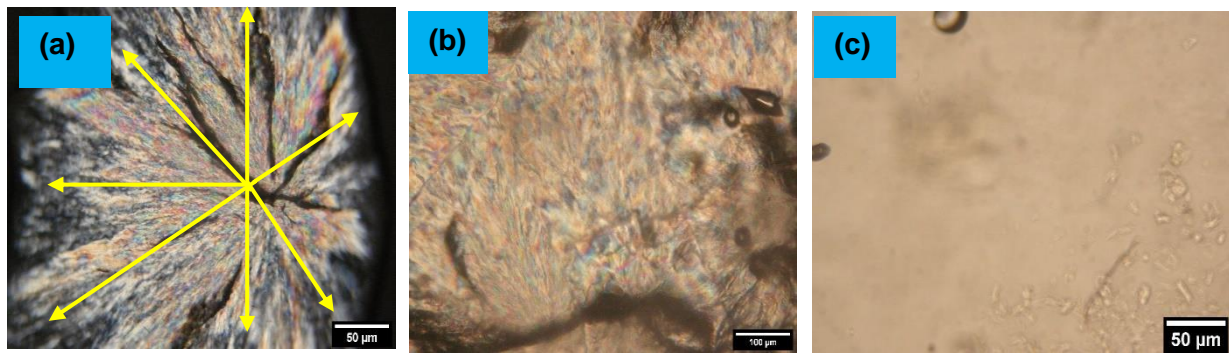
Figure 6. 14 Typical crystal morphology of PEG8000 film (a) at room temperature; (b) during melting at 70°C; and (c) in its melted state.

Figures 6.15 and 6.16 illustrate the POM images of the TCA crosslinked composite PCMs below and above its phase transition temperature. The observations made regarding the crystal morphological changes of PEG8000 after TCA crosslinking reaction are discussed in the following section. Observations indicated that the characteristic spherulite morphology of PEG8000 was not visible in the TCA crosslinked composite PCMs which indicated that TCA chemical crosslinking had altered the crystal structure of PEG.

Results suggested that incorporation of CF (e.g., amorphous polymer) had reduced the crystallinity of PEG greatly. Also, no significant changes in the crystal morphology of the TCA crosslinked composite PCMs were observed by varying the chemical composition. Therefore, it can be concluded that TCA crosslinking had destructed the crystal lattice of PEG which resulted in increasing the number of crystal defects; and since crystal defects are concentrated in the amorphous regions, the number of amorphous domains were subsequently increased undesirably.

Figures 6.15 and 6.16 illustrated that the opaque composite PCM did not convert into a transparent homogenous state during the melting process which indicated that the PEG segments did not undergo melting or even if it melted no leakage occurred because it was able to retain its original solid state due to the crosslinked network formed. Moreover, results indicated that no liquid phase was generated during the phase transition process which confirms successful shape stabilisation of PEG8000 after TCA crosslinking reaction.
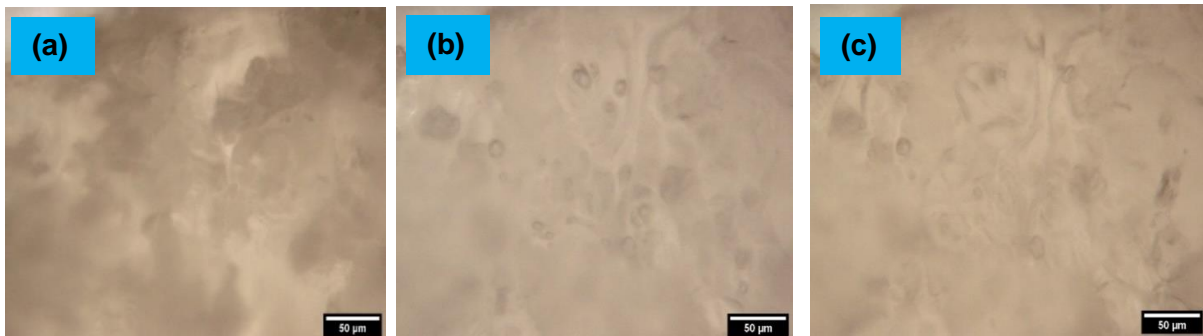
Figure 6. 15 POM images of composite PCM with 26.67 wt.% PEG8000 at (a) Room temperature; (b) melting; and (c) crystallisation.
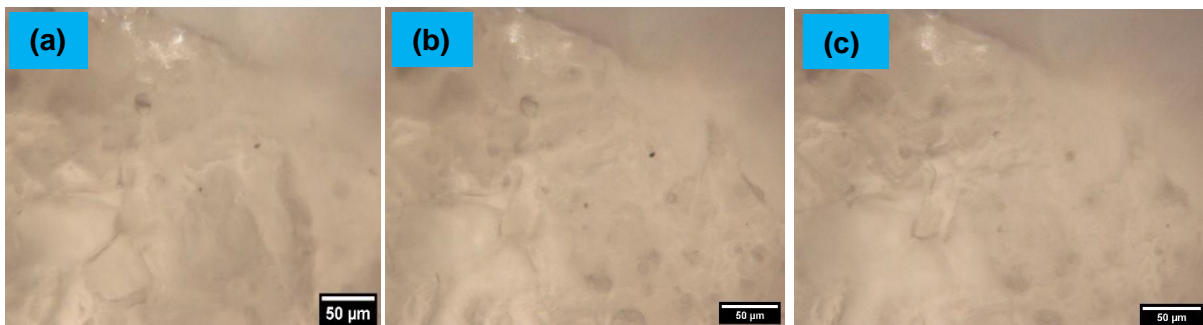
Figure 6. 16 POM images of composite PCM with blend ratio 4.0:1:7.5 and 32 wt.% PEG8000 at (a) Room temperature; (b) melting; and (c) crystallisation.

Figures 6.17 and 6.18 present the POM images of PEG8000 and the TCA crosslinked composite PCM containing 26.67 wt.% of PEG8000. Observations indicated that the typical spherulitic crystal structures become less visible, and the size of the spherulite crystals had reduced after the TCA crosslinking reaction (see marked circles in Figure 6.18 (b)) (Li et al., 2013). This was attributed to the impregnation of PEG8000 into CF, which resulted in confining the free movement of the PEG chain by the crosslinked network formed.

Figure 6.17 demonstrates that PEG was enwrapped completely by CF which was the main reason why the spherulite crystals of PEG became less visible after the chemical crosslinking reaction (Chen et al., 2020). Also, the 'mosaic-like' domains (see Figure

Figure 6. 17 Close-up view of the crystal morphology of the TCA crosslinked composite PCM.
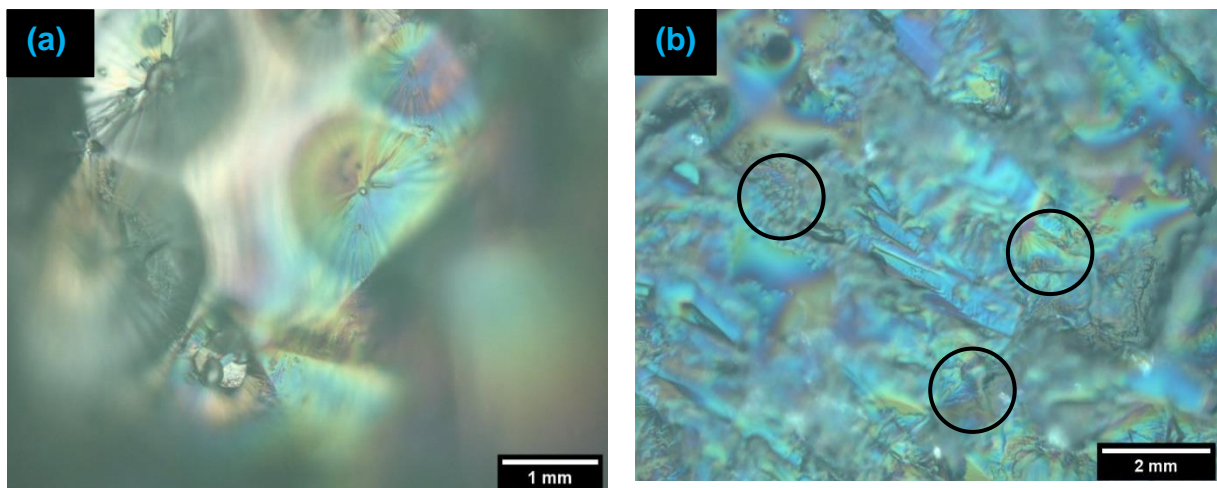
Figure 6. 18 Crystal morphology of (a) pristine PEG8000; and (b) PEG-CF composite PCM.

6.18 (b)) were observed which indicated the presence of structural irregularities in the TCA crosslinked composite PCM attributed to its inhomogeneous surface morphology.

196

6.4.6 Studying the surface morphology of the TCA crosslinked composite PCMs

Figure 6.19 presents the SEM images of the composite PCM with blend ratio 3.0:1:3 containing 42.86, 14.29 and 42.86 wt.% of PEG, CF, and CA to study its surface morphology, and to investigate the compatibility between PEG and CF. Observations indicated that the crosslinked composite PCM exhibited a highly porous structure. This suggested that CF had poor compatibility with PEG in the corresponding composite PCM. This was attributed to the formation of weak intermolecular forces between PEG and CF during chemical crosslinking reaction due to the presence of insufficient CA.
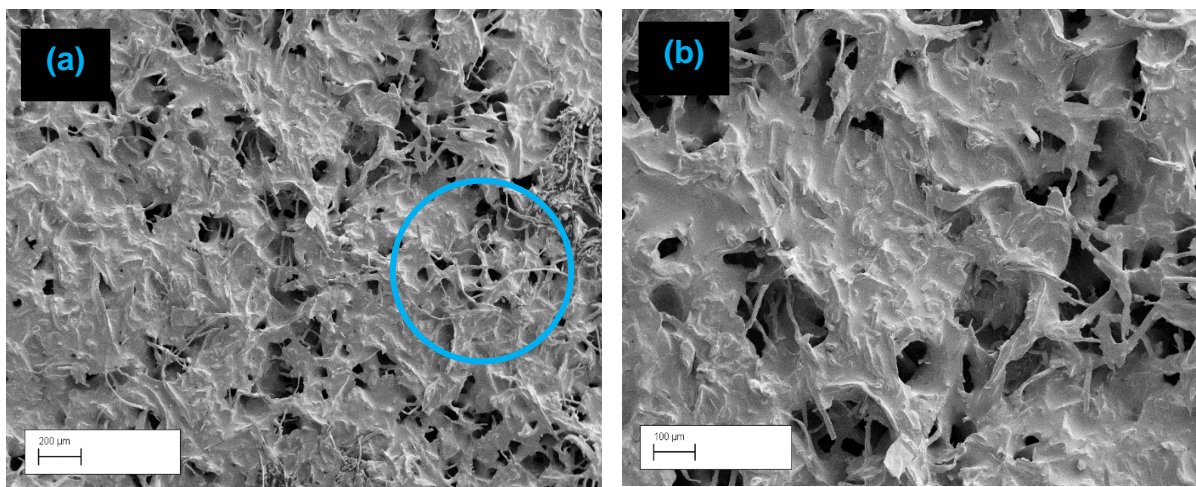
Figure 6. 19 (a) SEM image of TCA composite PCM; and (b) Close-up view of area marked with the circle.

Figure 6.20 presents the SEM images of the composite PCM with blend ratio 3.5:1:3 containing 46.67, 13.33 and 40.00 wt.% of PEG, CF, and CA. Observations indicated that increasing the PEG content from 42.86 to 46.67 wt.% provided that the CF and CA content was decreased from 14.29 to 13.33 wt.% and from 42.86 to 40.0 wt.% resulted in reducing the number of pores drastically and few cracks were appeared to have formed. This was attributed to the enhanced compatibility between PEG and CF.
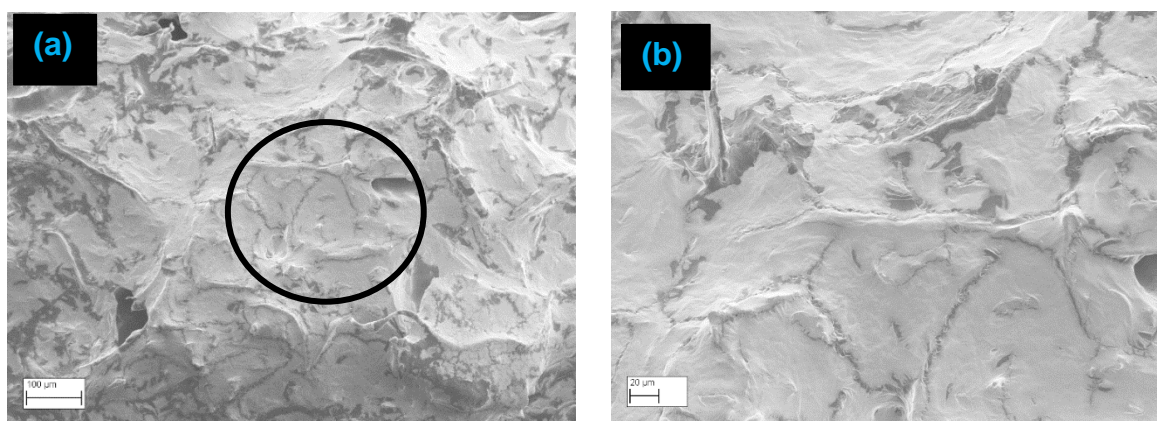
Figure 6. 20 (a) SEM image of TCA composite PCM; (b) Close-up view of area marked with the circle.

Figure 6.21 presents the SEM images of the composite PCM with blend ratio 3.0:1:5 containing 33.33, 11.11 and 56.56 wt.% of PEG, CF, and CA. Reducing the PEG content in the composite PCM resulted in changing the homogeneity of the composite PCM. Hence, a three-dimensional network with voids and aggregates of CF had formed.
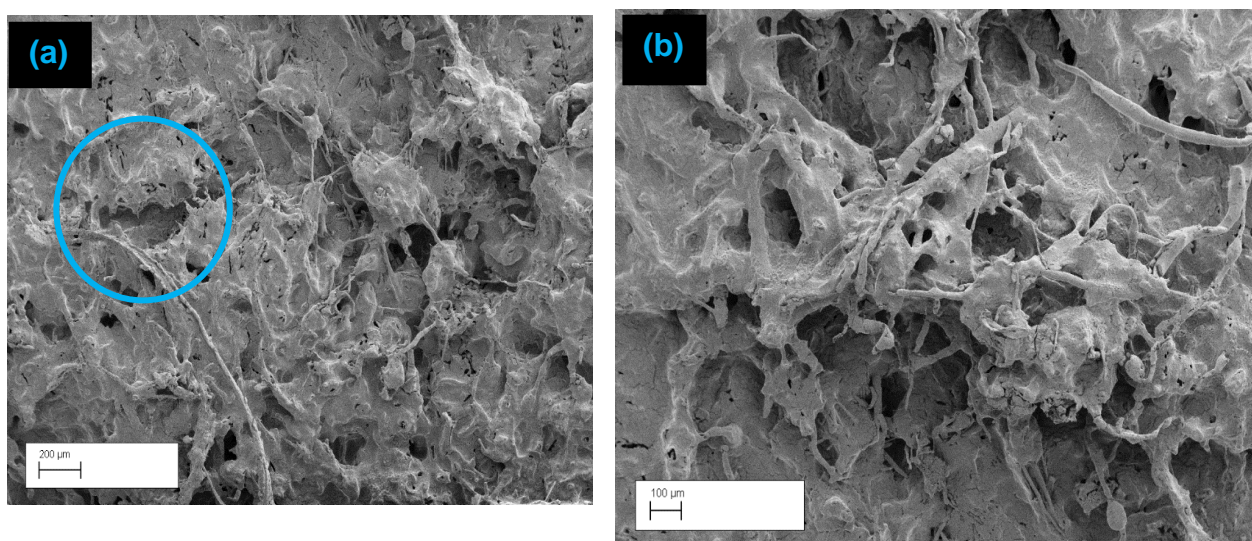
Figure 6. 21 (a) SEM image of TCA composite PCM; (b) Close-up view of area marked with the circle.

Figure 6.22 presents the SEM images of the composite PCM with blend ratio 3.0:0.85:10 containing 24.39, 5.92 and 69.69 wt.% of PEG, CF, and CA. Increasing the CA content resulted in enhancing the interfacial compatibility between PEG and CF since the number of pores and aggregates had reduced which was attributed to the enhanced dispersion of PEG in CF. This indicated that the interfacial compatibility

of PEG and CF was improved in the corresponding composite PCM which led to the formation of a compact structure.
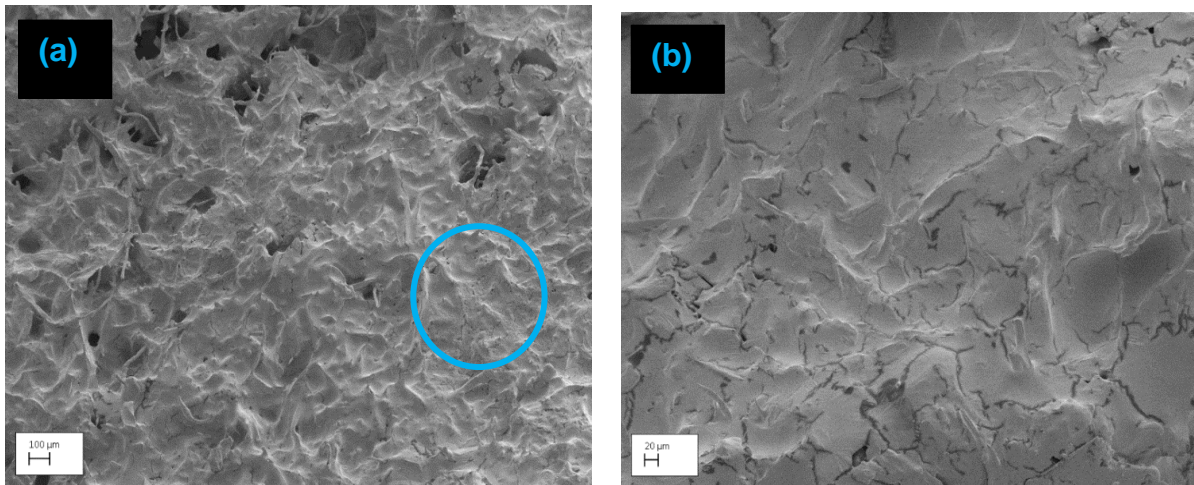
Figure 6. 22 (a) SEM image of TCA composite PCM; (b) Close-up view of area marked with the circle.

Figure 6.23 presents the SEM images of the composite PCM with blend ratio 3.5:1:10 containing 24.14, 6.90 and 68.97 wt.% of PEG, CF, and CA. Results indicated that decreasing the PEG and CA content insignificantly from 24.39 to 24.14 wt.% (e.g.,1.03% decrease); and from 69.69 to 68.97 wt.% (e.g.,1.03% decrease) provided that the CF content increased from 5.92 to 6.90 wt.% (e.g.,16.55% increase) resulted in enhancing the interfacial compatibility of PEG and CF. This was demonstrated by the compact microstructure shown in Figure 6.23. Also, the surface roughness was observed to increase with increased CF content. Therefore, results suggested that the compatibility between PEG and CF was influenced mainly by the chemical composition of the TCA crosslinked composite PCM. Moreover, it indicated that increasing the CF or CA content sufficiently resulted in improving the surface morphology of the composite PCMs.
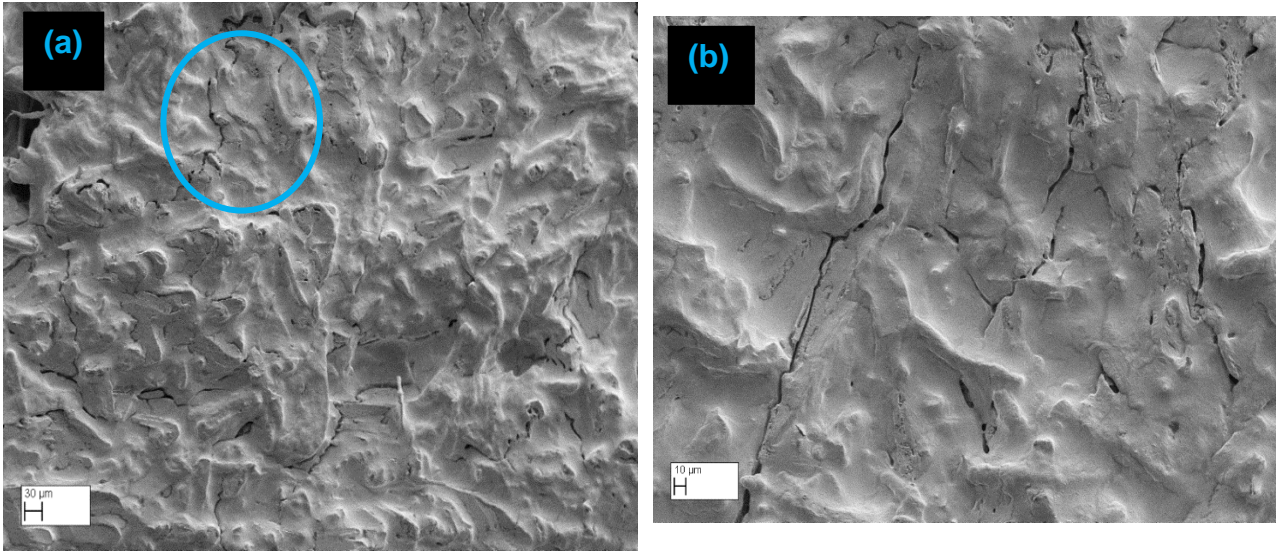
Figure 6. 23 (a) SEM image of TCA composite PCM; (b) Close-up view of area marked with the circle.

6.4.7 Interim Conclusions

In this Chapter PEG was successfully shape stabilised via the facile and feasible TCA crosslinking reaction using environmentally friendly materials only. A series of PEG-CF crosslinked composite PCMs with various PEG loadings were prepared successfully via the environmentally friendly TCA crosslinking reaction. Moreover, TCA crosslinking reaction resulted in producing a series of TCA crosslinked composite PCMs with enhanced thermal properties compared to the one prepared via the PU crosslinking reaction (see Chapter 5). The chemical structure, thermal properties, crystalline properties of the TCA crosslinked composite PCMs were investigated using FTIR, DSC, XRD and POM analysis. The conclusions and outcomes of current research are summarised below.

6.4.7.1 Outcomes

➢ Results demonstrated that CA could be used as a crosslinker for the preparation of environmentally friendly PEG based composite PCMs of enhanced thermal properties.

➢ FTIR results confirmed the preparation of TCA crosslinked composite PCMs via the formation of ester linkages between PEG and CF.

➢ XRD results indicated that the crystallinity of PEG had reduced drastically after TCA crosslinking reaction which was attributed to the formation of the crosslinked network. Optimisation of PEG content in the composite PCM resulted in decreasing the crystallinity because the amorphous phases were observed to have increased.

➢ DSC results indicated that the thermal properties of PEG had changed after the TCA crosslinking reaction because the latent heat capacity of PEG decreased by more than 50% after the TCA crosslinking reaction which was attributed to the destruction caused to its crystal lattice which encouraged the formation of crystal defects.

➢ Changes in the phase transition temperature of PEG after chemical crosslinking was due to the structural changes at lamellar level. Hence, the lamellar thickness and structure of PEG had changed since the spherulites were observed to have reduced in size. Results indicated that by changing the chemical composition of the composite PCM it is possible to tailor the phase transition temperature to match the operating temperature of the intended building application.

- Sufficient CA content was required to form ester linkages between PEG and CF; however, optimising the CA content resulted in declining the thermal and crystalline properties of PEG in the crosslinked composite PCMs.
- Supercooling temperature of PEG had decreased after the TCA crosslinking reaction which was attributed to the increased number of nucleating sites.
- SEM analysis indicated that the surface morphology of the TCA crosslinked composite PCMs depends mainly upon the chemical composition. Results indicated that incorporating insufficient CA content resulted in producing composite PCMs of porous structures. This was attributed to the poor compatibility between PEG and CF.

6.4.7.2 Outlooks

- MW irradiation treatment is reported to speed up the rate of chemical reaction.
- Results from Chapter 4 indicated that MW irradiation treatment enhanced the thermal and crystalline properties of PEG by rearranging its crystalline segments. Therefore, need to determine the effects of MW irradiation treatment on the thermal properties of the TCA crosslinked composite PCMs.
- Need to determine the thermal stability of the TCA crosslinked composite PCMs, and the influence of MW irradiation on the thermal stability of the crosslinked composite PCMs.
- Need to determine a suitable approach to improve the compatibility between PEG and CF at microlevel to form homogeneous composite PCMs of enhanced structural integrity.

Chapter 7: Synthesis of composite PCMs via the innovative Microwave radiation assisted TCA crosslinking reaction

Abstract

In this Chapter a series of TCA crosslinked composite PCMs with different PEG loadings were prepared via the environmentally friendly MW radiation assisted TCA crosslinking reaction. Its chemical structure, crystalline properties, thermal properties, thermal stability, crystal morphology and surface morphology were investigated and studied using FTIR, XRD, DSC, TGA, POM and SEM analysis. XRD results showed that MW irradiation treatment could enhance the crystallinity of PEG in the TCA crosslinked composite PCMs by rearranging the crystalline phases which consequently resulted in producing composite PCMs of better thermal performance. The thermal stability of PEG had improved after the TCA crosslinking reaction. This Chapter aims at meeting specific objectives 5 and 6 listed in section 1.4.

7.1 Introduction

Tricarboxylic acid (TCA) crosslinking reaction is very slow; and therefore, to speed up the rate of reaction an acid catalyst like sulfuric acid is conventionally used. However, major drawbacks of acid catalysts include corrosiveness, toxic, harmful, and difficult to handle. Microwave (MW) irradiation treatment is one of the commonly used approaches to accelerate the rate of chemical reactions by heating at a molecular level; and it involves utilising an electromagnetic radiation in the microwave range with a frequency in the range 300 MHz to 300 GHz.

In the recent times it is conventionally used for the synthesis of composites in biomedical applications due to the numerous desirable benefits it exhibits including shorter processing time and utilises less energy making it environmentally friendly. TCA crosslinking reaction resulted in producing highly porous, non-homogenous TCA crosslinked composite PCMs (see Chapter 6). MW irradiation technique is commonly used to prepare homogenous composites by improving the interfacial compatibility between PEG and CF.

7.2 Methods

ATR-FTIR analysis

FTIR analysis was performed to evaluate the influence of MW irradiation treatment on the chemical structure of the crosslinked TCA composite PCMs formed.

Powder XRD analysis

XRD analysis was performed to determine the crystalline properties of the TCA crosslinked composite PCMs.

DSC analysis

DSC analysis was performed to evaluate the thermal properties of the TCA crosslinked composite PCMs.

TG analysis (TGA)

TGA was performed to determine the thermal stability of TCA crosslinked composite PCMs by studying its thermal degradation process in nitrogen atmosphere at a heating rate of 10 °C/min from 30 to 650°C.

SEM analysis

SEM analysis was performed to study the surface morphology of the TCA crosslinked composite PCMs mainly to evaluate the influence of MW irradiation treatment on the interfacial compatibility between PEG and CF.

POM/ hot stage analysis

This was performed to study the crystal morphology and structure of PEG8000 in the TCA crosslinked composite PCMs.

7.3 Results and discussion

7.3.1 Functional groups of the MW irradiated TCA crosslinked composite PCMs

The FTIR spectra of the unirradiated and MW irradiated TCA crosslinked composite PCMs are presented in Figure 7.1. Observations indicated that the absorption bands all appear in three wavenumber regions of 3600 to 2900 cm^{-1}, 2700 to 2900 cm^{-1} and 1800 to 1500 cm^{-1}. Also, MW irradiation is observed to cause no major changes to the FTIR spectra of the TCA crosslinked composite PCMs. This confirms that the chemical structure of the resulting product was unaffected by MW irradiation. The characteristic peaks of PEG8000 at 3480, 2800 and 1960 cm^{-1} attributed to the O-H and C-H stretching vibrations are also appearing in the FTIR spectra of the MW irradiated TCA crosslinked composite PCMs; and the sharp peak at 3480 cm^{-1} arises from the

stretching vibration of the unreacted intermolecular bonded O-H groups (Sundararajan et al., 2019). The intensity of this peak was appeared to have increased after MW irradiation. This suggested that the number of OH groups had increased. For composite PCM with blend ratio 2.5:1:5 no noticeable changes are observed in the FTIR pattern; however, the intensity of peak at 1740 cm^{-1} indicating the formation of ester linkages (e.g., covalent bond) appears to have become more intense after 10 min MW radiation exposure but the intensity appears to have dropped after 20 min MW radiation. This was attributed to the change in length of the C=O bond. The changes in wavenumber after chemical reaction demonstrated the presence of weak intermolecular forces of attraction in the prepared composite PCMs (Sarı et al., 2018). Overall, no major changes had occurred to the FTIR pattern of the TCA crosslinked composite PCMs after the MW irradiation treatment.
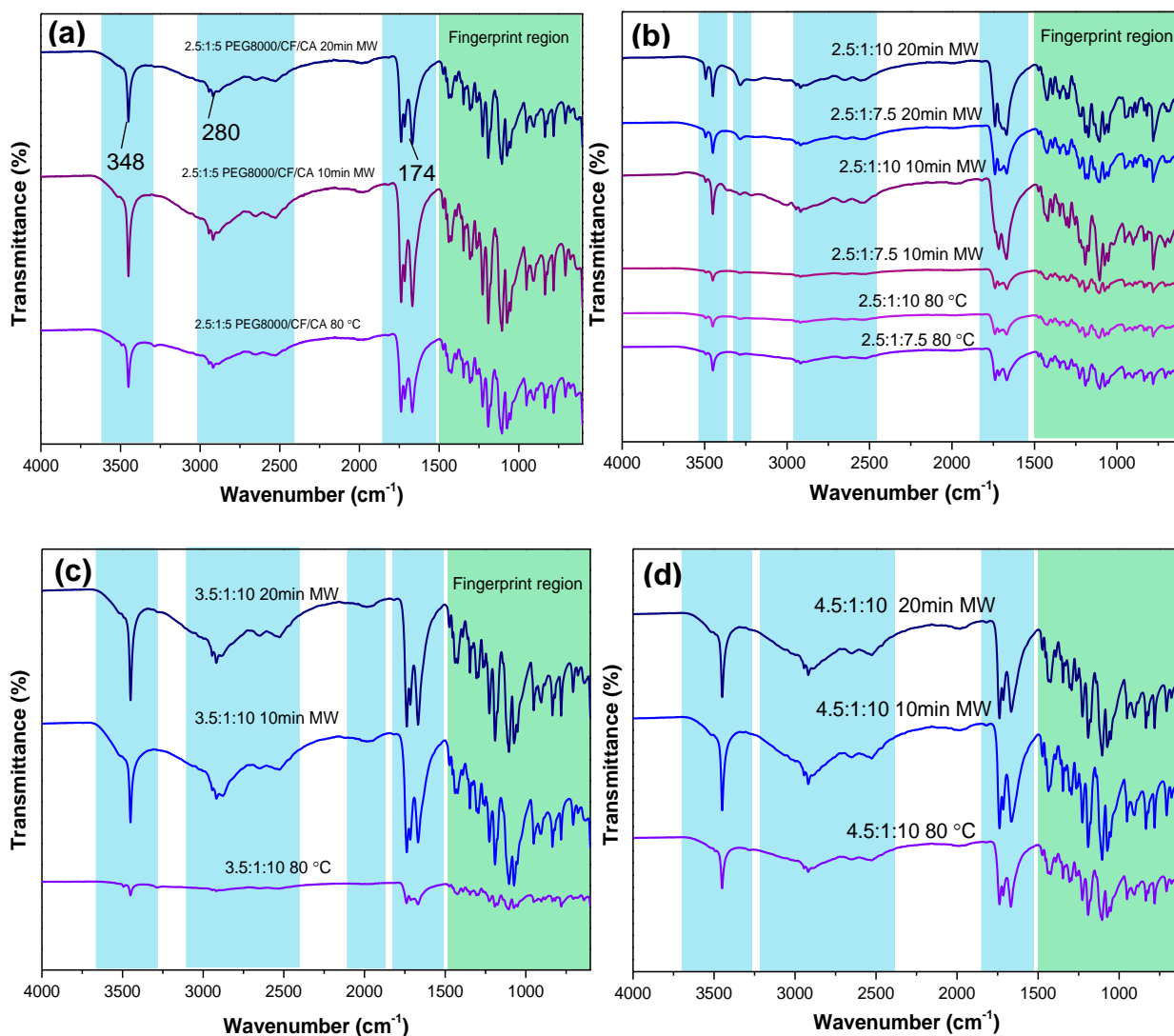
Figure 7. 1 The FTIR spectra of the unirradiated and MW irradiated TCA composite PCMs with different blend ratios: (a) 2.5:1:5; (b) 2.5:1:10; (c) 3.5:1:10; and (d) 4.5:1:10.

7.3.2 Impact of MW irradiation on the crystalline properties of PEG8000 in the TCA crosslinked composite PCMs

The XRD patterns of the unirradiated and MW irradiated TCA crosslinked composite PCMs with blend ratio 2.5:1:3, 2.5:1:5, 2.5:1:7.5, 3.0:1:5, 3.0:1:7.5 and 3.0:1:10 containing 38.46, 29.41, 22.73, 33.33, 26.09 and 21.43 wt.% of PEG8000 are presented in Figure 7.2. Observations indicated that 10 min MW irradiation caused the crystalline regions to rearrange since the intensity of the crystalline peaks had increased which demonstrated increased crystallinity (M. Wang et al., 2019). Figure 7.2 (c) indicated that the crystallinity of the composite PCMs with blend ratios 2.5:1:3, 2.5:1:5, 2.5:1:7.5 and 3:1:7.5 increased after 10 min MW irradiation from 8.92, 43.69,

40.17 and 35.44 to 38.11, 45.51, 43.81 and 47.73%. This was attributed to thermal effect of MW irradiation that resulted in enhancing the crystalline phases in PEG8000 by reducing the imperfect crystalline regions (He and Zhang, 2008). Moreover, results showed that the degree of enhancement caused to the crystallinity was influenced mainly by the chemical composition and the CI value. Hence, the composite PCM with blend ratio 2.5:1:3 had the lowest CI value of 8.92%; and 10 min MW irradiation was observed to cause significant improvement in CI value from 8.92 to 38.11% while in composite PCMs with high CI values no significant improvements in crystallinity occurred. When CI value was 43.69%, 10 min MW irradiation caused CI value to increase insignificantly to 45.51% (e.g., 4.17% increase) while in the composite PCMs with blend ratios 3.0:1:5 and 3.0:1:7.5 the CI was observed to decrease drastically from 41.50 to 26.69% (e.g.,35.69% decrease); and from 57.07 to 40.26% (e.g.,29.46% decrease). This was attributed to the reduced crystallite size caused by MW irradiation which subsequently resulted in decreasing its crystallinity. This was accompanied by the enlargement of the amorphous phases (Abiona and Osinkolu, 2010; Golitsyn et al., 2019).

Moreover, observations indicated that the impacts of MW irradiation were higher in composites containing higher contents of PEG and CF because composite PCM containing 33.33 and 11.11 wt.% of PEG and CF experienced 35.69% reduction in CI value while the CI value of composite PCM containing 22.73 and 9.09 wt.% of PEG and CF reduced to 29.46%. Results indicated that 10 min MW irradiation had a positive impact on the crystallinity of composite PCMs which initially had very low CI values. Also, the degree of enhancement caused to the crystallinity depended mainly upon the chemical composition of the composite PCM.
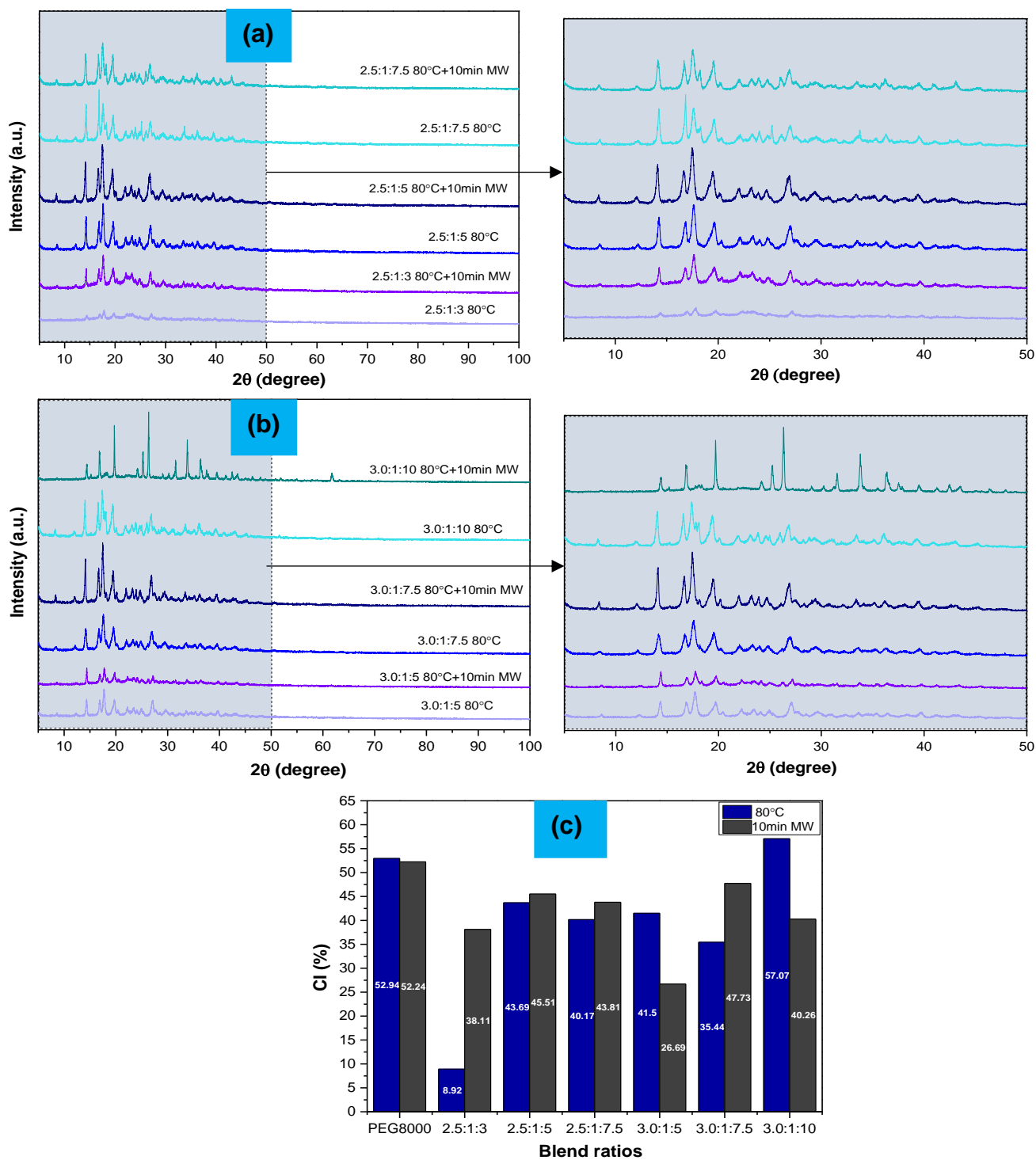
Figure 7. 2 (a) and (b) XRD pattern of the MW irradiated TCA crosslinked composite PCMs; and (c) CI of the crosslinked composite PCMs.

7.3.3 Impact of MW irradiation duration on the crystalline properties of PEG8000 in the TCA crosslinked composite PCMs

Results had demonstrated that MW irradiation can cause the rearrangement of the crystalline segments of PEG in the crosslinked structure. However, the impact of MW irradiation duration needs to be determined to evaluate whether it causes further improvements in the crystallinity of PEG.

The XRD patterns of the unirradiated and MW irradiated composite PCMs with blend ratios of 2.5:1:3, 2.5:1:5, 2.5:1:7.5, 4.0:1:5, 4.0:1:7.5 and 4.0:1:10 are presented in Figure 7.3 (a) and (b) while (c) compares the CI values of the different composite PCMs. Results indicated that 20 min MW irradiation had a desirable effect on the crystallinity of composite PCMs with blend ratio of 2.5:1:7.5 since its CI value was observed to increase from 40.17 to 49.00% (e.g., 21.98% increase); and the same pattern was observed to occur in the composite PCM with blend ratio 2.5:1:10 since CI value had increased from 29.30 to 48.24% (e.g., 64.64% increase).

Results suggested that the enhancement caused to the crystallinity of PEG in the composite PCM depended mainly upon the PEG and CF content because composite PCM containing 18.52 and 7.41 wt.% of PEG and CF (e.g., low content of PEG and CF) had experienced 64.64% increase in crystallinity while the composite PCM containing 22.73 and 9.09 wt.% of PEG and CF (e.g., high content of PEG and CF) had experienced a relatively lower improvement in crystallinity (e.g., 21.98% increase). Moreover, for the corresponding blend ratios 20 min MW irradiation was observed to cause better enhancement of PEG crystallinity compared to the 10 min MW irradiation since the latter only caused CI value to increase from 40.17 to 43.81%; and from 29.30 to 48.06% (e.g., 9.06 and 64.03% increase).

In composite PCM with blend ratio 2.5:1:5 containing 29.41 and 11.76 wt.% of PEG and CF content, 10 min MW irradiation was observed to cause insignificant enhancement of crystallinity since the CI value increased from 43.69 to 45.51% (4.17% increase); and MW irradiation of 20 min resulted in decreasing the CI value from 43.69 to 37.47% (e.g., 14.24% decrease). Therefore, for the corresponding composite PCM containing high content of PEG and CF no major improvements in crystallinity were caused by MW irradiation. Results showed that in the composite PCM with blend ratio of 4.0:1:5 10 containing 40.0 and 10.0 wt.% of PEG and CF, 10

min MW irradiation had a negative impact on the crystallinity since the CI value was observed to decrease drastically from 19.41 to 12.26 % (e.g., 36.84% decrease); however, 20 min MW irradiation resulted in enhancing the CI value insignificantly from 19.41 to 21.60% (e.g.,11.28% increase).

Moreover, MW irradiation had no remarkable impacts on the crystallinity of composite PCMs containing high PEG and CF contents since decreasing PEG and CF content from 40.0 to 32.0 wt.% and from 10.0 wt.% to 8.0 wt.% in the composite PCM with blend ratio 4.0:1:7.5 resulted in increasing the CI value significantly from 35.65 to 47.96% (e.g.,34.53% increase) after 10 min MW irradiation. The same pattern was observed after 10 min MW irradiation in composite PCM with blend ratio 4.0:1:10 containing 26.67 and 6.67 wt.% of PEG and CF since the CI value was observed to increase significantly from 33.61 to 43.31% (e.g.,28.86% increase). This indicated that CA content also impacts the degree of improvements in crystallinity since decreasing the CA content insignificantly from 66.67 to 60.00 wt.% (e.g.,10.00% decrease) resulted in enhancing the CI value significantly from 28.86 to 34.53% (e.g.,19.65% increase). Also, for composite PCM with blend ratio of 4.0:1:7.5 containing high content of PEG, CF, and CA, 20 min MW irradiation was observed to decline the CI value from 35.65 to 32.32% (e.g., 9.34% decrease) while in the composite PCM with blend ratio 4.0:1:10 containing low PEG, CF, and CA content 20 min MW irradiation was observed to enhance the CI value from 33.61 to 45.41% (e.g.,35.11% increase). Overall, results demonstrated the possibility of enhancing the crystallinity of PEG in the TCA crosslinked composite PCMs using MW irradiation treatment since its thermal effect resulted in melting the amorphous phases, and thereby increased the number of crystalline phases.
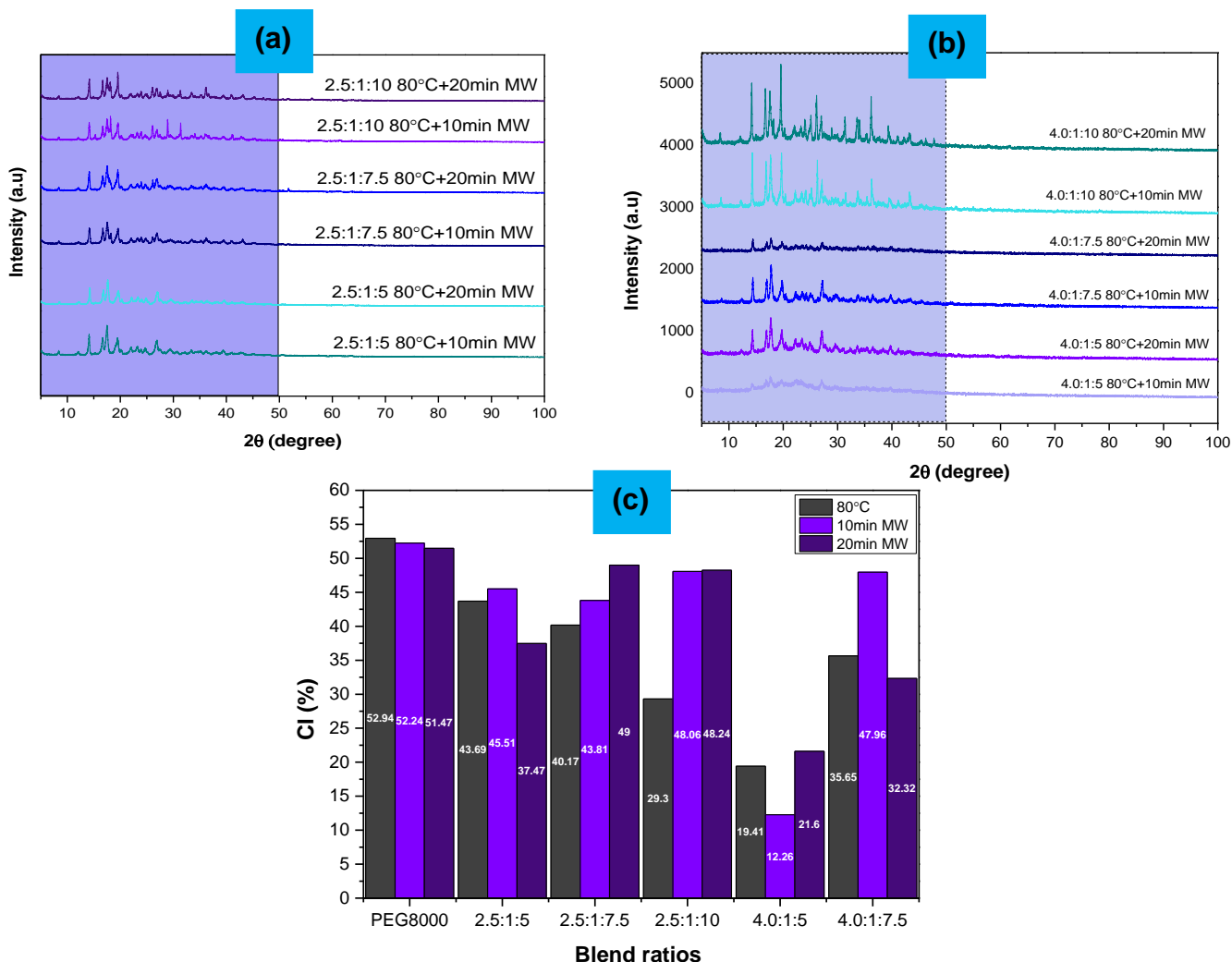
Figure 7. 3 (a) and (b) XRD pattern of the MW irradiated TCA crosslinked composite PCMs; and (c) CI values of the crosslinked composite PCMs.

7.3.4 Impact of MW irradiation and CF content on the crystalline properties of PEG8000 in the TCA crosslinked composite PCMs

Figure 7.4 presents the XRD patterns and the CI values of the unirradiated and MW irradiated TCA crosslinked composite PCMs with blend ratios of 4.0:0.80:5, 4.0:0.80:7.5 and 4.0:0.80:10 containing 40.82, 32.52 and 27.03 wt.% of PEG8000. The crystallinity of the composite PCM containing 40.82 wt.% of PEG8000 was observed to reduce after ten and twenty min MW irradiation from 45.68 to 41.61 % and 34.56% (e.g., 8.91 and 24.34% decrease). This indicated that MW irradiation had an undesirable effect on the crystallinity in composite PCMs with high PEG content. In composite PCM with blend ratio of 4.0:0.80:7.5 containing 32.39 wt.% of PEG, 6.88 wt.% of CF and 60.73 wt.% of CA, 10 min MW irradiation was observed to reduce the

211

CI value from 46.12 to 34.64% (e.g.,24.89% decrease); and 20 min MW irradiation also resulted in decreasing the CI value from 46.12 to 38.61% (e.g.,16.28% decrease). Overall, results indicated that for the corresponding blend ratio, the thermal effect of MW radiation had destructed the crystal lattice structure of PEG due to the presence of CF in lower content. Results indicated that sufficient CF content must be present in the composite PCM for the shielding of the crystal structure of PEG during the MW irradiation process; and thereby, preserve its crystallinity (Forster et al., 2019).

In the composite PCM with blend ratio of 4.0:0.80:10 containing 26.85 wt.% of PEG, 6.04 wt.% of CF and 67.11 wt.% of CA, 10 min MW irradiation was observed to enhance the CI value significantly from 39.45 to 48.12% (e.g.,21.98% increase) while 20 min MW irradiation had caused the CI value to increase insignificantly from 39.45 to 43.39% (e.g.,9.99% increase). Moreover, results indicated the importance of incorporating sufficient CF content in the composite PCMs for the enhancement of its crystallinity via MW irradiation treatment. Hence, MW irradiation was observed to attack the crystalline domains of PEG in the composite PCMs when the CF content was low due to insufficient shielding.
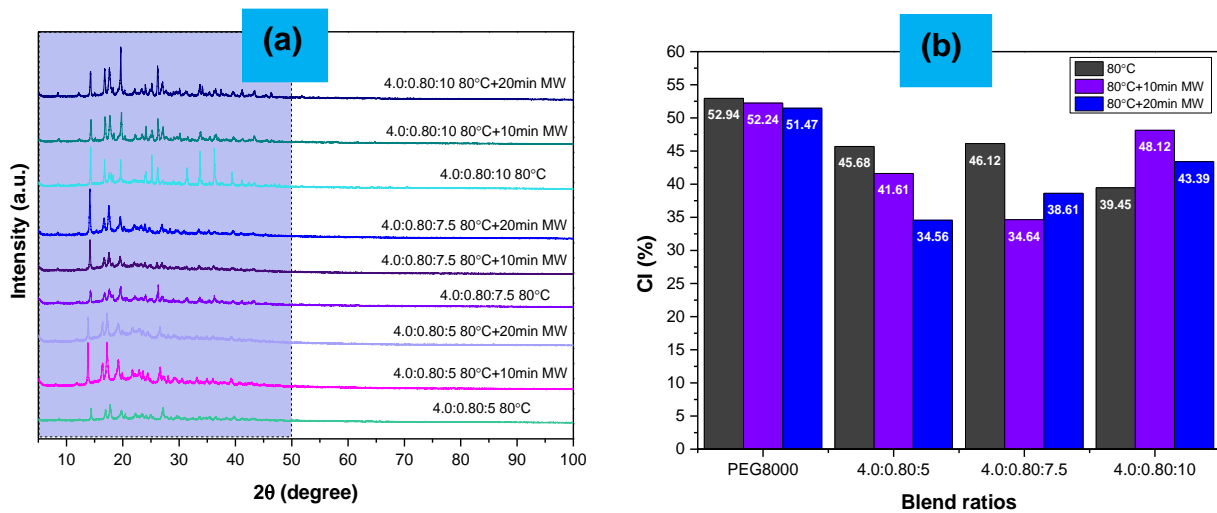
Figure 7. 4 (a) The XRD patterns of the unirradiated and MW irradiated TCA composite PCMs; and (b) CI values of the composite PCMs.

7.3.5 Thermal properties of the MW irradiated TCA crosslinked composite PCMs

Figure 7.5 presents the DSC heating and cooling curves of the unirradiated, and MW irradiated TCA crosslinked composite PCMs with blend ratios of 3.5:1:5, 3.5:1:7.5 and 3.5:1:10 containing 36.84, 29.17 and 24.14 wt.% of PEG8000; and table 7.1 summarises its thermal properties. The thermograms demonstrated that all the curves exhibited a single endothermic and exothermic peak which indicated the existence of one type of crystal structure in the TCA crosslinked composite PCMs and was attributed to the melting and crystallisation of PEG8000 in the composite PCMs (Kong et al., 2017). The melting and crystallisation enthalpy of the TCA crosslinked composite PCMs lied in the range 26.39 to 69.20 J/g; and 24.90 to 67.24 J/g while pristine PEG8000 had a melting and crystallisation enthalpy of 181.5 and 182.1 J/g.

Observations indicated that MW irradiation resulted in changing the area under the endothermic and exothermic peaks. This was attributed to the changes caused to the latent heat of melting and crystallisation. Composite PCM containing 36.84 wt.% of PEG8000 experienced significant reduction and enhancement of latent heat after 10 and 20 min MW irradiation. Ten min MW irradiation resulted in decreasing the latent heat of melting and crystallisation from 58.09 and 55.75 J/g to 47.64 and 45.83 J/g (e.g.,17.99 and 17.79% decrease); and 69.20 and 67.24 J/g (19.13 and 20.61% increase). Results suggested that 10 min MW irradiation had increased the number of crystal defects which was accompanied by an increase in the number of amorphous phases (e.g., non-crystallisable component).

However, an additional 10 min of MW irradiation (e.g., 20 min MW irradiation) was observed to melt the amorphous phases which consequently resulted in increasing the number of crystalline phases; and thus, resulted in enhancing the latent heat of melting and crystallisation. The same phenomenon was repeated for the composite PCMs containing 29.17 and 24.14 wt.% of PEG8000 since 10 min MW irradiation resulted in decreasing the latent heat of melting and crystallisation from 38.64 and 37.62 J/g to 38.51 and 36.29 J/g (e.g.,0.34 and 3.54% decrease); and from 26.39 and 24.90 J/g to 24.93 and 23.61 J/g (e.g., 5.53 and 5.18% decrease). While 20 min MW irradiation resulted in enhancing the latent heat of melting and crystallisation from 38.64 and 37.62 J/g to 41.29 and 38.47 J/g (e.g.,6.86 and 2.60% increase) and from 26.39 and 24.90 J/g to 31.76 and 30.89 J/g (e.g.,20.35 and 24.06% increase). Overall, results suggested that the degree of destruction or enhancement caused to the latent

heat capacity depends mainly upon the PEG content since composite PCM with optimum PEG content of 36.84 wt.% experienced optimum enhancement in its latent heat capacity after 20 min MW irradiation (e.g.,20% increase) while reducing the PEG content to 29.17 wt.% (e.g.,20.82% decrease) only enhanced the latent heat capacity by less than 10%. However, further reduction in PEG content to 24.14 wt.% resulted in enhancing the latent heat capacity by more than 20% after 20 min MW irradiation.

Table 7. 1 Thermal properties of unirradiated and MW irradiated TCA crosslinked composite PCMs.

Sample name	Phase transition temperature		Latent heats	
	T_m (°C)	T_c (°C)	H_m (J/g)	H_c (J/g)
PEG8000	63.12	43.78	181.5	182.1
3.5:1:5 80 °C	64.11	45.11	58.09	55.75
3.5:1:7.5 80 °C	50.69	41.60	38.64	37.62
3.5:1:10 80 °C	58.22	44.44	26.39	24.90
3.5:1:5 10 min MW	57.68	42.06	47.64	45.83
3.5:1:7.5 10 min MW	55.48	40.86	38.51	36.29
3.5:1:10 10 min MW	53.78	38.50	24.93	23.61
3.5:1:5 20 min MW	60.12	40.20	69.20	67.24
3.5:1:7.5 20 min MW	53.43	40.48	41.29	38.47
3.5:1:10 20 min MW	56.55	39.40	31.76	30.89
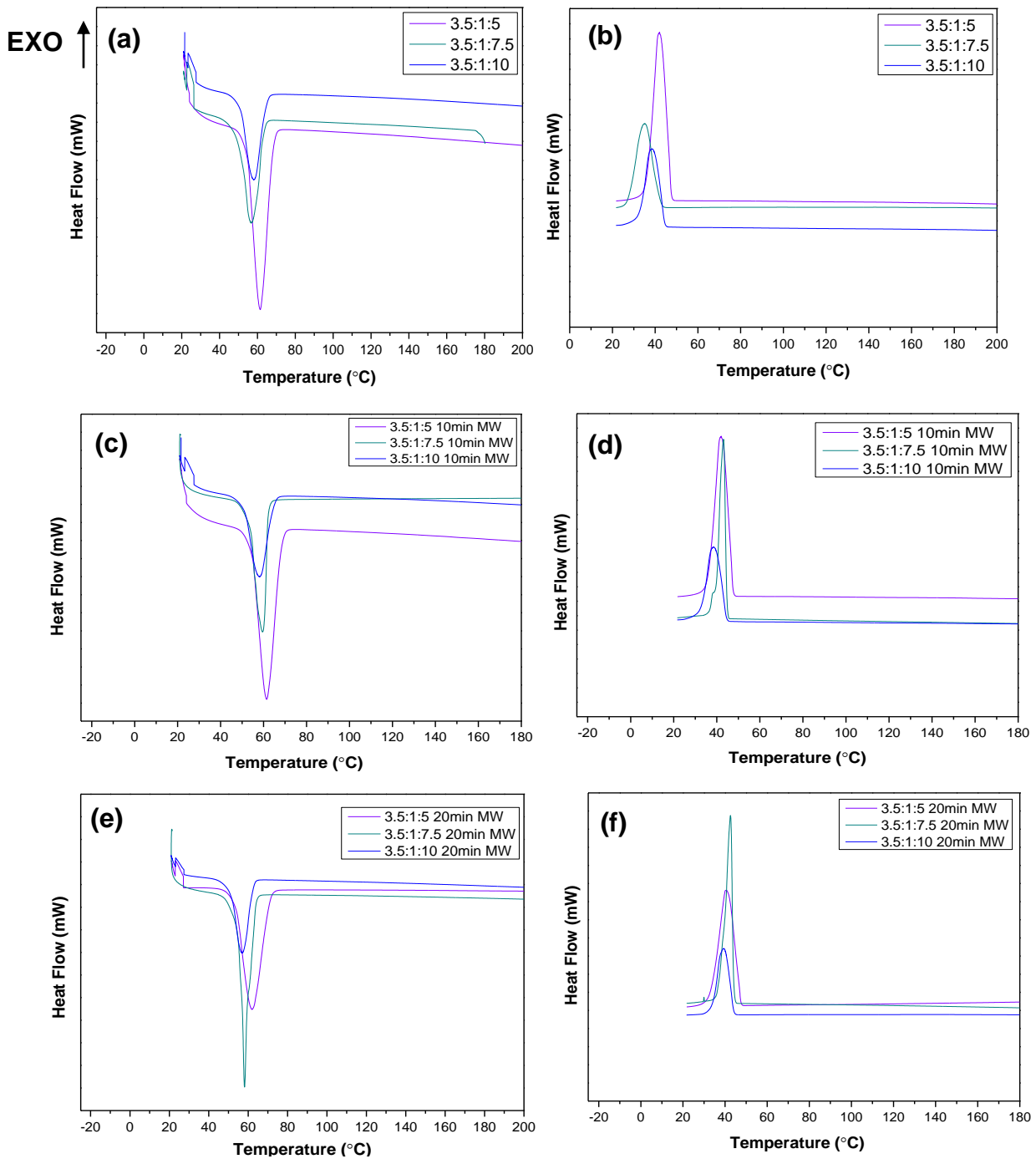
Figure 7. 5 DSC (a), (c) and (e) heating; and (b), (d) and (f) cooling curves of the unirradiated and MW irradiated TCA crosslinked composite PCMs.

Figure 7.6 (a) to (e) illustrates the impacts caused by MW irradiation to the thermal properties of PEG8000 in the TCA crosslinked composite PCMs.
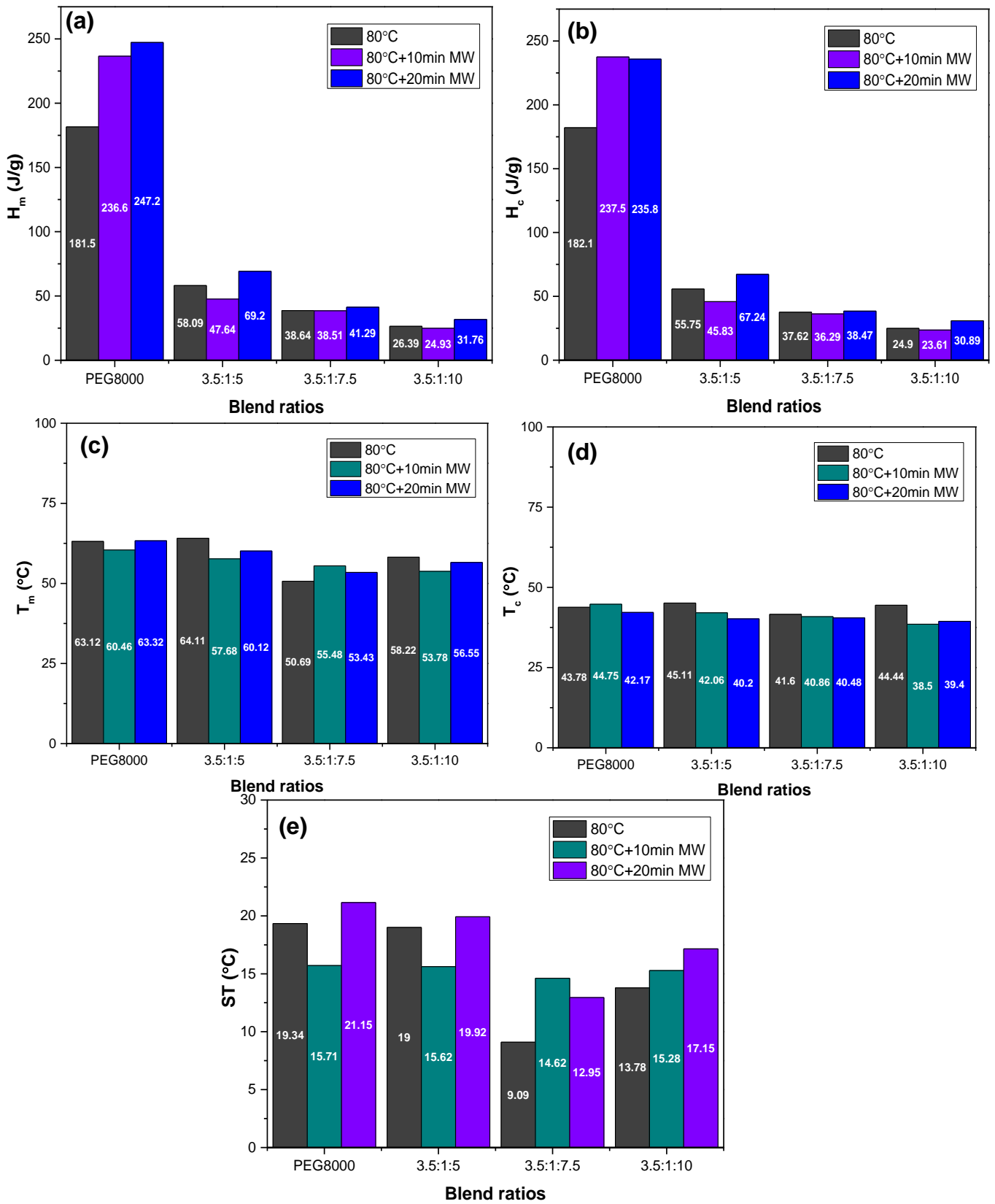
Figure 7. 6 The thermal properties of the different TCA crosslinked composite PCMs: (a) and (b) Latent heat of melting and crystallisation; (c) and (d) Phase transition temperatures; and (e) Supercooling temperatures.

Figure 7.7 (a) and (b) shows the DSC heating and cooling curves of the unirradiated, and MW irradiated composite PCMs with blend ratios of 3.5:0.85:7.5 and 3.5:0.85:10 containing 29.17 and 24.39 wt.% of PEG content, 7.17 and 5.92 wt.% of CF content and 63.29 and 69.69 wt.% of CA. MW irradiation was observed to enhance the latent heat of melting and crystallisation of composite PCM containing 29.17 wt.% of PEG8000 from 32.80 and 31.10 J/g to 40.03 and 37.84 J/g and 39.26 and 40.15 J/g. Observations indicated that sufficient CF content should be present in the composite PCM in order to enhance the thermal properties using MW irradiation treatment because decreasing the CF content from 7.17 to 5.92 wt.% (e.g.,17.43% decrease) resulted in reducing the latent heat of meting and crystallisation from 40.11 and 38.30 J/g to 32.08 and 30.87 J/g and 31.53 and 28.54 J/g after 10 and 20 min MW irradiation. The T_m and T_c temperatures (see Table 4.8) of the composite PCMs lied in the range 54.37 to 59.36 °C and 33.47 to 41.98 °C, which was lower than the phase transition temperature of PEG8000. This was attributed to the reduced thickness of the lamellae; and therefore, the corresponding composite PCMs consisted of low melting crystals. The supercooling temperatures (ST) of the composite PCMs lied in the range 14.55 to 24.38 °C. Results showed that MW irradiation resulted in increasing the ST from 14.88 to 17.38 and 24.38 °C in composite PCM with blend ratio 3.5:0.85:7.5 which was attributed to the reduced number of nucleation sites. The same trend was observed to occur in composite PCM with blend ratio 3.5:0.85:10 since MW irradiation resulted in increasing the ST from 14.55 to 17.42 and 16.48°C; however, the ST of the corresponding composite PCM was lower than the one of pristine PEG8000 which was 19.34°C. Figure 7.8 (a) to (e) summarises the thermal properties of the unirradiated and MW irradiated TCA crosslinked composite PCMs.
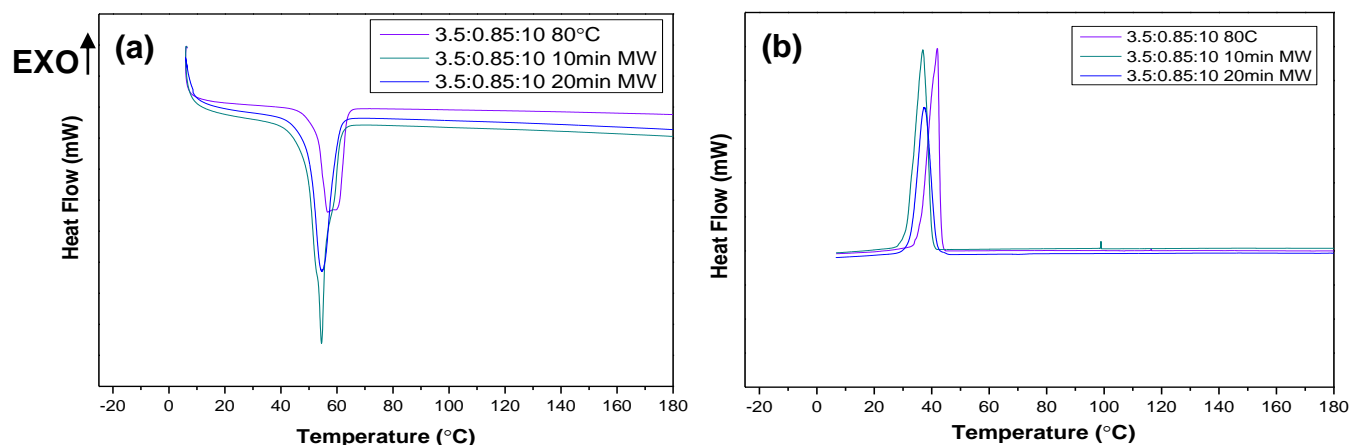
Figure 7. 7 DSC (a) heating; and (b) cooling curves of the TCA crosslinked composite PCMs.

Table 7. 2 Thermal properties of the TCA crosslinked composite PCMs.

Sample name	Phase transition temperature		Latent heats	
	T_m (°C)	T_c (°C)	H_m (J/g)	H_c (J/g)
PEG8000	63.12	43.78	181.5	182.1
3.5:0.85:7.5 80 °C	55.22	40.34	32.80	31.10
3.5:0.85:7.5 10 min MW	59.36	41.98	40.03	37.84
3.5:0.85:7.5 20 min MW	57.79	33.47	39.26	40.15
3.5:0.85:10 80 °C	56.49	41.94	40.11	38.30
3.5:0.85:10 10 min MW	54.37	36.95	32.08	30.87
3.5:0.85:10 20 min MW	54.39	37.91	31.53	28.54
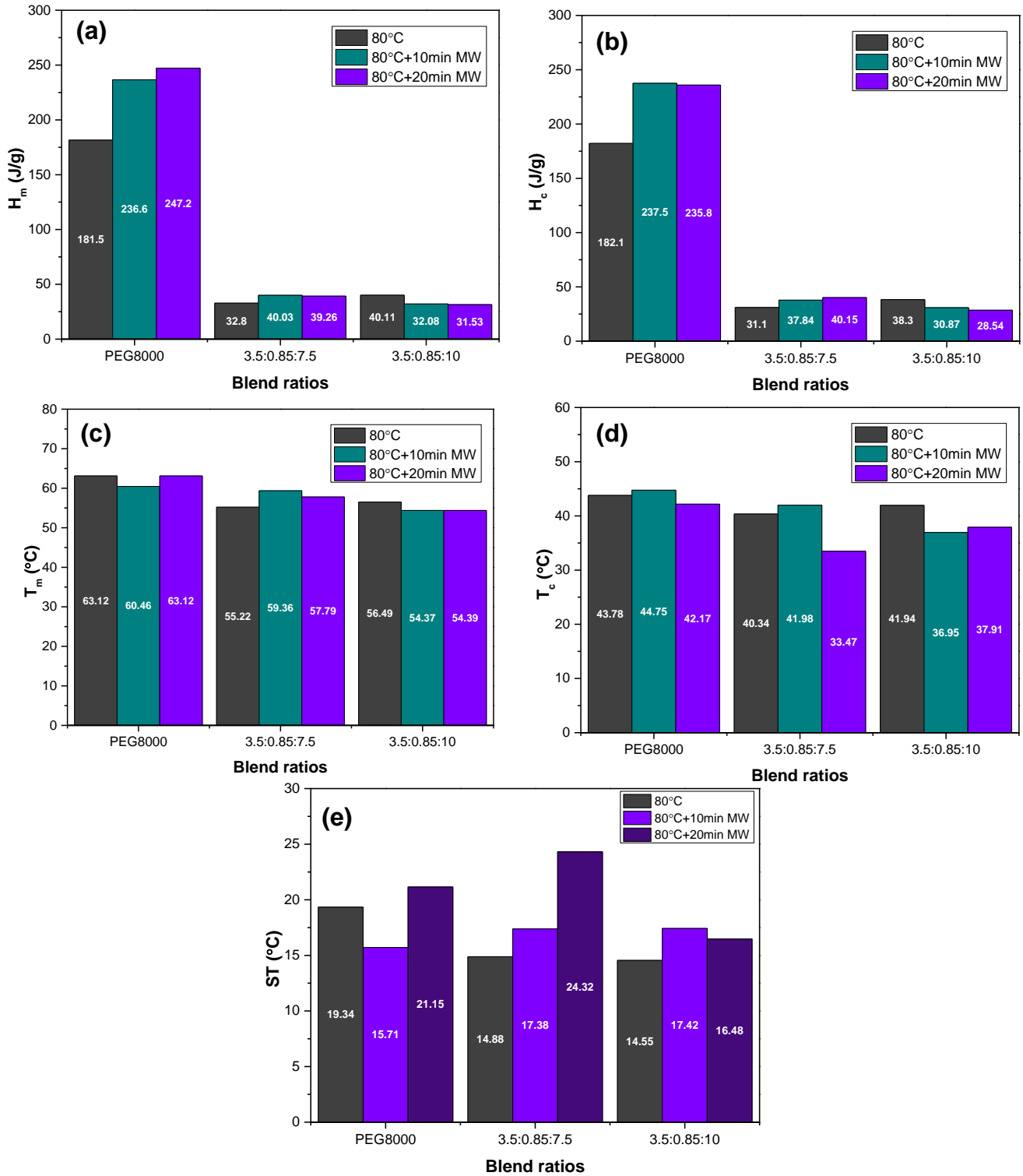
Figure 7. 8 The thermal properties of the different TCA crosslinked composite PCMs: (a) and (b) Latent heat of melting and crystallisation; (c) and (d) Phase transition temperatures; and (e) Supercooling temperatures.

7.3.6 Impact of MW irradiation and Mw on the thermal properties of PEG in the TCA crosslinked composite PCMs

Figure 7.9 shows the DSC heating and cooling curves of the unirradiated, and MW irradiated composite PCMs with blend ratio 4.0:1:10 prepared using PEG8000 (P8) and PEG4000 (P4). The area under the endothermic and exothermic peaks of P8 and P4 were observed to have reduced after TCA crosslinking reaction. This was attributed to the reduction in latent heat of melting and crystallisation of PEG after the chemical crosslinking reaction. In the composite PCM prepared using PEG4000, 10 min MW irradiation was observed to increase the latent heat of melting and crystallisation from 35.84 and 34.04 J/g to 39.74 and 38.06 J/g (e.g.,6.19 and 11.80% increase) while 20 min MW irradiation resulted in decreasing the latent heat of melting and crystallisation from 35.84 and 34.04 J/g to 33.86 and 30.88 J/g (e.g., 5.52 and 9.28% decrease).

MW irradiation of composite PCM prepared using PEG8000 resulted in decreasing the latent heat of melting from 43.28 and 43.79 J/g to 27.48 and 25.69 J/g and 35.46 and 33.81 J/g. Overall, results indicated that for TCA crosslinked composite PCM with blend ratio 4.0:1:10 experienced no remarkable enhancement in its thermal properties after the MW irradiation treatment; and changing the M_w was observed to have no desirable effects. The phase transition temperatures were also observed to have reduced after the TCA crosslinking reaction which indicated that the lamellae thickness had reduced; and the composite PCMs consisted of low melting crystals (see Chapter 6 for more information regarding this mechanism).
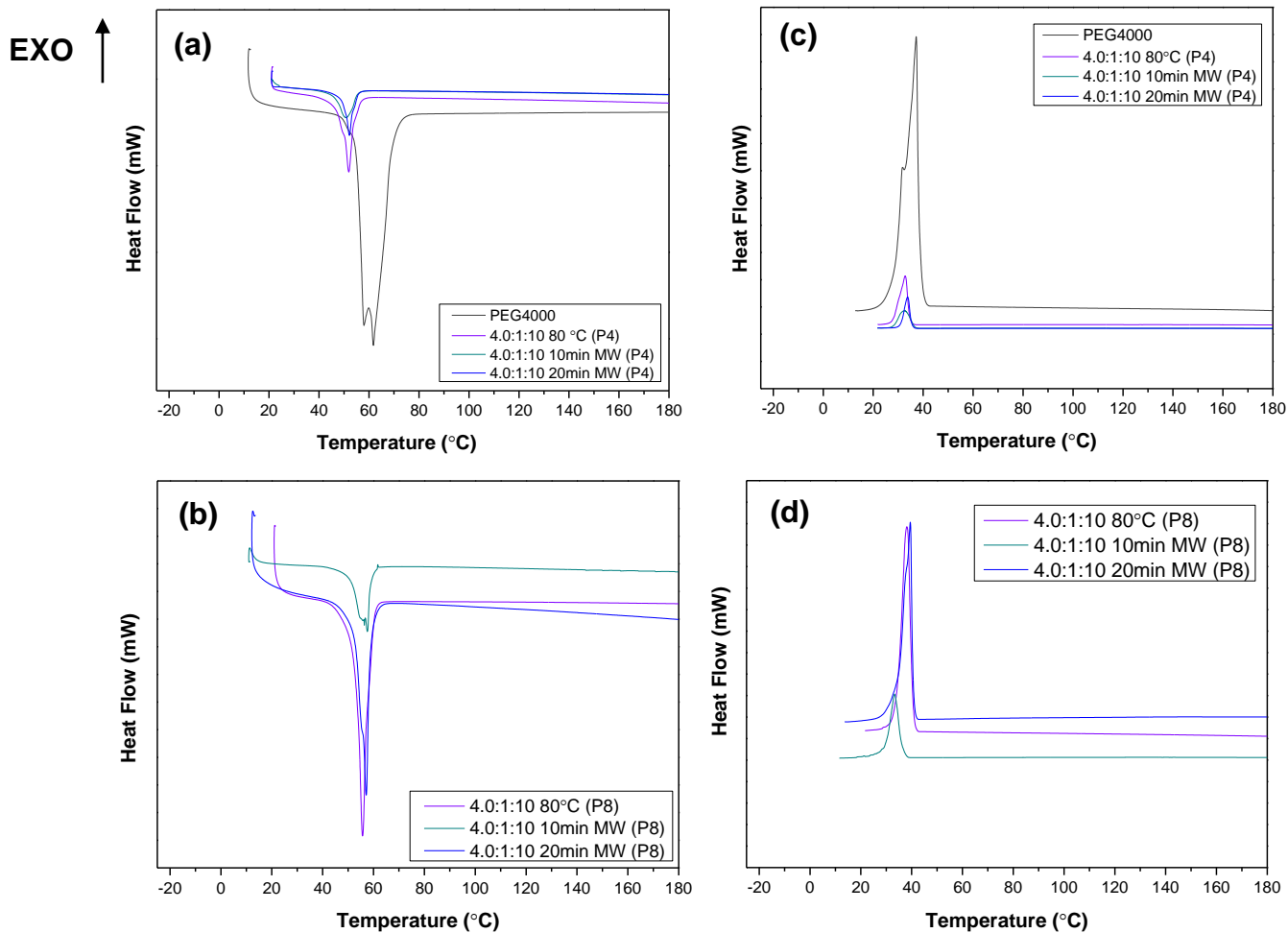
Figure 7. 9 DSC (a) and (b) heating; and (c) and (d) cooling cycles of unirradiated and MW irradiated composite PCM with blend ratio 4.0:1:10 prepared with PEG4000 (P4) and PEG8000 (P8).

Table 7. 3 The thermal properties of TCA crosslinked composite PCMs.

Sample name	Phase transition temperature		Latent heats	
	T_m (°C)	T_c (°C)	H_m (J/g)	H_c (J/g)
PEG8000 (P8)	63.12	43.78	181.5	182.1
4.0:1:10 80 °C (P8)	55.68	37.97	43.28	43.79
4.0:1:10 10 min MW (P8)	54.88	33.32	27.48	25.69
4.0:1:10 20 min MW (P8)	54.11	39.87	35.46	33.81
PEG4000 (P4)	57.84	37.06	170.3	173.2
4.0:1:10 80 °C (P4)	52.05	32.68	35.84	34.04
4.0:1:10 10 min MW (P4)	48.29	32.80	39.74	38.06
4.0:1:10 20 min MW (P4)	50.12	35.34	33.86	30.88
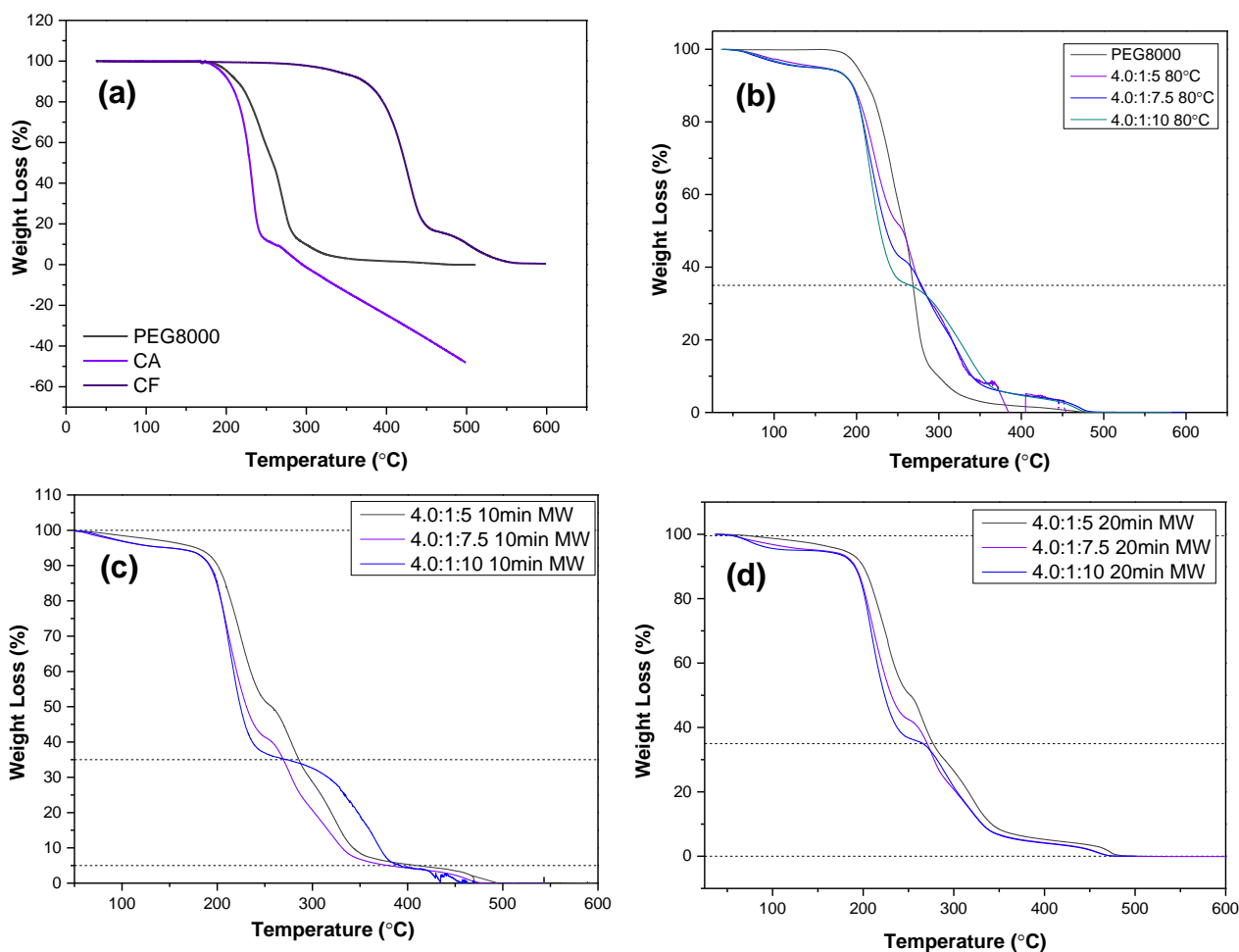
Figure 7. 10 TGA curve of the unirradiated (a) PEG8000, CA and CF; and (b), (c) and (d) unirradiated and MW irradiated TCA crosslinked composite PCMs.

7.3.7 Thermal stability of TCA crosslinked composites

The TGA curves of PEG8000, CA, CF and the TCA crosslinked composite PCMs are presented in Figure 7.10 (a) to (d). TGA results determined at the different degradation stages are summarised in Table 7.4. Observation indicated that PEG8000 and the TCA crosslinked composite PCMs were stable up to approximately 200 °C.

Observations indicated that increasing the onset temperature caused thermal decomposition of PEG8000 and the TCA crosslinked composite PCMs. The composite PCMs experienced mass loss in 2 to 4 stages while PEG8000 experienced mass loss in 2 stages only. Table 7.2 shows that the TCA crosslinked composite PCMs had an onset and maximum temperature in the range 127.81 to 201.24 °C and 363.79 to 489.64 °C while PEG8000 had an onset and maximum temperature of 189.90°C and 479.50 °C. Therefore, results demonstrated that the TCA crosslinked composite PCMs had better thermal stability than pristine PEG8000 even though the crosslinked composite PCMs had lower crystallinity than PEG8000. The onset temperature of the

unirradiated composite PCM with blend ratio 4.0:1:5 containing 40.0 wt.% of PEG8000, 10 wt.% of CF and 50 wt.% of CA was 198.18 °C which was higher than the one of PEG8000 (e.g., 189.90°C). Therefore, results indicated that after TCA crosslinking the onset temperature was enhanced by 4.36% which confirms improved thermal stability of PEG after chemical crosslinking. Results suggested that the degree of enhancement caused to onset temperature was influenced by the chemical composition since decreasing the PEG and CF content while increasing the CA content was observed to decrease the onset temperature of the composite PCMs. Hence, decreasing the PEG content from 40 to 32 and 26.67 wt.% and CF content from 10 to 8 and 6.67 wt.% while increasing the CA content from 50 to 60 and 66.67 wt.% resulted in decreasing the onset temperature from 198.18 to 195.51 and 127.87 °C.

MW irradiation was observed to enhance the thermal stability of the composite PCM containing 40 wt.% of PEG8000 since the onset temperature increased from 198.18 to 199.82 and 201.24 °C after ten and twenty min MW radiation exposure. Ten and twenty min MW irradiation resulted in increasing the onset temperature of composite PCM containing 26.67 wt.% of PEG8000 from 127.81 to 197.06 and 193.17 °C. However, MW irradiation was observed to reduce the thermal stability of the composite PCM containing 32 wt.% of PEG8000 since the onset temperature decreased from 195.51 to 193.77 and 193.99 °C. Overall, results demonstrated that the thermal stability of the TCA crosslinked PCMs were enhanced by MW irradiation.

For PEG8000 and the composite PCMs, the mass loss that occurred below 100 °C was attributed to the loss of absorbed moisture and corresponded to the melting of PEG8000. The second stage of major mass loss was in the temperature range varying from 170 up to 270 °C and corresponded to the thermal decomposition of PEG8000, CF and the crosslinked network (Devangamath et al., 2020). The third and fourth stage of mass loss occurred in the temperature range 300 to 500 °C and was attributed to the thermal decomposition of CA and the crosslinked structure.

Table 7. 4 TGA results of PEG and the TCA crosslinked composite PCMs.

Name	Mass loss (%)				T_{onset} (°C)	T_{max} (°C)
	Stage 1	Stage 2	Stage 3	Stage 4		
PEG8000	85.92	13.99	NA	NA	189.90	479.60
4.0:1:5 80°C	91.46	5.26	NA	NA	198.18	363.79
4.0:1:7.5 80°C	57.95	35.02	6.81	NA	195.51	489.64
4.0:1:10 80°C	4.39	59.30	30.79	5.24	127.81	479.85
4.0:1:5 10min MW	49.78	48.08	1.84	NA	199.82	467.76
4.0:1:7.5 10min MW	58.85	37.22	3.72	NA	193.77	416.18
4.0:1:10 10min MW	57.91	36.19	NA	NA	197.06	461.61
4.0:1:5 20min MW	50.17	20.49	24.56	4.71	201.24	413.12
4.0:1:7.5 20min MW	58.85	34.96	5.99	0.171	193.99	475.77
4.0:1:10 20min MW	4.84	58.57	36.29	NA	193.17	470.92

7.3.8 Effect of MW irradiation on the crystal morphology and structure of PEG8000 in the TCA crosslinked composite PCMs

Figure 7.11 presents a series of POM images of the unirradiated and MW irradiated PEG8000 particles, mainly to study the changes caused to the crystal morphology of PEG8000 after the MW irradiation treatment. Observations indicated that at room temperature no obvious changes in shape or size had occurred to the PEG8000 particle after 10- and 20-min MW irradiation; however, the clarity of the cross-extinction pattern had reduced after the MW irradiation treatment. This was attributed to the destruction caused to the spherulite crystals of PEG8000. The spherulite crystals were observed to be overlapping one another as result of the thermal effect induced by the MW irradiation treatment; and literature names this phenomenon as 'impingement' in which the spherulites growing in the outward direction from single nucleating point meet (Crist and Schultz, 2016). Therefore, results demonstrated that the perfection of the crystal lattice of PEG was not enhanced by the MW irradiation thermal effect. Also, the size of the crystals was observed to have reduced to a greater extent with an increase in the duration of MW irradiation treatment.
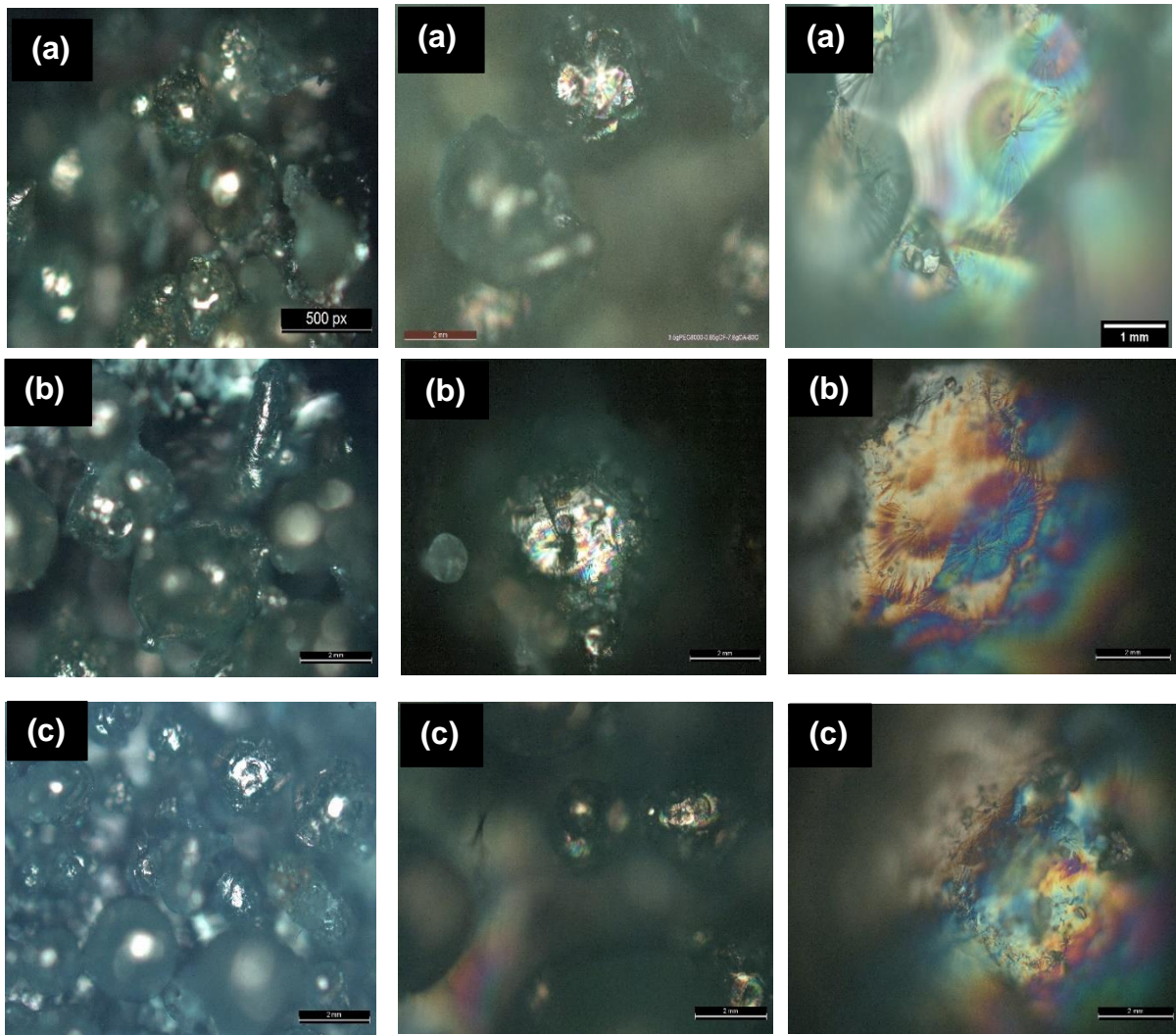
Figure 7. 11 POM images of (a) unirradiated; (b) 10min MW irradiated; and (c) 20min MW irradiated PEG8000 particles.

Figure 7.12 shows the POM image of the unirradiated TCA crosslinked composite PCM with bend ratio 4.0:1:10 below and above its phase transition temperature. Observations indicated that the characteristic spherulite morphology of PEG8000 had changed after TCA crosslinking reaction since the spherulites were not visible in the TCA crosslinked composite PCMs because PEG was enwrapped in CF after the crosslinking reaction which resulted in restricting the chain mobility. The TCA crosslinked composite PCM are observed to contain 'opaque' domains which indicated the presence of the crystalline phases. However, TCA crosslinked composite PCMs

appeared less opaque compared to pristine PEG8000 (see Chapter 4 for more information) which was attributed to its reduced crystallinity.
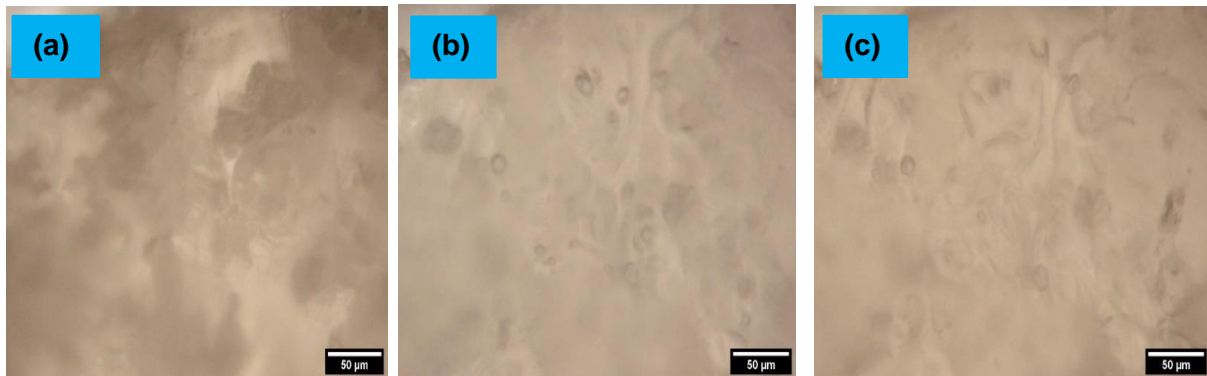
Figure 7. 12 POM images of composite PCM with 4.0:1:10 and 26.67 wt.% PEG8000 at (a) Room temperature; (b) melting; and (c) crystallisation.

Figure 7.13 shows the POM image of the 10 min MW irradiated TCA crosslinked composite PCM with bend ratio 4.0:1:10 below and above its phase transition temperature. Observations indicated that the opacity of the composite PCM had increased attributed to the increased number of crystalline phases due to the melting of the amorphous phases by the MW irradiation treatment (e.g., thermal effect of MW radiation). However, the characteristic spherulite structures were not observed. Figure 6.27 shows the POM image of the 20 min irradiated composite PCM with the same blend ratio. Observations indicated that the spherulite crystals were embedded in the CF matrix.
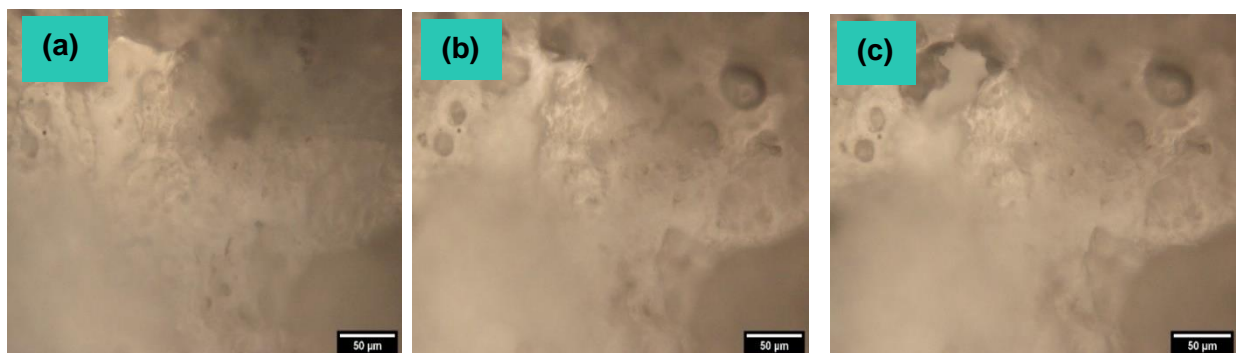
Figure 7. 13 POM images of 10 min MW irradiated composite PCM with 4.0:1:10 and 26.67 wt.% PEG8000 at (a) Room temperature; (b) melting; and (c) crystallisation.

7.3.9 Influence of MW irradiation on the surface morphology of the TCA crosslinked composite PCMs

Figure 7.14 compares the SEM images of the unirradiated and 10min MW irradiated composite PCM with blend ratio 3.0:1:5 containing 33.33, 11.11 and 55.56 wt.% of PEG, CF and CA. Observations indicated that 10 min MW irradiation treatment had caused significant changes to the surface morphology of the composite PCM since its highly porous three-dimensional network covered with aggregates of CF had disappeared completely. This was attributed to the thermal effect of the MW irradiation treatment that resulted in melting the aggregates to form a smoother surface. Hence, the interfacial compatibility between PEG and CF was improved by the 10 min MW irradiation since number of voids had reduced significantly which resulted in the formation a compact structure containing no voids.
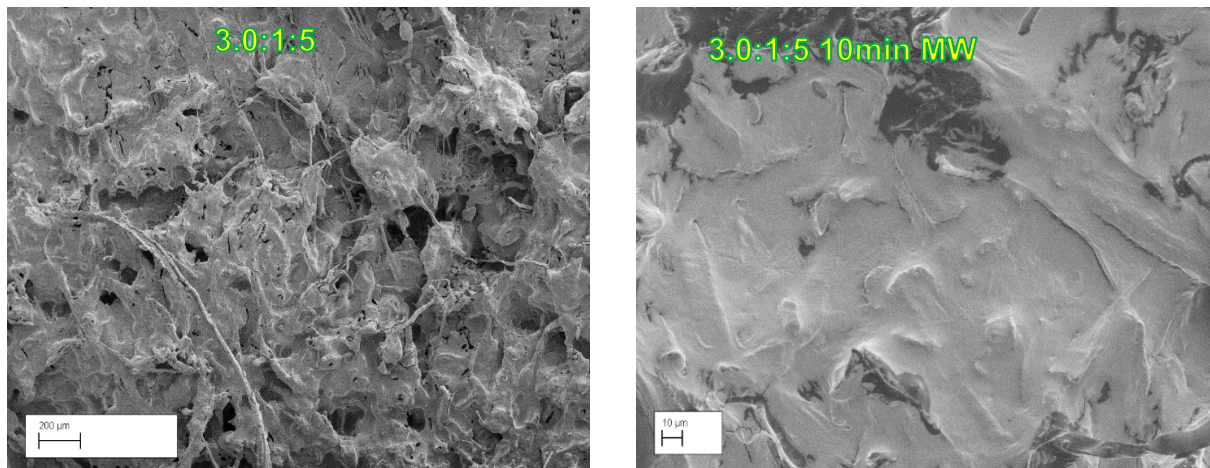
Figure 7. 14 SEM images of unirradiated and MW irradiated composite PCMs.

Figure 7.15 compares the SEM images of the unirradiated and 20min MW irradiated composite PCM with blend ratio 3.0:1:5 containing 29.17, 8.33 and 62.50 wt.% of PEG, CF, and CA. The unirradiated composite PCM exhibited a highly compact network of fibres with no voids and cracks. CF was observed to be embedded in the PEG-CA matrix and the surface morphology appeared to be rough. Overall, good interfacial compatibility existed between PEG and CF. Twenty min MW irradiation treatment was observed to have destructed the surface morphology of the corresponding composite PCM since pores and cracks were observed to have formed. The roughness of its surface was observed to have increased due to the thermal effect since 20 min MW irradiation resulted in reducing the moisture of the composite PCM. Therefore, poor interfacial compatibility existed between PEG and the CF.
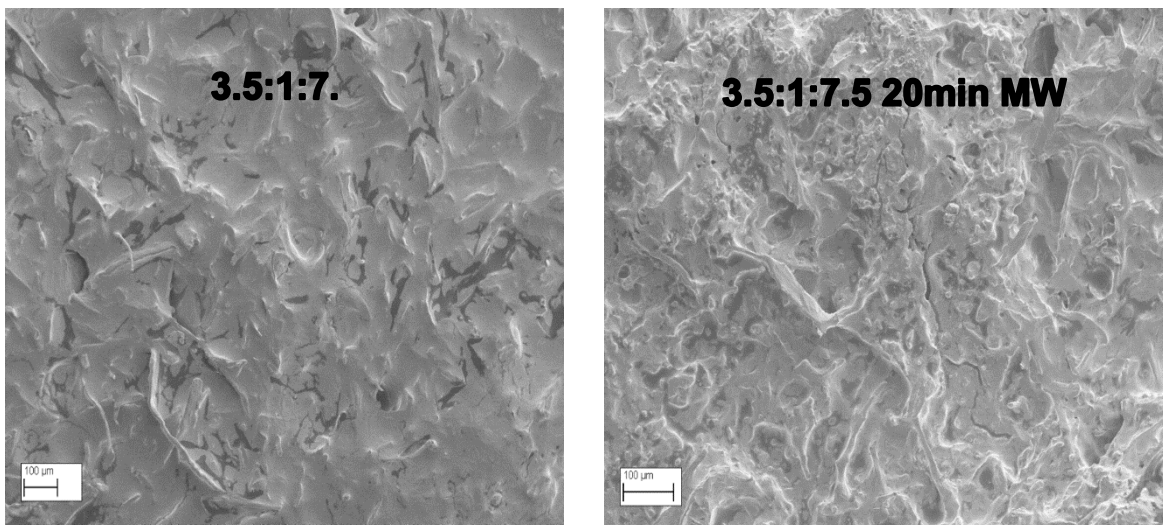
Figure 7. 15 SEM images of unirradiated and MW irradiated composite PCMs.

Figure 7.16 compares the unirradiated and MW irradiated composite PCMs with blend ratios of 2.5:1:7.5 and 3.0:1:10. The unirradiated composite PCMs exhibited a three-dimensional network of fibres. Reducing the CF and CA content resulted in forming a less compact network which consisted of many pores and voids. Hence, increasing the CA content from 68.18 to 71.43 provided that the PEG and CF content decreased from 22.73 to 21.43 wt.% and from 9.09 to 7.14 wt.% resulted in reducing the number of voids. The microstructure was observed to become compact which was attributed to the embedding of CF in the PEG-CA matrix. The interfacial compatibility between PEG and CF appears to have improved due to the formation of a highly crosslinked network. For the corresponding composite PCMs ten and twenty min MW irradiation treatments resulted in improving the interfacial compatibility between PEG and CF since composite PCMs are observed to exhibit compact microstructures; and they contained fewer voids /cracks. The aggregates of CF present in the unirradiated composite PCMs had disappeared as result of melting due to the thermal effect. Overall, the results demonstrated the possibility of enhancing the compatibility between PEG and CF using the MW irradiation treatment; thereby produce homogenous composite PCMs with enhanced structural integrity.
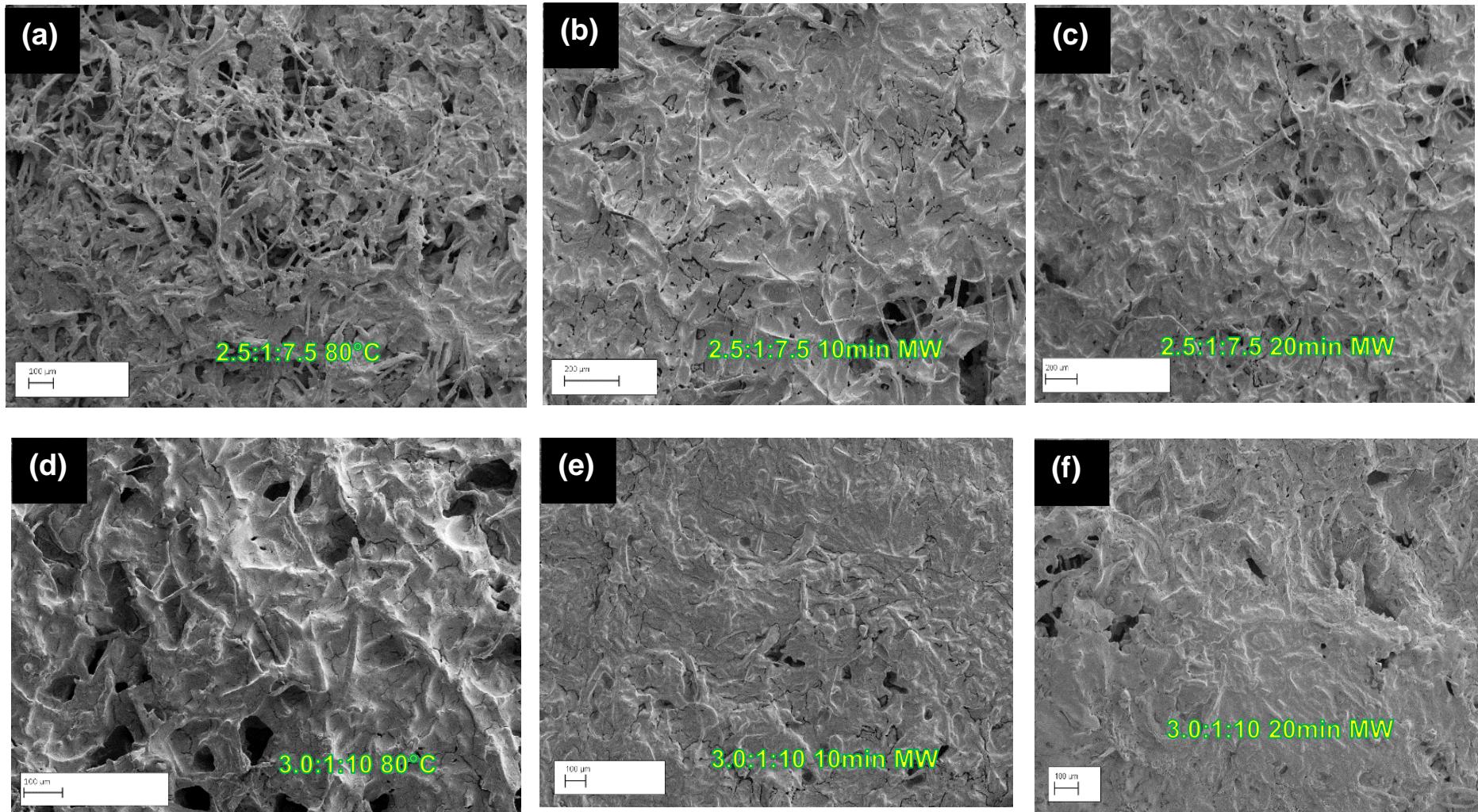
Figure 7. 16 SEM images of (a) unirradiated; (b) 10 min MW irradiated; and (c) 20 min MW irradiated composite PCMs with blend ratio of 2.5:1:7.5; (d) unirradiated; (e) 10 min MW irradiated; and (f) 20 min MW irradiated composite PCMs with blend ratio of 3.0:1:10.

7.4 Interim conclusions

In this Chapter PEG was shape stabilised successfully via an innovative 'MW radiation' assisted TCA crosslinking reaction. Results demonstrated that the thermal properties of the TCA crosslinked composite PCMs could be enhanced using the MW irradiation treatment provided that suitable blend ratios were selected and used. The conclusions and outcomes of current research are summarised below.

7.4.1 Outcomes

➢ MW irradiation was observed to have increased the rate of TCA crosslinking reaction since viscosity of the reaction mixture had increased after the MW irradiation treatment.

➢ FTIR results confirmed that MW irradiation caused no changes to the chemical structure of the TCA crosslinked composite PCMs.

➢ XRD results indicated that MW irradiation resulted in enhancing the crystallinity of composite PCMs which initially had poor crystallinity by melting the amorphous phases. For some blend ratios 10 min MW irradiation was enough for the enhancement of the crystallinity while in others 20 min MW irradiation was required.

➢ In composite PCMs containing low CF content MW irradiation was observed to decrease its crystallinity.

➢ MW irradiation had increased the supercooling behaviours of PEG in the TCA crosslinked composite PCMs since the unirradiated composite PCMs were observed to have lower supercooling temperatures (ST) than pristine PEG.

➢ Thermal stability of PEG was enhanced after the TCA crosslinking reaction. MW irradiation resulted in increasing the thermal stability further.

➢ SEM analysis demonstrated that the homogeneity of the TCA crosslinked composite PCMs were improved by the MW irradiation treatment.

Chapter 8: Conclusions and recommendations for future work

8.1 Major conclusions of current research

8.1.1 Conclusive statement for specific objective 1:

Research on stabilising the environmentally friendly solid-liquid PEG PCMs to overcome its leakage problem has been established several times in the previous literature via the vacuum impregnation approach (e.g., physical approach) but led to the production of composite PCMs prone to phase segregation. To produce durable PEG based composite PCMs chemical crosslinking approaches have been employed using toxic isocyanate based crosslinking agents like TDI and MDI. However, to encourage green chemistry it is crucial to utilise environmentally friendly materials to enhance the shape stability of PEG. Throughout this thesis environmentally friendly materials namely PEG, cellulose fibre and citric acid were used to prepare form-stable composite PCMs via a highly feasible solution casting approach. Unique formulations were developed and investigated to prepare functional composite PCMs of different PEG loadings using deionised water as solvent.

8.1.2 Conclusive statement for specific objective 2:

Results suggested that citric acid (CA) was the most suitable crosslinking agent for the shape stabilisation of PEG via the TCA crosslinking reaction because it was able to produce stable functional crosslinked composite PCMs. The conventionally used TDI was observed to produce highly toxic composite PCMs with very poor thermal performance and weak shape stability. The latent heat capacity of the corresponding composite PCMs were in the range 5.86 to 16.57 J/g; this was attributed to the thermal degradation of PEG during PU crosslinking reaction confirmed by its colour change from white to yellow. Therefore, results suggested that the crystal structure of PEG should experience minimal destruction during TCA crosslinking reaction to produce functional composite PCMs of enhanced thermal properties.

Incorporating adequate amount of CA was important for the formation of the TCA crosslinked composite PCMs. Hence, using low CA concentration (3 wt.%) resulted in producing very soft composites which poor physical properties since they were damaged during the demoulding process. However, results indicated that optimisation

232

of CA content resulted in increasing the hydrophilic nature attributed to the increased number of amorphous phases in the composite PCMs.

Overall, results suggested that composite PCMs containing high CF content should have a low CA content (e.g., high CF/CA ratio) to produce composite PCMs of enhanced thermal properties since composite PCMs containing high CF and low CA content (e.g., low CF/CA ratio) had lower latent heat capacity. Composite PCM with blend ratio 4:1:5 and CF/CA ratio of 0.20 had latent heat capacity of 50.78 J/g while composite PCM with blend ratio 4:1:10 and CF/CA ratio of 0.10 had a low latent heat capacity of 43.28 J/g.

8.1.3 Conclusive statement for specific objective 3:

In this thesis unique formulations were proposed, developed, and investigated to understand the impact of chemical composition on the thermal properties of the resulting TCA crosslinked composite PCMs.

Results indicated that the thermal properties of the TCA crosslinked composite PCMs depended mainly upon the PEG content, PEG/CF ratio and PEG/CA ratio.

The latent heat capacity of the composite PCM increased from 33.18 to 47.35 and 58.09 J/g as result of increasing PEG content from 29.41 to 33.33 and 36.84 wt.% provided this was accompanied by an increase in PEG/CF ratio from 2.50 to 3.00 and 3.50; and PEG/CA ratio from 0.50 to 0.60 and 0.70. This was attributed to the increased mobility of the PEG chain which resulted in producing crystallisable composite PCMs.

Further increase in PEG content from 36.84 to 40 wt.% (e.g., 8.58% increase) accompanied by an increase in PEG/CF ratio from 3.50 to 4.00; and PEG/CA content from 0.70 to 0.80 resulted in decreasing the latent heat capacity from 58.09 to 50.78 J/g (e.g.,12.58 decrease). This suggested that overloading the TCA composite PCM with PEG hindered the crystallisability of the PEG chain (e.g., its ability to form crystals).

Therefore, results demonstrated that the thermal properties of the TCA crosslinked composite PCMs were mainly dictated by the PEG content, PEG/CF ratio and PEG/CA ratio.

The current study had demonstrated the possibility of producing composite PCMs of enhanced thermal performance with low PEG loadings. Hence, composite PCM with PEG content of 36.84 wt.% had a latent heat of melting and crystallisation of 58.09 and 55.75 J/g.

8.1.4 Conclusive statement for specific objective 4:

8.1.4.1 Effects of TCA crosslinking on crystalline and thermal properties

TCA crosslinking reaction resulted in forming ester linkages between the OH group of PEG and CF. As result the flexibility of PEG chain was reduced greatly. The degree of restriction of PEG chain mobility (e.g., crystallinity) was dictated by the chemical composition. Results indicated that the crystallinity and latent heat capacity of the TCA crosslinked composite PCMs were governed by the number of crystalline and amorphous phases present in its structure. Presence of amorphous phases in higher content resulted in reducing the crystallinity; and the latent heat capacity of the resulting composite PCMs.

Formation of structures with higher number of covalent bonds (e.g., high density crosslinked structure) resulted in producing non-crystallisable composite PCMs. The crystallinity index (CI) value of pristine PEG8000 was 52.94% while the CI value of the TCA crosslinked composite PCMs were in the range 8.92 to 45.3%. This was attributed to the formation of crystal defects after the chemical crosslinking reaction.

For composite PCMs with PEG/CF ratio of 2.50 increasing the PEG content from 29.41 to 29.41 to 38.46 wt.%, PEG/CA ratio from 0.50 to 0.83 and CF content from 11.76 to 15.38 wt.% the CI value was observed to decrease significantly from 43.69 to 8.92% (79.58%); however, the latent heat capacity was observed to increase from 33.18 to 46.27 J/g (e.g., 39.45% increase). This suggested that the crystalline phases of composite PCM with CI value of 8.92% hidden by the amorphous phases.

Composite PCM with blend ratio of 2.5:1:7.5 had latent heat capacity of 24.93 J/g and a CI value of 40.17% while composite PCM with blend ratio of 3.0:1:5 had a latent heat capacity of 47.35 J/g with a CI value of 41.5%. This indicated that despite having similar CI values, both composite PCMs had different latent heat capacities which confirms the fact that both thermal performance and crystallinity of the resulting composite PCMs are dictated by its chemical composition. Results suggested that

there is no direct relationship between the crystallinity and the thermal properties of the resulting TCA crosslinked composite PCMs.

PEG8000 exhibited supercooling temperature of 19.34 °C. Results demonstrated that the TCA crosslinking reaction had reduced the supercooling temperature of PEG8000 since the supercooling temperature of the crosslinked composite PCMs ranged from 9.09 to 14.88 °C which was attributed to the formation of extra nucleation sites. Hence, supercooling behaviours of PEG can therefore be reduced without using any nucleating agents while stabilising it through the TCA crosslinking reaction.

8.1.4.2 Effects of TCA crosslinking on thermal stability

TGA results indicated that the TCA crosslinked composite PCMs had better thermal stability than pristine PEG despite having lower crystallinity. Observations indicated that the TCA crosslinked composite PCMs experienced mass loss in four stages. Melting of PEG8000 and moisture loss appeared to occur in stage 1 while majority of the mass loss attributed to the thermal decomposition of PEG8000, CF and CA occurred in stage 2. In the remaining two stages, thermal decomposition of the remaining crosslinked structure occurred.

Results indicated that composite PCM containing high CA content had poor thermal stability which was attributed to the increased hydrophilic nature due to the presence of CA in high concentration. Hence, increasing PEG content from 40 to 32 and 26.67 wt.% which was accompanied by a decrease in PEG/CA ratio from 0.80 to 0.53 and 0.40 since CA content increased from 50 to 60 and 66.67 wt.% resulted in decreasing the onset temperature from 198.18 to 195.51 and 127.87 °C.

8.1.4.3 Effects of TCA crosslinking on crystal morphology

POM analysis indicated that the typical spherulitic crystal structures of PEG became less prominent in the TCA crosslinked composite PCMs, and size of the crystals had reduced. Mainly because PEG chain appeared to be enwrapped completely by the crosslinked CF network in the TCA crosslinked composite PCMs. Results indicated that the crystallinity of PEG was impacted greatly by the chemical crosslinking reaction due to the destruction of the PEG crystal lattice. Crystal defects had formed, and amorphous phases appeared to dominate the crystalline phases in the composite PCMs.

8.1.5 Conclusive statement for specific objective 5:

8.1.5.1 Effect of MW radiation on crystalline properties

Results indicated that ten minutes MW radiation exposure was able to rearrange the crystalline regions which consequently resulted in enhancing the crystallinity of the TCA crosslinked composite PCMs. The degree of enhancement on crystallinity was dictated by the chemical composition and crystallinity index (CI) value.

Composite PCM with low CI value had experienced significant enhancement in crystallinity by 10 minutes MW radiation exposure mainly because amorphous phases are more likely to be attacked by the thermal effect since, they have higher moisture content than the crystalline phases. Hence, composite PCM with blend ratio of 2.5:1:3 experienced an increase in CI value from 8.92 to 38.11% (e.g.,76.59% increase) after 10 minutes MW radiation exposure.

Results suggested that composite PCMs with low content of PEG and CF, but high content of CA experienced a desirable effect by 10 minutes MW radiation exposure. Hence, composite PCM with blend ratio of 2.5:1:10 experienced a significant enhancement of CI value from 29.08 to 48.06% (e.g.,65.28% increase) after 10 minutes MW irradiation. The same phenomenon was observed to occur for composite PCM with blend ratio of 4.0:1:7.5 because ten minutes MW radiation exposure enhanced the CI value from 35.65 to 47.96%. This indicated that CA provided a shielding effect to prevent destruction of the crystal lattice structure of PEG by the thermal effect of MW radiation.

Results suggested that twenty minutes MW irradiation had an adverse effect on crystallinity since it appeared to reduce the crystallinity of some composite PCMs. For instance, in composite PCMs with blend ratio 2.5:1:5 the crystallinity of ten and twenty minutes MW irradiation was 45.51 and 37.47%. Therefore, results suggested that ten minutes MW radiation was sufficient to optimise the CI value of the TCA crosslinked composite PCMs.

8.1.5.2 Effect of MW radiation on thermal properties

Results indicated that twenty minutes MW irradiation had enhanced the latent heat capacity of the TCA crosslinked composite PCMs despite having an adverse effect on its crystallinity. This was attributed to the reduction in the number of amorphous phases by the thermal effect. This was accompanied by a reduction in the number of

crystal defects. The effect on latent heat of the composite PCM by MW irradiation was influenced mainly by the PEG content and PEG/CA ratio. For composite PCM with blend ratio 3.5:1:5 and PEG/CA ratio of 0.70, ten minutes MW radiation had decreased the latent heat capacity from 58.09 to 47.64 J/g (e.g.,17.99% decrease) while twenty minutes MW irradiation had enhanced the latent heat capacity from 58.09 to 67.24 J/g (e.g.,15.75% increase).

For composite PCMs containing low CF content, the CA content had to be low (e.g., high PEG/CA ratio) for it to experience a desirable effect on crystallinity by MW radiation because low CF content meant less shielding was available. Hence, composite PCM with blend ratio of 3.5:0.85:10 contained 5.92 wt.% of CF (e.g., low CF content) and a PEG/CA ratio of 0.35 experienced an undesirable effect on latent heat capacity after MW radiation exposure since latent heat capacity reduced from 40.11 to 32.08 and 31.53 J/g after ten and twenty minutes MW radiation exposure. Increasing CF content from 5.92 to 7.17 and PEG/CA ratio from 0.35 to 0.47 was observed to be a desirable combination since latent heat capacity had increased from 32.80 to 40.03 and 39.26 J/g after ten and twenty minutes MW radiation exposure. Overall results demonstrated the possibility of enhancing the thermal properties of TCA crosslinked composite PCM using MW radiation treatment during the crosslinking reaction.

8.1.6 Conclusive statement for specific objective 6:

8.1.6.1 Surface morphology of the TCA crosslinked composite PCMs

Results indicated that the interfacial bonding existing between PEG, CF and CA was influenced greatly by the CF and CA content. Hence, composite PCM with a blend ratio of 3.0:1:3 containing 42.86 wt.% of PEG was observed to have a highly porous microstructure indicating poor interfacial bonding between PEG, CF, and CA. However, increasing PEG content from 42.86 to 46.67 wt.% provided this was accompanied by a reduction in CF and CA content from 14.29 to 13.33 wt.% and 42.86 to 40.0 wt.% the interfacial bonding was observed to improve significantly. Hence, corresponding composite PCM was observed to exhibit a compact structure with an even topography. Overall, reducing PEG content had an adverse effect on the homogeneity of the resulting composite PCMs and increasing CA content was observed to produce compact structures.

8.1.6.2 Effect of MW radiation exposure on surface morphology of the TCA crosslinked composite PCMs

The unexposed composite PCM with blend ratio of 3.0:1:5 consisted of a highly porous three-dimensional porous structure covered with coarse aggregates of CF. Ten minutes MW radiation exposure had melted down the coarse aggregates of CF which was attributed to its thermal effect. The surface was observed to become smoother, and the number of voids appearing on surface had reduced significantly which indicated that the interfacial bonding between PEG, CF and CA had enhanced significantly after ten minutes MW radiation exposure.

However, for composite PCM with blend ratio of 3.5:1:7.5 twenty MW radiation exposure resulted in destructing the surface morphology. The compact structure was observed to contain higher number of voids and cracks after MW radiation exposure mainly because the samples had experienced significant moisture loss. This resulted in producing composite PCM with an uneven topography, and poor interfacial bonding.

8.2.1 The remarkable findings of the current study are summarised below:

➤ The crystallinity of PEG8000 was 52.94% which indicated that it was comprised of both crystalline and amorphous phases. Crosslinked composite PCM with blend ratio 2.5:1:5 containing 29.41 wt.% of PEG8000 was observed to have an optimum crystallinity of 43.69%. The corresponding latent heat of melting and crystallisation was 33.18 and 33.31 J/g. Therefore, this shows that minimal destruction should be caused to the crystalline phases of PEG8000 during chemical reaction to encourage the formation of composite PCMs of enhanced thermal properties which could be achieved by adjusting the chemical composition. Reduction in crystallinity was attributed to the increased number of crystal defects which resulted in increasing the number of amorphous phases because crystal defects are concentrated in the amorphous regions.

➤ Literature stated that increasing the PEG content resulted in enhancing the crystallinity. Results from the current study showed that optimisation of PEG content in the composite PCM had an adverse effect on the crystallinity and the thermal properties because the number of amorphous phases had also increased. However, incorporating enough PEG content was observed to improve the crystallinity which subsequently improved the thermal properties since increasing the PEG content from 24.14 to 36.84 wt.% (e.g., 52.61% increase) resulted in the

latent heat of melting and crystallisation significantly from 26.39 and 24.90 J/g to 58.09 and 55.75 J/g. The phase transition temperatures were observed to increase undesirably from 58.22 to 64.11 °C.

➢ Ten and twenty MW irradiation treatment was observed to cause changes to the crystallinity of the TCA crosslinked composite PCMs. In the composite PCM with blend ratio 3.5:1:5, ten and twenty min MW irradiated resulted in changing its thermal properties since latent heat of melting and crystallisation had decreased and increased from 58.09 and 55.75 J/g to 47.64 and 45.83 J/g; and 69.20 and 67.24 J/g. Results indicated that for the corresponding composite PCM twenty min MW irradiation was required to enhance its crystallinity by melting the amorphous phases.

➢ PEG8000 exhibited supercooling temperature of 19.34 °C. Results demonstrated that the TCA crosslinking reaction had reduced the supercooling temperature of PEG8000 since the supercooling temperature of the crosslinked composite PCMs ranged from 9.09 to 14.88 °C which was attributed to the formation of extra nucleation sites. Hence, supercooling behaviours of PEG can therefore be reduced without using any nucleating agents while stabilising it through the TCA crosslinking reaction.

8.2.2 Recommendations for future work

➢ Throughout the current study PEG8000 was mostly used in the TCA crosslinking reaction. For the preparation of composite PCMs for building construction application is would be ideal to select PEGs with lower molecular weights (e.g.,1000 g/mol) for further investigation using the formulations developed and presented within this thesis since then only TCA crosslinking reaction will lead to the production of PEG-cellulose composite PCMs with phase transition temperatures matching the operating temperature of the intended building construction application.

➢ PEG is a hydrophilic polymer and reducing its hydrophilic nature after the shape stabilisation process is desirable; however, it is still unknown whether the hydrophilicity of PEG had reduced after TCA crosslinking reaction. Therefore, further investigations like the 'contact angle' test should be carried out which will determine the nature of the surface (e.g., hydrophilic, or hydrophobic).

- Literature reports that increasing CA content results in increasing the hydrophilic nature of the resulting composite PCMs. Therefore, the influence of moisture content on the thermal and crystalline properties of PEG in the TCA crosslinked composite PCMs needs to be investigated and evaluated.

- Results indicated that MW irradiation was able to enhance the interfacial compatibility between PEG and CF which was required to prepare composite PCMs of improved structural integrity. The impact of changing molecular weight of PEG on the interfacial compatibility needs to be investigated since for building applications PEGs of lower molecular weights would be used in the TCA crosslinking reaction.

- TCA crosslinking reaction was observed to have reduced the supercooling temperature of PEG8000; however, it is still unknown whether CF or CA was responsible for providing the extra nucleating sites. Therefore, it would be necessary to investigate this so that chemical compositions can be adjusted accordingly for the preparation of TCA crosslinked composite PCMs exhibiting almost no supercooling behaviours.

References

Abhat, A., 1983. Low temperature latent heat thermal energy storage: Heat storage materials. Solar Energy 30, 313–332. https://doi.org/10.1016/0038-092X(83)90186-X

Abiona, A.A., Osinkolu, A.G., 2010. Gamma-irradiation induced property modification of polypropylene, International Journal of Physical Sciences.

Akeiber, H., Nejat, P., Majid, M.Z.A., Wahid, M.A., Jomehzadeh, F., Zeynali Famileh, I., Calautit, J.K., Hughes, B.R., Zaki, S.A., 2016. A review on phase change material (PCM) for sustainable passive cooling in building envelopes. Renewable and Sustainable Energy Reviews 60, 1470–1497. https://doi.org/10.1016/j.rser.2016.03.036

Alberdi, M., Esp1, E., Fernandez-Berridi, M.J., Iruin, J.J., 1994. Influence of the Blending Method and Poly(methyl methacrylate) Tacticity in Its Miscibility with Poly(hydroxy ether of bisphenol A, phenoxy), Polymer Journal.

Alemdar, A., Güngör, N., Ece, O.I., Atici, O., 2005. The rheological properties and characterization of bentonite dispersions in the presence of non-ionic polymer PEG. J Mater Sci 40, 171–177. https://doi.org/10.1007/s10853-005-5703-4

Ali, Z.I., Eisa, W.H., 2013. Characterization of Electron Beam Irradiated Poly Vinyl Alcohol/Poly Ethylene Glycol Blends. Journal of Scientific Research 6, 29–42. https://doi.org/10.3329/jsr.v6i1.13071

Alkan, C., Günther, E., Hiebler, S., Ensari, Ö.F., Kahraman, D., 2012. Polyurethanes as solid-solid phase change materials for thermal energy storage. Solar Energy 86, 1761–1769. https://doi.org/10.1016/j.solener.2012.03.012

Alkan, C., Sari, A., 2008. Fatty acid/poly(methyl methacrylate) (PMMA) blends as form-stable phase change materials for latent heat thermal energy storage. Solar Energy 82, 118–124. https://doi.org/10.1016/j.solener.2007.07.001

Alva, G., Lin, Y., Liu, L., Fang, G., 2017. Synthesis, characterization and applications of microencapsulated phase change materials in thermal energy storage: A review. Energy Build 144, 276–294. https://doi.org/10.1016/j.enbuild.2017.03.063

Al-Yasiri, Q., Szabó, M., 2023. Experimental study of PCM-enhanced building envelope towards energy-saving and decarbonisation in a severe hot climate. Energy Build 279. https://doi.org/10.1016/j.enbuild.2022.112680

Amaral, C., Vicente, R., Marques, P.A.A.P., Barros-Timmons, A., 2017. Phase change materials and carbon nanostructures for thermal energy storage: A literature review. Renewable and Sustainable Energy Reviews 79, 1212–1228. https://doi.org/10.1016/j.rser.2017.05.093

Arpagaus, C., Collenberg, A., Rütti, D., Assadpour, E., Jafari, S.M., 2018. Nano spray drying for encapsulation of pharmaceuticals. Int J Pharm 546, 194–214. https://doi.org/10.1016/j.ijpharm.2018.05.037

Athanasoulia, I.G., Tarantili, P.A., 2017. Preparation and characterization of polyethylene glycol/poly(L-lactic acid) blends, in: Pure and Applied Chemistry. Walter de Gruyter GmbH, pp. 141–152. https://doi.org/10.1515/pac-2016-0919

Atinafu, D.G., Dong, W., Huang, X., Gao, H., Wang, G., 2018. Introduction of organic-organic eutectic PCM in mesoporous N-doped carbons for enhanced thermal conductivity and energy storage capacity. Appl Energy 211, 1203–1215. https://doi.org/10.1016/j.apenergy.2017.12.025

Ayyappan, S., Mayilsamy, K., Sreenarayanan, V. V., 2016. Performance improvement studies in a solar greenhouse drier using sensible heat storage materials. Heat and Mass Transfer/Waerme- und Stoffuebertragung 52, 459–467. https://doi.org/10.1007/s00231-015-1568-5

Barreneche, C., Vecstaudza, J., Bajare, D., Fernandez, A.I., 2017. PCM/wood composite to store thermal energy in passive building envelopes. IOP Conf Ser Mater Sci Eng 251. https://doi.org/10.1088/1757-899X/251/1/012111

Bayés-García, L., Ventolà, L., Cordobilla, R., Benages, R., Calvet, T., Cuevas-Diarte, M.A., 2010. Phase Change Materials (PCM) microcapsules with different shell compositions: Preparation, characterization and thermal stability. Solar Energy Materials and Solar Cells 94, 1235–1240. https://doi.org/10.1016/j.solmat.2010.03.014

Bayon, A., Liu, M., Sergeev, D., Grigore, M., Bruno, F., Müller, M., 2019. Novel solid–solid phase-change cascade systems for high-temperature thermal energy storage. Solar Energy 177, 274–283. https://doi.org/10.1016/j.solener.2018.10.085

Behzadi, S., Farid, M.M., 2014. Long term thermal stability of organic PCMs. Appl Energy 122, 11–16. https://doi.org/10.1016/j.apenergy.2014.01.032

Berardi, U., Gallardo, A.A., 2019. c. Energy Build 199, 402–414. https://doi.org/10.1016/j.enbuild.2019.07.014

Bhat, A., Budholiya, S., Raj, S.A., Sultan, M.T.H., Hui, D., Shah, A.U.M., Safri, S.N.A., 2021. Review on nanocomposites based on aerospace applications. Nanotechnol Rev 10, 237–253. https://doi.org/10.1515/ntrev-2021-0018

Blanco-Rodríguez, P., Rodríguez-Aseguinolaza, J., Gil, A., Risueño, E., D'Aguanno, B., Loroño, I., Martín, L., 2015. Experiments on a Lab Scale TES Unit using Eutectic Metal Alloy as PCM. Energy Procedia 69, 769–778. https://doi.org/10.1016/j.egypro.2015.03.087

Borreguero, A.M., Valverde, J.L., Rodríguez, J.F., Barber, A.H., Cubillo, J.J., Carmona, M., 2011. Synthesis and characterization of microcapsules containing Rubitherm®RT27 obtained by spray drying. Chemical Engineering Journal 166, 384–390. https://doi.org/10.1016/j.cej.2010.10.055

Butala, V., Stritih, U., 2009. Experimental investigation of PCM cold storage. Energy Build 41, 354–359. https://doi.org/10.1016/j.enbuild.2008.10.008

Cabaleiro, D., Agresti, F., Barison, S., Marcos, M.A., Prado, J.I., Rossi, S., Bobbo, S., Fedele, L., 2019. Development of paraffinic phase change material nanoemulsions for thermal energy storage and transport in low-temperature applications. Appl Therm Eng 159. https://doi.org/10.1016/j.applthermaleng.2019.113868

Cabaleiro, D., Hamze, S., Fal, J., Marcos, M.A., Estellé, P., Żyła, G., 2020. Thermal and physical characterization of PEG phase change materials enhanced by carbon-based nanoparticles. Nanomaterials 10, 1–24. https://doi.org/10.3390/nano10061168

Cabane, E., Keplinger, T., Merk, V., Hass, P., Burgert, I., 2014. Renewable and functional wood materials by grafting polymerization within cell walls. ChemSusChem 7, 1020–1025. https://doi.org/10.1002/cssc.201301107

Cao, X., Dai, X., Liu, J., 2016. Building energy-consumption status worldwide and the state-of-the-art technologies for zero-energy buildings during the past decade. Energy Build 128, 198–213. https://doi.org/10.1016/j.enbuild.2016.06.089

Capanema, N.S.V., Mansur, A.A.P., de Jesus, A.C., Carvalho, S.M., de Oliveira, L.C., Mansur, H.S., 2018. Superabsorbent crosslinked carboxymethyl cellulose-PEG hydrogels for potential wound dressing applications. Int J Biol Macromol 106, 1218–1234. https://doi.org/10.1016/j.ijbiomac.2017.08.124

Cárdenas, B., León, N., 2013. High temperature latent heat thermal energy storage: Phase change materials, design considerations and performance enhancement techniques. Renewable and Sustainable Energy Reviews 27, 724–737. https://doi.org/10.1016/j.rser.2013.07.028

Chami Khazraji, A., Robert, S., 2013. Interaction effects between cellulose and water in nanocrystalline and amorphous regions: A novel approach using molecular modeling. J Nanomater 2013. https://doi.org/10.1155/2013/409676

Chanda, S., Bajwa, D.S., 2021. A review of current physical techniques for dispersion of cellulose nanomaterials in polymer matrices. Reviews on Advanced Materials Science. https://doi.org/10.1515/rams-2021-0023

Chen, C., Liu, W., Wang, Z., Peng, K., Pan, W., Xie, Q., 2015. Novel form stable phase change materials based on the composites of polyethylene glycol/polymeric solid-solid phase change material. Solar Energy Materials and Solar Cells 134, 80–88. https://doi.org/10.1016/J.SOLMAT.2014.11.039

Chen, C., Liu, W., Yang, H., Zhao, Y., Liu, S., 2011a. Synthesis of solid-solid phase change material for thermal energy storage by crosslinking of polyethylene glycol with poly (glycidyl methacrylate). Solar Energy 85, 2679–2685. https://doi.org/10.1016/j.solener.2011.08.002

Chen, C., Liu, W., Yang, H., Zhao, Y., Liu, S., 2011b. Synthesis of solid-solid phase change material for thermal energy storage by crosslinking of polyethylene

glycol with poly (glycidyl methacrylate). Solar Energy 85, 2679–2685. https://doi.org/10.1016/j.solener.2011.08.002

Chen, C., Wang, L., Huang, Y., 2009. Crosslinking of the electrospun polyethylene glycol/cellulose acetate composite fibers as shape-stabilized phase change materials. Mater Lett 63, 569–571. https://doi.org/10.1016/j.matlet.2008.11.033

Chen, K., Wang, C., Wang, T., Zhu, Z., Ma, R., Jiang, H., 2020. Preparation and performances of form-stable polyethylene glycol/methylcellulose composite phase change materials. Journal of Polymer Research 27. https://doi.org/10.1007/s10965-020-02150-0

Chen, K., Yu, X., Tian, C., Wang, J., 2014. Preparation and characterization of form-stable paraffin/polyurethane composites as phase change materials for thermal energy storage. Energy Convers Manag 77, 13–21. https://doi.org/10.1016/j.enconman.2013.09.015

Chen, W., Lv, G., Hu, W., Li, D., Chen, S., Dai, Z., 2018. Synthesis and applications of graphene quantum dots: A review. Nanotechnol Rev 7, 157–185. https://doi.org/10.1515/ntrev-2017-0199

Cheng, P., Gao, H., Chen, X., Chen, Y., Han, M., Xing, L., Liu, P., Wang, G., 2020. Flexible monolithic phase change material based on carbon nanotubes/chitosan/poly(vinyl alcohol). Chemical Engineering Journal 397. https://doi.org/10.1016/j.cej.2020.125330

Cho, J.S., Kwon, A., Cho, C.G., 2002. Microencapsulation of octadecane as a phase-change material by interfacial polymerization in an emulsion system. Colloid Polym Sci 280, 260–266. https://doi.org/10.1007/s00396-001-0603-x

Comunian, T.A., Favaro-Trindade, C.S., 2016. Microencapsulation using biopolymers as an alternative to produce food enhanced with phytosterols and omega-3 fatty acids: A review. Food Hydrocoll 61, 442–457. https://doi.org/10.1016/j.foodhyd.2016.06.003

Crist, B., Schultz, J.M., 2016. Polymer spherulites: A critical review. Prog Polym Sci. https://doi.org/10.1016/j.progpolymsci.2015.11.006

Deng, Y., Yang, L., 2017. Preparation and characterization of polyethylene glycol (PEG) hydrogel as shape-stabilized phase change material. Appl Therm Eng 114, 1014–1017. https://doi.org/10.1016/j.applthermaleng.2016.11.207

Deshpande, M., Sundararajan, S., Samui, A.B., Kulkarni, P.S., 2021. Microwave Assisted Preparation of Poly(ethylene) glycol/Lignin Blends for Thermal Energy Storage. J Energy Storage 35. https://doi.org/10.1016/j.est.2021.102338

Devangamath, S.S., Lobo, B., Masti, S.P., Narasagoudr, S., 2020. Thermal, mechanical, and AC electrical studies of PVA–PEG–Ag2S polymer hybrid material. Journal of Materials Science: Materials in Electronics 31, 2904–2917. https://doi.org/10.1007/s10854-019-02835-3

Dindi, A., Lopez Ferber, N., Gloss, D., Rilby, E., Calvet, N., 2020. Compatibility of an Aluminium-Silicon metal alloy-based phase change material with coated stainless-steel containers. J Energy Storage 32, 101961. https://doi.org/10.1016/j.est.2020.101961

Ding, W.D., Koubaa, A., Chaala, A., Belem, T., Krause, C., 2008a. Relationship between wood porosity, wood density and methyl methacrylate impregnation rate. Wood Mater Sci Eng 3, 62–70. https://doi.org/10.1080/17480270802607947

Ding, W.D., Koubaa, A., Chaala, A., Belem, T., Krause, C., 2008b. Relationship between wood porosity, wood density and methyl methacrylate impregnation rate. Wood Mater Sci Eng 3, 62–70. https://doi.org/10.1080/17480270802607947

Eanest Jebasingh, B., Valan Arasu, A., 2020. A comprehensive review on latent heat and thermal conductivity of nanoparticle dispersed phase change material for low-temperature applications. Energy Storage Mater 24, 52–74. https://doi.org/10.1016/j.ensm.2019.07.031

el Karim, Y., Grosu, Y., Faik, A., Lbibb, R., 2019. Investigation of magnesium-copper eutectic alloys with high thermal conductivity as a new PCM for latent heat thermal energy storage at intermediate-high temperature. J Energy Storage 26, 100974. https://doi.org/10.1016/j.est.2019.100974

Elias, C.N., Stathopoulos, V.N., 2019. A comprehensive review of recent advances in materials aspects of phase change materials in thermal energy

storage. Energy Procedia 161, 385–394. https://doi.org/10.1016/j.egypro.2019.02.101

Entrop, A.G., Halman, J.I.M., Dewulf, G.P.M.R., Reinders, A.H.M.E., 2016. Assessing the Implementation Potential of PCMs: The Situation for Residential Buildings in the Netherlands. Energy Procedia 96, 17–32. https://doi.org/10.1016/j.egypro.2016.09.090

Ernest Ravindran, R.S., Subha, V., Ilangovan, R., 2020. Silver nanoparticles blended PEG/PVA nanocomposites synthesis and characterization for food packaging. Arabian Journal of Chemistry 13, 6056–6060. https://doi.org/10.1016/j.arabjc.2020.05.005

Fabiani, C., Piselli, C., Pisello, A.L., 2020. Thermo-optic durability of cool roof membranes: effect of shape stabilized phase change material inclusion on building energy efficiency. Energy Build 207, 109592. https://doi.org/10.1016/j.enbuild.2019.109592

Fallahi, A., Guldentops, G., Tao, M., Granados-Focil, S., van Dessel, S., 2017. Review on solid-solid phase change materials for thermal energy storage: Molecular structure and thermal properties. Appl Therm Eng 127, 1427–1441. https://doi.org/10.1016/j.applthermaleng.2017.08.161

Fang, G., Li, H., Chen, Z., Liu, X., 2011. Preparation and properties of palmitic acid/SiO2 composites with flame retardant as thermal energy storage materials. Solar Energy Materials and Solar Cells 95, 1875–1881. https://doi.org/10.1016/j.solmat.2011.02.010

Fang, G., Li, H., Yang, F., Liu, X., Wu, S., 2009. Preparation and characterization of nano-encapsulated n-tetradecane as phase change material for thermal energy storage. Chemical Engineering Journal 153, 217–221. https://doi.org/10.1016/j.cej.2009.06.019

Fang, Y., Kang, H., Wang, W., Liu, H., Gao, X., 2010. Study on polyethylene glycol/epoxy resin composite as a form-stable phase change material. Energy Convers Manag 51, 2757–2761. https://doi.org/10.1016/j.enconman.2010.06.012

Farid, M.M., Khudhair, A.M., Razack, S.A.K., Al-Hallaj, S., 2004. A review on phase change energy storage: Materials and applications. Energy Convers Manag 45, 1597–1615. https://doi.org/10.1016/j.enconman.2003.09.015

Fashandi, M., Leung, S.N., 2017. Preparation and characterization of 100% bio-based polylactic acid/palmitic acid microcapsules for thermal energy storage. Mater Renew Sustain Energy 6, 1–10. https://doi.org/10.1007/s40243-017-0098-0

Fei, B., Lu, H., Qi, K., Shi, H., Liu, T., Li, X., Xin, J.H., 2008. Multi-functional microcapsules produced by aerosol reaction. J Aerosol Sci 39, 1089–1098. https://doi.org/10.1016/j.jaerosci.2008.07.007

Forster, A.L., Tsinas, Z., Al-Sheikhly, M., 2019. Effect of irradiation and detection of long-lived polyenyl radicals in highly crystalline ultra-high molar mass polyethylene (UHMMPE) fibers. Polymers (Basel) 11. https://doi.org/10.3390/polym11050924

Gök, Ö., Alkan, C., Konuklu, Y., 2019. Developing a poly(ethylene glycol)/cellulose phase change reactive composite for cooling application. Solar Energy Materials and Solar Cells 191, 345–349. https://doi.org/10.1016/j.solmat.2018.11.038

Golitsyn, Y., Pulst, M., Samiullah, M.H., Busse, K., Kressler, J., Reichert, D., 2019. Crystallization in PEG networks: The importance of network topology and chain tilt in crystals. Polymer (Guildf) 165, 72–82. https://doi.org/10.1016/j.polymer.2019.01.018

Hawlader, M.N.A., Uddin, M.S., Khin, M.M., 2003. Microencapsulated PCM thermal-energy storage system. Appl Energy 74, 195–202. https://doi.org/10.1016/S0306-2619(02)00146-0

Hawlader, M.N.A., Uddin, M.S., Zhu, H.J., 2000. Preparation and evaluation of a novel solar storage material: Microencapsulated paraffin. International Journal of Solar Energy 20, 227–238. https://doi.org/10.1080/01425910008914357

He, Q., Zhang, A., 2008. Effect of microwave irradiation on crystalline structure and dielectric property of PVDF/PZT composite. J Mater Sci 43, 820–823. https://doi.org/10.1007/s10853-007-2153-1

Hospodarova, V., Singovszka, E., Stevulova, N., 2018. Characterization of Cellulosic Fibers by FTIR Spectroscopy for Their Further Implementation to Building Materials. Am J Analyt Chem 09, 303–310. https://doi.org/10.4236/ajac.2018.96023

Hua, W., Zhang, L., Zhang, X., 2021. Research on passive cooling of electronic chips based on PCM: A review. J Mol Liq. https://doi.org/10.1016/j.molliq.2021.117183

Huang, J., Wang, T., Zhu, P., Xiao, J., 2013. Preparation, characterization, and thermal properties of the microencapsulation of a hydrated salt as phase change energy storage materials. Thermochim Acta 557, 1–6. https://doi.org/10.1016/j.tca.2013.01.019

Huang, X., Guo, J., He, J., Gong, Y., Wang, D., Song, Z., 2017. Novel phase change materials based on fatty acid eutectics and triallyl isocyanurate composites for thermal energy storage. J Appl Polym Sci 134, 1–8. https://doi.org/10.1002/app.44866

Huo, X., Li, W., Wang, Y., Han, N., Wang, J., Wang, N., Zhang, X., 2018. Chitosan composite microencapsulated comb-like polymeric phase change material via coacervation microencapsulation. Carbohydr Polym 200, 602–610. https://doi.org/10.1016/j.carbpol.2018.08.003

Jeong, S.G., Jeon, J., Lee, J.H., Kim, S., 2013. Optimal preparation of PCM/diatomite composites for enhancing thermal properties. Int J Heat Mass Transf 62, 711–717. https://doi.org/10.1016/j.ijheatmasstransfer.2013.03.043

Jiang, Y., Ding, E., Li, G., 2001. Study on transition characteristics of PEG/CDA solid-solid phase change materials. Polymer (Guildf) 43, 117–122. https://doi.org/10.1016/S0032-3861(01)00613-9

Jing, R., Zhang, H., Huang, C., Su, F., Wu, B., Sun, Z., Xu, F., Sun, L., Xia, Y., Peng, H., Lin, X., Li, B., Zou, Y., Chu, H., Huang, P., Yan, E., 2022. Construction

of double cross-linking PEG/h-BN@GO polymeric energy-storage composites with high structural stability and excellent thermal performances. Colloids Surf A Physicochem Eng Asp 638. https://doi.org/10.1016/j.colsurfa.2021.128193

Jouhara, H., Zabnienska-Gore, A., Khordehgah, N., Ahmad, D., Lipinski, T., 2020. Latent Thermal Energy Storage Technologies and Applications : A Review. International Journal of Thermofluids 6, 100039. https://doi.org/10.1016/j.ijft.2020.100039

Kaewprachu, P., Jaisan, C., Rawdkuen, S., Tongdeesoontorn, W., Klunklin, W., 2022. Carboxymethyl cellulose from Young Palmyra palm fruit husk: Synthesis, characterization, and film properties. Food Hydrocoll 124. https://doi.org/10.1016/j.foodhyd.2021.107277

Kahraman, D., Biçer, A., Sar, A., Alkan, C., 2018. Microencapsulated n -alkane eutectics in polystyrene for solar thermal applications. Solar Energy 160, 32–42. https://doi.org/10.1016/j.solener.2017.11.072

Karaman, S., Karaipekli, A., Sar, A., Biçer, A., 2011. Polyethylene glycol (PEG)/diatomite composite as a novel form-stable phase change material for thermal energy storage. Solar Energy Materials and Solar Cells 95, 1647–1653. https://doi.org/10.1016/j.solmat.2011.01.022

Kasaeian, A., Pourfayaz, F., Khodabandeh, E., 2017. Experimental studies on the applications of PCMs and nano-PCMs in buildings : A critical review. Energy Build 154, 96–112. https://doi.org/10.1016/j.enbuild.2017.08.037

Kee, S.Y., Munusamy, Y., Ong, K.S., 2018. Review of solar water heaters incorporating solid-liquid organic phase change materials as thermal storage. Appl Therm Eng 131, 455–471. https://doi.org/10.1016/j.applthermaleng.2017.12.032

Kenisarin, M., Mahkamov, K., 2016. Salt hydrates as latent heat storage materials:Thermophysical properties and costs. Solar Energy Materials and Solar Cells 145, 255–286. https://doi.org/10.1016/j.solmat.2015.10.029

Kim, Y.U., Park, J.H., Yun, B.Y., Yang, S., Wi, S., Kim, S., 2021. Mechanical and thermal properties of artificial stone finishing materials mixed with PCM

impregnated lightweight aggregate and carbon material. Constr Build Mater 272. https://doi.org/10.1016/j.conbuildmat.2020.121882

Kong, W., Yang, Y., Zhou, C., Lei, J., 2017. Novel thermosetting phase change materials with polycarbonatediol based curing agent as supporting skeleton for thermal energy storage. Energy Build 146, 12–18. https://doi.org/10.1016/j.enbuild.2017.04.040

Krieghoff, J., Gronbach, M., Schulz-Siegmund, M., Hacker, M.C., 2021. Biodegradable macromers for implant bulk and surface engineering. Biol Chem. https://doi.org/10.1515/hsz-2021-0161

Kuru, A., Aksoy, S.A., 2014. Cellulose–PEG grafts from cotton waste in thermo-regulating textiles. Textile Research Journal 84, 337–346. https://doi.org/10.1177/0040517513494251

Lafri, D., Semmar, D., Hamid, A., Ouzzane, M., 2019. Experimental investigation on combined sensible and latent heat storage in two different configurations of tank filled with PCM. Appl Therm Eng 149, 625–632. https://doi.org/10.1016/j.applthermaleng.2018.12.028

Lai, W.C., Cai, Y.T., Cai, Y.L., 2020. Novel green and sustainable shape-stabilized phase change materials for thermal energy storage. J Taiwan Inst Chem Eng 117, 257–264. https://doi.org/10.1016/j.jtice.2020.12.013

Lai, W.C., Liau, W. Bin, Lin, T.T., 2004. The effect of end groups of PEG on the crystallization behaviors of binary crystalline polymer blends PEG/PLLA. Polymer (Guildf) 45, 3073–3080. https://doi.org/10.1016/j.polymer.2004.03.003

Lashgari, S., Mahdavian, A.R., Arabi, H., Ambrogi, V., Marturano, V., 2018. Preparation of acrylic PCM microcapsules with dual responsivity to temperature and magnetic field changes. Eur Polym J 101, 18–28. https://doi.org/10.1016/j.eurpolymj.2018.02.011

Lee, S.Y., Shin, H.K., Park, M., Rhee, K.Y., Park, S.J., 2014. Thermal characterization of erythritol/expanded graphite composites for high thermal storage capacity. Carbon N Y 68, 67–72. https://doi.org/10.1016/j.carbon.2013.09.053

Li, G., 2016. Sensible heat thermal storage energy and exergy performance evaluations. Renewable and Sustainable Energy Reviews. https://doi.org/10.1016/j.rser.2015.09.006

Li, J., Hu, X., Zhang, C., Luo, W., Jiang, X., 2021. Enhanced thermal performance of phase-change materials supported by mesoporous silica modified with polydopamine/nano-metal particles for thermal energy storage. Renew Energy 178, 118–127. https://doi.org/10.1016/j.renene.2021.06.021

Li, J., Yao, M., Shao, Y., Yao, D., 2018. The application of bio-nanotechnology in tumor diagnosis and treatment: A view. Nanotechnol Rev 7, 257–266. https://doi.org/10.1515/ntrev-2018-0011

Li, S., Kong, L., Wang, H., Xu, H., Li, J., Shi, H., 2018. Thermal performance and shape-stabilization of comb-like polymeric phase change materials enhanced by octadecylamine-functionalized graphene oxide. Energy Convers Manag 168, 119–127. https://doi.org/10.1016/j.enconman.2018.05.014

Li, W., Klemeš, J.J., Wang, Q., Zeng, M., 2022. Salt hydrate–based gas-solid thermochemical energy storage: Current progress, challenges, and perspectives. Renewable and Sustainable Energy Reviews 154, 111846. https://doi.org/10.1016/j.rser.2021.111846

Li, W., Zhang, X.X., Wang, X.C., Niu, J.J., 2007. Preparation and characterization of microencapsulated phase change material with low remnant formaldehyde content. Mater Chem Phys 106, 437–442. https://doi.org/10.1016/j.matchemphys.2007.06.030

Li, W.D., Ding, E.Y., 2007. Preparation and characterization of cross-linking PEG/MDI/PE copolymer as solid-solid phase change heat storage material. Solar Energy Materials and Solar Cells 91, 764–768. https://doi.org/10.1016/j.solmat.2007.01.011

Li, X., Sanjayan, J.G., Wilson, J.L., 2014. Fabrication and stability of form-stable diatomite/paraffin phase change material composites. Energy Build 76, 284–294. https://doi.org/10.1016/j.enbuild.2014.02.082

Li, Y., Li, F., Yang, Y., Ge, B., Meng, F., 2021. Research and application progress of lignin-based composite membrane. Journal of Polymer Engineering 41, 245–258. https://doi.org/10.1515/polyeng-2020-0268

Li, Y., Li, J., Deng, Y., Guan, W., Wang, X., Qian, T., 2016. Preparation of paraffin/porous TiO2 foams with enhanced thermal conductivity as PCM, by covering the TiO2 surface with a carbon layer. Appl Energy 171, 37–45. https://doi.org/10.1016/j.apenergy.2016.03.010

Li, Y., Liu, R., Huang, Y., 2008. Synthesis and Phase Transition of Cellulose-graft-Poly(ethylene glycol) Copolymers. J Appl Polym Sci 116, 2658–2667. https://doi.org/10.1002/app

Li, Y., Ma, Q., Huang, C., Liu, G., 2013. Crystallization of poly (ethylene glycol) in poly (methyl methacrylate) networks. Medziagotyra 19, 147–151. https://doi.org/10.5755/j01.ms.19.2.4430

Li, Y., Wu, M., Liu, R., Huang, Y., 2009. Cellulose-based solid–solid phase change materials synthesized in ionic liquid. Solar Energy Materials and Solar Cells 93, 1321–1328. https://doi.org/10.1016/J.SOLMAT.2009.02.005

Liang, C., Lingling, X., Hongbo, S., Zhibin, Z., 2009. Microencapsulation of butyl stearate as a phase change material by interfacial polycondensation in a polyurea system. Energy Convers Manag 50, 723–729. https://doi.org/10.1016/j.enconman.2008.09.044

Liang, X.H., Guo, Y.Q., Gu, L.Z., Ding, E.Y., 1995. Crystalline–Amorphous Phase Transition of a Poly(ethylene glycol)/Cellulose Blend. Macromolecules 28, 6551–6555. https://doi.org/10.1021/ma00123a023

Liu, L., Peng, B., Yue, C., Guo, M., Zhang, M., 2019. Low-cost, shape-stabilized fly ash composite phase change material synthesized by using a facile process for building energy efficiency. Mater Chem Phys 222, 87–95. https://doi.org/10.1016/j.matchemphys.2018.09.072

Liu, L., Xiong, B., Men, Y., 2017. Facile preparation of porous plaster board containing phase change capsules using gel template. Energy Build 156, 134–139. https://doi.org/10.1016/j.enbuild.2017.09.074

Liu, P., Gao, H., Chen, X., Chen, D., Lv, J., Han, M., Cheng, P., Wang, G., 2020. In situ one-step construction of monolithic silica aerogel-based composite phase change materials for thermal protection. Compos B Eng 195. https://doi.org/10.1016/j.compositesb.2020.108072

Liu, P., Chen, W., Liu, C., Tian, M., Liu, Pengju, 2019. A novel poly (vinyl alcohol)/poly (ethylene glycol) scaffold for tissue engineering with a unique bimodal open-celled structure fabricated using supercritical fluid foaming. Sci Rep 9. https://doi.org/10.1038/s41598-019-46061-7

Liu, X., Yang, F., Li, M., Sun, C., Wu, Y., 2022. Development of cost-effective PCM-carbon foam composites for thermal energy storage. Energy Reports. https://doi.org/10.1016/j.egyr.2021.12.065

Liu, X., Zhuang, K., Lin, S., Zhang, Z., Li, X., 2017. Determination of supercooling degree, nucleation and growth rates, and particle size for ice slurry crystallization in vacuum. Crystals (Basel) 7. https://doi.org/10.3390/cryst7050128

Liu, Z., Yu, Z. (Jerry), Yang, T., Qin, D., Li, S., Zhang, G., Haghighat, F., Joybari, M.M., 2018. A review on macro-encapsulated phase change material for building envelope applications. Build Environ 144, 281–294. https://doi.org/10.1016/j.buildenv.2018.08.030

Liu, Z., Zang, C., Ju, Z., Hu, D., Zhang, Y., Jiang, J., Liu, C., 2020. Consistent preparation, chemical stability and thermal properties of a shape-stabilized porous carbon/paraffin phase change materials. J Clean Prod 247. https://doi.org/10.1016/j.jclepro.2019.119565

Lu, S., Shen, T., Xing, J., Song, Q., Shao, J., Zhang, J., Xin, C., 2018. Preparation and characterization of cross-linked polyurethane shell microencapsulated phase change materials by interfacial polymerization. Mater Lett 211, 36–39. https://doi.org/10.1016/j.matlet.2017.09.074

Lucht, N., Hinrichs, S., Gro ßmann, L., Pelz, C., Felgenhauer, E., Clasen, E., Schwenk, M., Hankiewicz, B., 2021. Synthesis of magnetic ferrogels: A tool-box approach for finely tuned magnetic- A nd temperature-dependent properties. Physical Sciences Reviews. https://doi.org/10.1515/psr-2019-0120

Ma, G., Sun, J., Zhang, Y., Jing, Y., Jia, Y., 2019. Preparation and thermal properties of stearic acid-benzamide eutectic mixture/expanded graphite composites as phase change materials for thermal energy storage. Powder Technol 342, 131–140. https://doi.org/10.1016/j.powtec.2018.09.074

Madene, A., Jacquot, M., 2006. Review Flavour encapsulation and controlled release – a review. Int J Food Sci Technol 41, 1–21. https://doi.org/10.1111/j.1365-2621.2005.00980.x

Magdalena, A., Pop, A., Cimpeanu, C., Turcus, V., 2018. European Journal of Medicinal Chemistry Nanoencapsulation techniques for compounds and products with antioxidant and antimicrobial activity - A critical view. Eur J Med Chem 157, 1326–1345. https://doi.org/10.1016/j.ejmech.2018.08.076

Malekipirbazari, M., Sadrameli, S.M., Dorkoosh, F., Sharifi, H., 2014. Synthetic and physical characterization of phase change materials microencapsulated by complex coacervation for thermal energy storage applications. Int J Energy Res 31, 135–147. https://doi.org/10.1002/er

Martins, I.M., Barreiro, M.F., Coelho, M., Rodrigues, A.E., 2014. Microencapsulation of essential oils with biodegradable polymeric carriers for cosmetic applications. Chemical Engineering Journal 245, 191–200. https://doi.org/10.1016/j.cej.2014.02.024

Maruoka, N., Sato, K., Yagi, J.I., Akiyama, T., 2002. Development of PCM for recovering high temperature waste heat and utilization for producing hydrogen by reforming reaction of methane. ISIJ International 42, 215–219. https://doi.org/10.2355/isijinternational.42.215

Mathis, D., Blanchet, P., Landry, V., Lagière, P., 2018. Impregnation of wood with microencapsulated bio-based phase change materials for high thermal mass engineered wood flooring. Applied Sciences (Switzerland) 8. https://doi.org/10.3390/app8122696

Mehrali, Mohammad, Latibari, S.T., Mehrali, Mehdi, Metselaar, H.S.C., Silakhori, M., 2013. Shape-stabilized phase change materials with high thermal conductivity based on paraffin/graphene oxide composite. Energy Convers Manag 67, 275–282. https://doi.org/10.1016/j.enconman.2012.11.023

Mehrpooya, M., Pakzad, P., 2020. Introducing a hybrid mechanical – Chemical energy storage system: Process development and energy/exergy analysis. Energy Convers Manag 211, 112784. https://doi.org/10.1016/j.enconman.2020.112784

Meints, T., Hansmann, C., Gindl-Altmutter, W., 2018. Suitability of different variants of polyethylene glycol impregnation for the dimensional stabilization of oak wood. Polymers (Basel) 10. https://doi.org/10.3390/polym10010081

Meißner, D., Jutzi, P., 2009. Amphiphilic Long-chain Citric Acid Ethers.

Methaapanon, R., Kornbongkotmas, S., Ataboonwongse, C., Soottitantawat, A., 2020. Microencapsulation of n-octadecane and methyl palmitate phase change materials in silica by spray drying process. Powder Technol 361, 910–916. https://doi.org/10.1016/j.powtec.2019.10.114

Milián, Y.E., Gutiérrez, A., Grágeda, M., Ushak, S., 2017. A review on encapsulation techniques for inorganic phase change materials and the in fl uence on their thermophysical properties. Renewable and Sustainable Energy Reviews 73, 983–999. https://doi.org/10.1016/j.rser.2017.01.159

Mondal, S., 2008. Phase change materials for smart textiles - An overview. Appl Therm Eng 28, 1536–1550. https://doi.org/10.1016/j.applthermaleng.2007.08.009

Mousavi, S., Rismanchi, B., Brey, S., Aye, L., 2021. PCM embedded radiant chilled ceiling: A state-of-the-art review. Renewable and Sustainable Energy Reviews. https://doi.org/10.1016/j.rser.2021.111601

Nazir, H., Batool, M., Bolivar Osorio, F.J., Isaza-Ruiz, M., Xu, X., Vignarooban, K., Phelan, P., Inamuddin, Kannan, A.M., 2019. Recent developments in phase change materials for energy storage applications: A review. Int J Heat Mass Transf 129, 491–523. https://doi.org/10.1016/j.ijheatmasstransfer.2018.09.126

Negoro, T., Thodsaratpreeyakul, W., Takada, Y., Thumsorn, S., Inoya, H., Hamada, H., 2016. Role of Crystallinity on Moisture Absorption and Mechanical Performance of Recycled PET Compounds, in: Energy Procedia. Elsevier Ltd, pp. 323–327. https://doi.org/10.1016/j.egypro.2016.05.042

Ng, D.Q., Tseng, Y.L., Shih, Y.F., Lian, H.Y., Yu, Y.H., 2017. Synthesis of novel phase change material microcapsule and its application. Polymer (Guildf) 133, 250–262. https://doi.org/10.1016/j.polymer.2017.11.046

Nomura, T., Okinaka, N., Akiyama, T., 2009. Impregnation of porous material with phase change material for thermal energy storage. Mater Chem Phys 115, 846–850. https://doi.org/10.1016/j.matchemphys.2009.02.045

Nor Azlan, A.Y.H., Katas, H., Mh Busra, M.F., Salleh, N.A.M., Smandri, A., 2021. Metal nanoparticles and biomaterials: The multipronged approach for potential diabetic wound therapy. Nanotechnol Rev. https://doi.org/10.1515/ntrev-2021-0046

Oh, S.Y., Yoo, D. Il, Shin, Y., Seo, G., 2005. FTIR analysis of cellulose treated with sodium hydroxide and carbon dioxide. Carbohydr Res 340, 417–428. https://doi.org/10.1016/j.carres.2004.11.027

Oliver, A., 2012. Thermal characterization of gypsum boards with PCM included: Thermal energy storage in buildings through latent heat. Energy Build. https://doi.org/10.1016/j.enbuild.2012.01.026

Onder, E., Sarier, N., Cimen, E., 2007. Encapsulation of phase change materials by complex coacervation to improve thermal performances of woven fabrics. Thermochim Acta 467, 63–72. https://doi.org/10.1016/j.tca.2007.11.007

Park, J.H., Kang, Y., Lee, J., Wi, S., Chang, J.D., Kim, S., 2019. Analysis of walls of functional gypsum board added with porous material and phase change material to improve hygrothermal performance. Energy Build 183, 803–816. https://doi.org/10.1016/j.enbuild.2018.11.023

Pasupathy, A., Velraj, R., Seeniraj, R. V., 2008. Phase change material-based building architecture for thermal management in residential and commercial establishments. Renewable and Sustainable Energy Reviews 12, 39–64. https://doi.org/10.1016/j.rser.2006.05.010

Pedrosa, P., Pomposo, J.A., Calahorra, E., Cortiizar, M., 1995. E I'N FR OR Crystallization of poly(ethylene oxide) in binary blends containing poly(p-vinyl phenol).

Peng, K., Chen, C., Pan, W., Liu, W., Wang, Z., Zhu, L., 2016. Preparation and properties of β-cyclodextrin/4,4′-diphenylmethane diisocyanate/polyethylene glycol (β-CD/MDI/PEG) crosslinking copolymers as polymeric solid-solid phase change materials. Solar Energy Materials and Solar Cells 145, 238–247. https://doi.org/10.1016/j.solmat.2015.10.031

Pielichowska, K., Głowinkowski, S., Lekki, J., Biniaś, D., Pielichowski, K., Jenczyk, J., 2008. PEO/fatty acid blends for thermal energy storage materials. Structural/morphological features and hydrogen interactions. Eur Polym J 44, 3344–3360. https://doi.org/10.1016/j.eurpolymj.2008.07.047

Pielichowski, K., Flejtuch, K., 2002. Differential scanning calorimetry studies on poly(ethylene glycol) with different molecular weights for thermal energy storage materials. Polym Adv Technol 13, 690–696. https://doi.org/10.1002/pat.276

Polińska, M., Rozanski, A., Galeski, A., Bojda, J., 2021. The Modulus of the Amorphous Phase of Semicrystalline Polymers. Macromolecules 54, 9113–9123. https://doi.org/10.1021/acs.macromol.1c01576

Polu, A.R., Rhee, H.W., 2015. Nanocomposite solid polymer electrolytes based on poly(ethylene oxide)/POSS-PEG (n=13.3) hybrid nanoparticles for lithium ion batteries. Journal of Industrial and Engineering Chemistry 31, 323–329. https://doi.org/10.1016/j.jiec.2015.07.005

Pomianowski, M., Heiselberg, P., Zhang, Y., 2013. Review of thermal energy storage technologies based on PCM application in buildings. Energy Build 67, 56–69. https://doi.org/10.1016/j.enbuild.2013.08.006

Prieto, C., Cooper, P., Fernández, A.I., Cabeza, L.F., 2016. Review of technology: Thermochemical energy storage for concentrated solar power plants. Renewable and Sustainable Energy Reviews 60, 909–929. https://doi.org/10.1016/j.rser.2015.12.364

Qin, Y., Chen, K., Zhang, H., Luo, X., Liang, S., Tian, C., Wang, J., Zhang, L., 2019a. Structure-property correlation of poly(ethylene glycol) based form stable phase change materials with different crosslinking structure. Solar Energy Materials and Solar Cells 203, 110192. https://doi.org/10.1016/j.solmat.2019.110192

Qin, Y., Chen, K., Zhang, H., Luo, X., Liang, S., Tian, C., Wang, J., Zhang, L., 2019b. Structure-property correlation of poly(ethylene glycol) based form stable phase change materials with different crosslinking structure. Solar Energy Materials and Solar Cells 203, 110192. https://doi.org/10.1016/j.solmat.2019.110192

Rahimi Kord Sofla, M., Brown, R.J., Tsuzuki, T., Rainey, T.J., 2016. A comparison of cellulose nanocrystals and cellulose nanofibres extracted from bagasse using acid and ball milling methods. Advances in Natural Sciences: Nanoscience and Nanotechnology 7. https://doi.org/10.1088/2043-6262/7/3/035004

Rai, M., Pandit, R., Gaikwad, S., Yadav, A., Gade, A., 2015. Potential applications of curcumin and curcumin nanoparticles: From traditional therapeutics to modern nanomedicine. Nanotechnol Rev 4, 161–172. https://doi.org/10.1515/ntrev-2015-0001

Rajabi, H., Ghorbani, M., Mahdi, S., Sadeghi, A., Rajabzadeh, G., 2015. Food Hydrocolloids Retention of saffron bioactive components by spray drying encapsulation using maltodextrin , gum Arabic and gelatin as wall materials. Food Hydrocoll 51, 327–337. https://doi.org/10.1016/j.foodhyd.2015.05.033

Ranu, B.C., Adak, L., Ghosh, T., 2021. Learning Green Chemistry and its principles from Nature's process and development of green procedures mimicking nature. Chemistry Teacher International 0. https://doi.org/10.1515/cti-2021-0023

Rathore, P.K.S., Shukla, S.K., 2021. Enhanced thermophysical properties of organic PCM through shape stabilization for thermal energy storage in buildings: A state of the art review. Energy Build. https://doi.org/10.1016/j.enbuild.2021.110799

Saafi, K., Daouas, N., 2019. Energy and cost efficiency of phase change materials integrated in building envelopes under Tunisia Mediterranean climate. Energy 187, 115987. https://doi.org/10.1016/j.energy.2019.115987

Salunkhe, P.B., Shembekar, P.S., 2012. A review on effect of phase change material encapsulation on the thermal performance of a system. Renewable and Sustainable Energy Reviews 16, 5603–5616. https://doi.org/10.1016/j.rser.2012.05.037

Samantha, S.C., Bruna, A.S.M., Adriana, R.M., Fabio, B., Sandro, A.R., Aline, R.C.A., 2015. Drying by spray drying in the food industry: Micro-encapsulation, process parameters and main carriers used. African Journal of Food Science 9, 462–470. https://doi.org/10.5897/ajfs2015.1279

Sánchez, L., Sánchez, P., Carmona, M., de Lucas, A., Rodríguez, J.F., 2008. Influence of operation conditions on the microencapsulation of PCMs by means of suspension-like polymerization. Colloid Polym Sci 286, 1019–1027. https://doi.org/10.1007/s00396-008-1864-4

Sánchez, L., Sánchez, P., de Lucas, A., Carmona, M., Rodríguez, J.F., 2007. Microencapsulation of PCMs with a polystyrene shell. Colloid Polym Sci 285, 1377–1385. https://doi.org/10.1007/s00396-007-1696-7

Sánchez, P., Sánchez-Fernandez, M.V., Romero, A., Rodríguez, J.F., Sánchez-Silva, L., 2010. Development of thermo-regulating textiles using paraffin wax microcapsules. Thermochim Acta 498, 16–21. https://doi.org/10.1016/j.tca.2009.09.005

Sangwal, K., 1996. EFFECTS OF IMPURITIES ON CRYSTAL GROWTH PROCESSES, Crystal Growth and Charact.

Sari, A., 2014. Composites of polyethylene glycol (PEG600) with gypsum and natural clay as new kinds of building PCMs for low temperature-thermal energy storage. Energy Build 69, 184–192. https://doi.org/10.1016/j.enbuild.2013.10.034

Sari, A., Alkan, C., Özcan, A.N., 2015. Synthesis and characterization of micro/nano capsules of PMMA/capric-stearic acid eutectic mixture for low temperature-thermal energy storage in buildings. Energy Build 90, 106–113. https://doi.org/10.1016/j.enbuild.2015.01.013

Sari, A., Karaipekli, A., 2009. Preparation, thermal properties and thermal reliability of palmitic acid/expanded graphite composite as form-stable PCM for thermal energy storage. Solar Energy Materials and Solar Cells 93, 571–576. https://doi.org/10.1016/j.solmat.2008.11.057

Sari, A., Karaipekli, A., 2007. Thermal conductivity and latent heat thermal energy storage characteristics of paraffin/expanded graphite composite as phase change

material. Appl Therm Eng 27, 1271–1277. https://doi.org/10.1016/j.applthermaleng.2006.11.004

Sarier, N., Onder, E., 2012. Organic phase change materials and their textile applications: An overview. Thermochim Acta. https://doi.org/10.1016/j.tca.2012.04.013

Sarı, A., Biçer, A., Alkan, C., 2017. Thermal energy storage characteristics of poly(styrene-co-maleic anhydride)-graft-PEG as polymeric solid–solid phase change materials. Solar Energy Materials and Solar Cells 161, 219–225. https://doi.org/10.1016/j.solmat.2016.12.001

Sarı, A., Bicer, A., Al-Sulaiman, F.A., Karaipekli, A., Tyagi, V. v., 2018. Diatomite/CNTs/PEG composite PCMs with shape-stabilized and improved thermal conductivity: Preparation and thermal energy storage properties. Energy Build 164, 166–175. https://doi.org/10.1016/j.enbuild.2018.01.009

Shafigh, P., Asadi, I., Mahyuddin, N.B., 2018. Concrete as a thermal mass material for building applications - A review. Journal of Building Engineering 19, 14–25. https://doi.org/10.1016/j.jobe.2018.04.021

Shah, A.H., Zhang, Y., Xu, X., Dayo, A.Q., Li, X., Wang, S., Liu, W., 2018. Reinforcement of stearic acid treated egg shell particles in epoxy thermosets: Structural, thermal, and mechanical characterization. Materials 11. https://doi.org/10.3390/ma11101872

Shamseddine, I., Pennec, F., Biwole, P., Fardoun, F., 2022. Supercooling of phase change materials: A review. Renewable and Sustainable Energy Reviews. https://doi.org/10.1016/j.rser.2022.112172

Sharma, A., Tyagi, V. v., Chen, C.R., Buddhi, D., 2009. Review on thermal energy storage with phase change materials and applications. Renewable and Sustainable Energy Reviews 13, 318–345. https://doi.org/10.1016/j.rser.2007.10.005

Shetty, P., Mu, L., Shi, Y., 2019. Polyelectrolyte cellulose gel with PEG / water : Toward fully green lubricating grease. Carbohydr Polym 115670. https://doi.org/10.1016/j.carbpol.2019.115670

Shi, W., Yang, J., Zhang, Y., Luo, J., Liang, Y., Han, C.C., 2012. Lamellar orientation inversion under dynamic interplay between crystallization and phase separation. Macromolecules 45, 941–950. https://doi.org/10.1021/ma202046c

Shin, Y., Yoo, D. il, Son, K., 2005. Development of thermoregulating textile materials with microencapsulated Phase Change Materials (PCM). II. Preparation and application of PCM microcapsules. J Appl Polym Sci 96, 2005–2010. https://doi.org/10.1002/app.21438

Silva, T., Vicente, R., Rodrigues, F., 2016. Literature review on the use of phase change materials in glazing and shading solutions. Renewable and Sustainable Energy Reviews 53, 515–535. https://doi.org/10.1016/j.rser.2015.07.201

Singh Rathore, P.K., Shukla, S.K., Gupta, N.K., 2020. Potential of microencapsulated PCM for energy savings in buildings: A critical review. Sustain Cities Soc. https://doi.org/10.1016/j.scs.2019.101884

Sivanathan, A., Dou, Q., Wang, Y., Li, Y., Corker, J., Zhou, Y., Fan, M., 2020. Phase change materials for building construction: An overview of nano-/micro-encapsulation. Nanotechnol Rev 9, 896–921. https://doi.org/10.1515/ntrev-2020-0067

Song, P., Zhou, F., Li, F., Han, Z., Wang, L., Xu, J., Zhang, Bo, Wang, M., Fan, J., Zhang, Bolin, 2021. Superfine pulverisation pretreatment to enhance crystallinity of cellulose from Lycium barbarum L. leaves. Carbohyd Polym 253. https://doi.org/10.1016/j.carbpol.2020.117207

Souayfane, F., Fardoun, F., Biwole, P.H., 2016. Phase change materials (PCM) for cooling applications in buildings: A review. Energy Build 129, 396–431. https://doi.org/10.1016/j.enbuild.2016.04.006

St-Onge, V., Cui, M., Rochon, S., Daigle, J.C., Claverie, J.P., 2021. Reducing crystallinity in solid polymer electrolytes for lithium-metal batteries via statistical copolymerization. Commun Mater 2. https://doi.org/10.1038/s43246-021-00187-2

Strassburg, S., Mayer, K., Scheibel, T., 2020. Functionalization of biopolymer fibers with magnetic nanoparticles. Physical Sciences Reviews. https://doi.org/10.1515/psr-2019-0118

Su, W., Darkwa, J., Kokogiannakis, G., 2015. Review of solid-liquid phase change materials and their encapsulation technologies. Renewable and Sustainable Energy Reviews 48, 373–391. https://doi.org/10.1016/j.rser.2015.04.044

Subin, M.C., Chowdhury, S., Karthikeyan, R., 2021. A review of upgradation of energy-efficient sustainable commercial greenhouses in Middle East climatic conditions. Open Agric. https://doi.org/10.1515/opag-2021-0017

Sundararajan, S., Samui, A.B., Kulkarni, P.S., 2019. Crosslinked polymer networks of poly(ethylene glycol) (PEG) and hydroxyl terminated poly(dimethyl siloxane) (HTPDMS) as polymeric phase change material for thermal energy storage. Solar Energy 181, 187–194. https://doi.org/10.1016/j.solener.2019.01.091

Sundararajan, S., Samui, A.B., Kulkarni, P.S., 2017a. Shape-stabilized poly(ethylene glycol) (PEG)-cellulose acetate blend preparation with superior PEG loading via microwave-assisted blending. Solar Energy 144, 32–39. https://doi.org/10.1016/j.solener.2016.12.056

Sundararajan, S., Samui, A.B., Kulkarni, P.S., 2017b. Synthesis and characterization of poly(ethylene glycol) (PEG) based hyperbranched polyurethanes as thermal energy storage materials. Thermochim Acta 650, 114–122. https://doi.org/10.1016/j.tca.2017.02.011

Sundararajan, S., Samui, A.B., Kulkarni, P.S., 2016. Interpenetrating phase change polymer networks based on crosslinked polyethylene glycol and poly(hydroxyethyl methacrylate). Solar Energy Materials and Solar Cells 149, 266–274. https://doi.org/10.1016/j.solmat.2015.12.040

Sunku Prasad, J., Muthukumar, P., Desai, F., Basu, D.N., Rahman, M.M., 2019. A critical review of high-temperature reversible thermochemical energy storage systems. Appl Energy 254, 113733. https://doi.org/10.1016/j.apenergy.2019.113733

Tang, Y., Jia, Y., Alva, G., Huang, X., Fang, G., 2016. Synthesis, characterization and properties of palmitic acid/high density polyethylene/graphene nanoplatelets composites as form-stable phase change materials. Solar Energy Materials and Solar Cells 155, 421–429. https://doi.org/10.1016/j.solmat.2016.06.049

Tangthuam, P., Pimoei, J., Mohamad, A.A., Mahlendorf, F., Somwangthanaroj, A., Kheawhom, S., 2020. Carboxymethyl cellulose-based polyelectrolyte as cationic exchange membrane for zinc-iodine batteries. Heliyon 6. https://doi.org/10.1016/j.heliyon.2020.e05391

Tanpichai, S., Witayakran, S., Wootthikanokkhan, J., Srimarut, Y., Woraprayote, W., Malila, Y., 2019. Mechanical and antibacterial properties of the chitosan coated cellulose paper for packaging applications: Effects of molecular weight types and concentrations of chitosan. Int J Biol Macromol 15–17. https://doi.org/10.1016/j.ijbiomac.2019.11.128

Tatsidjodoung, P., le Pierrès, N., Luo, L., 2013. A review of potential materials for thermal energy storage in building applications. Renewable and Sustainable Energy Reviews 18, 327–349. https://doi.org/10.1016/j.rser.2012.10.025

Trigui, A., Karkri, M., Boudaya, C., Candau, Y., Ibos, L., 2013. Development and characterization of composite phase change material: Thermal conductivity and latent heat thermal energy storage. Compos B Eng 49, 22–35. https://doi.org/10.1016/j.compositesb.2013.01.007

Tyagi, V. v., Kaushik, S.C., Tyagi, S.K., Akiyama, T., 2011. Development of phase change materials based microencapsulated technology for buildings: A review. Renewable and Sustainable Energy Reviews 15, 1373–1391. https://doi.org/10.1016/j.rser.2010.10.006

Umair, M.M., Zhang, Y., Iqbal, K., Zhang, S., Tang, B., 2019. Novel strategies and supporting materials applied to shape-stabilize organic phase change materials for thermal energy storage–A review. Appl Energy 235, 846–873. https://doi.org/10.1016/j.apenergy.2018.11.017

Urwin, S.J., Yerdelen, S., Houson, I., ter Horst, J.H., 2021. Impact of impurities on crystallization and product quality: A case study with paracetamol. Crystals (Basel) 11. https://doi.org/10.3390/cryst11111344

Uyanga, K.A., Daoud, W.A., 2021. Carboxymethyl cellulose-chitosan composite hydrogel: Modelling and experimental study of the effect of composition on microstructure and swelling response. Int J Biol Macromol 181, 1010–1022. https://doi.org/10.1016/j.ijbiomac.2021.04.117

Vadhera, J., Sura, A., Nandan, G., Dwivedi, G., 2018. Study of Phase Change materials and its domestic application. Mater Today Proc 5, 3411–3417. https://doi.org/10.1016/j.matpr.2017.11.586

Vehring, R., Snyder, H., Lechuga-Ballesteros, D., 2020. Drying Technologies for Biotechnology and Pharmaceutical Applications.

Wahid, M.A., Hosseini, S.E., Hussen, H.M., Akeiber, H.J., Saud, S.N., Mohammad, A.T., 2017. An overview of phase change materials for construction architecture thermal management in hot and dry climate region. Appl Therm Eng 112, 1240–1259. https://doi.org/10.1016/j.applthermaleng.2016.07.032

Wang, G., Xu, C., Wei, G., Du, X., 2019. Numerical study of a novel dual-PCM thermal energy storage structure filled with inorganic salts and metal alloy as the PCMs. Energy Procedia 158, 4423–4428. https://doi.org/10.1016/j.egypro.2019.01.774

Wang, H., Yuan, Y., Rong, M., Zhang, M., 2009. Microencapsulation of styrene with melamine-formaldehyde resin. Colloid Polym Sci 287, 1089–1097. https://doi.org/10.1007/s00396-009-2072-6

Wang, M., Sun, M., Zhang, Y., Chen, Y., Wu, Y., Ouyang, J., 2019. Effect of microwave irradiation-retrogradation treatment on the digestive and physicochemical properties of starches with different crystallinity. Food Chem 298. https://doi.org/10.1016/j.foodchem.2019.125015

Wang, W., Yang, X., Fang, Y., Ding, J., Yan, J., 2009. Preparation and thermal properties of polyethylene glycol/expanded graphite blends for energy storage. Appl Energy 86, 1479–1483. https://doi.org/10.1016/j.apenergy.2008.12.004

Wang, Y., Zhang, Y., Xia, T., Zhao, W., Yang, W., 2014. Effects of fabricated technology on particle size distribution and thermal properties of stearic-

eicosanoic acid/polymethylmethacrylate nanocapsules. Solar Energy Materials and Solar Cells 120, 481–490. https://doi.org/10.1016/j.solmat.2013.09.028

Wei, J., Li, Z., Liu, L., Liu, X., 2013. Preparation and characterization of novel polyamide paraffin MEPCM by interfacial polymerization technique. J Appl Polym Sci 127, 4588–4593. https://doi.org/10.1002/app.37681

Wen, R., Jia, P., Huang, Z., Fang, M., Liu, Y., Wu, X., Min, X., Gao, W., 2018. Thermal energy storage properties and thermal reliability of PEG/bone char composite as a form-stable phase change material. J Therm Anal Calorim 132, 1753–1761. https://doi.org/10.1007/s10973-017-6934-8

Wijesena, R.N., Tissera, N.D., Rathnayaka, V.W.S.G., Rajapakse, H.D., de Silva, R.M., de Silva, K.M.N., 2020. Shape-stabilization of polyethylene glycol phase change materials with chitin nanofibers for applications in "smart" windows. Carbohydr Polym 237, 116132. https://doi.org/10.1016/j.carbpol.2020.116132

Wilhelm, E., Richter, C., Rapp, B.E., 2018. Phase change materials in microactuators: Basics, applications and perspectives. Sens Actuators A Phys 271, 303–347. https://doi.org/10.1016/j.sna.2018.01.043

Wu, H.T., Tsai, H.M., Li, T.H., 2019. Formation of polyethylene glycol particles using a low-temperature supercritical assisted atomization process. Molecules 24. https://doi.org/10.3390/molecules24122235

Xi, P., Gu, X., Cheng, B., Wang, Y., 2009. Preparation and characterization of a novel polymeric based solid-solid phase change heat storage material. Energy Convers Manag 50, 1522–1528. https://doi.org/10.1016/j.enconman.2009.02.013

Xu, J., Wang, R.Z., Li, Y., 2014. A review of available technologies for seasonal thermal energy storage. Solar Energy 103, 610–638. https://doi.org/10.1016/j.solener.2013.06.006

Yahiaoui, M., Denape, J., Paris, J.Y., Ural, A.G., Alcalá, N., Martínez, F.J., 2014. Wear dynamics of a TPU/steel contact under reciprocal sliding. Wear 315, 103–114. https://doi.org/10.1016/j.wear.2014.04.005

Yang, J., Qi, G.Q., Liu, Y., Bao, R.Y., Liu, Z.Y., Yang, W., Xie, B.H., Yang, M.B., 2016. Hybrid graphene aerogels/phase change material composites: Thermal

conductivity, shape-stabilization and light-to-thermal energy storage. Carbon N Y 100, 693–702. https://doi.org/10.1016/j.carbon.2016.01.063

Yang, X., Cai, Z., 2019. An analysis of a packed bed thermal energy storage system using sensible heat and phase change materials. Int J Heat Mass Transf 144. https://doi.org/10.1016/j.ijheatmasstransfer.2019.118651

Yang, Y., Pang, Y., Liu, Y., Guo, H., 2018. Preparation and thermal properties of polyethylene glycol/expanded graphite as novel form-stable phase change material for indoor energy saving. Mater Lett 216, 220–223. https://doi.org/10.1016/j.matlet.2018.01.025

Yang, Z., Peng, H., Wang, W., Liu, T., 2010. Preparation, Characterization, and Properties of Crosslinked Hydroxylated Poly(styrene-b- butadiene-b-styrene) Triblock Copolymer Guoliang. J Appl Polym Sci 116, 2658–2667. https://doi.org/10.1002/app

Yanshan, L., Shujun, W., Hongyan, L., Fanbin, M., Huanqing, M., Wangang, Z., 2014. Preparation and characterization of melamine/formaldehyde/polyethylene glycol crosslinking copolymers as solid-solid phase change materials. Solar Energy Materials and Solar Cells 127, 92–97. https://doi.org/10.1016/j.solmat.2014.04.013

Yazdani, M.R., Ajdary, R., Kankkunen, A., Rojas, O.J., Seppälä, A., 2021. Cellulose Nanofibrils Endow Phase-Change Polyethylene Glycol with Form Control and Solid-to-gel Transition for Thermal Energy Storage. ACS Appl Mater Interfaces 13, 6188–6200. https://doi.org/10.1021/acsami.0c18623

Yin, G.Z., Díaz Palencia, J.L., Wang, D.Y., 2021. Fully bio-based Poly (Glycerol-Itaconic acid) as supporter for PEG based form stable phase change materials. Composites Communications 27. https://doi.org/10.1016/j.coco.2021.100893

You, M., Wang, X., Zhang, X., Zhang, L., Wang, J., 2011. Microencapsulated n-Octadecane with styrene-divinybenzene co-polymer shells. Journal of Polymer Research 18, 49–58. https://doi.org/10.1007/s10965-010-9390-8

Yu, X., Chang, J., Huang, R., Huang, Y., Lu, Y., Li, Z., Wang, L., 2021. Sensitivity analysis of thermophysical properties on PCM selection under steady and

fluctuating heat sources: A comparative study. Appl Therm Eng 186. https://doi.org/10.1016/j.applthermaleng.2020.116527

Zangabad, P.S., Mirkiani, S., Shahsavari, S., Masoudi, B., Masroor, M., Hamed, H., Jafari, Z., Taghipour, Y.D., Hashemi, H., Karimi, M., Hamblin, M.R., 2018. Stimulus-responsive liposomes as smart nanoplatforms for drug delivery applications. Nanotechnol Rev 7, 95–122. https://doi.org/10.1515/ntrev-2017-0154

Zhan, S., Chen, S., Chen, L., Hou, W., 2016. Preparation and characterization of polyurea microencapsulated phase change material by interfacial polycondensation method. Powder Technol 292, 217–222. https://doi.org/10.1016/j.powtec.2016.02.007

Zhang, C., Hu, X., Xiao, S., Luo, W., Wang, H., Jiang, X., 2021. Enhanced thermal performance of phase-change material supported by nano-Ag coated eggplant-based biological porous carbon. J Energy Storage 43. https://doi.org/10.1016/j.est.2021.103174

Zhang, H., Sun, S., Wang, X., Wu, D., 2011. Fabrication of microencapsulated phase change materials based on n-octadecane core and silica shell through interfacial polycondensation. Colloids Surf A Physicochem Eng Asp 389, 104–117. https://doi.org/10.1016/j.colsurfa.2011.08.043

Zhang, H., Wang, X., 2009a. Synthesis and properties of microencapsulated n-octadecane with polyurea shells containing different soft segments for heat energy storage and thermal regulation. Solar Energy Materials and Solar Cells 93, 1366–1376. https://doi.org/10.1016/j.solmat.2009.02.021

Zhang, H., Wang, X., 2009b. Fabrication and performances of microencapsulated phase change materials based on n-octadecane core and resorcinol-modified melamine-formaldehyde shell. Colloids Surf A Physicochem Eng Asp 332, 129–138. https://doi.org/10.1016/j.colsurfa.2008.09.013

Zhang, L., Zhang, P., Wang, F., Kang, M., Li, R., Mou, Y., Huang, Y., 2016. Phase change materials based on polyethylene glycol supported by graphene-based mesoporous silica sheets. Appl Therm Eng 101, 217–223. https://doi.org/10.1016/j.applthermaleng.2016.02.120

Zhang, L., Zheng, T., Wu, L., Han, Q., Chen, S., Kong, Y., Li, G., Ma, L., Wu, H., Zhao, Y., Yu, Y., Yang, Y., 2021. Fabrication and characterization of 3D-printed gellan gum/starch composite scaffold for Schwann cells growth. Nanotechnol Rev 10, 50–61. https://doi.org/10.1515/ntrev-2021-0004

Zhang, X.X., Fan, Y.F., Tao, X.M., Yick, K.L., 2005. Crystallization and prevention of supercooling of microencapsulated n-alkanes. J Colloid Interface Sci 281, 299–306. https://doi.org/10.1016/j.jcis.2004.08.046

Zhang, X.X., Fan, Y.F., Tao, X.M., Yick, K.L., 2004. Fabrication and properties of microcapsules and nanocapsules containing n-octadecane. Mater Chem Phys 88, 300–307. https://doi.org/10.1016/j.matchemphys.2004.06.043

Zhang, Y., Zheng, S., Zhu, S., Ma, J., Sun, Z., Farid, M., 2018. Evaluation of paraffin infiltrated in various porous silica matrices as shape-stabilized phase change materials for thermal energy storage. Energy Convers Manag 171, 361–370. https://doi.org/10.1016/j.enconman.2018.06.002

Zhang, Z., Fang, X., 2006. Study on paraffin/expanded graphite composite phase change thermal energy storage material. Energy Convers Manag 47, 303–310. https://doi.org/10.1016/j.enconman.2005.03.004

Zhou, L., Shi, F., Liu, G., Ye, J.P., Han, P.S., Zhang, G., 2021. Fabrication and characterization of in situ cross-linked electrospun Poly(vinyl alcohol)/phase change material nanofibers. Solar Energy 213, 339–349. https://doi.org/10.1016/j.solener.2020.11.039

Zhou, L., Tang, L.S., Tao, X.F., Yang, J., Yang, M.B., Yang, W., 2020. Facile fabrication of shape-stabilized polyethylene glycol/cellulose nanocrystal phase change materials based on thiol-ene click chemistry and solvent exchange. Chemical Engineering Journal 396. https://doi.org/10.1016/j.cej.2020.125206